Anthropomorphic Surgical System for Soft Tissue Robot-Assisted Surgery

Antonia Tzemanaki

A **thesis** submitted in partial fulfilment of the requirements of the University of the West of England, Bristol for the degree of Doctor of Philosophy

Funded by the Bristol Urological Institute

Bristol Robotics Laboratory

Faculty of Environment and Technology

University of the West of England, Bristol

August 2016

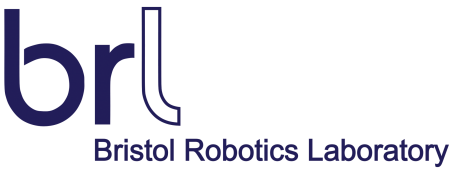

Abstract

Over the past century, abdominal surgery has seen a rapid transition from open procedures to less invasive methods such as laparoscopy and robot-assisted minimally invasive surgery (R-A MIS). These procedures have significantly decreased blood loss, postoperative morbidity and length of hospital stay in comparison with open surgery. R-A MIS has offered refined accuracy and more ergonomic instruments for surgeons, further minimising trauma to the patient.

This thesis aims to investigate, design and prototype a novel system for R-A MIS that can provide more natural and intuitive manipulation of soft tissues and, at the same time, increase the surgeon's dexterity. The thesis reviews related work on surgical systems and discusses the requirements for designing surgical instrumentation. From the background research conducted in this thesis, it is clear that training surgeons in MIS procedures is becoming increasingly long and arduous. Furthermore, most available systems adopt a design similar to conventional laparoscopic instruments or focus on different techniques with debatable benefits. The system proposed in this thesis not only aims to reduce the training time for surgeons but also to improve the ergonomics of the procedure by focusing on the gap between R-A MIS and open surgery.

In order to achieve this, a survey was conducted among surgeons, regarding their opinions on surgical training, surgical systems, how satisfied they are with them and how easy they are to use. A concept for MIS robotic instrumentation was then developed and a series of focus group meetings with surgeons were run to discuss it. The proposed system, named μ`Angelo`, is an anthropomorphic master-slave system that comprises a three-digit miniature hand that can be controlled using the master, a three-digit sensory exoskeleton. While multi-fingered robotic hands have been developed for decades, none have been used for surgical operations. As the system has a human-centred design, its relation to the human hand is discussed. Prototypes of both the master and the slave have been developed and their design and mechanisms are demonstrated. The accuracy and repeatability of the master as well as the accuracy and force capabilities of the slave are tested and discussed.

Acknowledgements

I would like to start by thanking my supervisors for giving me the opportunity to undertake this research and supporting me during my stay in the Bristol Robotics Lab. Dr Sanja Dogramadzi has encouraged my ideas and has given me continuous valuable feedback. She has been an inspiring role model and I will be eternally grateful for the trust she has shown in me as well as the opportunity to participate in teaching. Professor Tony Pipe has offered guidance, valuable advice and humour when it was most needed, for which I am very grateful. Professor Chris Melhuish has been a source of feedback, inspiration, music and great stories. BRL is an exciting place to work and I am thankful for having been part of it for the past 5 years.

I am very appreciative for the help of Mr Raj Persad and Mr David Gillatt as their clinical input has been invaluable. I would like to thank all the surgeons participating in the initial study of this project, and especially the Bristol Urological Institute for allowing me to observe surgical operations and offering priceless information. I would also like to express my deep gratitude to the BUI for funding the largest part of my PhD and creating this opportunity to work in Surgical Robotics.

My progression reviewers Dr Lyndon Smith and Dr Tom Mitchell have also played an important role in the development of my work. Their annual comments and advice have helped shape and improve my thesis. I specifically want to thank Dr Lenz for the detailed comments on my manuscripts which have been very beneficial.

I would like to thank collaborators that have contributed to this research project: Miss Allison Tse for her work on the data glove, Dr Tom Burton for his work on the exoskeleton design, Dr Lucasz Fracczak for his work on the instrument cables and Mr Ben Winstone for his help with image processing. I would also like to thank the BRL technicians, Ian Horsfield, Sam Coupland, Jason Welsby, Sam Forbes and Gareth Griffiths for their time, guidance and all the teasing, and especially for putting up with my long hours in the BRL and lending valuable equipment to me.

Thank you to Dimitris Tzionas, my colleague since our early academic years, for always offering advice and friendship. My cousin Stelios Kalogridakis, for always encouraging me and accompanying me to the best gigs. My tanguera, Evi Diamantidou, for her friendship and long calls. My friend Kasia Pilasiewicz for coming up with the 'microAngelo' name. Thank you to my BRL friends and colleagues.

It would be difficult to express my gratitude for Mr Charles F. Nevett. He has contributed in countless occasions during my PhD years, including proofreading, editing pictures, videos and posters, being the main user in the research and assisting in some ancient Alexandria mathematics. Most of all, I would like to thank him for his endless psychological and moral support.

Finally, I would like to dedicate this thesis to my parents, Konstantina and Eftihios, who have supported me throughout my life and unconditionally encouraged me to follow my dreams. My sisters Anika and Chrissoula and my brother in law Yannis have always stood by me and helped when I needed it. Thank you to little Matthildi and Agapi for sending me love and handcrafted art. My family has taught me to stay strong, persist through all struggles and crave for more knowledge.

"To [...] all the young people of the world, I offer one simple insight. In my life I have found two things of priceless worth – learning and loving. Nothing else — not fame, not power, not achievement for its own sake — can possibly have the same lasting value. For when your life is over, if you can say 'I have learned' and 'I have loved,' you will also be able to say 'I have been happy'."

Arthur C. Clarke
'Rendezvous with Rama'

Contents

Glossary

Angle vector form of expressing the rotary joint values of a serial manipulator at a given time, describing its layout. 147, 149, 151, 152

Anthropomorphic Human-like, in this particular report: human finger-like. 5–7, 44, 50, 56, 57, 59, 60, 62, 66–68, 95, 99–101, 110, 114, 115, 156, 159, 163, 167

CAD Computer-aided design. 4, 75, 76, 99, 104, 110, 205, 206

Cholecystectomy Surgical procedure for the removal of the gall bladder. 1, 9, 21, 61, 63

Closed-ended questions Question format that limits respondents with a list of answer choices from which they must choose to answer the question. 50, 51

CMC Carpometacarpal (Figure 4.1). 68, 69, 72, 76, 80, 83–86, 88, 89, 91, 94, 103, 111, 139, 149

Cystectomy Surgical procedure for the removal of all or part of the urinary bladder. 15, 16

DIP Distal interphalangeal (Figure 4.1). 68, 72, 75, 76, 78, 80, 83, 86, 91, 93, 97, 98, 111, 138, 153, 154

DOF Degree Of Freedom: in case of a mechanism made of several bodies, the number of possible independent relative motions between the links of the mechanism. DOFs is used to indicate plural. 14, 25–28, 30–34, 36, 37, 39, 40, 43, 48, 56, 58, 63, 68, 69, 71, 72, 74–76, 78, 80, 83, 84, 94, 101, 104, 107, 111, 112, 114–116, 122, 123, 125–133, 136, 139, 153–158, 161–163, 210–213, 216

FDA Food and Drug Administration. 2, 16, 21

FK Forward Kinematics. 70, 86, 89, 101, 141–143, 149, 151, 154

FLS Fundamentals of Laparoscopic Surgery. 23, 34, 164

FRS Fundamentals of Robotic Surgery. 22

Fulcrum effect It creates the need for surgeons to move their hand in the opposite direction in which the tip of the instrument is intended to go. 19, 61

Fundoplication A surgical procedure in which the upper portion of the stomach is wrapped around the lower end of the oesophagus and sutured in place as a treatment for the reflux of stomach contents into the oesophagus. 22

HALS Hand-assisted laparoscopic surgery: the surgeon inserts a hand through a small incision in the abdomen. 11, 12, 18, 21, 36, 45, 56, 65

Haptics Tactile feedback technology which takes advantage of the sense of touch by applying forces, vibrations, or motions to the user. 41, 82

Hernia An internal part of the body pushes through a weakness in the muscle or surrounding tissue wall (such as an abdominal surgical wound that has not fully healed). 11, 12, 20, 45, 53, 56

IK Inverse Kinematics. 149, 151, 154

Insufflation The process of injecting gas into the abdominal cavity in order to create more space for the surgical tasks. 10, 56

IP Interphalangeal (Figure 4.1). 68, 73, 76, 80, 81, 86, 91, 93, 97, 98, 111, 153, 154

Laparoscope A slender tubular camera-tool inserted through an incision in the abdominal wall for viewing the operating field. 10, 18, 20, 26

Laparoscopy Conventional MIS technique: the surgeon uses hand held tools to operate on the patients body through small incisions on the abdomen. 1, 10, 11, 13, 14, 18, 21, 23, 45, 51–56, 60, 61, 65, 166

Learning curve Graphical representation of surgical performance against gained experience. 15, 21, 29, 60, 62

Likert-scale In response to such a question, respondents specify their level of agreement or disagreement on a symmetric agree-disagree scale for a series of statements. 51

MCP Metacarpophalangeal (Figure 4.1). 68, 69, 73, 76, 80, 81, 83–86, 89, 91, 93, 97, 98, 111, 138, 147, 149, 151, 153

MIS Minimally Invasive Surgery. 1–4, 7, 9, 11, 16, 18, 20–22, 27, 29, 30, 34, 36, 45, 46, 49–53, 55, 56, 60–62, 65, 67, 159, 163, 164, 166, 167

MRI Magnetic Resonance Imaging. 35

Nitinol Metal alloy of nickel and titanium. 34

NOTES Natural Orifice Translumenal Endoscopic Surgery. 17, 18, 31–33, 39, 46

Open-ended question Unstructured question in which (unlike in a closed-ended question) possible answers are not suggested and the respondents answers in their own words. 50

Peritoneum Abdominal wall. 32

PIP Proximal interphalangeal (Figure 4.1). 68, 75, 76, 80, 83, 86, 93, 97, 98, 111, 138, 147–149, 151, 153

Pneumoperitoneum Air or gas in the abdominal (peritoneal) cavity. 12

Prostatectomy Surgical procedure for the removal of the prostate. 16, 61

PTFE Polytetrafluoroethylene. Synthetic material. 125–127

R-A MIS Robot-Assisted Minimally Invasive Surgery: the surgeon remotely operates articulated instruments attached to the end of robotic arms. 2, 3, 7, 12–16, 18, 22–24, 41, 46, 49–51, 53, 55, 56, 58, 60–62, 65, 67, 73, 138, 159, 160, 166–168

Randomised trials Study where the participating patients are randomly allocated one or other of the different treatments with ultimate goal to statistically determine which is the best. 61

Rapid Prototyping Group of techniques for quick manufacturing and prototyping. In this project: 3D printing of parts of an assembly using its CAD drawings. 4

Retractor A surgical instrument with which a surgeon can either actively separate the edges of a surgical incision or can hold back underlying organs and tissues. 36, 63, 161

Robotic cart The surgical unit that carries the robotic arms and instruments. 15

SMA Shape Memory Alloy. Wire which when heated it returns to its original shape. 8, 35, 39, 40, 99, 104–109, 130–132

SPA Single Port Access. 18–21, 31, 32, 34, 39, 40, 46, 52, 56, 65, 160

Sternotomy Surgery in which an incision is made along the sternum, after which the sternum itself is divided, or 'cracked'. 33

STT Similar Triangle Transform. Proposed method for mapping the thumb, index and middle finger to those of a robotic hand. 141, 142, 147, 150–154, 157, 162

Triangulation Trocars are usually placed in a triangular fashion in order to facilitate smooth instrument manipulation. 18–20

Trocar A sharp-pointed surgical instrument used to create ports in the abdomen as a means of introduction for laparoscopic cameras and tools. 10, 11, 18, 20, 36

Nomenclature

ΔL_{max} Maximum distance that the cable can be pulled so that the joint covers its entire range of motion

γ_g Radius of the gear supporting the pulley that the cable wraps around

γ_m Radius of the gear attached to the motor's shaft

Γ_S Radius of the pulley around which the cable wraps

γ_s Radius of the pulley around which the cable wraps and which is attached to the centre of the gear

λ Similarity proportion between distances A and a

Ωq Projection of Ωt on z axis

Ωt Radius of the two cones' common base formed with p_i and p_m as vertices and all possible solutions for p_t as base perimeter

Ω Centre of the common circular base formed with p_i and p_m as vertices and all possible solutions for p_t as base perimeter

ω_{31}-ω_{36} Angle limits for the 3rd DOF of the instrument's thumb, which define the path of the cable tJ_5

ω_{41}-ω_{45} Angle limits for the 4th DOF of the instrument's thumb, which define the path of the cable tJ_5

ω_{51}-ω_{512} Angle limits for the 5th DOF of the instrument's thumb, which define the path of the cable tJ_5

ϕ_I Angle between A and B

ϕ_i Angle between a and b

θ_j Angle of joint j

θ_I Angle vector of the exoskeleton's index finger's joints

θ_i Angle vector of the instrument's index finger's joints

θ_M Angle vector of the exoskeleton's middle finger's joints

θ_m Angle vector of the instrument's middle finger's joints

θ_t Angle vector of the exoskeleton's thumb's joints

θ_t Angle vector of the instrument's thumb's joints

A Distance between the tips of the exoskeleton's index and middle fingers

a Distance between the tips of the instrument's index and middle fingers

B Distance between the tips of the exoskeleton's index finger and thumb

b Distance between the tips of the instrument's index finger and thumb

C Distance between the tips of the exoskeleton's middle finger and thumb

c Distance between the tips of the instrument's middle finger and thumb

d Projection on the z axis of the distance between p_i and p_t

e Projection on the z axis of the distance between p_m and p_t

E_4 Tangential point on the O_4 shaft of the instrument's thumb

E_5 Tangential point on the O_5 shaft of the instrument's thumb

e_j Mapping error (relative distance) between the exoskeleton's and the instrument's digits

F_A Point where the cable intersects the horizontal from O_5

F_B Tangential point on the O_5 shaft as the cable extends to E_4

G_5 Point of narrowing on the shaft of link '2' of the instrument's thumb

G_B Point where cable 'tJ_5' exits the thumb and enters a sheath of constant length until it connects to the actuating motor

G_{31} G_{33} Diametrical points of the through hole of link 'a' of the instrument's thumb

G_{32} Point at the edge of link 'a'

I_K Tangential point on the O_4 shaft as the cable tJ_5 extends to G_{31}, where $K = AorB$ depending on which routing is used

in Projection of p_i on z axis

k Offset that is calculated from the three sensors when the MCP joint is at 0 position

O_j Origin of frame {j}, coincident with the centre of the shaft of the instrument's thumb's DOF j, where $j = 1, 2, 3, 4or5$

p'_{TI} Modified translation vector of the hand's index base {I} with regard to the thumb base {T} for use in iterative STT mapping

p'_{TM} Modified translation vector of the hand's middle base {I} with regard to the thumb base {T} for use in iterative STT mapping

P_2 Position of the 'locking' pin in link '1' of the instrument's thumb, where the cable tJ_2 is attached

P_5 Position of the 'locking' pin in link '3' of the instrument's thumb, where the cable tJ_5 is attached

p_I Position vector of the exoskeleton's index finger's tip

p_i Position vector of the instrument's index finger's tip

p_M Position vector of the exoskeleton's middle finger's tip

p_m Position vector of the instrument's middle finger's tip

p_T Position vector of the exoskeleton's thumb's tip

p_t Position vector of the instrument's thumb's tip

p_{TI} Translation vector of the hand's index base {I} with regard to the thumb base {T}

p_{ti} Translation vector of the instrument's index base {i} with regard to the thumb base {t}

p_{TM} Translation vector of the hand's middle base {I} with regard to the thumb base {T}

p_{tm} Translation vector of the instrument's middle base {i} with regard to the thumb base {t}

q_j MCP angle in degrees, derived using the three sensors around this joint

R_d Range of the MCP joint measured experimentally

R_r Range of the sensor value before joint calibration

r_s Radius of the joint shafts of the instrument's thumb

R_{TI} Rotation matrix of the base of the index/middle finger base {I} with regard to the thumb base {T} (for both the human hand and the instrument)

x_ω y_ω z_ω Coordinates of Ω on x, y and z axes respectively

x_i z_i The p_i coordinate on x and z axis respectively

x_m z_m The p_m coordinate on x and z axis respectively

x_p y_p Coordinate of 'locking' pin P_5 on x and y axes respectively

x_t z_t The p_t coordinate on x and z axis respectively

z_I The p_I coordinate on z axis

z_M The p_M coordinate on z axis

z_T The p_T coordinate on z axis

List of Figures

List of Tables

Chapter 1

Introduction

Minimally Invasive Surgery (MIS) refers to a wide range of surgical procedures where the size of the incisions made on the patient's body is limited as opposed to wider incisions used in open surgery. MIS made it "possible for surgeons neither to look directly nor touch the tissues or organs on which they operate" (Mack, 2001). Keyhole surgery or laparoscopy is a type of MIS, performed through small incisions on the patient's abdomen.

Examples of efforts in designing primitive versions of minimally invasive instruments have been recorded since 400 B.C. by Hippocrates. Later, in 1806, Philip Bozzini produced a tool that exploited reflecting light from a series of mirrors. Although not being accepted by the medical community of the time, it later set the grounds for endoscopy (St Peter and Holcomb, 2008). A variation of this instrument, called the cystoscope, made the first laparoscopy in an animal possible in 1901. Despite many advancements towards MIS in various medical procedures over the years, many consider that the revolution in MIS really began in 1987 when Philip Mouret performed the first laparoscopic cholecystectomy[1] (Mack, 2001; St Peter and Holcomb, 2008; Park and Lee, 2011), five years after the development of a high resolution camera that could be attached to the endoscope.

MIS procedures are becoming more common in hospitals because of their numerous advantages, such as decreased blood loss, reduced post-operative pain and morbidity, better cosmetic results, shorter hospital stay and thus, lower cost (Allemann et al., 2010). For example, laparoscopic hysterectomies increased from 17.7% to 46% between 2006-2009 (Jonsdottir et al., 2011). Park and Lee (2011) state that

[1]For terminology see the Glossary at the beginning of the thesis

if there had been no MIS approaches invented, the volume of patients nowadays could not possibly have been accommodated by existing hospitals.

Robotic technology, an evolution of the hand-held laparoscopic instruments, was introduced to surgery in order to add to and enhance the benefits of MIS. Robot-assisted MIS (R-A MIS) offers the possibility of improved precision, dexterity and refined accuracy, helping surgeons overcome limitations of current surgical techniques (Allemann et al., 2010). This, in combination with the more ergonomic surgical instruments, has consequently added to the popularity of the technique (Freschi et al., 2012). Furthermore, the indirect control of the surgical instruments creates the possibility of remote surgery, e.g. Lindbergh operation by Marescaux (2002), providing the ability to operate on patients at isolated locations or astronauts in space (Thirsk et al., 2007).

In 2000, the Food and Drug Administration (FDA) approved the teleoperated Da Vinci Surgical System (frequently referred to as Da Vinci) for various surgical procedures (Intuitive Surgical, 2016). At the time of writing this thesis, the Da Vinci remains the only commercially available R-A MIS system for general and abdominal surgery. Teleoperated R-A MIS systems, such as the Da Vinci, include two main components: the robotic manipulation unit with slender instruments that can be inserted into the operating field for carrying out surgical tasks and a surgical interface to remotely control the instruments. As will be discussed later, the main criticism of such systems is related to the high costs, the necessity of a large space in operating theatres and the limitations of their instruments (Baik, 2008). In fact, their efficiency and extent of contribution are doubted by a large part of the surgical population (Greenberg, 2013). In order to improve patient safety and the surgeon's efficiency, as well as increasing the number of surgical procedures for which these technologies can be applied, great efforts are being put into designing new MIS instruments by both the academic and industry sector. Additionally, the way that the instruments are controlled affects not only their efficacy, but also the ergonomics and learning process for the surgeon. It is, therefore, necessary that new

surgical instruments are partnered with appropriate controllers to form a complete teleoperated system. Research in such systems could have a significant impact in the advancement of R-A MIS.

1.1 Research Questions

> "The fact that there is a multiplicity of solutions on offer suggests that none of them are perfect. And if there was one ideal solution, we would all have adopted it. So the fact that the choice of instruments that are being developed is not finalised yet, indicates that there is room for development."
>
> Krukowski et al. (2010)

The purpose of this thesis' research has been to investigate, design and build a novel prototype of MIS robotic instrumentation for manipulation of soft tissue, such as in general surgery. For simplicity in this thesis, the term MIS refers to abdominal surgery unless stated otherwise.

Through the study of MIS techniques, review of existing surgical systems and devices as well as their limitations, the research presented in this thesis has aimed to further the understanding and use of robotics in the field of surgery. In order to achieve this, the following questions concerning the specifications of the system needed to be answered.

i. What are the issues and setbacks in R-A MIS when compared to other MIS techniques and open surgery?

ii. Can R-A MIS instruments be designed to utilise dexterous manipulations and ergonomics associated with open soft tissue (abdominal) surgery?

iii. How can an appropriate user interface be designed to match the dexterity of the instruments and enable remote manipulation?

1.2 Methodology

The research conducted in order to answer these research questions can be summarised in the following objectives:

1. Investigation of issues in MIS and review of existing systems and devices.
2. Further exploration of existing challenges in manipulation, ergonomics and requirements in MIS using feedback from surgeons.
3. Design of a novel master-slave concept for MIS instrumentation that could overcome identified challenges.
4. Development of kinematic models of proposed systems that agree with the kinematic model of the human hand and hence, offer the surgeon intuitive manipulation.
5. Computer-aided design (CAD) and rapid prototyping (RP) for implementation of the slave instrument to demonstrate feasibility of production and miniaturisation.
6. CAD and RP for implementation of a master device that is adjustable.
7. System trials to evaluate capabilities in grasping force and master-slave mapping to demonstrate possibility for effective teleoperation.

Each part has had a significant role in forming the succeeding phase of the research, revisiting previous phases and including iterations of previous designs when required. The methodology can be represented as in Figure 1.1.

1.3 Published Work

As a result of the research activity, parts of the thesis have been published in four conference proceedings, one journal and two relevant conference workshops. Furthermore, a journal paper describing the master-slave mapping of the μ`Angelo` system

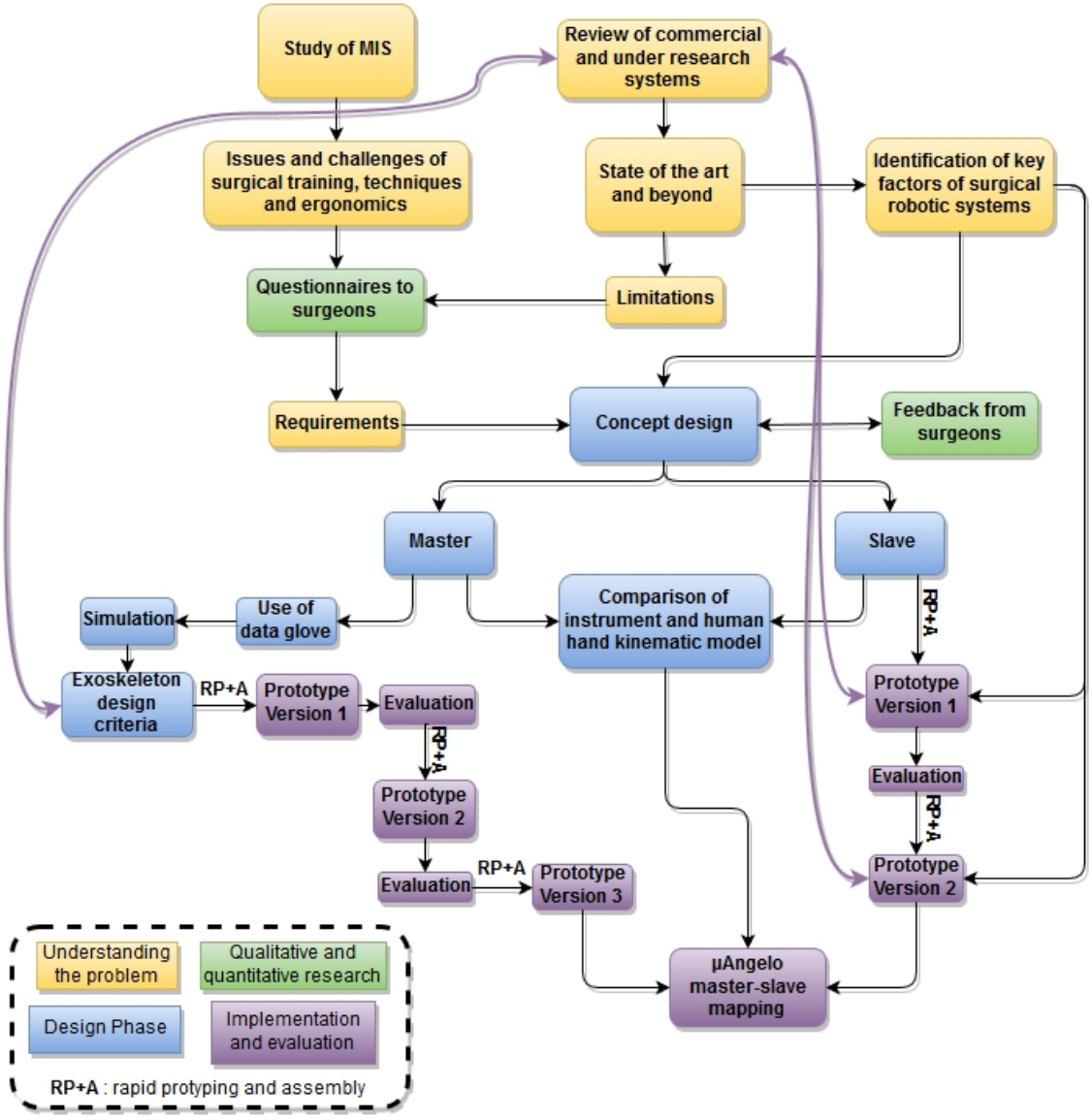

Figure 1.1: Research methodology

and the accuracy experiments of the exoskeleton and the surgical instrument is currently under development. More specifically (abstracts can be found on page 165):

- Edited versions of Sections 3.2, 4.1 and 5.1 have been published in:

  Tzemanaki, A., Dogramadzi, S., Pipe, T., and Melhuish, C. (2012). Towards an anthropomorphic design of minimally invasive instrumentation for soft tissue robotic surgery. In Advances in Autonomous Robotics. Springer, pages 455-456.

- An edited version of Section 4.3.1 has been published in:

Tzemanaki, A., Gao, X., Pipe, A. G., Melhuish, C., and Dogramadzi, S. (2013). Hand exoskeleton for remote control of minimally invasive surgical anthropomorphic instrumentation. In Yang, G.-Z. and Darzi, A., eds., The 6th Hamlyn Symposium on Medical Robotics. Imperial College London, pages 81-82.

- Edited versions of Sections 3.1, 3.3 and 5.2 have been published in:

  Tzemanaki, A., Walters, P., Pipe, A. G., Melhuish, C., and Dogramadzi, S. (2014). An anthropomorphic design for a minimally invasive surgical system based on a survey of surgical technologies, techniques and training. The International Journal of Medical Robotics and Computer Assisted Surgery, 10(3):368-378.

- Edited versions of Sections 4.3.2, 5.3.1 and 5.3.5 have been published in:

  Tzemanaki, A., Burton, T. M., Gillatt, D., Melhuish, C., Persad, R., Pipe, A. G., and Dogramadzi, S. (2014). μAngelo: A novel minimally invasive surgical system based on an anthropomorphic design. In 2014 5th IEEE RAS EMBS International Conference on Biomedical Robotics and Biomechatronics, pages 369-374.

- Edited versions of Sections 5.3.2, 5.3.3 and 6.1 have be published in:

  Tzemanaki, A., Fracczak, L., Gillatt, D., Koupparis, A., Melhuish, C., Persad, R., Pipe, A. G., Rowe, E. and Dogramadzi, S. (2016). Design of a multi-DOF cable-driven mechanism of a miniature serial manipulator for robot-assisted minimally invasive surgery. In 2016 6th IEEE RAS EMBS International Conference on Biomedical Robotics and Biomechatronics, pages 55-60.

Presentations:

- Tzemanaki, A., Pipe, A. G., Melhuish, C., and Dogramadzi, S. (2013). Hand exoskeleton for remote control of minimally invasive surgical anthropomorphic instrumentation. In 'Simulation, Robotics and Telemedicine' Conference of the Royal Society of Medicine and the Severn Deanery, Bristol, UK.

- Tzemanaki, A. and Dogramadzi S. (2015). µAngelo: A Novel System for Robot-Assisted Minimally Invasive Surgery. In 2015 Women in Robotics Workshop of the Robotics Science and Systems conference. Rome, Italy.

1.4 Thesis Roadmap

In Chapter 2, different types of MIS techniques are briefly described and the related issues are identified, leading to a discussion about the requirements of R-A MIS. Surgical systems that have been commercially available, as well as a few under-development, are reviewed.

In Chapter 3, a survey of surgical systems, training and techniques conducted among surgeons is presented and its findings are discussed. Furthermore, the concept of the proposed system (`µAngelo` surgical system) is introduced and feedback from surgeons is presented.

In Chapter 4, the proposed surgical interface (master) is described. A study of the joints and kinematics of the human hand and an investigation of an anthropomorphic approach using a commercial data glove are conducted. Following on from this, the development of various versions of the exoskeleton prototypes using Hall-effect sensors is demonstrated with tests for accuracy and repeatability. Although the final exoskeleton prototype includes provision for haptic feedback, this is not implemented as part of this thesis.

Chapter 5 describes the design of the anthropomorphic slave instrument of the `µAngelo` system and compares its kinematic model to that of the master exoskeleton. Two prototypes using different actuation mechanisms are described: shape memory

alloy (SMA) and cables connected to motors. Two ways of routing the cable-driven mechanism of the second prototype are further investigated and the method of deriving the input-output functions that drive the mechanism is explained. The theoretical model is tested experimentally using simple open-loop position control and the accuracy of the input-output functions is discussed.

Chapter 6 considers the master and slave as an integrated functional system. Firstly, it discusses the bio-inspiration of the slave instruments and their resemblance to the human hand to verify the degree of anthropomorphism in the design. Consequently, it suggests a method of mapping between the instruments and the exoskeleton and, by extension, the human hand. Using the proposed mapping method, simpler system designs with fewer degrees of freedom are considered and their performance in position accuracy is compared to the `μAngelo` design.

In Chapter 7, conclusions are drawn about the thesis' research and its contributions. Finally, limitations of the work are discussed and future directions for further research are identified.

Chapter 2

Background and Related Issues

Advances in MIS as well as related technologies in the course of the recent decade have led to a convergence of techniques available for treatment of various conditions. However, different surgical specialities use MIS techniques and routines that vary significantly, depending on which part of the body is operated on (e.g. abdominal surgery, neurosurgery), and hence, this research focuses mainly on general surgery (especially abdominal such as urology, gynaecology and colorectal surgery). Prostate cancer is the fourth most common cancer (12% all of cancer cases) and the most common cancer in men accounting for 25% of all cases in males in the United Kingdom in 2009 (Cancer Research UK, 2012), while bowel cancer accounts for 13% of all cancer incidents in the UK (2009). In addition, cholecystectomy (gall bladder removal) is one of the most frequent procedures, more than 80% of which are undertaken using MIS (Solly et al., 2006).

A brief presentation of the most popular MIS techniques will be followed by an overview of the existing commercial systems, as well as a number of relevant research activities and systems in the field. Comparison of different operating techniques will be made in order to help with understanding possible issues and challenges, while the importance and level of difficulty in training for these techniques will also be discussed.

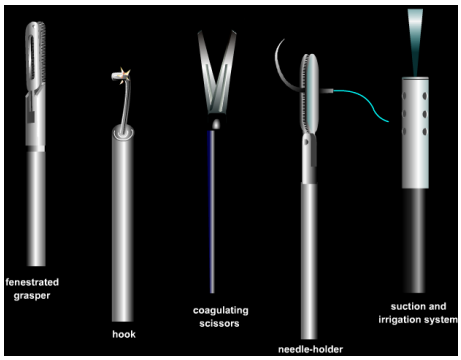

Figure 2.1: Basic laparoscopic instruments (©1999-2016 WeBSurg® IRCAD®, All Rights Reserved)

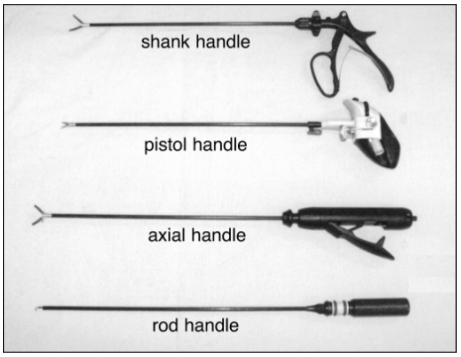

Figure 2.2: Laparoscopic instruments and their handles (Matern et al. (2001), under CC BY-NC-ND 3.0 license)

Figure 2.3: Rigid Laparoscope (with permission from Xion-Medical GmbH)

Figure 2.4: Laparoscopic trocars (©1999-2016 WeBSurg® IRCAD®, All Rights Reserved)

2.1 Types of MIS

2.1.1 Laparoscopic Surgery

There are usually three main incisions made in the abdomen during laparoscopy. Two are intended for the instruments (Figures 2.1 and 2.2) and the third is made for a laparoscope, a slender tube with a light source and a camera (Figure 2.3). The instruments and laparoscope are inserted, removed and swapped through trocars (Figure 2.4) in order to minimise the trauma to the abdominal wall and to stabilise the instrument's point of rotation as much as possible. As soon as the laparoscope is inserted into the body cavity, a gas (CO_2 in most cases) is used to insufflate the abdomen above the organs, in order to elevate the abdominal wall and make space for the instruments' movement (insufflation).

Specific Challenges Although the diagnostic value of laparoscopy has been proven since the 1960s, emergency therapeutic application is relatively recent, e.g. for acute abdominal pain (Golash and Willson, 2005), with specific complications during the procedure. According to Hashizume et al. (1997), 37.5% of complications are caused by incidents that occur during needle and trocar positioning, 70% of which occur during the positioning of the first trocar. Although rare (5 per 10,000 to 3 per 1,000 cases), these potentially preventable injuries have serious consequences with a mortality rate of 13% of the injured patients (Chandler et al., 2001).

The most common complication is the development of hernias, sometimes leading to the necessity of a follow-up operation for hernia repair. The risk increases with the diameter of the trocar (although it can also be due to abdominal wall trauma during the procedure). Kadar et al. (1993) reported one patient with hernia development out of 429 (0.23%) when a 10 mm trocar was used and 5 out of 161 (3.1%) when the diameter of the trocar was 12 mm. Furthermore, the bigger the size of the hernia, the higher the recurrence rate is in the following years (Hesselink et al., 1993).

Additionally, complications have been associated with increasing operative time in laparoscopy (Jackson et al., 2011), making advancement of instruments and technologies imperative, in order to improve surgical efficiency and speed.

2.1.2 Hand-Assisted Laparoscopic Surgery

Hand-Assisted Laparoscopic Surgery (HALS) is not a purely laparoscopic approach; the surgeon can insert a hand through a small incision in the abdomen (7-10 cm (Scott-Conner, 2012)), using it for sensory perception (tactile feedback) and to guide the surgical instruments, facilitating the mobilisation of the organs. It is used instead of a full conversion to open surgery, as it ensures better control and a significant time gain compared to laparoscopic techniques, especially true in complex procedures (Meijer et al., 2000; Scott-Conner, 2012). Conversion rates from MIS to HALS differ between hospitals and procedures, but range from 0 to 15% (Lin and Liu, 2015). Meijer et al. (2000) states:

> "HALS is a safe and efficient method by which it is possible to combine the established convenience and safety of open surgery with the advantages of minimally invasive surgery."

The main disadvantages of this technique include reduced working space taken up by the hand, potential for loss of pneumoperitoneum (CO_2) due to leaking and the cosmetic issues associated with an upper abdominal incision (also hernia development risk) (Rané and Wolf, 2005). Additionally, the surgeon's hand can block the visibility of the site (Scott-Conner, 2012).

In order to make this technique safer, several hand-assistance devices have been developed. An example of first generation devices is IntroMit (Figure 2.5), while GelPort (Figure 2.6) belongs to the second generation devices, which are more user-friendly but also more expensive (30% more than the first-generation devices) (Rané and Dasgupta, 2003).

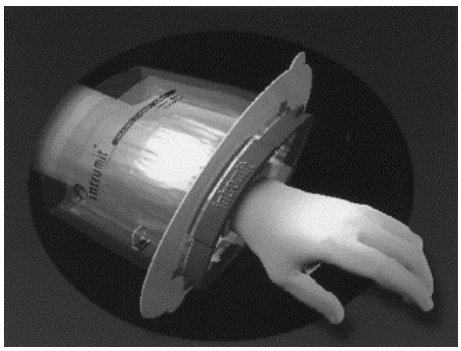

Figure 2.5: Intromit (reprinted from the work by Stifelman and Nieder (2002) with permission from Elsevier)

Figure 2.6: GelPort (Patel and Stifelman, 2004). Reprinted with permission from JOURNAL OF ENDOUROLOGY (Volume 18 & Issue 7), published by Mary Ann Liebert, Inc., New Rochelle, NY

2.1.3 R-A MIS and Commercial Systems

Since R-A MIS has been in use for less than 20 years, the commercially competitive environment of surgical robotics could be considered to be still in its infancy. Available systems for abdominal surgery are not autonomous but constitute master-

slave, remotely controlled systems. The surgeon performs surgery using a computer console that remotely controls small instruments attached to the robot.

The surgeon is usually able to perform more operations per day experiencing less fatigue due to improved ergonomics in comparison with laparoscopy. Furthermore, R-A MIS significantly improves the surgeon's technical capability, promotes surgical safety and consistency, recording detailed information for every procedure (Taylor, 2006). This allows better analysis and comparison between the outcomes of procedures which ultimately benefit training and future procedures in terms of safety. In laparoscopy, everyone shares the same view of the big screens leading to better collaboration between the surgeon and the medical staff during the procedure. In R-A MIS, this can be further improved with the addition of a mentoring console where surgeon and resident can operate on one patient simultaneously.

2.1.3.1 Da Vinci Surgical System

The most commonly used robotic system, and the only commercially available at the time of writing, is the Da Vinci Surgical System (Figure 2.7). Here, the surgeon operates by controlling the master handle shown in Figure 2.8. The system scales, filters and translates the surgeon's hand movements into more precise micro-movements of the instruments, which operate through small incisions in the body (Intuitive Surgical, Inc., 2016a).

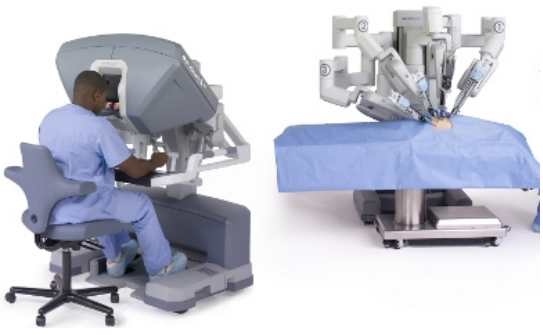

Figure 2.7: Da Vinci Surgical system (Intuitive Surgical, Inc. (2016c), ©2016 Intuitive Surgical, Inc.)

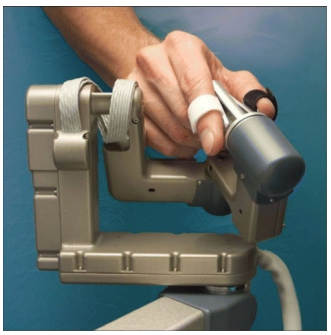

Figure 2.8: The Da Vinci master handle (©2005 by John Wiley & Sons)

Generally, laparoscopy is found to be faster (e.g. in rectal cancer as reported by Park et al. (2011) and endometrial cancer by Cardenas-Goicoechea et al. (2010)) or at least comparable to R-A MIS (in prostatectomy as reported by Rozet et al. (2007)), although the Da Vinci system offers some advantages in precision during finer tasks. In certain procedures, the Da Vinci improves visualisation and decreases the operator's distance from the surgical field, such as in rectal surgery due to the narrow pelvic cavity (Baik, 2008) or in laryngeal surgery (Hillel et al., 2008).

The instruments of the Da Vinci (Figure 2.9) carry a gripper with a wrist-like movement (named EndoWrist) at the end of a shaft. The shaft can be as small as 5 mm in diameter. The gripper comprises three Degrees Of Freedom (DOFs) and 90° of articulation, but its shaft is attached to a robotic arm resulting in a total of seven DOFs (Intuitive Surgical, Inc., 2016a) per instrument/arm. It is argued that the seven DOFs resemble the number of DOFs in the human arm; however, since its shaft is straight and rigid (lacking an elbow), the rotation at the point of the abdominal insertion has the same axis as the one at the EndoWrist joint and hence, the Da Vinci arm seems to have six DOFs when compared to the human arm which is considered to have seven (Hillel et al., 2008).

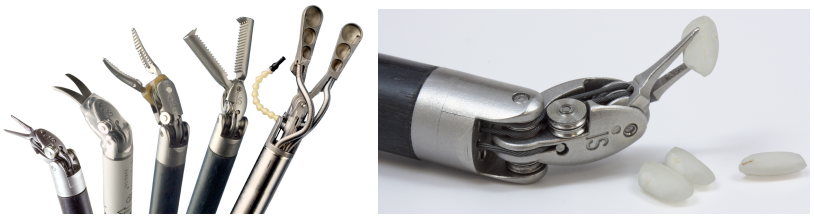

Figure 2.9: Da Vinci instruments (Intuitive Surgical, Inc., 2016a)

2.1.3.2 Zeus Robotic Surgical System

The Zeus Robotic Surgical System (Jones, 2011) was an alternative to the Da Vinci, originally produced by Computer Motion and later bought by Intuitive Surgical Inc., the company that produces Da Vinci (Lysaght, 2005), eliminating the competition and consequently establishing their monopoly in the field. According to Trehan

and Dunn (2013), lack of competition has allowed cost to be higher than necessary, although this could change with existing patents expiring in 2016 (Hoffman, 2010).

Zeus' layout and ergonomics were very similar to Da Vinci, with the addition of the AESOP robotic arm (Automated Endoscopic System for Optimal Positioning) which was voice activated and used to hold the endoscope. The Zeus robotic system was also being tested for wireless space surgery (Jones, 2011).

When comparing the two systems, Dakin and Gagner (2003) found that Da Vinci outperformed Zeus with regard to speed, attributing this to the articulation of the EndoWrist. Two years earlier, Sung et al. (2001) had concluded that the learning curve and operative time were shorter and movements also more inherently intuitive when using the Da Vinci System. These studies suggest that the Da Vinci is, at the moment, the only widely acceptable surgical robot.

2.1.3.3 Considerations

The benefits of the Da Vinci are often questioned due to its great size and cost (both purchase and maintenance), the lack of tactile feedback as well as the time-consuming docking and separation procedure of the robotic cart and the patient (Baik, 2008). The total population of the developed countries covers 14.6% of the world population, while the other 85.4% live in developing countries (Malik, 2013). Although a stay in a hospital in the UK or the US is considered expensive and efforts are focused on reducing it by treating the patients faster, in developing countries where the cost of hospital stay is not as high, e.g. the price in the US is more than 60% above the average (Koechlin et al., 2010), hospitals are not inclined to disperse funds for buying and maintaining expensive equipment such as the Da Vinci robot. The cost becomes even greater as hospitals may require permanent presence of a specialist for technical troubleshooting of the robotic system (Al-Naami et al., 2013).

Although R-A MIS in such procedures may offer decreased blood loss and transfusion rates, operative times are significantly longer compared to open techniques in complex procedures such as radical cystectomy. Open surgery is still the stan-

dard approach for them (Novara et al., 2015). It has been reported that only 3% of the R-A MIS cystectomies in the United States were completed without converting to the open technique (Smith et al., 2012). The slow adoption is perceived to be increased difficulty due to handling of sensitive structures as well as working in a confined space.

In 2013, the FDA conducted a survey with experienced surgeons who used the Da Vinci in a variety of procedures to understand arising challenges compared to conventional techniques (Center for Devices and Radiological Health et al., 2013). All respondents considered it to have a complex user-interface as time is needed for learning how to use the foot pedals, acquiring effective hand-eye coordination and performing procedures without the ability to use their hands to feel tissues, organs or use sutures. The biggest challenge of all might be how to position the arms to avoid collisions between them as well as in relation to the patient's incisions.

Furthermore, robotic surgery was named one of the top 10 health technology hazards for 2015 by the Emergency Care Research Institute (ECRI Institute, 2014). Factors contributing to events of patient harm were identified as *i*) the need to reposition team members, the patient (also accidental movement) or equipment mainly because of the size of the Da Vinci and *ii*) lapses in team communication. This agrees with the study by Wright et al. (2014) on 87,514 patients comparing complication rates and costs related to two types of surgeries when done laparoscopically or using the Da Vinci. R-A MIS in both types of surgery had statistically significant higher complication rates than those of conventional MIS, while the related costs were increased by $2,504 (oophrectomy) and $3,310 (cystectomy) per patient. Similarly, in the case of R-A MIS prostatectomy, complications such as eye injuries can arise due to the combination of long surgical duration and the patient being positioned head down. This position is specifically required for this procedure for better exposure and optimal robotic arm positioning (Sampat et al., 2015).

Main recommendation of the ECRI institute is better training, not only for the surgeon but also for the rest of the surgical team, including nurses, anaesthetists

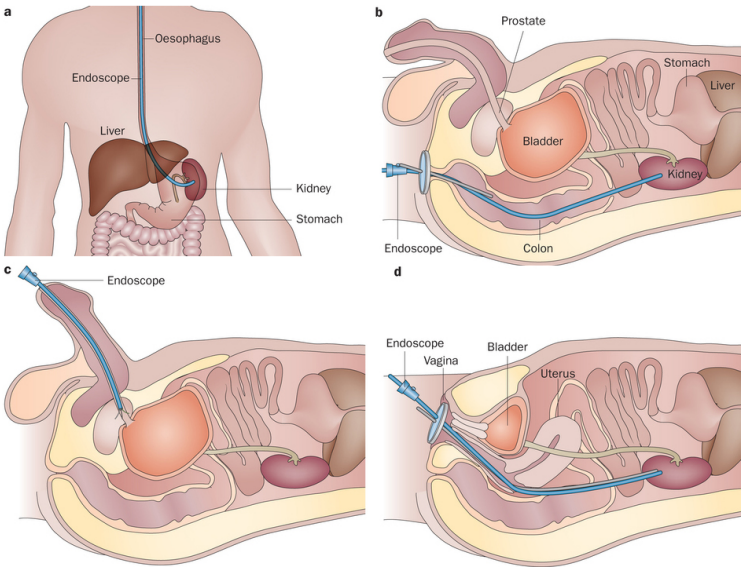

Figure 2.10: NOTES approaches (a) Transgastric nephrectomy (endoscopic access to the kidney via the stomach), (b) Transrectal nephrectomy (the instruments are progressed through the wall of the colon), (c) Tranurethral prostatectomy and (d) Transvaginal nephrectomy (Tyson and Humphreys (2014), permission by Nature Publishing Group[1])

and ancillary staff. This type of recommended training is exclusively related to the existing robotic technology, forcing surgeons to specialise and adapt to specific problems. However, a different approach could be that robotic technologies should instead adapt to the surgeon's needs.

2.1.4 Natural Orifice Translumenal Endoscopic Surgery

Natural Orifice Translumenal Endoscopic Surgery (NOTES) is a surgical technique that requires no external incisions. Instead of making a skin incision, an internal incision is made via a natural orifice (transgastric, transvaginal, transcolonic or transrectal) in order to reach internal organs. A variety of approaches is demonstrated in Figure 2.10. In some cases, as a hybrid technique that combines NOTES and a direct access approach, additional laparoscopic instruments are inserted through an incision in the umbilicus (Arulampalam et al., 2009). Robotic systems are also being developed specifically for this surgical technique (some are mentioned in Section 2.3.2).

[1]www.nature.com/nrurol/journal/v11/n6/full/nrurol.2014.96.html

At the time of writing this thesis, NOTES is considered an experimental surgical technique and is still in early stages of development. It entails high risks of infection and problems in closure of the internal incisions. More robust technologies or techniques will be needed in order to overcome the technical challenges (Flora et al., 2008).

2.1.5 Single Port Access

Single Port Access (SPA) or Single Access Surgery was developed as an alternative to conventional multi-port laparoscopy in order to improve some of the MIS results. Using one incision instead of many, it is expected to have better cosmetic results and less post-operative pain. Figure 2.11 shows one of the commercial devices used in SPA for introducing the laparoscope and instruments into the body cavity. Although a variety of such multichannel devices is on offer, they are expensive or even unaffordable for hospitals. Khiangte et al. (2010) present an improvised SPA glove port made out of readily available materials; however the suitability of some of the materials for human use is questioned by Uygun et al. (2013).

Figure 2.11: SILS Port (Ito et al. (2010), ©2010 by John Wiley & Sons)

In the techniques discussed in the preceding Sections (laparoscopy, HALS and R-A MIS), trocars are usually placed in a triangular fashion (Figure 2.12) in order to facilitate smooth instrument manipulation along with adequate visualisation. Using multiple instruments through a single insertion generates internal and external clashes, while achieving triangulation of the instruments (for example camera, grasping forceps and scissors) forces the surgeons to cross their hands and instru-

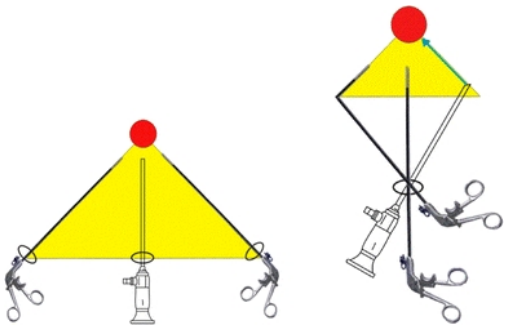

Figure 2.12: Triangulation of instruments in multi-port surgery (left) and SPA (right) (red dot: target organ) (Chiu et al. (2011), with permission of Springer, original caption: "Standard triangulation (left) and single-incision laparoscopic (SIL) appendectomy triangulation (right)")

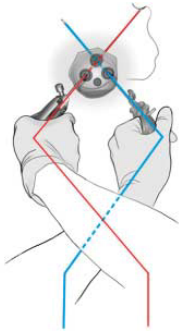

Figure 2.13: Position of hands in conventional SPA (Allemann et al. (2010), image courtesy of Pierre Allemann M.D., ©Archive of surgery, JAMA Surgery)

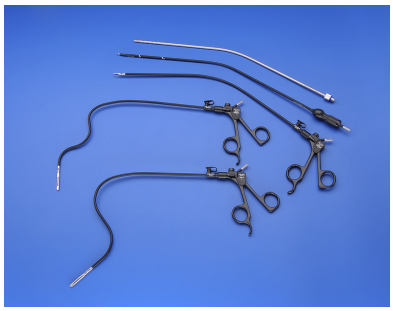

Figure 2.14: Dapri curved grasping forceps and scissors (©KARL STORZ - Endoskope, Germany)

ments in a non-ergonomic fashion as shown in Figure 2.13 (Allemann et al., 2010). This is often referred to as the 'fulcrum effect'.

The use of specialised curved instruments (Figure 2.14), where the curve is inside the patient's body, has been proposed and tested in order to overcome these conflicts (Dapri et al., 2011). It is claimed that, thanks to the double curvature, perfect triangulation of the tools is achieved at all times, despite the fact that they are working through a single incision. Allemann et al. (2010) compare two types of SPA surgery using externally semi-curved instruments: standard SPA where the surgeons hold the instruments and robot-assisted SPA surgery using the Da Vinci robot and a single-port device. In the case of the R-A approach, the surgeons operate the left instrument indirectly using their right hand and vice versa (the control of the instruments is inverted). This study showed that the mean operating time and the

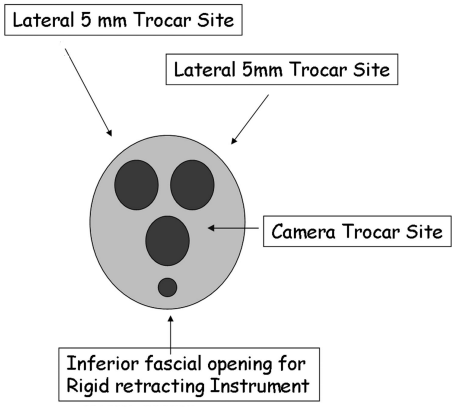

Figure 2.15: Schematic of SPA (adapted from the work by Rottman et al. (2010), under CC BY-NC-ND 3.0 license)

rate of internal and external conflicts were lower when using the R-A approach, while the junior surgeon's mean operative time when using the robot was similar to the senior surgeon's mean time when using the standard SPA approach.

The principle of triangulation is necessary in order to regain acceptable ergonomic conditions and reproduce important manoeuvres used in multi-port MIS. Nevertheless, the incision size is also an important issue. Despite minimising the number of incisions, SPA, not surprisingly, requires a larger port than the ones in multi-port MIS. Rao et al. (2011) report incisions anywhere between 17 and 50 mm depending on the port and the organ to be accessed/removed. Rottman et al. (2010) report a case where the umbilical single incision was 15 mm long and through which two 5 mm trocars for the instruments were inserted, as well as a trocar for a 5 mm laparoscope (Figure 2.15). However, one of the 5 mm trocars had to be up-sized to a 12 mm one in order to accommodate a larger diameter instrument. The authors report no complications or hernia formation after 18 months of the successful operation. Nevertheless, this cannot be considered a statistically significant result (only one patient included in the study). The benefits of SPA surgery, besides cosmetic, are not unambiguously proven and accepted by all surgeons due to extended operating times and higher risk of hernia (Zhang et al., 2012).

The Da Vinci robotic system was initially introduced into SPA by some innovative surgeons, such as Stein et al. (2010), using GelPort (Figure 2.6, page 12),

which, as previously mentioned, is intended for HALS. However, being originally designed for multi-port laparoscopy, it was argued whether the Da Vinci, a bulky robotic system, was suitable for SPA surgery due to the collision of its arms (Nam et al., 2011). Subsequently, Intuitive Surgical received FDA approval to market its single-site instrumentation for cholecystectomy procedures (Intuitive Surgical, 2011). Kroh et al. (2011) reported the successful results of thirteen such cases using the new Da Vinci single-site platform.

2.2 Surgeon's Needs

Da Vinci surgery is now widespread and is used by many surgeons. Although most hospitals proudly advertise the fact that they own one, "some have kept it low key" (Greenberg, 2013), being sceptical and cautious about its use. The benefits that robotics could bring to the surgical field are manifold but it is evident that a number of questions remain. Do the existing systems satisfy their users? Do surgeons suffer from bad ergonomics? And finally, has the surgical training experience improved with the use of technology? The following Sections give a brief overview of the existing literature on the subject.

2.2.1 Surgical Training and Techniques

Acquisition and mastery of basic laparoscopic skills is a prerequisite for performing complex laparoscopic operations, and thus, training surgeons in MIS procedures is becoming increasingly time-consuming (Society of American Gastrointestinal and Endoscopic Surgeons, 2009). When learning a new procedure, performance tends to improve with experience. The learning curve phase constitutes a very stressful part of a surgeon's career, while it is extensively cost inefficient and induces complications for the patients (Dankelman et al., 2010). In order to minimise this phase, the training of a new surgeon is intense and as efficient as possible, a fact stressed by Soot et al. (1999) and Tan et al. (2002), when discussing the transition from

open to laparoscopic fundoplication. The Society of American Gastrointestinal and Endoscopic Surgeons (2009) suggests that MIS training should be integrated into the surgical residency training and be done simultaneously with open surgery training, since this would provide a synergistic effect in the surgical education (Kano et al., 2010).

Apart from laparoscopic training, many surgeons undergo robotic training as well. Herron and Marohn (2007) point out the need for a simulator that could provide adequate training, equivalent to using the actual robotic system. Relevant information can also be obtained from the survey by Liu et al. (2003), which investigates and praises the usefulness of surgical teaching simulators. The survey by Duchene et al. (2006) examines to what extent surgical residents participate in R-A MIS operations. Only 38% of the respondents rated their laparoscopic training experience satisfactory, a number that did not increase even 7 years later (Furriel et al., 2013). Gobern et al. (2011) show that most frequently there is no formal curriculum in place, which limits the ability to incorporate robotic training into residency.

The use of surgical robotics could enhance and shorten the learning process: multiple big screens with better vision capabilities lead to better collaboration and communication between the surgeon and the medical staff, which also means that the trainees can learn faster. Besides, it has been shown that the mentoring console of the Da Vinci (where surgeon and resident operate on one patient simultaneously) enhances training and improves performance in complex surgical tasks (Hanl et al., 2006). The 'Red Dragon' is a simulator for training in MIS procedures which, through its manipulator and graphical interface, measures position and orientation of the tools as well as the forces and torques applied to them by the surgeon (Gunther et al., 2007). Its purpose is to objectively assess the skills of the surgeon and to study translation from a simulation environment to animal trials. Additionally, intensive training with Da Vinci using the Fundamentals of Robotic Surgery (FRS), a simulation-based training curriculum for R-A MIS analogous to the Fundamentals

of Laparoscopic Surgery (FLS) (Ragle, 2012), is very important for any resident before they feel confident to perform surgery on a patient (Macgregor et al., 2012).

2.2.2 Ergonomics

Studies have shown that surgeons frequently report problems such as neck, shoulder/arm, hand/wrist and back pain/stiffness, while suffering from mental fatigue after a series of laparoscopic procedures (Doné et al., 2004; Reyes et al., 2006). It is also mentioned that surgeons are not able to perform precise motions and that they find the instruments awkward to manipulate (Doné et al., 2004). The adjustability of the device is a significant factor, and as Berguer and Hreljac (2004) have reported, laparoscopic instrument users with smaller hand size have difficulty operating them and also experience musculoskeletal problems.

Increasingly, R-A MIS is replacing conventional laparoscopic surgery and it is essential to determine whether robotic systems are adjusted to the surgeons' needs and comfort. In the survey by Santos-Carreras et al. (2012) among 24 surgeons with R-A MIS experience, 28% complained about neck and finger discomfort, followed by 20% complaining about back pain. Generally, however, Da Vinci operations scored better than laparoscopy and open surgery regarding the surgeons' comfort during the procedure.

2.2.3 Need for Innovation

> "The operating room of the year 2030 will be a totally different environment than today. Mass screening and early diagnosis will have a major impact on the type and invasiveness of required surgical procedures."
>
> Sir Alfred Cuschieri, MD, 2000

Apart from instruments and robotic systems, the operating room also needs to be adjusted and improved (Herron and Marohn, 2007). At the moment, the Da Vinci system has entered hospitals and is hosted in the same operating rooms that had

been used even before laparoscopic procedures had been established. This suggests that the system's operating conditions are not optimally suited. Its docking and undocking procedure is long, while the volume of the robot leaves limited free space in the operating room, even leading to patient harm as previously discussed (ECRI Institute, 2014).

Instead, special operating rooms for R-A MIS procedures could be tailored according to the advantages of the robotic systems so that they offer the optimal conditions for best patient care. Al-Naami et al. (2013) anticipate improvements including more flexible robotic arms that can be pulled from the ceiling and with automatic loading and unloading of the instruments (instead of the manual procedure currently performed by the surgical assistant). Ease of use is also a very significant factor; ideally, a tele-surgical system integrated with every surgeon's computer would simplify the procedure.

For true innovation and progress, the current systems should be reconsidered and the established surgical routines challenged. The need for more articulated and efficient instruments is apparent, as is the need for more universal instruments able to perform a variety of tasks without having to change between them frequently. Mutter and Marescaux (2004) state that "the change in instrument position is the most time-demanding part of the operation".

Although this thesis is dedicated to surgical instruments that are in direct contact with the operating field and less, for example, with the robotic arms that may hold them, it is useful to consider the system and environment as a whole. More specifically regarding the use and manipulation of robotic surgical instruments, important attributes to surgeons would include dexterity that expands surgical capability, improved flexibility for further reach in the abdomen without reconfiguration, and haptic feedback (Herron and Marohn, 2007). "Research in surgical robotics should not be tethered to the surgeon-at-a-console paradigm" (Herron and Marohn, 2007) but instead could adopt modular and portable systems with 'plug and play' capabilities. Furthermore, ability to customise the system for different users could

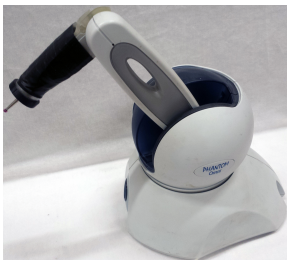

Figure 2.16: Phantom Omni with a modified tip

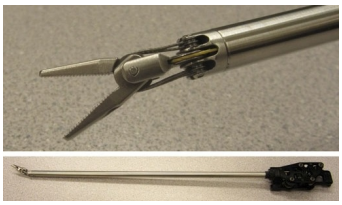

Figure 2.17: Raven II instrument (Hannaford et al. (2013), ©2013 IEEE)

contribute to good ergonomics and avoid musculoskeletal problems, as Berguer and Hreljac (2004) report.

2.3 Surgical Systems in Development

The following Sections present a review of various research robotic surgical systems. This does not aim to be exhaustive but to present examples of robotic systems intended for use in the surgical techniques mentioned previously and to highlight their main aspects. A comparison table summarising some of their features can be found on page 48.

2.3.1 Master-Slave Systems

Raven is a system similar to the Da Vinci but aimed towards academic research (Hannaford et al., 2013). The surgical manipulators have seven DOFs (Lum et al., 2009) and the surgeon is using a Phantom Omni (Geomagic, 2013) to control the position and orientation of the instrument's tip (Figure 2.16). Initially being funded by the US military for treating soldiers on the front line as soon as possible after an injury, seven systems of the 2nd generation of the robot, Raven II, were distributed to universities in the USA in order to advance the technology even more by collaboration. The instrument used for the Raven II is shown in Figure 2.17.

MiroSurge is another research master-slave platform (Thielmann et al., 2010). It includes the surgeon's console and three surgical robotic arms (MIRO) that carry two

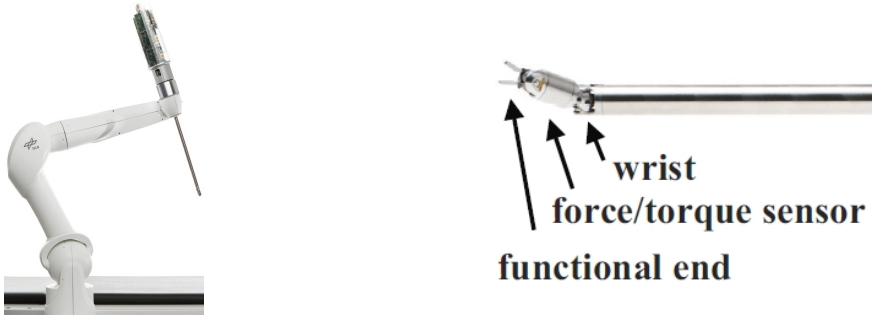

Figure 2.18: MIRO arm and MICA instrument (Thielmann et al. (2010), ©2010 IEEE)

surgical instruments (MICA) and a stereo video laparoscope (Figure 2.18). Surgeons are using an Omega7 (Figure 2.19), which, through its parallel kinematics, tracks the hand/arm movements and transfers them to the robotic arms and instruments. The MIRO arms have seven joints, each with serial kinematics resembling a human arm (shoulder, upper arm, elbow, forearm and wrist) (Hagn et al., 2010). Due to the robot's light weight (10 kg), unlike the Da Vinci, alternative setups including ceiling/wall mounting are feasible. Furthermore, the elbow joint of the MIRO arm can contribute to arm collision prevention.

Unlike the Da Vinci instruments, MICA has force feedback capabilities, using one six-DOF force/torque sensor integrated into its two-DOF wrist, as well as a gripping force sensor for its functional end-effector. The three motors that control these movements are integrated into the instrument for versatility: the tool is detachable with standalone actuation and sensing capabilities for the same platform to be used for different procedures. Issues related to cost and maintenance of such specialised instruments after multiple sterilisations are likely to arise. Although MiroSurge and Raven II look promising as alternatives to Da Vinci, their concept is similar in respect to the instrument design, which is also the concept of conventional laparoscopic instruments: long shaft with an articulated gripper at its end.

In a similar context, RobIn Heart (Figure 2.20 (a)) is a master-slave robot intended for cardiac surgery (Niewola et al., 2013). Its slave arm has one translational and three rotational DOFs and holds the tool which has two DOFs, as well as opening and closing of the tooltip. This arm is mounted on a column next to the

Figure 2.19: Omega7 haptic device (Courtesy of Force Dimension, Switzerland)

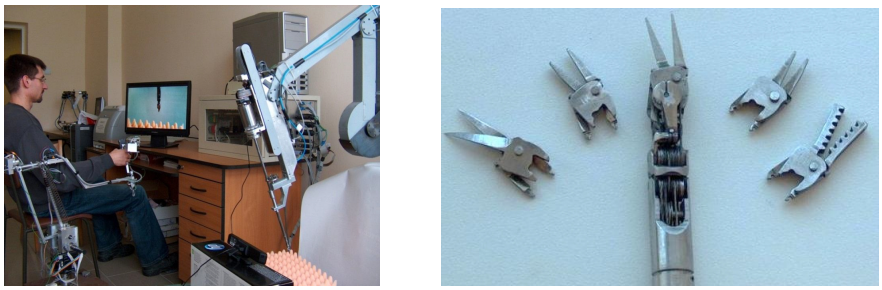

(a) (b)

Figure 2.20: Robin Heart (a) master-slave and (b) tool and tooltips (Niewola et al. (2013), ©2011-2016 by Walter de Gruyter GmbH)

surgical table, while an additional arm (one translational and three rotational DOF) is mounted on the operating table to hold the endoscope. Finally, the master manipulator has six DOFs that control the corresponding DOFs of the arm and tool as well as a capability to open and close the tooltip. The user can switch between controlling the endoscope arm and the one that holds the tool. The system supports two major innovations: *i*) the tools can have changeable tooltips (Figure 2.20 (b)), which reduces the time needed for removing the tool and attaching the new tool to the arm before re-entering the operating field (Niewola et al., 2013) and *ii*) the tools can be attached to a separate holder that allows conversion to manual MIS in the case of emergency (Nawrat and Kostka, 2014).

Arata et al. (2005) developed a master-slave system where two master arms (three rotational, three translational DOFs and opening/closing of the grasper) control two arms that hold the instruments and one that holds the endoscope. The master (desktop) arms are equipped with encoders for position tracking but also support force feedback. The developed instrument that the slave arm holds also has grasping

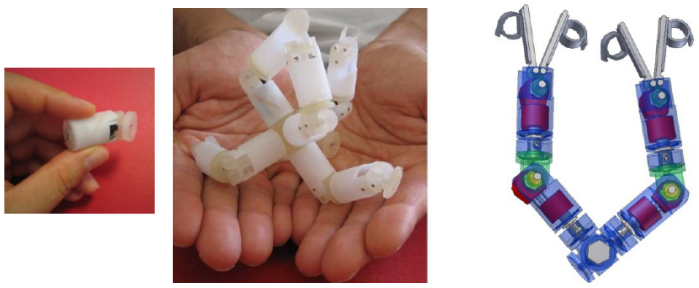

(a) (b)

Figure 2.21: ARES (a) module and assembly and (b) master device (Watanabe et al. (2010), ©2010 IEEE)

force sensing capability. However, the design of the instrument is not very different from the Da Vinci, as it is a two-DOF gripper.

A divergent approach followed by the robotic system ARES (Assembling Reconfigurable Endoluminal Surgical System) involves the patient swallowing 10-15 robotic modules which are then assembled in the stomach cavity in a planned configured topology (Watanabe et al., 2010). They propose tissue sample collecting and storing, while the camera module enables vision. The authors go on to suggest that the sample could be brought out of the body through normal excretion, which, however, could involve great technical difficulties. In order to control the robot, a master device configured to the exact specifications of the slave module is being developed (Figure 2.21 (b)).

Likewise, Sang et al. (2011) developed their own master manipulator for their system 'MicroHand A'. The slave manipulator, shown in Figure 2.22, has two arms, each having a three-DOF instrument at the tip and a third arm for the camera. Each arm has a six-DOF passive part for adjustments before surgery, and a three-DOF active part which accommodates the instruments. The overall design is similar to the Da Vinci and was developed as its alternative, specifically targeting the Chinese market (Zhang et al., 2013). In fact, the instruments have the same number of DOFs as the Da Vinci instruments (Figure 2.22).

The master manipulator that was developed is shown in Figure 2.23 (a) and is a serial robot with seven DOFs, which include position, rotation, force and grasping

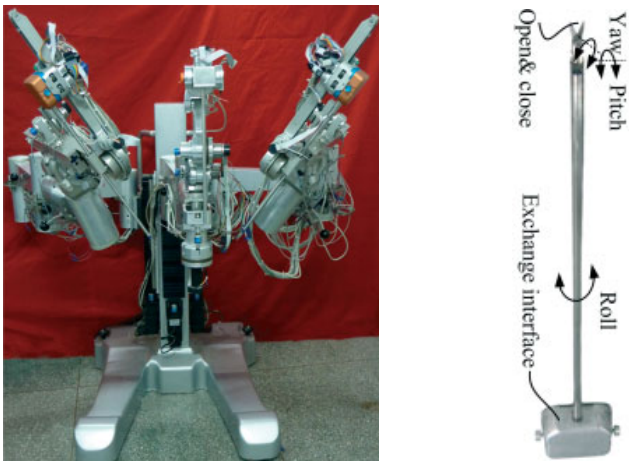

Figure 2.22: 'Microhand A' slave manipulators and 3-DOF instrument (Sang et al. (2011), ©2011 by John Wiley & Sons)

information in a similar way to the previously mentioned Phantom Omni (Figure 2.16). An alternative master manipulator for the 'MicroHand A' slave robot was developed by Zhang et al. (2013), based on the concept of a more direct manipulation of the instruments so that surgeons do not need specialised training for MIS after their open surgery training. Figure 2.23 (b) shows the knife-master and the forceps-master which are used to control the position and orientation of a surgical knife and forceps respectively. Using sensors and an electromagnetic tracking system, it allows hand motions similar to those executed in open surgery. This concept dictates manufacturing of a variety of master devices in order to control the various surgical instruments such as scissors and hooks, possibly resulting in a high-cost set. Furthermore, as the masters do not incorporate motors, force feedback to the surgeon cannot be implemented. The authors propose a safety procedure for tracking the master's position integrated into the control architecture and use of graphical feedback by augmenting the visual display in relation to the applied force as replacement to the force feedback. Experiments using the mechanical master device and the forceps-master showed that the learning curve was steeper with the latter, indicating that a direct relationship between the master and the slave can improve the efficiency of the procedure.

Direct manipulation is also demonstrated in the 'Hyper Finger', developed by

(a) (b)

Figure 2.23: 'Microhand A' (a) mechanical master and (b) forceps-master and knife-master (Sang et al. (2011); Zhang et al. (2013), ©2011,2013 by John Wiley & Sons)

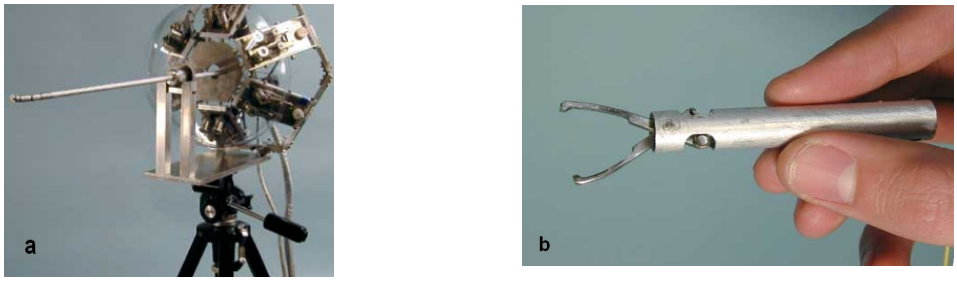

Figure 2.24: (a) Slave and (b) gripper of the 'Hyper Finger' (Ikuta et al. (2003), ©2003 IEEE)

Ikuta et al. (2003), where the slave is a miniature version (10 mm diameter) of the master (Figures 2.24 and 2.25). Each finger is tendon-driven and has multiple links with nine DOFs and a detachable gripper. Ikuta et al. (2003) have shown that one finger can sufficiently grasp and hold a porcine liver.

Finally, a different approach has been adopted by Dikaiakos et al. (2014). Although not a master-slave system, this mechatronic MIS instrument (Figure 2.26) has the same number of DOFs as the Da Vinci gripper. The design is inspired by the movement of the human eye and is controlled by antagonistic cables that allow it to have a wrist-like movement. The device is handheld by the surgeon who controls the gripper at the distal end, using the thumb-stick and button at the proximal end

Figure 2.25: Master of the 'Hyper Finger' (Ikuta et al. (2003), ©2003 IEEE)

of the shaft. It has motors incorporated into the handle, which could inhibit its use due to the added weight. Furthermore, the device has a re-configurable joint, which allows the surgeon to change the orientation of the shaft for more efficient and ergonomic access to the operating field.

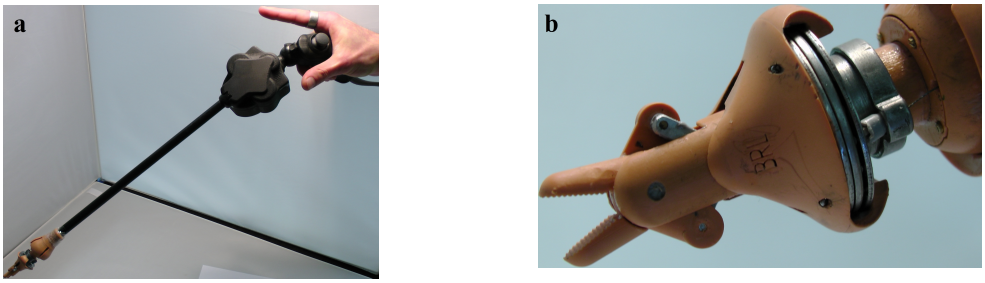

Figure 2.26: (a) Handheld mechatronic instrument and (b) its gripper (Dikaiakos et al. (2014), ©2014 IEEE)

2.3.2 SPA and NOTES Robots

Although SPA surgery (page 18) is not widely accepted as it encompasses many risks and difficulties (Zhang et al., 2012), many researchers believe that this is a step forward in surgical robotics. The SPRINT system (Single-Port lapaRoscopy bImaNual roboT) (Figure 2.27) comprises two miniature arms, each with six DOFs and a gripper. The arms are inserted through a 30 mm incision in the umbilicus (Piccigallo et al., 2010). The arms have a diameter of 23 mm and length of 142 mm and are actuated by four on-board brushless D.C. motors for the four distal DOFs (elbow and wrist) and by two external motors for the two proximal DOFs (shoulder). The authors propose that a stereoscopic camera holder and a third arm could also be inserted. A real-time control architecture is implemented using a custom environment (Sánchez et al., 2011) while the robot is controlled using an Omega7 master manipulator (Figure 2.19).

Alternative forms of the slave instrument, camera design and control are required for NOTES, since the rigid laparoscopic instruments are not suitable for this technique. The ViaCath instrument (Figure 2.28) has a flexible steerable three-DOF shaft of 16 mm diameter and 90 cm length which provides two manipulating arms

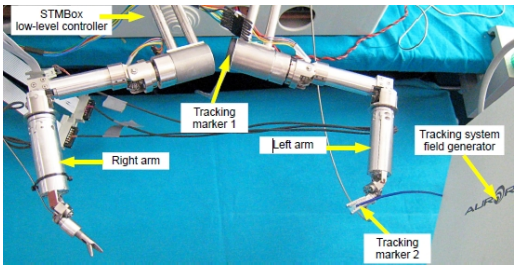

Figure 2.27: Prototype of the SPRINT slave robot (Sánchez et al. (2011), ©2011 IEEE)

with seven DOFs each, able to manoeuvre a variety of end-effectors. In addition, a camera, a light source and a suction channel are included (Abbott et al., 2007). The system was developed at EndoVia Medical which was later bought by Hansen Medical (Boston Business Journal, 2005).

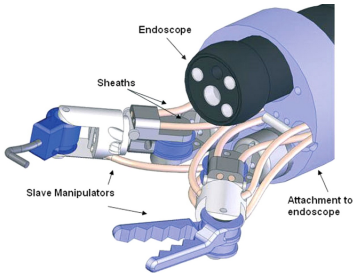

Figure 2.28: ViaCath system (reprinted from the work by Yeung and Gourlay (2012) with permission from Elsevier)

A different concept for use in SPA is proposed by Natali et al. (2012): miniature robotic arms and a camera enter the body cavity through a single entry point and are operated by external robotic arms via a trans-abdominal active magnetic linkage on the peritoneum. Following the same idea, Montellano Lopez et al. (2012) present an intra-abdominal robot which is able to carry a small camera and attach itself to the peritoneum. In contrast to the work by Natali et al. (2012), this robot does not use a magnetic field, but has adhesive surfaces made of a bio-compatible polymer nano-imprinted with a pattern inspired by geckos (tree frogs).

Continuum Surgical Robots

A very popular configuration, especially for SPA surgery and NOTES, incorporates continuum mechanisms that mimic snake movement. The previously men-

tioned 'Hyper Finger' belongs to this category (Ikuta et al., 2003). Another of these mechanisms is shown in Figure 2.29, where a flexible endoscope is illustrated. It includes two modules, each with two DOFs, while a spring backbone is responsible for the flexibility and back-drivability of the system, i.e. the actuators react to the external force, making collisions with tissue and organs safe (Yoon et al., 2010). A scaled-up version was developed as its master manipulator (Yoon and Yi, 2015).

Figure 2.29: 4-DOF flexible continuum robot (reprinted from Yoon et al. (2010) with permission from the authors

A surgical robot, called 'i-Snake', is developed and intended for NOTES using biologically inspired articulation (Shang et al., 2011). It has a serial joint architecture with five segments and seven independently actuated DOFs (two universal joints and three one-DOF joints). The robot (Figure 2.30) is mounted on a rigid shaft, while each DOF is actuated by a micromotor embedded in the corresponding segment. The surgeon is controlling the robot via a handle equipped with potentiometers, a thumb-stick and a push switch. Inside the robot, one sheath is used for the camera and power wires. The robot essentially acts as a vehicle, with another sheath used for passing surgical instruments to the operating field. During preclinical animal trials, a complete surveillance of the workspace was achieved and an endoscopic clip was delivered through the 'instrument sheath'. Tissue manipulation is limited due to the lack of triangulation (Vitiello et al., 2013), while real-time control has to deal with the non-intuitive toggling between each joint.

Ota et al. (2008) designed the CardioARM (Figure 2.31) and presented the preliminary tests obtained in animal and cadaver studies for cardiac surgery. Flexible instruments, unlike rigid-type systems, can navigate through complex tridimensional paths and a full sternotomy can be avoided. The 35 mm radius arm is composed of 50 rigid cylindrical links serially connected by three cables. The links are not

Figure 2.30: 'i-Snake' instrument (Shang et al. (2011), ©2011 IEEE)

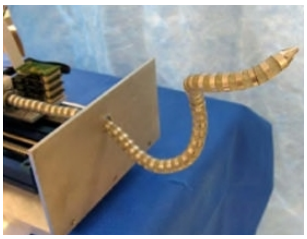

Figure 2.31: CardioARM (reprinted from Ota et al. (2008) with permission from Elsevier)

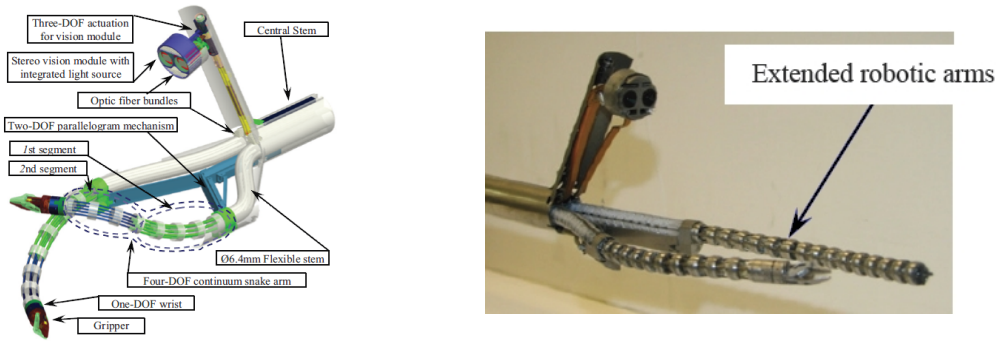

Figure 2.32: IREP robot for SPA (Xu et al. (2009); Xu and Zheng (2012), ©2009, 2012 IEEE)

controlled individually, but implement a 'follow the leader' configuration.

Xu et al. (2009) analysed a workspace of a seventeen-DOF Insertable Robotic Effector Platform (IREP) for SPA surgery, composed of two snake-like arms and a controllable stereoscopic camera (Figure 2.32). The skeleton of the arms consists of super-elastic nitinol tubes. A simulation-based comparison between three different configurations of the continuum arms concluded that the optimal comprises three-DOF continuum segments and one-DOF rotary wrist (Xu and Zheng, 2012). After the integration of IREP into a master-slave system using a Phantom Omni (Bajo et al., 2012), experiments in basic tasks from the FLS (Ragle, 2012) demonstrated good dexterity, with the exception of suture passing which proved difficult due to the limited rotation of the wrists ($\pm 60°$).

Snake-like units were also used in the development of a slave system for MIS of the upper airway by Simaan et al. (2004), carrying four super-elastic nitinol tubes. This design supported miniaturisation and removed dependency on small universal joints and wires, hence reducing the manufacturing cost. There is one central and

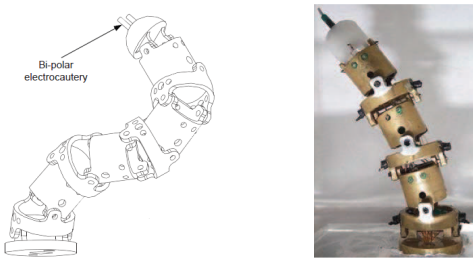

Figure 2.33: MINIR schematic and initial design (Ho et al. (2011), ©2011 IEEE)

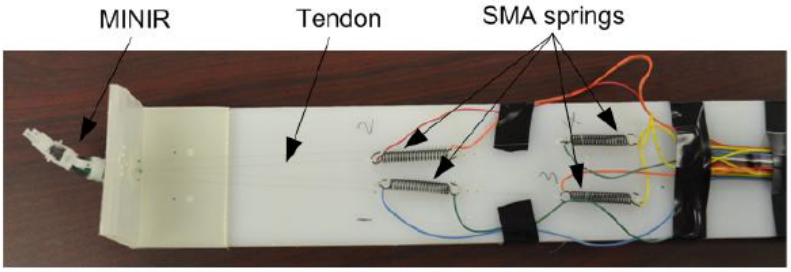

Figure 2.34: Revised layout of MINIR (Ho and Desai (2012), ©2012 IEEE)

primary backbone and three surrounding tubes for secondary support. The authors showed that the load on the central backbone can be significantly reduced because of the secondary ones, preventing the thin backbone from buckling (Simaan, 2005).

Ho et al. (2011) developed an MRI compatible Minimally Invasive Neurosurgical Intracranial Robot (MINIR) structured by several links and actuated by shape memory alloy (SMA). The robot consists of four revolute joints (Figure 2.33), each of which is connected to two antagonistic SMA wires using temperature as feedback. Using a tendon-sheath mechanism (Figure 2.34), the SMA springs were transferred outside of the main robot body, achieving $\pm 45°$ rotational range of each joint (Ho and Desai, 2012). The maximum force that each SMA spring can generate is 5.3 N at 50° C, in contrast to a maximum of 1.4 N at 75° C generated using the previous design (Ho et al., 2011).

Robots in the form of flexible needles also belong to this category, and are intended as an alternative to straight and rigid needles when it is required to reach an area by avoiding 'risk zones'. One method to achieve this is using concentric tube robots. These are composed of multiple pre-curved tubes that are nested inside their subsequent one, in such a way, that the relative rotation between them allows

the robotic sequence to change shape and move along curved paths and around obstacles. However, the number of tubes composing the body of the robot limits the number of curves in the path and consequently the range of their application (Ko and Rodriguez y Baena, 2013). Conversely, Morimoto et al. (2016)propose that concentric tube robots can not only be 3D printed but also be both patient and procedure specific while they have developed a virtual reality based environment for surgeons to design such robots 'on-the-fly' according to the patient's specific anatomy. In a different and biologically inspired approach, aiming to improve the applicability of such robots, Ko and Rodriguez y Baena (2013) proposed a steerable needle, called STING (Soft Tissue Intervention and Neurosurgical Guide). STING uses a "programmable bevel" to control its tip angle and to steer by adjusting the relative offset between its segments. An electromagnetic sensor embedded into the prototype measures position and orientation of its tip so that they two-segment needle can follow a 2D trajectory.

2.3.3 Robotic HALS

HALS was described in Section 2.1.2 as a semi-conversion from MIS to a more invasive approach. In order to exploit the advantages of this technique, Ohshima et al. (2008) have developed a three-fingered miniature hand with five DOFs (named '3f5d hand' and shown in Figure 2.35) that could carry out assistive tasks in surgery as the non-dominant hand of the surgeon. The total number of fingers is based on the assumption that two fingers are not adequate to push aside an organ, while a hand with more fingers would be too complex. Each unit of the '3f5d hand' has a diameter of 12 mm so that they can be individually inserted through a trocar and assembled together in the abdomen. The assembly process requires two free trocars and can be time consuming and difficult to achieve. The best achieved assembly time was 74 seconds after repeated practice, and during animal trials it was 6 minutes. This would prevent quick removal of the instrument in case of an emergency. While this instrument can be used as an assistive surgical retractor, more complex tasks

cannot be carried out due to the limited number of DOFs.

The '3f9d hand' is the second version of the instrument by Oshima et al. (2010) and has nine DOFs in total, three actuated DOFs for each finger. The combination of the three base joints of the fingers acts as a three-joint alternative to a wrist. It can perform a few different types of manipulation, including grasping, pushing and holding. The assembly process is simplified and faster as the connection to the actuation module happens externally (after the assembly). However, the concept of the assembly still seems problematic as it requires incisions for two trocars which are placed diametrically on the patient's abdomen. Such incisions are not common as they do not support triangulation of the instruments. The authors propose the use of one of these incisions for the trocar that will hold the assembled hand; even if this trocar in the specific location is useful for the surgeon, the second (diametrical) incision might be impractical for the surgeon to use during the operation. Furthermore, as discussed on page 11, the complexity that this assembly introduces during the instruments' insertion to the abdomen can contribute to more patient complications.

Figure 2.35: Three-fingered five-DOF hand (Ohshima et al. (2008), ©2008 IEEE)

Luo and Wang (2011) designed a three-digit gripper (Figure 2.36a) with ten DOFs which is deployed in the patient's abdomen through a single 24 mm incision using a four-bar mechanism. This hand is controlled by a master glove carrying potentiometers (Figure 2.36b), which are mapped to the joints of the instruments depending on its layout and how it is used at any given time. For this mapping, the master glove is adjusted manually by the surgeon to correspond to the new instrument kinematics.

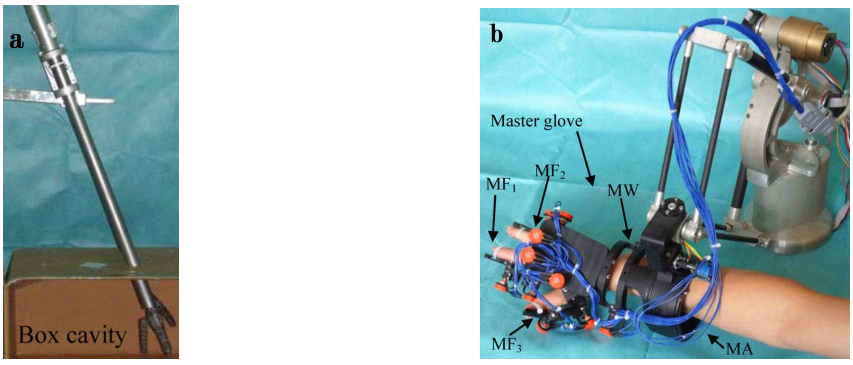

Figure 2.36: (a) Three-digit gripper and (b) master glove by Luo and Wang (2011) (©2011 IEEE)

Two vs. Three-digit Grasp in Surgery

The two robotic HALS systems mentioned use miniature hand-like instruments with three digits. The rationale behind such a design is worth considering further. Wolfe et al. (2010) categorised seven basic functions of the hand to include precision pinch, opposition pinch, key pinch, chuck grip, hook grip, span grasp, and power grasp. According to the authors, these functions, apart from power grasping, can be performed using the thumb, index and middle fingers. This is also supported by Napier (1956), stating that precision grips of small objects require only these three digits while the ring and little fingers simply provide extra stability. Furthermore, experiments with primates with opposable or pseudo-opposable thumbs showed that these three digits accounted for 86% of the observed precision grips (Costello and Fragaszy, 1988). More specifically in surgery, Zhang et al. (2006) found that the fingertips of the thumb, index and middle fingers are mainly involved in the movements of surgeons during 'soft tissue' open surgical procedures. They classified these observed motions and types of contact with tissues as precision grasping.

On the other hand, two-digit grippers, as in the Da Vinci, may be able to grasp objects firmly, however, they allow "manipulations to only be done by movements of the wrist and arm" (Iberall, 1987), limiting the surgeon's dexterity. A third digit could add stability but more importantly enhance capabilities of manipulation and palpation, as observed in open surgery. Furthermore, its functionality could be extended by carrying tools that assist e.g. in suturing (see Sections 3.2 and 6.1.1).

2.3.4 Actuation Mechanisms

Systems discussed in the previous Sections are summarised in Table 2.1 (page 48). Note that opening and closing of an end-effector has not been included in the number of DOFs and that the DOFs in continuum robots may not be independently actuated. In the actuation mechanism column, the generalised term 'cable' is used which could be substituted by tendon, wire or super-elastic NiTi depending on the specified robot.

Table 2.1 also offers a comparison between cable-driven mechanisms in robotic instruments or fingers. Cable-driven mechanisms impose coupling of the joints' motion and complicate their actuation and control, while there is also the risk of tendons breaking during an operation. Arata et al. (2005) use a rigid link mechanism with the drive unit integrated into the instrument's shaft to avoid cable breaking.

The literature also shows that there is a compromise between the size of a manipulator and the number of its independently actuated DOFs. For example, MICA's end-effector (universal joint) is controlled by a cable-pulley system via a 10 mm diameter shaft. The Da Vinci (Intuitive Surgical, Inc., 2016b) and the Raven instruments (Hannaford et al., 2013) use a cable and pulley system as well. The shaft of Da Vinci instruments is 8 mm in diameter, with a few exceptions at 5 mm. In a non-surgical context, the DLR (Deutsches Zentrum für Luft und Raumfahrt e.V. - German Aerospace Centre) Hand has fingers that have 4 actuated DOFs each using an antagonistic pair of tendons for each DOF and a total of 8 motors, while its size is comparable to a human hand (Grebenstein et al., 2011).

SMA springs are an alternative method of actuation as they have the property to contract when heated. These actuators are small enough to be integrated into the structure of a miniature robot, without posing problems of coupling between the joints. An example of such a mechanism is MINIR (Ho et al., 2011).

Robotic instruments with snake-like motion are very common in techniques such as NOTES or SPA. Especially in NOTES, such mechanisms can offer good manoeuvrability as they can navigate through complex paths, avoiding structures and

penetrating deeper into otherwise inaccessible areas. For SPA, they offer possibility for the required triangulation of the instruments without needing additional joints as for example with the SPRINT robot (Figure 2.27). On the other hand, snake-like motion differs from the human hand and digit motion and thus, can be difficult to map to a master device operated by surgeons, as was the case for i-snake (Vitiello et al., 2013).

Force Requirements

The number of DOFs and size of a robotic instrument or finger determine the magnitude of exerted force at the tip. Ability to produce adequate manipulation forces is an important attribute of a surgical instrument. Cable-driven mechanisms seem to be more successful in produced forces at the end-effector. Ho et al. (2011) were able to triple the produced force of their robot (MINIR) when adding a tendon-sheath mechanism (5.3 N).

Although coverage of this critical subject is incomplete in the literature, Madhani et al. (1998) carried out tests where surgeons pulled tissue samples with similar forces as they would do during surgery (as judged empirically by the surgeons). According to their results, average pulling forces lie in the range of 2-9 N, while the required force to hold a needle securely is approximately 48 N. Moreover, in a study with five expert level surgeons, the 'Red Dragon' (previously mentioned on page 22) measured forces of up to 30 N while suturing (Gunther et al., 2007).

To address challenges of miniaturisation and force capabilities, Raghavaiah et al. (2005) combined a motor and SMA to create a hybrid actuator of 5 mm diameter and 40 mm length. The actuator was used to actuate 10 mm long needle driver jaws, generating a gripping force of 5.5 N. Similar forces are produced by some of the reviewed systems (shown in Table 2.1).

2.3.5 Haptics

Another issue often addressed in R-A MIS is the lack of haptics for the surgeon. Haptics, generally, refers to the sense of touch; the surgeon performing a R-A MIS procedure uses a teleoperated system and hence indirectly controls the instruments. Without special measures taken, this removes valuable information regarding the force being applied by the instruments or the texture and type of tissues. Having the ability to provide this feedback to the surgeon could vastly help with tasks requiring highly dexterous manipulation of tissues within the body (Meijden and Schijven, 2009). Haptic feedback can be tactile ('feeling' of edges and shape of an object or texture) or kinaesthetic (force). As the field of surgical haptics is a very broad one and is beyond the scope of this thesis, only a brief review will follow.

Tholey and Desai (2007) presented a modular laparoscopic grasper with tridirectional force measurement capability during grasping and palpation tasks. In a similar context, Roke et al. (2012) created a deformation-based tactile feedback system and tested it for palpation of soft tissues. Their experiments demonstrated detection of objects inside the tissues with better accuracy and in less time compared to when there was only visual and kinaesthetic feedback. Haptic systems can be integrated in manipulators such as the two-finger gripper of Spiers et al. (2012), a closed chain serial manipulator that imitates the rolling motion of the thumb and index finger.

An example of visual and visual-audio (different auditory tones) feedback, as an alternative solution to kinaesthetic feedback, is the work by Tavakoli et al. (2006) and Kitagawa et al. (2005) . The signal from sensors is used to either augment the visual display by graphically representing the applied force of the instrument's tip in the height and shade of coloured bars or play a single tone when the exerted force reaches a certain magnitude. As mentioned previously, these techniques are the only possibility for haptic feedback in master devices such as the one of 'MicroHand A' (Zhang et al., 2013). Gwilliam et al. (2009) reported that any form of feedback contributes to better control and prevents unnecessarily large gripping forces. However,

visual feedback did not improve the accuracy of experienced surgeons who instead performed better with kinaesthetic feedback.

2.3.6 Master Interfaces

In the previous Sections, a few physical (as opposed to graphical) master interfaces were described. Phantom Omni (Figure 2.16) and Omega7 (Figure 2.19) are master devices with force feedback that can be used for various applications. If the instruments to be teleoperated were more complex, more complex master devices would be required. Custom made ones that fit the properties of their slave robots include the master arm of RobIn Heart (Figure 2.20 (a)), the ARES master device (Figure 2.21 (b)), the 'Microhand A' mechanical master manipulator or its forceps/knife-masters (Figures 2.23 (a) and (b), page 30) and the master of the 'Hyper Finger' (Figure 2.25, page 30).

A common property of these master devices is that their design emulates the motion of the surgeon's hands (and arms). Simorov et al. (2012) have reviewed various surgical platforms and user interfaces, including the use of arm exoskeletons to control surgical instruments, as well as data gloves with 'motion-detecting sensors' attached to the joints of the surgeon's hand. However, problems such as cost, lack in precision and durability have been overlooked (Dipietro et al., 2008). It is useful to explore hand/arm tracking not necessarily intended for surgery; specifically, user-worn hand/arm devices with an addition of a 3D vision headset for the surgeon can increase the portability of a system, improving its ergonomics further (Simorov et al., 2012).

Generally, current devices for hand motion tracking span from on-the-hand hardware, based on flexible sensor technology or rigid links with encoders for each joint (such as the master glove by Luo and Wang (2011)), to external imaging systems based on intensive image processing and often covering a limited field of view. Rigid joint mechanisms can give precise joint flexion angles but can be heavy and restrictive to the operator's hand during prolonged use.

Data gloves are typically lightweight and can be cheap to manufacture but joint resolution could be too low for surgical use as the sensors give a more generalised impression of a gesture rather than detailed joint tracking. Furthermore, such gloves lack durability, are non-adjustable and cannot suit all users (Dipietro et al., 2008). The WB-1R system by Zecca et al. (2007) can measure the movements of the head, arms and hands. It uses a fifteen-DOF custom-made data glove with flexible sensors that detect bending due to the change of resistance. The angle error in the WB-1R system can be as great as 27°, showing only intention of the user (Zecca et al., 2007). Cyberglove, on the other hand, is a commercial data glove that offers higher joint resolution with 22 flex sensors and 1° accuracy (Liarokapis et al., 2013). However, it requires calibration for each user and has a prohibitively high cost. Cyberglove supports haptic feedback only if another device, Cybergrasp, is worn at the same time by the user (CyberGlove Systems LLC, 2016). Apart from negating the major advantage of a data glove, i.e. being lightweight and comfortable, Cybergrasp has been criticised for posing difficulty with applying small forces (Peer et al., 2008).

Other low-cost sensors, such as Kinect (Microsoft, 2016) and Leapmotion (Leap Motion Inc, 2016) have been frequently used for body, arm or hand tracking. Leap Motion has sub-millimetre accuracy (Weichert et al., 2013) and has been used as a user controller for manipulating virtual bone fragments (Dagnino et al., 2015). Kinect lacks the precision for hand digit tracking but has good application in hand gesture recognition (Qian et al., 2013). Another example of optical tracking is 'Digits', a wrist-worn real time hand tracker which avoids burdening of the hand with extra load although it comprises a structure attached to the user's forearm (Kim et al., 2012). The structure accommodates a camera-based sensor for hand digit tracking and an IMU for wrist and forearm movements. The authors state that tracking wrist rotations (or when the wrist is completely straight) is problematic using this method. Limitations of such systems include occlusions resulting from overlapping fingers. Vision systems also depend on environment lighting and this can be problematic for surgical application. Finally, they are unable to support

haptic feedback without additional hardware.

2.3.7 Human and Robot Hand Mapping

In teleoperation, depending on the nature of the master-slave system, a mapping algorithm that correlates the behaviour of the master to the slave is required. The algorithm is more complex when the master and slave systems are not of a corresponding design. Some of the most common methods for kinematic mapping in the literature include *i*) joint-to-joint mapping, where there is a simple correspondence between the joints of the two systems without any transformation, *ii*) pose mapping where the pose of the master is detected among known poses and then replicated in a similar predetermined way in the slave and *iii*) point-to-point mapping where the fingertip position of the master is the input to the inverse kinematic (IK) model of the slave.

An example of pose mapping is the work by Gorce and Rezzoug (2004), where neural network algorithms were used for learning grasping gestures of multi-fingered hands. Although pose mapping is an appropriate solution for simple, easily distinguished hand postures, it could be unsuitable for precision movements required in surgical applications. This is mainly due to possible unpredictable switching between different grasps even with small changes in the master (Peer et al., 2008; Gioioso et al., 2013). Joint-to-joint mapping is mostly suitable for anthropomorphic manipulators. Even in such cases, the kinematic models of the master and slave are not typically identical and grasping gestures can fail.

When precision grasps are considered, point-to-point mapping is more suitable. Peer et al. (2008) mapped a human hand wearing Cyberglove with Cybergrasp to a three-fingered under-actuated robot hand (BarretHand[2]). Both kinematic and force mapping are attempted using a projection of the human finger workspace onto an estimated trajectory of the robot finger. Using this method, the authors state that no knowledge about the object properties or library of pre-defined grasps is required.

[2]www.barrett.com/products-hand.htm

However, not all of the workspace of the human hand could be mapped to robot motions. Furthermore, although a soft grasp could be distinguished from a strong grasp, smaller steps in force were not detected due to the difference between the robot's sensors (torque sensors in the joints) and the human hand sensing technique (force sensing at fingertips).

To address the lack of generality of the aforementioned methods, Gioioso et al. (2013) presented a procedure where human hand synergies are mapped to robotic hands with dissimilar kinematics. In this method, a 'virtual sphere' represents the minimum volume that includes a set of reference points on the fingertip of the human hand. When the human hand moves, motion of these reference points is generated resulting in motion of the virtual object (sphere) 'held' by the robot hand. Such techniques are based on neuroscience research (Santello et al., 1998) that suggests that there are very few combinations that are used in basic grasps. Although this can be true for every-day-life grasps (Gioioso et al., 2013), precision movements in surgical tasks do not necessarily adhere to such classification.

In a combination of methods, Liarokapis et al. (2013) use demonstrations of users and forward/inverse kinematics (point-to-point) for mapping the human-robot arm motion and joint-to-joint mapping for the human-robot hand. Their method, 'functional anthropomorphism', has as priority the execution of a task and subsequently optimises the motion to be more human-like.

2.4 Summary

After reviewing MIS techniques and considering the surgical requirements as well as the difficulties during resident training, it has been made clear that there is room for research and improvement. In laparoscopy, most complications occur during the positioning of the first trocar while the risk of hernia development increases with the diameter of the instruments' shaft. This risk is even greater in HALS, with additional issues regarding reduced visibility and workspace, loss of insufflation gas

and non-cosmetic surgical outcome. Although NOTES and SPA focus on producing the best cosmetic result after the surgery, these techniques pose different concerns. In NOTES, there are difficulties in closing the internal incisions and the risk of infection is greater, while SPA is time consuming and involves expensive equipment as well as bad ergonomics for the surgeon. Finally, the Da Vinci robot is a costly, bulky high-maintenance system with no haptic feedback, has a time consuming patient docking and separation procedure, and thus, its use is not endorsed by many surgeons.

Nevertheless, robotic systems can make a significant contribution to the surgical field. Further research should be conducted, to determine how challenging the training for surgeons is and how they adapt to the new robotic techniques. The relevant research projects are innovative in their approach but focus more on new surgical techniques, such as SPA or NOTES, which are not accepted by many surgeons. These techniques entail many problems and it seems that the technology to support them is not readily available.

Despite surgical instruments (both commercial and under-development) having a high degree of dexterity for manipulation of soft tissues, the surgeon still has to be thoroughly trained to use them, just like with conventional laparoscopic instruments. The present paradigm is a limited one (Herron and Marohn, 2007); the layout of the Da Vinci has to be evaluated, and improved if needed. Systems such as the 'MicroHand A' and the 'Hyper Finger' (Zhang et al., 2013; Ikuta et al., 2003), adopting a more direct manipulation method, seem promising in terms of ease of control and ameliorating the learning process. The design and concept of robotic instruments should be revised, so that their manipulation is more intuitive for the operating surgeon.

Furthermore, new teleoperation interfaces should improve surgical efficacy, so that their applicability is expanded to more complex surgical procedures. For advanced and more complex surgical operations, open techniques are used instead of R-A MIS (Novara et al., 2015). Therefore, a proposed master-slave system forMIS should attempt to close the gap between open surgery and R-A MIS techniques. It

should therefore be surgeon-centred with increased dexterity as well as easy manipulation through an intuitive user interface. With a goal to reduce operation time and using a simple process for the instruments' abdominal insertion, complication rates could also be reduced (page 11). With regard to technical specifications, the diameter of each incision should be as small as possible for minimal risk of hernia development (page 11). Finally, grasping/pulling forces for soft tissue should be in the range of 2-9 N and the needle-grasping force approximately 30 N.

Table 2.1: Summary of teleoperated surgical systems

Surgical System	Slave manipulator				Master device	Type of surgery
	DOFs	Actuation	S.D.* (mm)	Force (N)		
Da Vinci	7 (3 on the tool)	cable-driven	5	n/a	finger grips	multi-port/SPA
Zeus	6 (2 on the tool)	cable-driven	n/a	n/a	voice activated+handles	multi-port
Raven II	7 (3 on the tool)	cable-driven	10	n/a	Phantom Omni	multi-port
MiroSurge	7 (2 on the tool)	cable-driven	10	10	Omega7	multi-port
RobIn Heart	6 (2 on the tool)	cable-driven	10	n/a	6-DOF arm	multi-port cardiac
ARES	4 in two modules	motors, magnets	n/a	n/a	handles similar to slave	NOTES
MicroHand A	6 (3 on the tool)	cable-driven	8	12	desktop manipulator or forceps-master	multi-port
Hyper Finger	9	cable-driven	10	n/a	scaled-up slave	multi-port
Dikaiakos et al.	3	cable-driven	30	n/a	hand-held	multi-port
Arata et al. (2005)	6 (2 on the tool)	rigid link	10	n/a	desktop haptic arms	multi-port
SPRINT	12 (6 in each arm)	cable-driven	30	5	direct actuation	SPA
ViaCath	6	cable-driven	16	0.5	haptic console	NOTES
Yoon et al. (2010)	4	cable-driven	8	n/a	scaled-up slave	
i-snake	7 in 5 segments	micromotors	12.5	0.5	handle with thumb-stick	NOTES
CardioARM	105 (follow the leader)	cable-driven	10	n/a	2-DOF joystick	cardiac
IREP	10 (5 in each arm)	cable-driven	15	n/a	Phantom Omni	SPA
Simaan (2005)	5	cable-driven	4	1	direct actuation	throat and upper airway
MINIR	3	SMA	12.5	5.3	direct actuation	neurosurgery
3f9d hand	9 in 3 fingers (assembly needed)	cable-driven	12.7	7.3	direct actuation	Robotic HALS
Luo and Wang (2011)	10 in 3 fingers	cable-driven and 4-bar	24	n/a	glove with encoders	Robotic HALS
DLR Hand	4 in 1 finger	cable-driven	n/a**	30	not a teleoperated surgical system	

* **S.D.**: Diameter of the shaft of the tool or digit if applicable (essentially the size of the required incision)
n/a: not applicable or not available ** Similar to a human finger

Chapter 3

Concept Design and Evaluation

The preceding background research and review of the related literature has offered a good understanding of R-A surgery, the incidental technological advances and limitations. Several MIS techniques were described and their challenges were identified. This will help answer the first research question of Section 1.1 (page 3). Surgeons, however, may still be sceptical about the benefits of robotic surgical systems (Greenberg, 2013) and further investigation should be conducted to identify why this technology adoption, with all its patient benefits, is not in widespread use at the time of writing.

Close collaboration and discussions with surgeons have been instrumental in getting an insight into problems that surgeons encounter when using R-A MIS. Therefore, an initial step into this research was to conduct a survey to gather surgeons' views on surgical training and transition from open to MIS techniques. The surgeons also expressed their views on preferred surgical techniques, the ease of use of MIS systems and accompanying instrument design. Following on from the survey, a novel concept for MIS was designed based on dexterous manipulation that can potentially reduce training time for new surgeons. This concept was further discussed with surgeons in a short series of focus group meetings.

This Chapter presents the results of the survey as well as outlines the rationale of a novel user-centred MIS system. Finally, the outcome of the focus group meetings is compared with the survey results and feedback regarding the proposed system is reviewed.

The research presented in Sections 3.1, 3.2 and 3.3 is an edited version of the work published in the following conference proceedings and journal:

Tzemanaki, A., Dogramadzi, S., Pipe, T., and Melhuish, C. (2012). Towards an anthropomorphic design of minimally invasive instrumentation for soft tissue robotic surgery. In Advances in Autonomous Robotics. Springer, pages 455-456 (with permission of Springer).

Tzemanaki, A., Walters, P., Pipe, A. G., Melhuish, C., and Dogramadzi, S. (2014). An anthropomorphic design for a minimally invasive surgical system based on a survey of surgical technologies, techniques and training. The International Journal of Medical Robotics and Computer Assisted Surgery, 10(3):368-378.

3.1 Surgeons' Survey

The survey, in the form of questionnaires, was designed to establish current experiences of surgeons and explore advantages and limitations in current surgical techniques. Based on real needs of MIS, the ultimate goal was to define a novel R-A MIS concept. Qualitative and quantitative (statistical) data were used to establish sufficient requirements.

3.1.1 Survey Preparation

The questionnaire comprised a selection of both 'open-ended' and 'closed-ended' questions to elicit information including the following:

- Duration of laparoscopic/robotic training
- Laparoscopic/robotic training complexity/difficulty
- Difficulty in adjusting from open surgery to MIS
- Satisfaction with the cost/performance of the existing systems
- Willingness to adapt to new methods/instruments
- Preference of surgical techniques

- Posture and ergonomic issues
- Preferences in surgeon-system interfaces

Two methods were used for extracting information with the questionnaire: *i*) hand it directly to the participants and allow two weeks for response (local hospitals) and *ii*) send the web link of an electronic version to the surgeons (contacted via personal email or via the medical centre they were affiliated with). In some cases, questionnaires were translated into the user's language before being sent.

Eleven questionnaires were first sent to a target group as a pilot to ensure that the questions were not misinterpreted. No problems were encountered amongst seven collected responses, and hence, the survey moved to the main phase. According to the respondents of the pilot phase, the questionnaire took between 5 and 20 minutes to complete.

As suggested by Boynton and Greenhalgh (2004); Boynton (2004); Walonick (2010), the questionnaire started with the most important questions and ended with demographic and personal details of the user. Different types of closed-ended questions, such as multiple choice, Likert-scale and rating scale formats were used in order to make the survey more interesting to the participants.

Population Sample

Out of approximately 90 questionnaires that were sent, 35 surgeons responded. Despite being a limited sample, the responses were considered sufficient for exploring the topics in question and defining requirements.

The respondents were surgeons from the UK (16), Spain (15), France (2), Japan (1) and USA (1), 35-64 years old, of both genders (the ratio of women to men being 1:4) and experience in at least one MIS technique. 91% had more than six years of experience in open and 77% had more than six years using MIS (this included both laparoscopy and R-A MIS). 12 respondents had never performed a R-A MIS operation on a patient, although most of them had limited R-A MIS experience. Their surgical specialities included general surgery, urology, gynaecology, digestive

system and bariatric surgery. Their level of seniority in open and MIS surgery, as they would personally rate themselves, is shown in Figure 3.1. The questionnaire can be found in Appendix I.

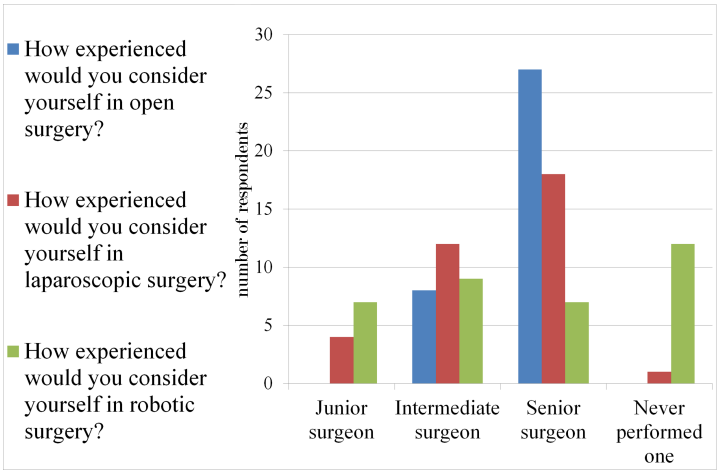

Figure 3.1: Experience of the respondents in surgical techniques

3.1.2 Surgical Systems

In one of the questions, the respondents were asked to list the main benefits (Figure 3.2) of the Da Vinci Surgical System. Their answers praised it for the 3D vision (mentioned by 43% of the respondents), articulation of instruments (31%), intuitive manipulation (28%) and better precision (23%) compared with conventional laparoscopy. Regarding the cost-performance balance of the Da Vinci system, more than 45% responded that the system is too expensive to buy, 40% thought that it is expensive but worth buying, while no respondent believed that the price is fair. Besides its high cost, respondents mentioned the size of the robot, the long docking process (preparation and installation of the robot near the patient) and possible equipment failures as shortcomings.

3.1.3 Surgical Training and Techniques

Questions related to SPA surgery showed that 32 out of 35 surgeons prefer multi-port to SPA. Their responses regarding the benefits of SPA (compared to multi-port) in-

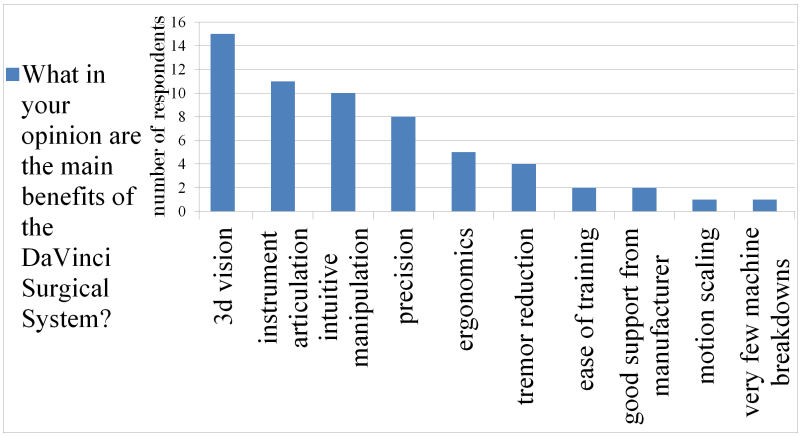

Figure 3.2: Main benefits the Da Vinci Surgical System

cluded mainly 'more cosmetic results' (21 surgeons) and 'less incisions to be healed' (6 surgeons), while two respondents considered it to have no benefits. The drawbacks included difficult operation of instruments (22 surgeons), increased duration of operation (6 surgeons), limited movements and poor dexterity (5 surgeons), poor ergonomics (4 surgeons) and increased risk of hernia development (4 surgeons), the latter being a fact also discussed by Zhang et al. (2012).

When asked how complex they considered their laparoscopic surgery training to be (Figure 3.3), 25 surgeons (out of the 34 that had such training - 73.5%) responded with 'very complex' or 'complex' opposed to only 9 surgeons believing that it is 'not so complex' or 'simple'. The numbers regarding R-A surgery were 15 (out of 28 - 53.5%) and 13 surgeons respectively. This shows that training for R-A surgery is generally considered simpler.

However, all but 1 respondent had previously undergone training for laparoscopy, which possibly affected their answers since they trained in R-A MIS after being already accustomed to the basic concept of MIS. Anticipating this, the issue of transition from one surgical technique to another needed to be discussed (Figure 3.3). Although R-A MIS techniques differ from the ones used in laparoscopy, only 3 participants found the transition from conventional to R-A MIS to be difficult. In addition, surgeons seemed to be divided into two categories: those who had experience in basic or advanced laparoscopy and then moved on to do robotic training, and

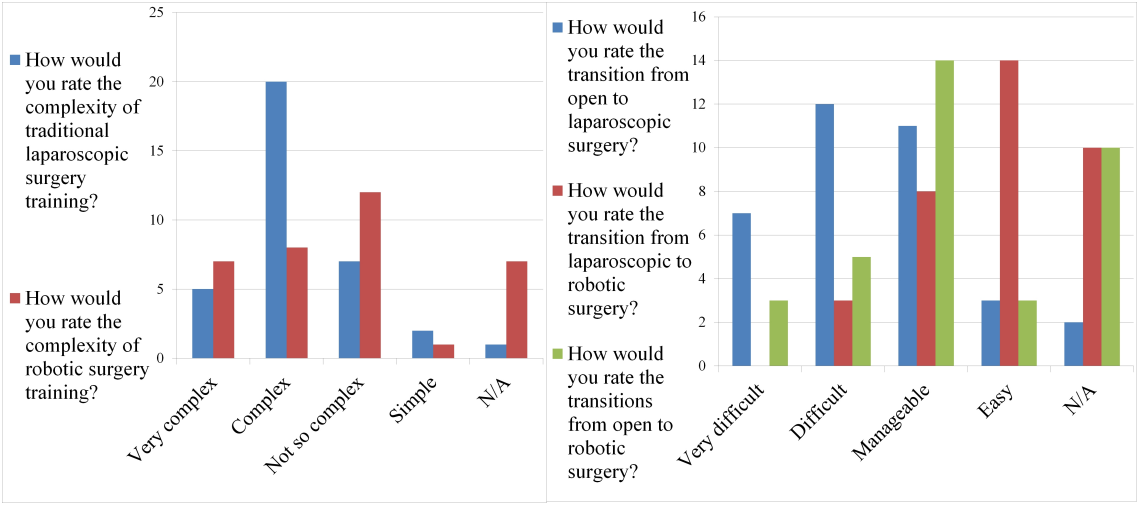

Figure 3.3: Surgical training and transitions between surgical techniques

those who were trained directly in R-A surgery after completing their open surgery training. After being trained in open surgery, about 56% of the respondents found it 'very difficult' or 'difficult' to get adjusted to laparoscopy, in contrast to only 29% having trouble to adjust from open to R-A surgery.

3.1.4 Ergonomics in R-A Surgery

Figure 3.4 presents the data concerning the surgeons' satisfaction with their posture during surgery. Despite the fact that 25 surgeons stated being 'very happy' or 'happy' with their posture during laparoscopy, 21 respondents mentioned preferring a seating position, while only 3 favoured standing. This could be an indication of eagerness to change or try different techniques, instead of settling for what their hospital has to offer.

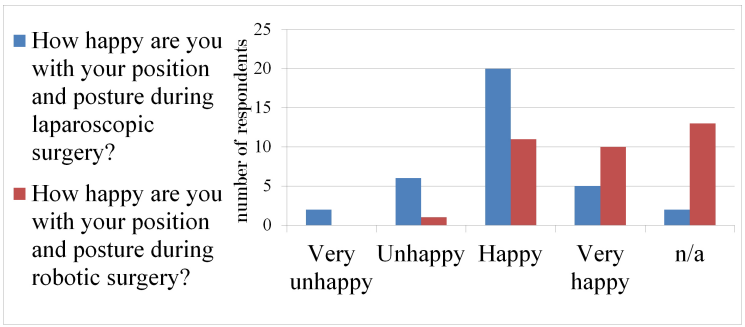

Figure 3.4: Posture during MIS

Subsequently, a rating scale was used to determine how willing they are to try new instruments. This was distinguished into two categories: *i*) those that do not change their routine during MIS and *ii*) those that would suggest adapting to new methods that may change their routine. Results showed that in both cases they were willing to try new instruments with 32 surgeons answering 'I am very happy to try' in the first case and 28 surgeons willing to adapt to new routines.

3.1.5 Main Ideas

All of the respondents knew of the Da Vinci and half of them were aware of the Zeus system as well. With Da Vinci being the only commercial surgical system in use, R-A MIS was understood specifically as Da Vinci surgery. The results of the survey agree with Baik (2008) and the report by the ECRI Institute (2014) regarding the shortcomings of the Da Vinci (e.g. long docking process and possible equipment failures).

The results also agree with the FDA survey (Center for Devices and Radiological Health et al., 2013), as the respondents found the transition to R-A MIS after laparoscopy training simple. In addition, not all surgeons performing R-A surgery have experience in laparoscopic techniques. If, in fact, it is not necessary to be trained in laparoscopy before using robotic systems, a question to be asked is, why do robotic instruments have to resemble laparoscopic instruments? "Are they merely an adjunct to manual MIS?" (Marcus et al., 2013)

It is, therefore, necessary to go beyond the incremental results of the current robotic methods and adopt more progressive approaches. The suggestion that a new concept of instruments for R-A MIS could separate itself from the design of existing laparoscopic tools was well received by the respondents. Manipulating tissue with laparoscopic instruments (e.g. forceps) is more difficult than using the hands; organs and tissue slipping from the grasp of the instruments is common, and perhaps this indicates that the design of laparoscopic graspers is not as effective as it could be (Heijnsdijk et al., 2002). At the same time, surgeons are not satisfied with the level

of dexterity and ergonomics of current instruments available for laparoscopy or R-A MIS (also reported by Doné et al. (2004)).

Finally, an important finding of this exploration was that SPA is seen in a negative way by most surgeons, as being unnecessary or even having no benefits at all. Zhang et al. (2012) suggest that this is due to the many risks and difficulties entailed in such a procedure.

3.2 Concept of an Anthropomorphic MIS System

Following on from the completion of the survey and towards answering the second research question (page 3), a concept for MIS robotic instruments was developed.

Multi-port MIS and HALS are the starting points of this research. The overall system layout is similar to the master-slave system of the Da Vinci system and consists of two basic subsystems: the instruments and the surgeon's interface. Three incisions are needed: one for the camera and two for the instruments. Each instrument carries an articulated three-digit robotic mechanism that represents and can imitate the movements of the surgeon's thumb, index and middle finger. Therefore, one digit has five DOFs ('thumb' of the instrument) while the other two have four DOFs (more on the kinematics of the instrument in relation to the human hand in Sections 4.1 and 6.1). The three-digit concept, as discussed on page 38, is based on the fact that the thumb, index and middle fingers are responsible for precision grips (Napier, 1956). The hand-like instrument design approach is illustrated in Figure 3.5.

In abdominal surgery, the insufflation of the abdomen allows for safe unfolding of the instruments into an open position. At the same time, the desired maximum diameter is 15-20 mm so that risk of hernia is minimised (page 11). Therefore, the thumb in the multi-joint anthropomorphic structure is foldable to minimise the total diameter of the instrument (Figure 3.6) during insertion and retraction.

Furthermore, each digit could carry a different tool: a combination of two digits

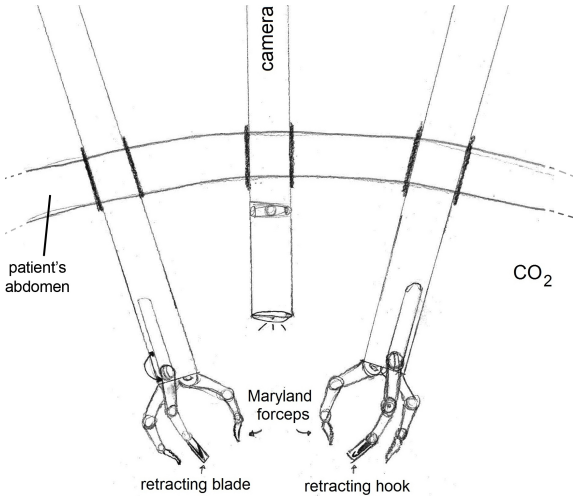

Figure 3.5: Proposed instruments with camera inside the abdomen

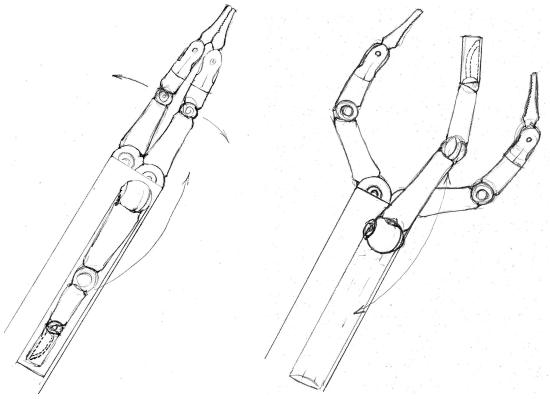

Figure 3.6: Folded – extended position

could be used as grasping forceps, while the third could be used for extra support. Alternatively, the third digit could also carry a retractable blade or other knot-tying assisting gripper. This leads to a surgical concept where one surgeon could be able to use two tools with one hand, reducing the need for a surgical assistant: for example, one hand could create traction with the thumb and middle finger (equivalent of grasping forceps) and operating a blade with the index finger while the other could operate Maryland forceps - using electrocautery and an irrigation tool.

The anthropomorphic system design aims to *i*) reduce the 'cognitive gap' between the way that instruments are manipulated and the surgeon's natural hand movements (Figure 3.7), *ii*) offer increased dexterity and workspace reachability and *iii*) allow more demanding manoeuvres to be done. Through these properties, the

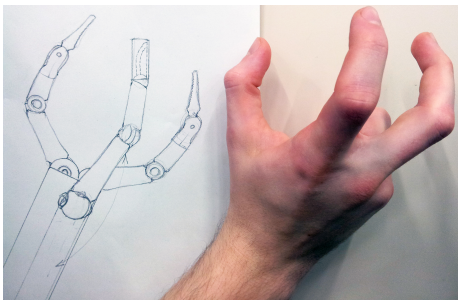

Figure 3.7: Comparison of concept drawing with a hand (the 'index' of the instruments has a retractable blade inside its last link)

system will enable R-A MIS to be adopted in more complex procedures that include sensitive structures and where manipulation is difficult due to limited workspace (Novara et al. (2015), see page 15). Therefore, the way that the instruments are controlled is very important. The manipulation of the instruments affects not only their efficacy, but also the ergonomics and the learning process for the surgeon. For this reason, the master device needs to be lightweight, adjustable and have a provision for sensing movement of the surgeon's digit joints in order to translate them to movements in the hand-like instrument's joints.

As discussed in Section 2.3.6, hand exoskeletons tend to be bulky and heavy when they are aimed at actuation of hands or arms, e.g. for hand rehabilitation from a stroke (Wege and Hommel, 2005; Burton et al., 2011). By removing the motors, the design can be simplified. The design of the master device that teleoperates the proposed anthropomorphic instruments is presented in Chapter 4. The final design is an adjustable sensory exoskeleton with lightweight sensors.

The proposed surgical system has been named μ`Angelo`. The relationship between its components in comparison with the Da Vinci surgical robot is shown in Figure 3.8. The Da Vinci has a fixed master, whereas the μ`Angelo` exoskeleton is portable. Furthermore, the slave instruments of the Da Vinci have limited DOFs and a design that requires long training to get accustomed to. The μ`Angelo` slave instrument aims at increased dexterity with DOFs and a user-centred design.

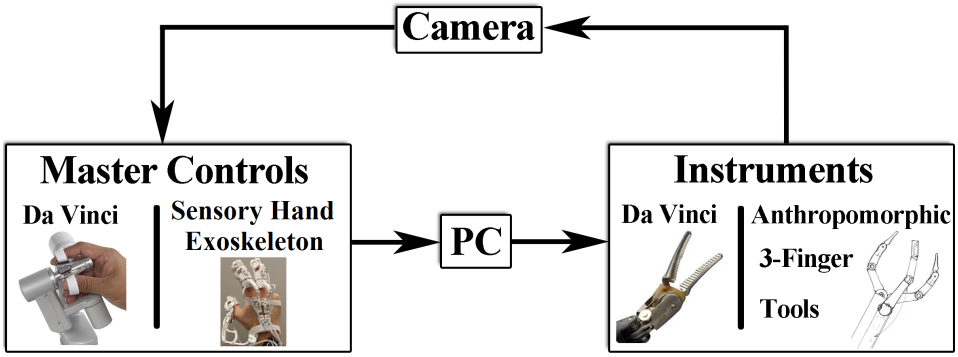

Figure 3.8: System schematic and comparison with the Da Vinci main components

3.3 Focus Group Analysis

The anthropomorphic master-slave concept was evaluated by conducting two focus group meetings with surgeons. The first one comprised one moderator and four surgical registrars from the Bristol Urological Institute, UK and lasted 1.5 hours. The second focus group meeting, lasting 25 minutes, included two senior surgeons (UK and Italy) and two moderators, one of which was a surgeon (UK).

Each session was audio/video recorded, then transcribed and processed using content analysis, i.e. deriving information from the transcripts using techniques for data coding such as identifying 'signed vehicles' and their frequency of occurrence to locate important structures and provide a meaningful reading (Krippendorff, 2004). 'Signed vehicles' can be a set of words or even gestures and facial expressions that carry information that should not be overlooked. More specifically, deductive category application was initially used to code the transcript with predetermined themes related to the concepts that were read (Mayring, 2000). Following the first method, inductive category development was applied to code ideas not previously identified, but deduced in a step-by-step manner (Mayring, 2000).

The participants were given three concepts to read (the material presented to them can be found in Appendix I). The first concept described a surgeon claiming that a patient should have open surgery as a treatment, while in the second concept a different surgeon counter-proposed that the same patient should choose R-A surgery instead. The major themes emerging from these two concepts (Focus Group 1) were:

- advantages of open compared to R-A surgery
- advantages of R-A surgery compared to conventional laparoscopy
- differences between learning curve techniques of all three surgical techniques

The third concept (Focus Groups 1 and 2) described in detail the design of the anthropomorphic master-slave system (Section 3.2) and the emerging themes included:

- value of hand-like movement for surgical tasks
- potential applications and how it would be used in MIS
- suggestions/alterations of the design

The questions for each of the three concepts were:

i. What do you think is good about the concept?

ii. What do you think is bad about the concept?

iii. What do you think could be done differently?

The following Sections represent the analysis of the discussions between the participating surgeons.

3.3.1 R-A MIS vs. Open Surgery

The participants claimed that R-A MIS surgery takes longer than the open equivalent. With R-A MIS, the surgeon has difficulty replicating open surgery techniques, ascribing this to *i*) the limited field of view, also reported by Paul et al. (2013), *ii*) a range of movements of the surgical robot ("its arms often clash with each other") and *iii*) its big volume. In addition, the lack of tactile feedback during R-A surgery was considered a big issue. This was reported as: "you cannot use your fingers to do what the fingers do".

With respect to complex procedures, the participating surgeons said that they would generally prefer using the open technique. This was attributed to what is considered as the 'gold standard' for a surgical procedure at a given time, which they connected directly to the statistical success of a certain technique and indirectly to its cost. "If R-A MIS was less expensive, conventional laparoscopy could become a thing of the past". Despite R-A MIS requiring a big investment, as hospitals have to also disburse funds for disposable robotic tools, medical and economic benefits of the system are not clearly proven yet, with no randomised trials comparing the Da Vinci surgery to other MIS techniques (Paul et al., 2013). Furthermore, surgeons training on R-A MIS start with simple procedures: according to Al-Naami et al. (2013), cholecystectomy is the most suitable procedure for beginners.

In favour of R-A surgery, reduced pain and blood loss, quicker recovery and better cosmetic results were mentioned.

3.3.2 R-A MIS vs. Conventional Laparoscopy

The main benefits of R-A MIS compared to conventional MIS were narrowed down to the 3D vision, which was emphasised as an asset that foregrounds R-A surgery. The next important benefit accounts for improved ergonomics. Conventional MIS is often considered a more tedious and physically demanding process (e.g. for prostatectomy) as the surgeon has an unnatural upper body posture for often more than three hours.

R-A MIS was also considered to be more intuitive and straightforward to familiarise with than conventional MIS. High instrument articulation, flexible movement, reduced blood loss, less post-operative required analgesia and quicker recovery were all considered to be advantages of R-A MIS. The fulcrum effect, being eliminated in R-A MIS, was mentioned as a downfall of conventional MIS.

3.3.3 Learning Curve

It has been noted in the literature that the learning process for MIS is longer than that for open surgery (Duchene et al., 2006; Gobern et al., 2011; Furriel et al., 2013)

and this agreed with the participants' experience. They believed that happened because their training began with open surgery and they were exposed to MIS techniques only much later in their careers. The participants also associated this with the 'gold standard' and the way surgery has evolved over the years. They stated that they used MIS techniques only for simple procedures initially (as also mentioned by the Society of American Gastrointestinal and Endoscopic Surgeons (2009)). They believed that with wider acceptance of MIS in simple procedures, the technique would spread to more complex ones.

When comparing conventional with R-A MIS, however, the learning curve of the former was viewed as being much longer than the latter. This was attributed to better ergonomics, ease of instrument control and enhanced vision during R-A surgery.

3.3.4 Feedback for the Anthropomorphic Concept

Table 3.1 summarises the main points of the discussion regarding the proposed concept of anthropomorphic instruments and master controls for R-A MIS (Section 3.2). The participants supported the hand-like instrument concept by describing it as an extension of their fingers with added versatility and attributes that make it possible to perform tasks that they cannot do using just their hands. Apart from noting that tactile feedback would be very important, they commented more specifically on the actual movement of the instrument. They welcomed the idea of an instrument that behaves exactly like their hands and thought that its manipulation would be easy. In addition, the ability to work symmetrically using both of their hands in the same way as well as to perform more anthropomorphic grasps would help reproduce the movements they use during open surgery.

When considering potential uses of such an instrument and its advantages over the existing ones, the surgeons mentioned the ability to perform more actions using a single hand. Figure 3.9 shows four types of manipulations which occur during surgery, as observed by Ohshima et al. (2008). Apart from being able to perform

Table 3.1: Focus group feedback summary

Hand-like movement	Potential usage	Suggestions/modifications
Behaves the same as your hand	More actions using one hand	Scissors preferred to a blade
Natural movement of manipulation	As a retractor	Integration of irrigation system
Grasping without pinching/traumatising	As both grasper and needle holder	Integration of a hook
Ability to work symmetrically	Traction using 2 digits, cutting with the 3rd	Tips should be strong enough to hold a needle
Ability to follow the natural curve of an organ	Bowel surgery (large diameter object grasping)	
Extension of the fingers with added versatility	Ability to use all links or just tips	
Reproduction of movements during open surgery	Smoother grasping (e.g. ureter)	
Advantages of the hand plus tips able to perform tasks the hand cannot do	Liver surgery, cholecystectomy (retraction with one hand, surgery with the other)	

these movements, the participants noted that surgeons would potentially use their thumb and middle finger for traction (Figure 3.9 d) and the third (index finger) to dissect tissue (if it carried a blade or scissors), while the other hand (three more digits) could be used as a retractor. This would minimise the need for an assistant, as for example in the case of cholecystectomy, where the assistant needs to retract the liver while the surgeon is using both hands for traction and dissection of gall bladder.

Furthermore, the instrument's digits could support dual grasping. In one configuration (digit-mode) grasping would be performed using all digit links in a similar way that the human hand grasps an object. The digits would then wrap around the contour of the organ or tissue using all available DOFs as shown in Figure 3.9a, especially if it is of a large diameter (e.g. in bowel surgery) and without traumatising it (e.g. sensitive structures such as the ureter or liver). In the second configuration (forceps-mode), two digits (thumb and index) would be used with all links but the last (end-effector) joined together to yield a more conventional grasper with strong tips, for example for needle-holding (similar type of grasp as in Figure 3.9 c).

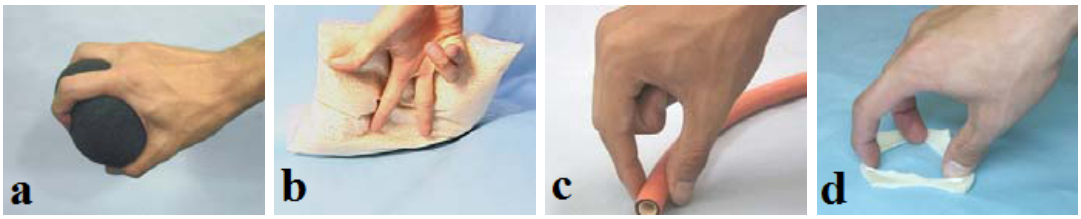

Figure 3.9: Manipulations performed during surgery (©2008 IEEE)

The integration of a blade inside one of the digits was not popular among the participants. Instead, scissors were preferred, while the integration of a hook or irrigation system that comes out with a push button (or foot pedal) seemed appealing. The discussion on potential tools for the fingertips of each instrument led to the concept of instruments with interchangeable tips. Such a feature would offer added flexibility to the surgeon as well as reduce the time-consuming changing of instruments. There could be two types of possible fingertips:

- Interchangeable ones, fitting over the digit's last link: *i*) single surfaced, e.g. hook, scalpel, which are carried by one digit and *ii*) double surfaced, e.g. graspers, needle holders, clamps etc., which require two digits (middle finger and thumb) in order to form the tool.

- Permanent ones that have an intricate mechanism included inside the digit. For example, irrigation requires a tube inside the digit and shaft, while scissors involve two surfaces on one digit (Figure 3.10) as well as an external button in the master device for the surgeon to control opening/closing.

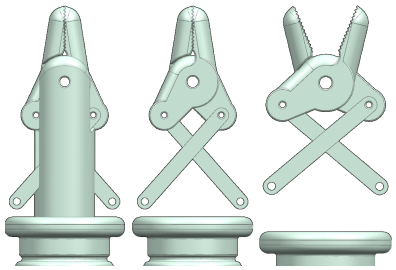

Figure 3.10: Example of scissors on a digit's last link (Dikaiakos et al. (2014), ©2014 IEEE)

3.4 Summary

The survey presented in Section 3.1 helped to define inadequacies of the existing systems and consequently form a better understanding of how they could be improved. The analysis emerging from the first focus group meeting confirmed the preceding

results from the survey regarding the cost as well as the benefits of the Da Vinci Surgical System, which mainly regarded its vision capabilities and ergonomics. Despite this, the ergonomics of the Da Vinci are still not comparable to those of conventional open surgery, in which there is a wider range of possible instrument movements.

The chosen design (Section 3.2) aims to combine the best aspects of the current surgical approaches (open, laparoscopy, HALS and R-A MIS). It differs from approaches in use at the moment as it includes an opposable thumb, which the surgeon could use to manipulate tissues and organs as in open surgery. By applying such techniques and adopting ergonomics of open surgery, use of R-A MIS could be extended to more complex procedures.

In addition, beyond being simple miniature hand replicas, each digit of the instruments could be equipped with a different tip. For example, one of the instruments could have two tips that, when joined together, form a grasper, while the third digit carries a set of scissors (as suggested in the focus groups). The other instrument could have two tips that form a needle driver and one for irrigation. This way, two hand-like instruments would be equivalent to having four different surgical tools being operated by one person at the same time. Furthermore, as discussed in the focus groups, the ability to actuate each joint of the digits provides surgeons with the option of using the instrument's digits as their own for manipulation and grasping of larger surfaces or using them as normal miniature forceps by collapsing all links but the last together.

Therefore, the concept design meets the requirements arising from the survey such as the need to improve articulation and ergonomics. Justified by the survey, the proposed design focuses on the concept of multi-port MIS (32 out of 35 surgeons answered that they prefer multi-port to SPA). Furthermore, the feedback from the surgeons during the focus group meetings was positive, supporting the intuitiveness of the concept. On reflection of the feedback regarding the instruments (summarised in Table 3.1), strong grasping with the fingertips needs to be addressed, while the concept of having interchangeable tips on the digits of the instruments should be

explored.

Finally, for an anthropomorphic based surgical end-effector, the most intuitive interface for surgeons to use is one that fits around their hand and allows control of the instrument as if it is simply an extension of their own body. The user-interface must simplify teleoperation, while surgeons can choose their preferred body posture. Therefore, the master controls (Figure 3.8, page 59) must be lightweight, adjustable and allow for unrestricted motion.

Chapter 4

Master manipulator

The survey and focus groups that were presented in the previous Chapter agree with the literature review (Sections 2.2.2 and 3.3.1) in that although surgeons experience better ergonomics in R-A MIS compared to conventional MIS, there is still room for improvement, especially when compared to the ergonomics of open surgery. Reported impacts on their health (Santos-Carreras et al., 2012) can also affect their efficacy and competence, which directly affects patient outcomes.

In order to control anthropomorphic instruments such as the ones outlined in Section 3.2 and to allow surgeons to execute hand movements similar to those of everyday life, a system for hand and digit motion capturing is required. Hand motion capturing systems are discussed in Section 2.3.6 but their inherent limitations render them unsuitable for the surgical environment. Bad ergonomics (heavy and bulky mechanisms) and lack of required precision are the main limitation. At the same time, vision based systems suffer from occlusions between fingers and depend on lighting conditions, while integration with haptics would need a separate complementary system.

Exploring what constitutes a suitable master manipulator is carried out in this chapter through a brief study of the human hand. This has contributed to the understanding of hand kinematics and required motions that a surgical master would need to follow. In order to identify requirements for an ergonomic and efficient design in more detail, a commercial data-glove was initially used to capture hand motion. Finally, the design of the master developed for the μ`Angelo` system is presented. The prototypes of the master described in this chapter focus on the tracking of the hand digits' position, while inclusion of haptics is only catered for and will be

implemented in future work.

The research presented in Sections 4.1, 4.3.1 and 4.3.2 is an edited version of the work published in the following conference proceedings:

Tzemanaki, A., Dogramadzi, S., Pipe, T., and Melhuish, C. (2012). Towards an anthropomorphic design of minimally invasive instrumentation for soft tissue robotic surgery. In Advances in Autonomous Robotics. Springer, pages 455-456 (with permission from Springer).

Tzemanaki, A., Gao, X., Pipe, A. G., Melhuish, C., and Dogramadzi, S.(2013). Hand exoskeleton for remote control of minimally invasive surgical anthropomorphic instrumentation. In Yang, G.-Z. and Darzi, A., eds., The 6th Hamlyn Symposium on Medical Robotics. Imperial College London, pages 81-82.

Tzemanaki, A., Burton, T. M., Gillatt, D., Melhuish, C., Persad, R., Pipe, A. G., and Dogramadzi, S. (2014). μAngelo: A novel minimally invasive surgical system based on an anthropomorphic design. In 2014 5th IEEE RAS EMBS International Conference on Biomedical Robotics and Biomechatronics, pages 369-374 (©2014 IEEE).

4.1 Joints of the Human Hand

Examining the joints of the human hand and constructing a kinematic model is instrumental in understanding the specifics of its movement. Figure 4.1 depicts the joints of the fingers and the thumb. The proximal interphalangeal (PIP) and distal interphalangeal (DIP) joints of the fingers are hinge joints capable of only flexion and extension (one DOF each). The metacarpophalangeal (MCP) joints at the base of the index and middle finger, however, are saddle joints, and hence capable of abduction and adduction as well (two DOFs). The thumb can also be modelled by having two 1-DOF (interphalangeal-IP and MCP) and one 3-DOF (Carpometacarpal-CMC) joints. Although some authors consider the base joint of the thumb (CMC) to have two DOFs (Weghe et al., 2004; Cerveri et al., 2007), there is a considerable rotation

at the base, even when the axial rotation (pronation/supination of the thumb) is constrained (Buchholz and Armstrong, 1992).

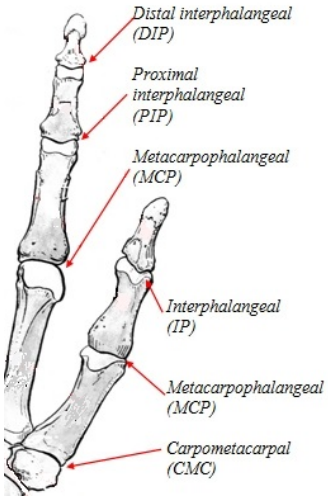

Figure 4.1: Joints of the human hand digits (sydneyhandsurgeryclinic.com)

Using a different model, the hand can be represented by a rigid linkage system incorporating 22+3 DOFs (three added DOFs for the wrist). This model considers the MCP and the CMC joints of the thumb having two and three DOFs respectively, which means six DOFs in total for the thumb (Yang et al., 2007; Choi, 2008).

Dragulescu et al. (2007) also consider four DOFs for the fingers and three DOFs for the thumb, adding three DOFs for the wrist. Furthermore, Cobos et al. (2008) suggest that each of the index, middle, ring and little fingers is defined by five DOFs and four links, while the thumb is defined by four DOFs and three links.

The model that was adopted in this research (regarding the thumb, index and middle finger) is summarised in Table 4.1. Each digit has three links and the model has 13 DOFs in total. This was considered adequate for all functional moves and was chosen for its relatively low degree of complexity.

Kinematic Model

Figure 4.2 illustrates the model of the thumb and index finger (the middle finger is similar to the index) as described in Table 4.1. The Denavit-Hartenberg parameters of the hand model are given in Table 4.2. The lengths of the digit links are denoted

Table 4.1: Model of the human digits

Digits	Type of joint	DOFs
Index and middle	distal interphalangeal (DIP)	1
	proximal interphalangeal (PIP)	1
	metacarpophalangeal (MCP)	2
Thumb	interphalangeal (IP)	1
	metacarpophalangeal (MCP)	1
	Carpometacarpal (CMC)	3

ℓ_t and ℓ_i for the thumb and index respectively and $\{t_j\}$ is the frame of the fingertip. The base of the thumb was used as the reference frame. The virtual model of the three digits is shown in Figure 4.3, while a detailed forward kinematics (FK) model is given in Appendix II.

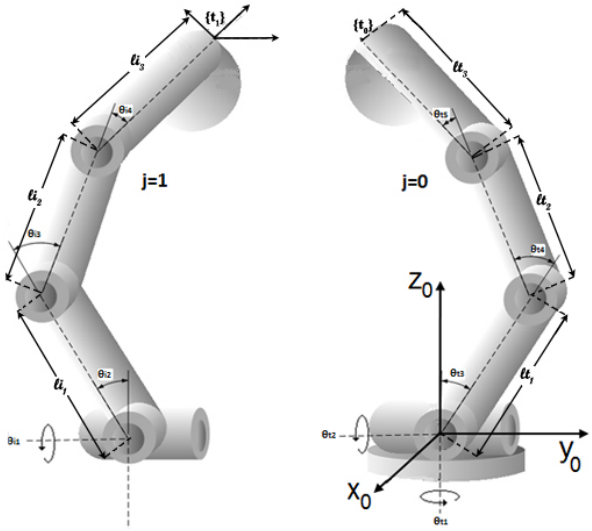

Figure 4.2: Graphical model of a 5-DOF (thumb, j=0) and 4-DOF finger (index, j=1)

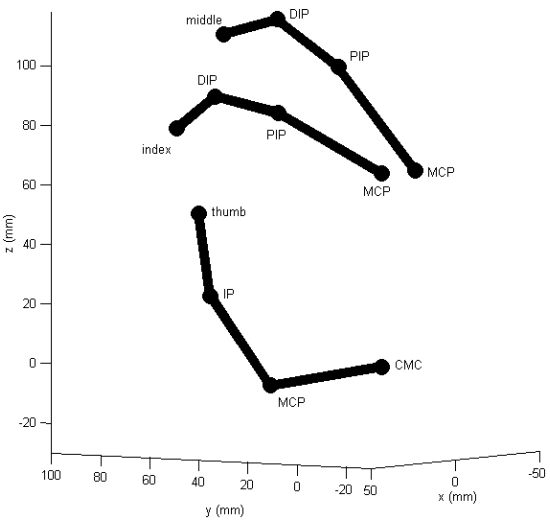

Figure 4.3: Virtual model of the human thumb, index and middle fingers

4.2 Data Glove

The 5DT Glove Ultra (Fifth Dimension Technologies, 2005), shown in Figure 4.4, is a commercial data glove based on fibre optics technology and measuring individual digit flexion and abduction. An optical fibre inside the glove is connected to a light source; the light beam travels through the fibre which has core and cladding made of materials with different refractive indices, allowing detection of the fibre flexion.

Table 4.2: Denavit-Hartenberg parameters for 5 and 4-DOF manipulators

5-DOF digit

joint	a_j	α_j	d_j	θ_j
1	0	-90	0	θ_{t1}
2	0	-90	0	θ_{t2}
3	ℓ_{t1}	0	0	θ_{t3}
4	ℓ_{t2}	0	0	θ_{t4}
5	ℓ_{t3}	0	0	θ_{t5}

4-DOF digit

joint	a_j	α_j	d_j	θ_j
1	0	-90	0	θ_{i1}
2	0	0	0	θ_{i2}
3	ℓ_{i1}	0	0	θ_{i3}
4	ℓ_{i2}	0	0	θ_{i4}

The model which was used in this work has 14 sensors in total: two on each digit and one between two adjacent digits. The three digits of interest (thumb, index and middle) therefore have eight sensors.

The data from the sensors are being transmitted to a PC in packets of 29 bytes using Bluetooth. The glove must be calibrated to the user's hand by reading in sensors values for the entire range of motion of each digit and storing maximum and minimum values ('maxSensor' and 'minSensor'). These values are then scaled to a predetermined angle range for each sensor, from 0° to a maximum ('MaxAngle'), as given in Table 4.3. The values in degrees for each sensor are calculated by linearly scaling the raw sensor data (sensorRaw) to the corresponding angle. For the sensors of the digits, the following formula is used:

$$sensorAngle = \frac{MaxAngle}{maxSensor - minSensor} \left| sensorRaw - minSensor \right| \quad (4.1)$$

For the abduction between thumb/index and between index/middle fingers, increasing sensor values correspond to decreasing flexion angles, and the formula is:

$$sensorAngle = \frac{MaxAngle}{maxSensor - minSensor} \left| maxSensor - sensorRaw \right| \quad (4.2)$$

Digit Tracking Using the Data Glove

Using a simplified version of the kinematic model presented in Section 4.1, a simulation environment can be created, where a user wearing the data glove can interact with virtual objects. This can evaluate the data glove as a master manipulator and

Sensor	Digit	Joint	Max. Angle
1	Thumb	MCP	90
2		IP	90
3	Thumb-Index abduction		60
4	Index	MCP (flexion)	90
5		PIP	90
6	Index-Middle abduction		45
7	Middle	MCP (flexion)	90
8		PIP	90

Table 4.3: Maximum angle values

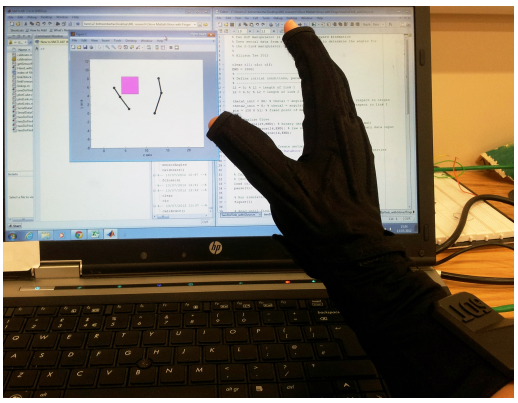

Figure 4.4: Using the 5DT glove to interact with a simulation environment

identify its potential as a surgical master.

A basic 2D environment, shown in Figure 4.4, has been created in MATLAB. It involves two digits with two DOFs and two links manipulating a cubical object (the cube has one DOF) in real time. Only data from the two flexion sensors in each digit were used in this experiment. In a second experiment (Figure 4.5), the abduction sensor between the thumb and index finger was used, as well as the flexion sensors of the two digits. Therefore, each of the two displayed digits has three links and three DOFs. The third DOF of the base joint of the thumb (CMC) is not detected (Table 4.1) and hence, the inaccurate registration of the thumb in 3D space led to unsuccessful pinch grasps during this test.

As expected, the experiments proved that the glove lacks the precision required for hand tracking in surgical tasks as it provides insufficient data for the CMC joint of the thumb and no data for the DIP joints of the fingers. Furthermore, its size cannot be adjusted, which means that the same sensor could be aligned with the

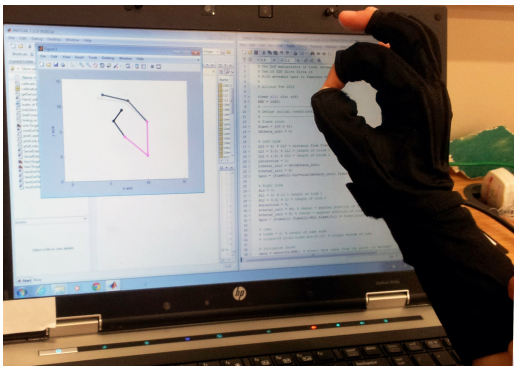

Figure 4.5: Attempting a pinch grasp

thumb's IP joint in small hands or the MCP joint in larger hands. This can lead to further inaccuracies in digit and grasp tracking.

4.3 Sensory Exoskeleton

The preceding exploration of the data glove helped to determine issues in digit motion capturing. Concluding from the experiments and the inadequacy of the data glove for detailed joint tracking, it was decided to develop a hand tracking device which will address the identified challenges. In Section 2.3.6, a few such systems were reviewed, with rigid joint mechanisms (a.k.a. hand exoskeletons) being one of the concepts. The μ`Angelo` exoskeleton is not 'active', i.e. will not be aimed at actuation of the hands, and hence can be lighter than the exoskeleton designs found in the literature.

Design Criteria

As part of the design process for a hand exoskeleton, a number of requirement criteria needed to be prioritised to make it suitable for R-A MIS. Namely, the exoskeleton must:

- Accurately obtain joint angles during digit flexion and abduction/adduction as well as thumb pronation/supination for precision tracking of the surgeon's digits.

- Be lightweight to prevent fatigue during extended periods of use.
- Correspond to the full hand model presented in Table 4.1, so that it does not impede normal hand function and the surgeon can have full dexterity during operations.
- Correspond to the motion range of the slave instrument's joints.
- Be adjustable so that it fits a wide range of hand sizes and, hence, not being limited to use by a single surgeon.
- Have a design with provision for haptic feedback to the surgeon, which, as seen in the literature, could vastly help with tasks requiring highly dexterous manipulations of tissue within the body.

Following on from the set criteria, three prototypes were developed and are presented in the following Sections. These passive hand exoskeletons can sense the movements of the surgeon's digits' joints and translate them to movements in the instrument's joints.

4.3.1 Prototype 1

4.3.1.1 Joint Tracking

In order to track the motion of the hand digits, small and lightweight sensors should be integrated with the exoskeleton. Two types of Hall-effect sensors where chosen: MLX90316 and MLX90333 (Melexis, Belgium) can measure the change of an angle in 1-DOF and 3-DOF respectively. Hall-effect sensors' output voltage varies in response to the change of a detected magnetic field perpendicular to the current across the conductor. The MLX90316 is only sensitive to the flux density applied orthogonally to its surface, while the MLX90333 sensor is also sensitive to the flux density applied parallel to it[1].

[1]More information can be found in the datasheets and the manufacturer's website: https://www.melexis.com/en/product/MLX90316/Absolute-Rotary-Position-Sensor-IC and http://www.melexis.com/mlx90333

The sensors were chosen for their small size and simple design. They have 10-bit angular accuracy and 12-bit resolution and can be calibrated to any angular range. A PTC-04 (Melexis, Belgium) commercial programmer was used to precisely calibrate the sensors to the required operating range. The 1-DOF sensor can give absolute angular position of a small diametric magnet located parallel to the sensor in a rotary type joint, while the 3-DOF sensor detects orientation of an axial magnet and can be suitable for a ball type joint.

4.3.1.2 Kinematic Model

As a first exploration of a simplified exoskeleton design, the PIP and DIP of the index and middle fingers were considered coupled. In fact, these joints in the human hand are often considered coupled, with Kamper et al. (2003) deriving an approximate relationship between their motion during reach-and-grasp tasks. An example of this relationship is shown in Figure 4.6. This approximation seems insufficient for the precision required in surgical applications and, hence, was not used in the subsequent prototypes of the exoskeleton. In prototype 1, however, the goal was also to evaluate this approach as early as possible, hence the prototype carries only one sensor for the PIP joint, while the position of the DIP is approximated by the relationship between the PIP and the DIP.

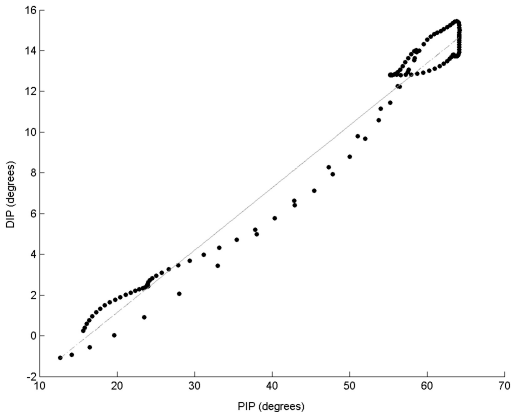

Figure 4.6: Example of relation between PIP and DIP joint of the same digit (Kamper et al., 2003)

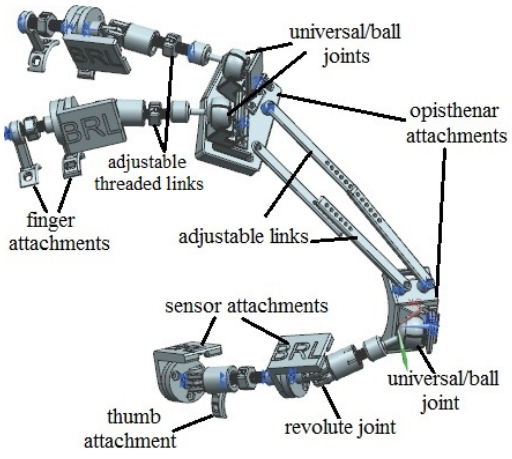

Figure 4.7: CAD drawing of the exoskeleton assembly

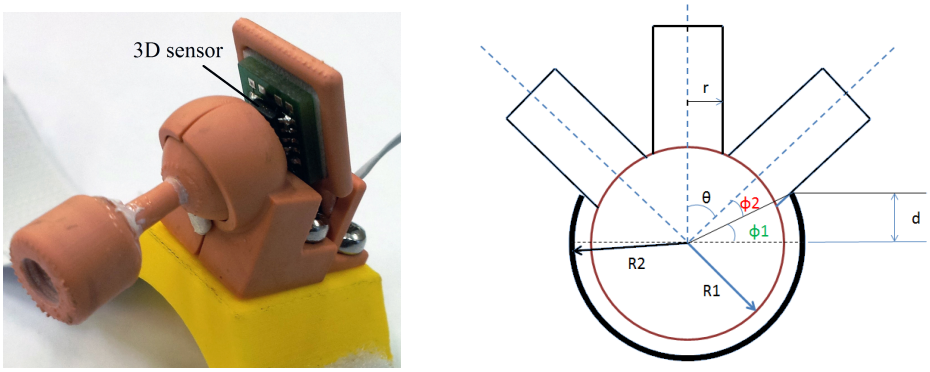

Figure 4.8: Ball joint prototype and range of motion calculation

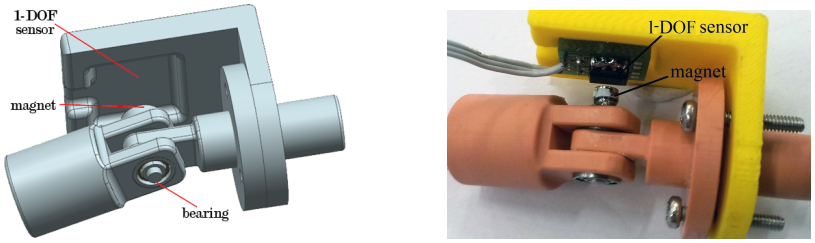

(a) (b)

Figure 4.9: Revolute joint (a) CAD and (b) 3D printed part

4.3.1.3 Layout and Assembly

The CAD drawing of the exoskeleton assembly is shown in Figure 4.7. The overall structure was designed to be as compact as possible and it has eleven DOFs. Apart from the lack of two DOFs of the DIP joints, the design followed the model of Table 4.1 (page 70). It comprises seven sensors in total: three 3-DOF sensors for the MCP joints of the index and middle fingers (only two of these DOFs were used) and the CMC of the thumb, and four 1-DOF for the PIP joints of the index and middle fingers and the IP and MCP of the thumb. The MCP and CMC joints were designed as ball joints in order to reduce the volume and the complexity of the component. The sensors are attached to the non-contacting parts at the side of each joint (Figures 4.8 and 4.9).

The typical range of motion of each joint can be considered as: 0-90° for the MCP, 0-110° for the PIP and 0-70° for the DIP. From the parameters of Figure 4.8,

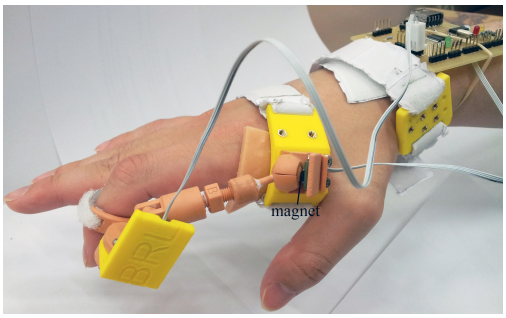

Figure 4.10: Testing the exoskeleton on one finger

the range of the ball joint can be calculated using equation (4.3).

$$2\theta = 2(90 - \phi_1 - \phi_2) = 2(90 - sin^{-1}(\frac{d}{R_2}) - sin^{-1}(\frac{r}{R_2})) \tag{4.3}$$

To ensure unrestricted motion, the range of the ball joint was set to be at least 90°, by choosing $R_2 = 6$ mm, $d = 3$ mm and $r = 1.5$ mm.

The exoskeleton was fabricated using 3D printing (NanoCure, Envisiontec, Germany). Figure 4.10 shows part of the exoskeleton fitted on the side of the index finger and the electronics attached to the wrist.

4.3.1.4 Adjustability

Each exoskeleton joint is fastened to the digit with an adjustable attachment and the joints are connected to each other via double threaded links (Figure 4.11) that make it possible to vary the link lengths according to the digit links of the user. One side of a double threaded link has a left-hand thread, while the other has a right-hand thread: by rotating the link, it can be extended (clockwise) or shortened (anti-clockwise). The double thread links not only make the mechanism adjustable, but also allow the exoskeleton to be lightweight (approx. 130 gr for one digit including electronics), without added material for modifications. The two opisthenar attachments (base of fingers and wrist) are also connected to each other via adjustable links.

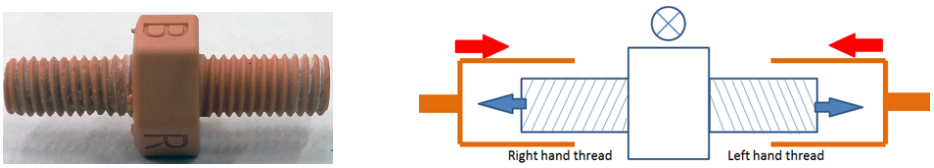

(a) (b)

Figure 4.11: Double-threaded link (a) printed part and (b) working principle

4.3.1.5 Evaluation

Figure 4.12 shows a snapshot from the initial tests to link the data from the sensors to the virtual model of the index finger (4 DOFs) in order to simulate the movement of the user's finger. The virtual model could, in general, follow the motion of the user's finger. However, the exoskeleton could not be firmly attached to the fingers, which occasionally led to inaccurate measurements. Encouraged by these early results of joint tracking, it was decided to improve the design in the form of a second prototype which would include *i*) secure attachments to the digits *ii*) sensing of the DIP joints and *iii*) more robust design.

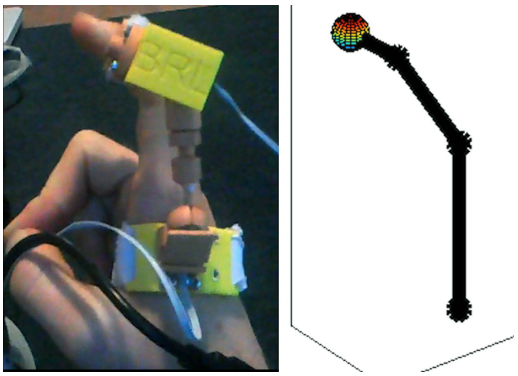

Figure 4.12: Simulation of the user's index finger motion

4.3.2 Prototype 2[2]

The new design was based on previous work on hand exoskeletons in the Bristol Robotics Laboratory presented by Burton et al. (2011). The new exoskeleton was designed to comfortably fit around the 5th to 95th percentile of hand lengths and

[2]Section 4.3.2 was collaborative work with by Dr Thomas M.W. Burton in the BRL in 2013.

breadths (5th percentile - 173 mm and 78 mm respectively and 95th percentile - 205 mm and 95 mm respectively) as described by Pheasant and Haslegrave (2006). The equations by Buchholz et al. (1992) were then used to estimate the maximum and minimum required length for the index, middle and thumb digit lengths. Designing the mechanism's digit lengths using these equations means that the device is able to have its joint axes aligned with the natural joint axes of the surgeon as in the work by Burton et al. (2011). Furthermore, it allows for the same Hall-effect sensors used in prototype 1 to be accurately positioned so that the correct joint angle is measured (1 mm distance from the magnet and 0.5 mm offset from the joint axis). This is an important aspect of the design as it means that the device is comfortable to wear for the surgeon while allowing for accurate information about the joint position to be extracted.

This prototype weighs 154 gr in total and is scalable to the range of hand sizes listed above via lead screws embedded into the mechanism, allowing each segment length of a digit to be elongated or contracted to suit an individual person's anatomy. Adjustment is achieved via a hex key inserted into each segment to turn the screw. This mechanism is shown in Figure 4.13.

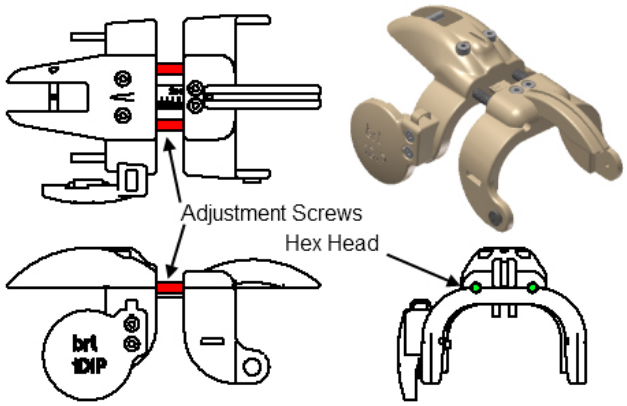

Figure 4.13: Mechanism for adjusting the lengths of the exoskeleton's segments to fit different sized hands

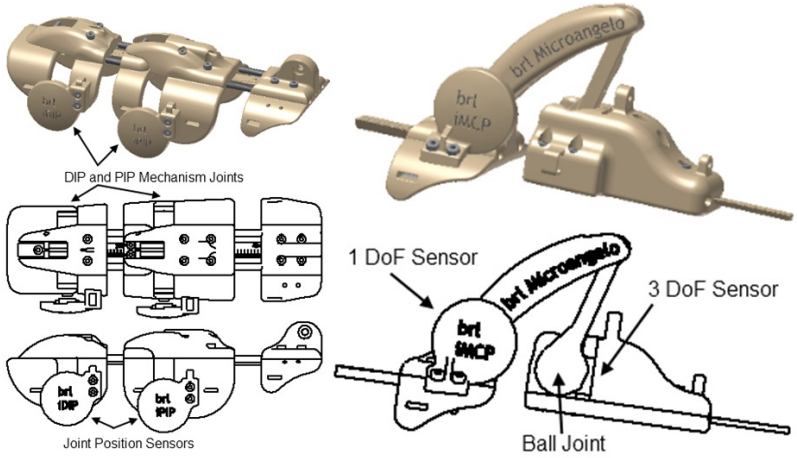

Figure 4.14: The DIP, PIP (left) and the MCP (right) joint mechanisms of the exoskeleton

4.3.2.1 Operation of the Exoskeleton

The new exoskeleton takes all joints of the digits into account to provide more accurate digit tracking and has a total of 13 DOFs. The DIP and PIP joints of the index and middle finger as well as the IP and MCP of the thumb use the 1-DOF sensors to detect angular rotation of the joint. The joints of each segment operate around miniature bearings placed either side of the joint to reduce friction. Use of the lead screw adjustment mechanism allows for the bearings to be positioned with their axes aligned with each joint's natural axis of rotation. The mechanisms and sensors for the IP joints are shown in Figure 4.14 (left).

However, the MCP joints of the fingers and the CMC of the thumb require more complex mechanisms to track their respective motions. For the index and middle MCP joints a ball and socket mechanism along with a 3-DOF sensor were used, combined with a 1-DOF sensor for the redundant link joint, to obtain MCP flexion/extension and abduction/adduction angles. The mechanism for this can be seen in Figure 4.14 (right).

The CMC joint of the thumb is a highly intricate and complex mechanism. The device developed for this joint has a similar mechanism to that used for the fingers' MCP joints in that a ball joint was used to allow for flexion/extension and abduction/adduction of the thumb with a 3-DOF sensor and the 1-DOF sensor of

the thumb MCP joint for the redundant link as well. However, unlike the fingers, the thumb has much larger segment lengths between the ball joint on the hand plate and the IP mechanisms. To ensure correct movement of the ball joint, an additional unconstrained four-bar mechanism was added to the design as shown in Figure 4.15.

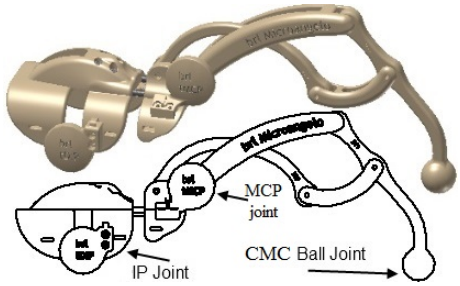

Figure 4.15: Thumb MCP joint mechanism showing ball joint and four bar mechanism

All of the electronics are electrically grounded onto a plate mounted onto the dorsal side of the hand. Digits were constrained to the exoskeleton via soft and adjustable straps to ensure a snug fit for correct operation as shown in Figure 4.16. Each sensor was also equipped with an LED to indicate power. This would provide the user with an indication of the type of problem, should one of the sensors fail. The full design in different digit configurations can be seen in Figure 4.17, which demonstrates its high digit manoeuvrability during dexterous tasks.

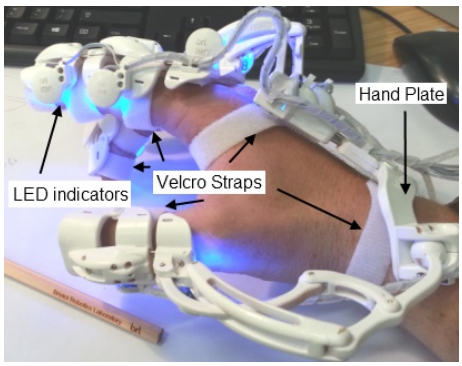

Figure 4.16: Mechanisms attached to hand plate. Also shown are the LED indicators and the straps to hold the mechanism to the hand

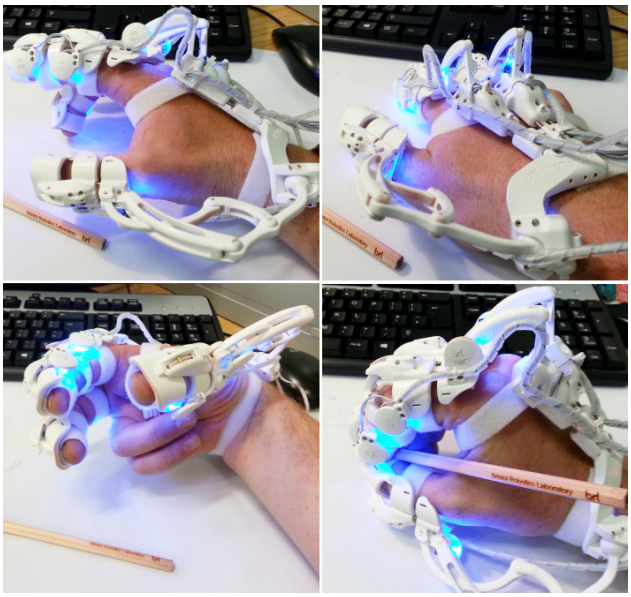

Figure 4.17: The Exoskeleton in different digit configurations

4.3.2.2 Suitability for Haptic Feedback

As mentioned in the design criteria (page 73), an important aspect of a teleoperated robotic surgical system is the ability to provide haptic feedback during operations. While not implemented as part of this thesis, the design is based around the work of Burton et al. (2011) in which similar mechanisms were actuated to provide hand rehabilitation for stroke patients. The work of Burton et al. (2011) was not focused on digit tracking but, instead, used motors to actively actuate the digits and facilitate the opening of the patient's hand.

As shown in Figure 4.18, using an open-pulley design with the centre of rotation coincident with the joint's axis, forces could be applied to each individual phalanx via a cable-driven system. Force applied to the cable at 'i' around the guide at 'ii' produces a force on the digit around the joint at 'iii' via the 'open-pulley'. This could in turn be used to provide haptics to surgeons during operations in the form of a resistive force as they flex their digits.

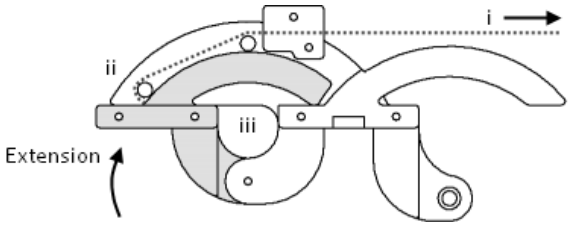

Figure 4.18: Force feedback module

4.3.2.3 Evaluation

The exoskeleton is linked to a virtual model, as in Section 4.3.1.5. Figure 4.19 illustrates parts of the simulation of the DIP and PIP joints of the user's middle finger. The visualization of the user's motions is successful, apart from the joints at the base of each digit, where the 3-DOF Melexis sensing range does not cover the joint range. In prototype 3 of the exoskeleton, in order to address this issue, the ball joints are replaced, despite their compact and lightweight design. The 3-DOF sensors are replaced by three 1-DOF sensors for the CMC joint of the thumb and the MCP joints of the index and middle fingers.

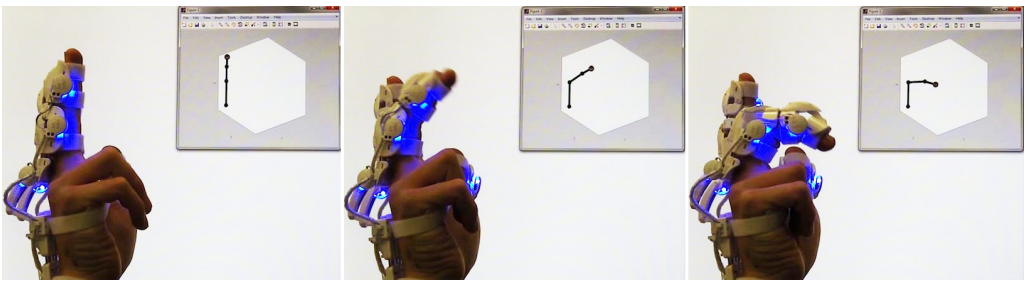

Figure 4.19: The user controls a virtual model of the finger using exoskeleton prototype 2

4.3.3 Prototype 3

The exoskeleton prototype 2 has been slightly modified, so that it comprises simple rotary joints which accommodate 1-DOF sensors, as these have proven to be more accurate compared to the 3-DOF ones. Specifically:

- The ball joints aligned with the MCP joints of the index and middle fingers have been removed and instead, the flexion of each of these MCP joints is

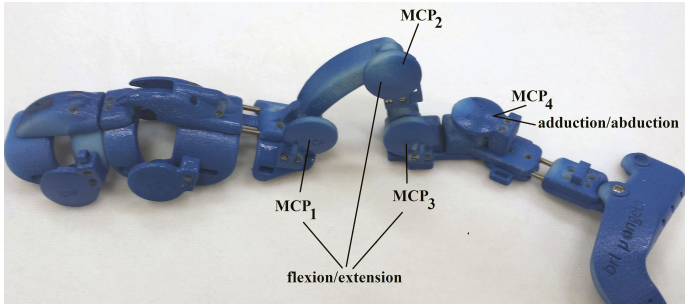

Figure 4.20: MCP_1, MCP_2 and MCP_3: sensors measuring flexion of MCP joint. MCP_4: sensor measuring abduction/adduction of MCP joint

calculated by the combined values of three 1-DOF sensors (Figure 4.20).

- The abduction/adduction of the index and middle fingers is measured by an additional 1-DOF sensor positioned at a 90° offset with respect to the flexion measuring sensors.

- The ball joint of the thumb has also been removed and the mechanism is similar to the ones of the fingers, with three 1-DOF sensors detecting the CMC flexion angle (similar to the MCP_1, MCP_2 and MCP_3 of Figure 4.20), and two 1-DOF sensors placed at 90° offset measuring the CMC abduction/adduction and pronation/supination.

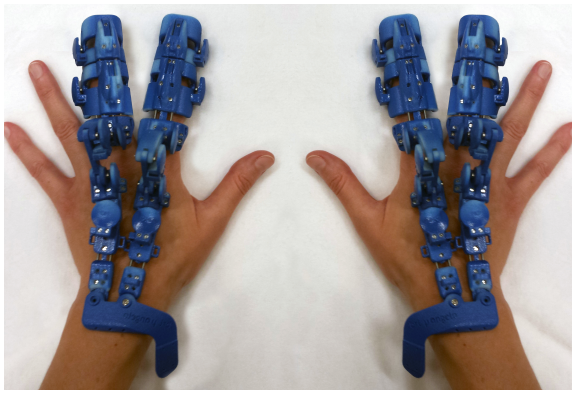

Figure 4.21: Modified exoskeleton for index and middle fingers

The index and the middle fingers of prototype 3 have six sensors each, while the thumb has seven sensors in total. Figures 4.20 and 4.21 show the mentioned modifications. The additional links of the MCP joint mechanism are necessary in

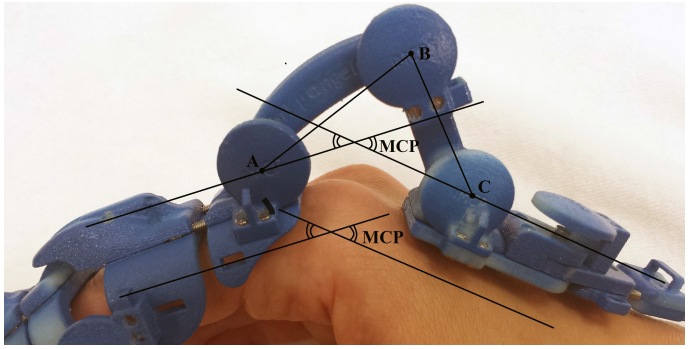

Figure 4.22: Additional sensors and relation with the flexion of the MCP joint of the index and middle fingers or the CMC flexion of the thumb

order for the exoskeleton to follow the natural motion of the user without restricting it. Figure 4.22 shows the three sensors around the MCP joint: for the particular mechanism, to calculate the position of the MCP joint flexion, three measurements are needed.

Figure 4.23 illustrates the principle: the angles that the sensors measure as well as the MCP angle that needs to be calculated are shown. Two triangles are formed: ABD and BCE. Without the MCP_2 sensor (Figure 4.20), there are only two known parameters for each triangle: θ_1 and θ_3 are the values from the sensors MCP_1 and MCP_3, while L_1 and L_2 are known link lengths from the exoskeleton design specification. Therefore, these triangles cannot be defined without an additional sensor. If θ_2 is the MCP_2 sensor measurement, it can be derived from triangle BCE:

$$\alpha = 180 - \theta_2 - (90 - \theta_1) = 90 - \theta_2 + \theta_1 \tag{4.4}$$

From the triangle AEO:

$$MCP = 180 - (180 - \alpha) - \theta_3 = \alpha - \theta_3 \tag{4.5}$$

They combination of equations (4.4) and (4.5) yields

$$MCP = 90 + \theta_1 - \theta_2 - \theta_3 \tag{4.6}$$

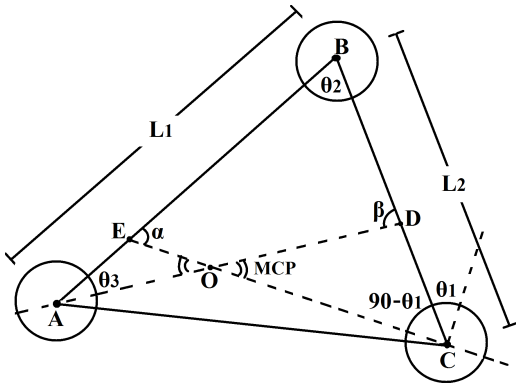

Figure 4.23: Geometrical calculation of the MCP or CMC flexion

4.3.3.1 Evaluation

In order to test the tracking accuracy of the exoskeleton, a series of tests were conducted. The exoskeleton was adjusted so that its joints are aligned with the digit joints of the user. For this experiment, coloured adhesive markers were placed at the side of each joint. The motion of these markers was tracked using image processing in order to compare their position to the joint position derived from the exoskeleton sensors. Image processing techniques included colour detection and blob tracking while each test was performed in a single plane of motion to avoid occlusions of the fingers as seen from the camera view. Figure 4.24 illustrates the different planes of motion: (a) side of index finger (DIP, PIP and flexion of MCP) (b) top of index finger (abduction/adduction of MCP) (c) side of thumb (IP, MCP and flexion of CMC) (d) top of thumb (abduction/adduction of MCP).

For each test, only the corresponding exoskeleton sensors were used. By calibrating the sensors to the correct angle range of each joint (smaller than the original 360° that they are calibrated to by the manufacturer) better resolution can be achieved. Following the calibration and using equation (4.6), the data from the sensors are input into the FK model of the hand so that the position of the joints and fingertip can be plotted. The procedure is illustrated in Figure 4.25.

Figure 4.26 (a) (in comparison to Figure 4.24 (a)) shows the first step of image processing where the video was colour-graded so that green is the most prominent colour. The joint and fingertip positions are exported and then plotted to simulate

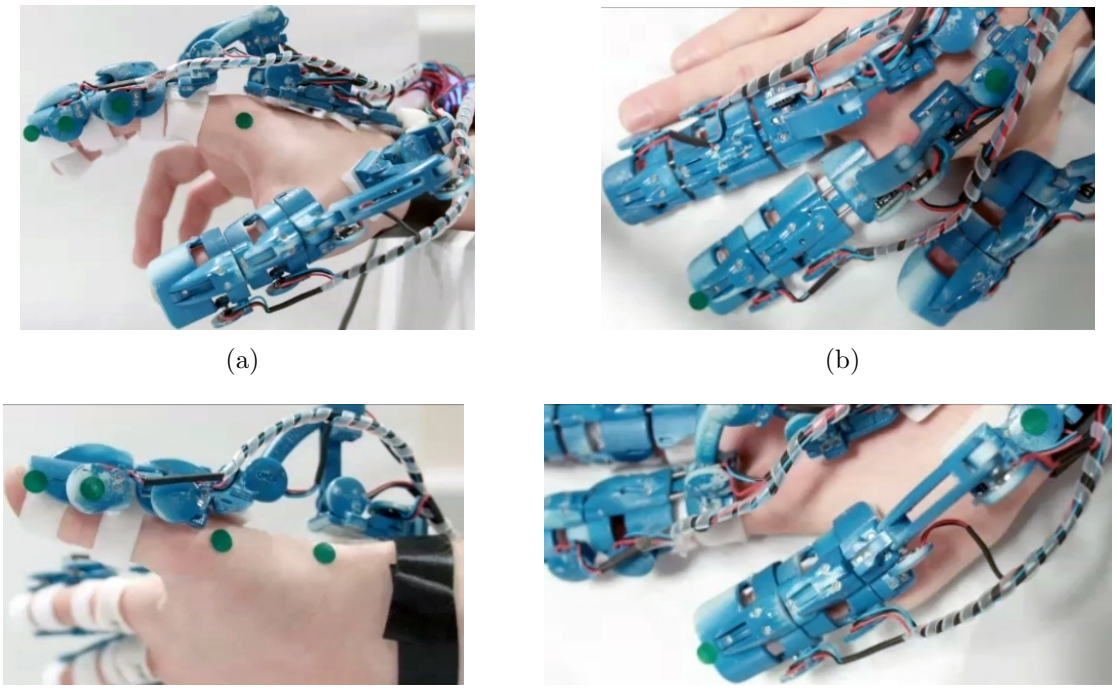

(a) (b)

(c) (d)

Figure 4.24: Planes of motion when tracking the digit joints using image processing (green markers): (a) side of index finger (b) top of index finger (c) side of thumb (d) top of thumb

the finger (Figure 4.26 (b)). The two types of plot are then compared. Figures 4.27 (a)-(d) show the trajectories captured by the two methods in the same graph: to achieve this, *i*) the trajectories derived by image processing were enlarged to fit the scale of the exoskeleton trajectories and *ii*) their orientation was manipulated to fit the orientation of the exoskeleton trajectories. The reason for this processing is that the distances between the markers captured by the camera are not necessarily the real lengths of the exoskeleton joints as this would change depending on the

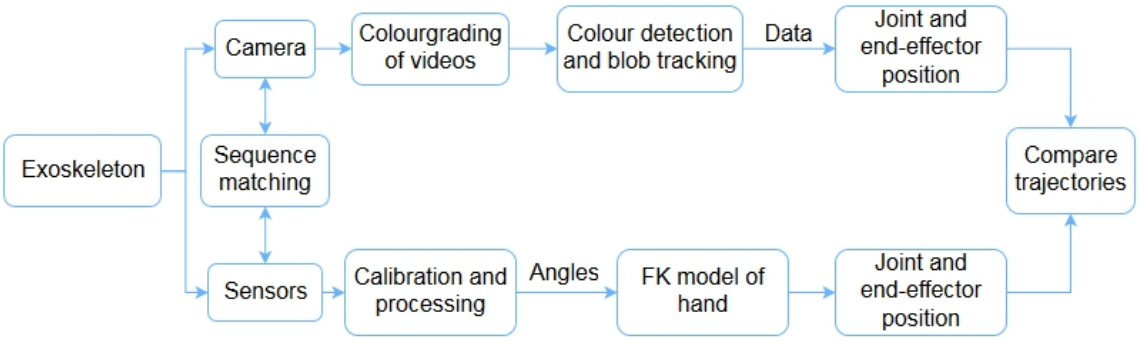

Figure 4.25: Accuracy testing procedure

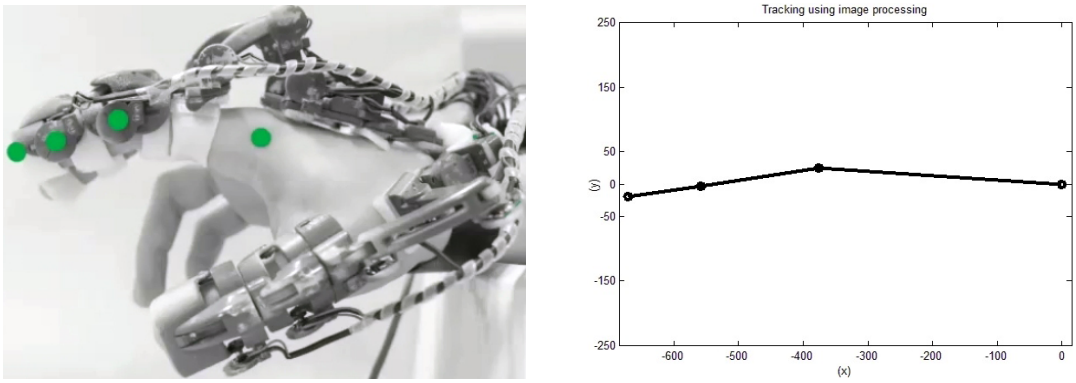

(a) (b)

Figure 4.26: (a) Frame of the side of the index video after colour-grading and (b) corresponding snapshot of the simulation using the green markers' position

distance and the angle between the camera and the exoskeleton. This also explains why the trajectories are not identical. Missing data from blob tracking is due to light reflections on the markers, as for example in Figure 4.27 (c).

The comparison shows that the trajectories match. However, in Figure 4.27 (b), there is considerable difference between the measured angles of motion. Figure 4.28 (a) shows these two trajectories: the sensor measures 4° of motion while the image processing gives a measurement of 10°. This can be due to false calibration of the sensor, as the corresponding measurement for the thumb was successful. This can be seen in Figure 4.28(b).

In a separate experiment, the user was asked to move the index finger from left to right while the palm lying flat on the table. This experiment was repeated eight times. Figure 4.29 shows the trajectory of the fingertip during one of the tests when repeating this motion seven times. By enlarging a small area of the graph, the greatest error can be calculated to be 12μm for this trial. The order of the maximum error was consistent in all five tests, with an average of 8μm ($\sigma = 0.005$).

4.3.3.2 Mapping to the Theoretical Model

The preceding evaluation includes all sensors but the CMC pronation/supination of the thumb. During all tests, the specific sensor did not record any significant change in angle. It has been concluded that the position of this sensor on the exoskeleton

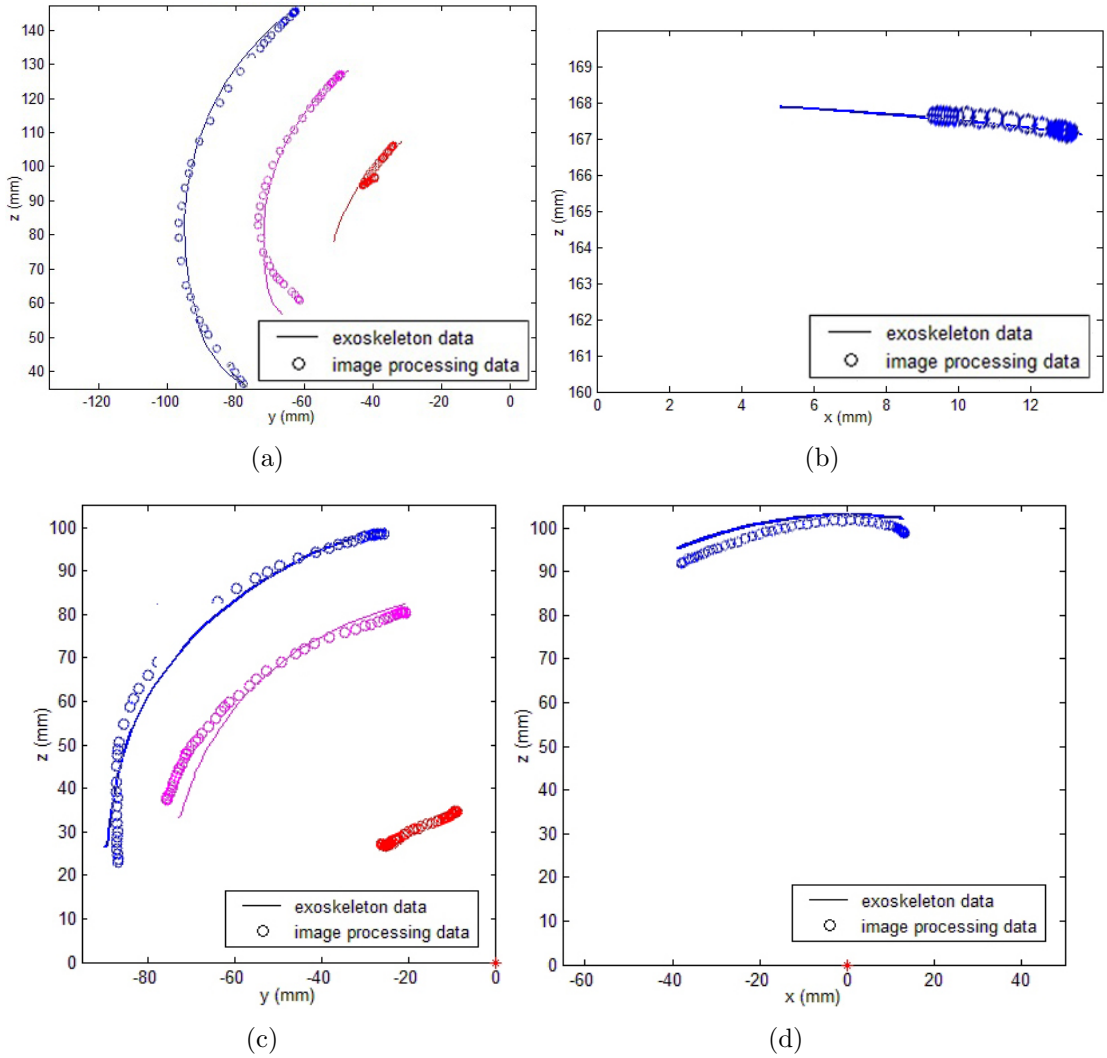

Figure 4.27: Comparison of trajectories derived by image processing with those derived using the exoskeleton sensors (a) side of index finger (b) top of index finger (c) side of thumb (d) top of thumb

is not optimal and therefore does not track the corresponding motion. Despite this, the exoskeleton has been mapped to the theoretical model with successful tracking of the digits' motion.

The data from the sensors simply constitute the input to the FK model for all joints except for the MCP joints of the index and middle finger and the CMC of the thumb, for which calibration is needed. The calibration consists of finding the extremes of the user's range of motion for the specific joints and using equation (4.7), where θ_j is the input to the FK for joint j, q_j is the sensor angle value in degrees (derived by equation (4.6)), k is the sensor angle value when the joint is at position

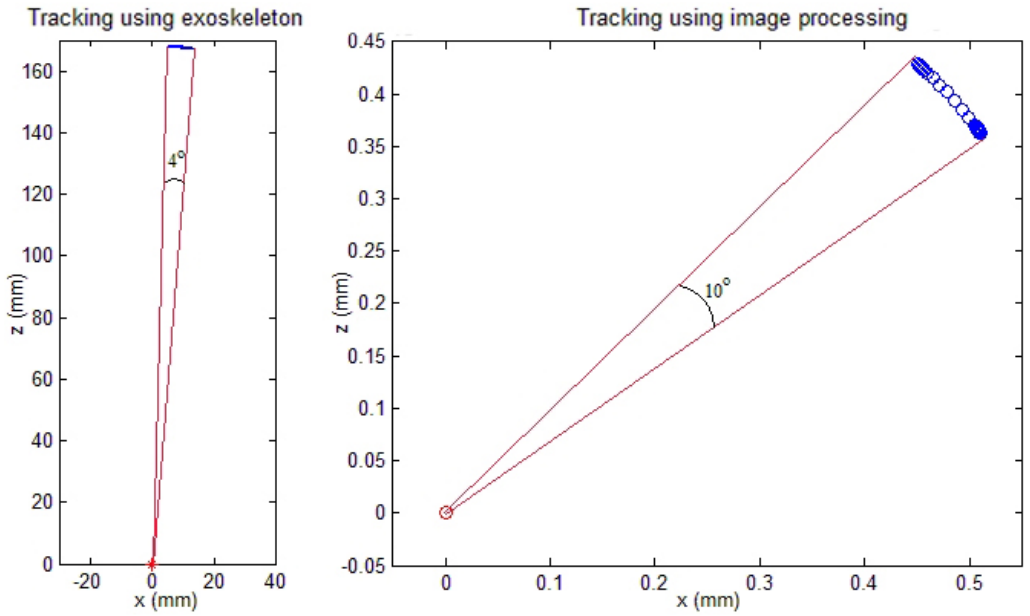

(a)

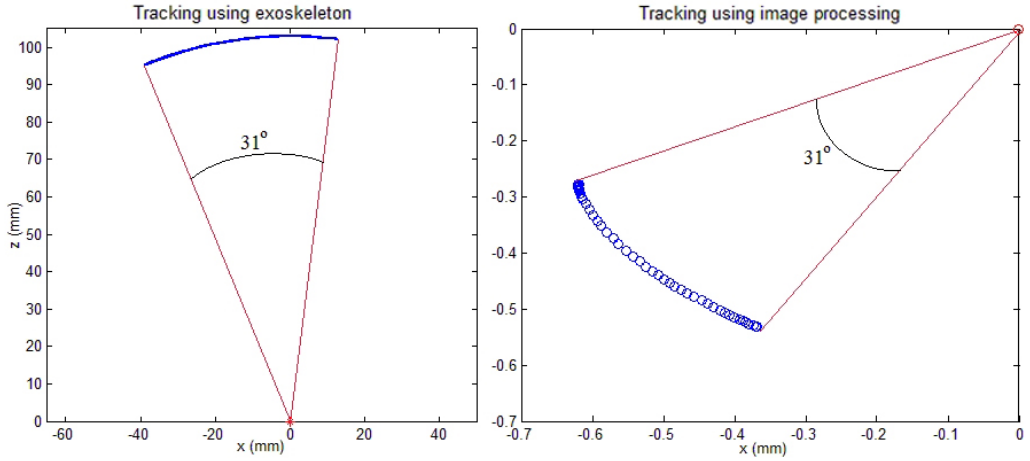

(b)

Figure 4.28: Measured angle between left and right movements of (a) index finger (b) thumb

0 (this offset can be negative or positive), R_d is the range of the joint measured experimentally (approximate value using a protractor) and R_r is the range of the sensor value before joint calibration.

$$\theta_j = (q_j + k)\frac{R_d}{R_r} \tag{4.7}$$

Figure 4.30 shows different types of grasp that were executed between thumb-

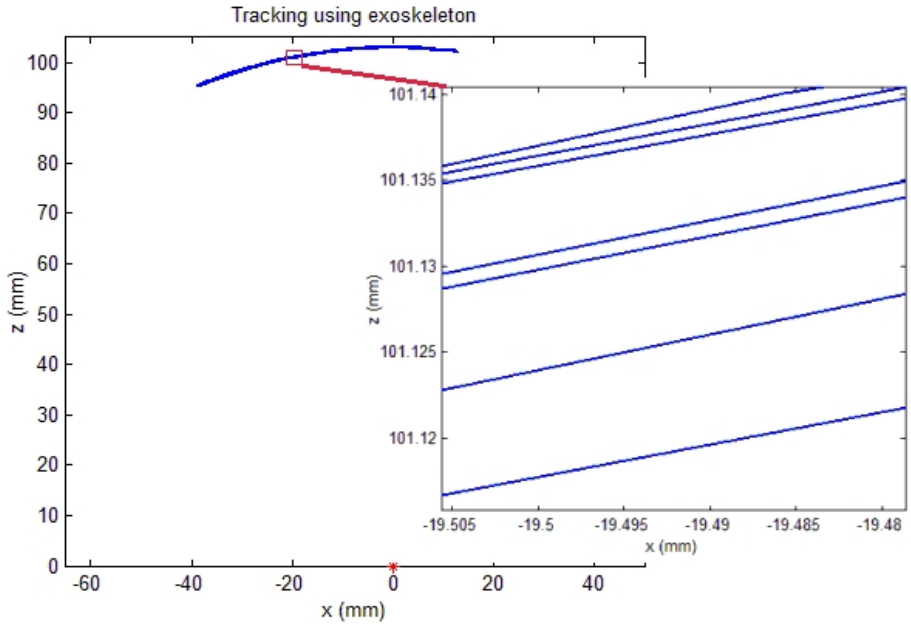

Figure 4.29: Seven trajectories during a left-right movement of the index finger

index finger and thumb-middle finger. Two examples of simulated grasps are shown in Figure 4.31. Among 11 trials, the error was calculated as the difference between the tip positions of the thumb and the index finger (or middle finger, depending on which formed the grasp in cooperation with the thumb). The minimum error was 5.39 mm, with a mean of 11.18 mm ($\sigma = 2.53$). This error can be due to imprecise calibration and the lack of complete data from the CMC joint. Furthermore, although the exoskeleton can be adjusted to fit the length of the user's digits, more improvements and adjustments are required to make it a better fit. It was observed that occasionally, the exoskeleton would 'slip' out of the predetermined position, affecting mostly the MCP joints of the index and middle fingers. This has contributed to the error magnitude as well as to the relatively high standard deviation.

4.3.3.3 Coupling Between Digit Joints

In comparison with prototype 1, prototype 3 includes sensors for the DIP and IP joints as this addition can offer a more precise illustration of the digit motion. In a series of experiments, the user performed *i*) movements of the three digits covering their entire range of motion and *ii*) index-thumb and middle-thumb pinch grasps.

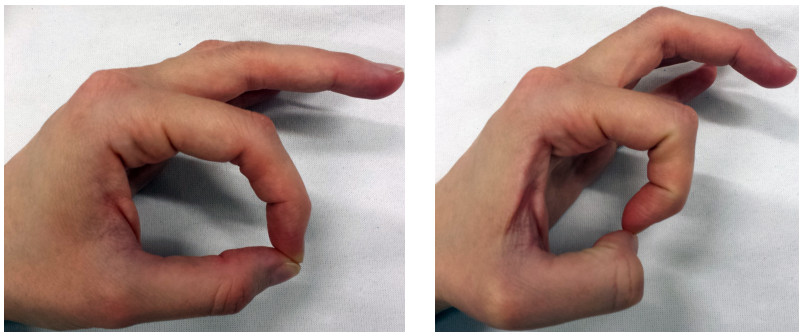

Figure 4.30: Types of pinch grasps between the thumb and index finger

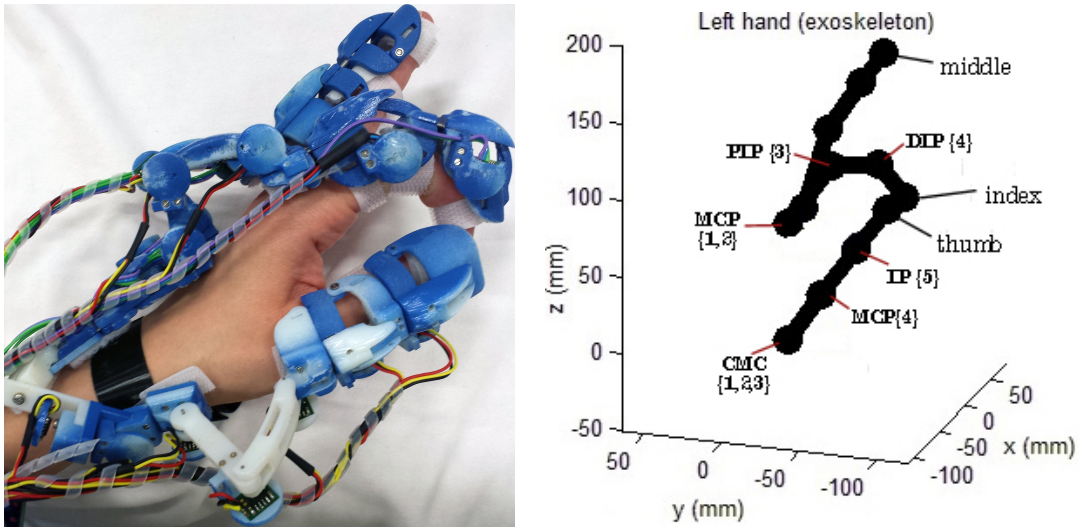

(a) (b)

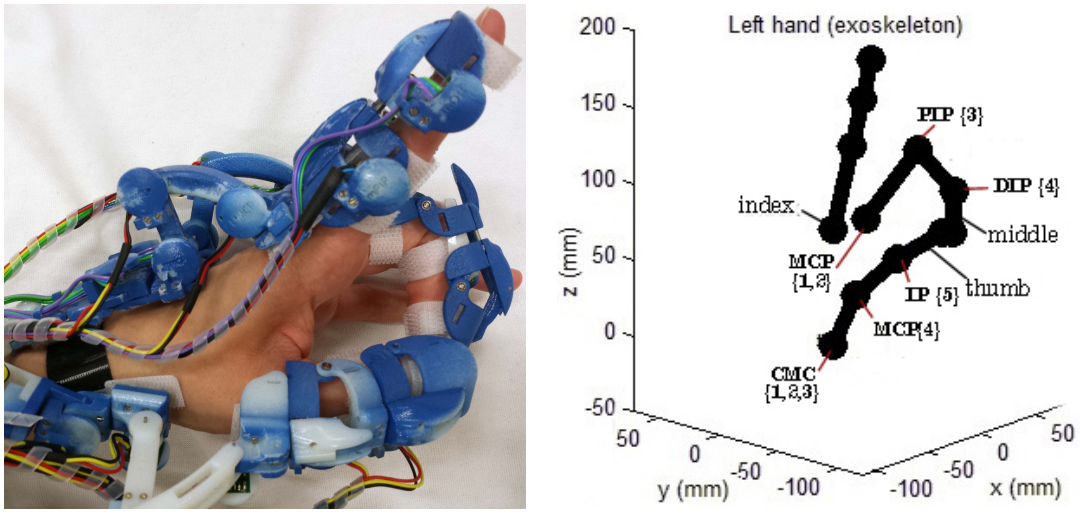

(c) (d)

Figure 4.31: Successful simulated pinch grasps between thumb-index (a-b) and thumb-middle finger (c-d)

These experiments aimed to determine the degree of coupling between the DIP and PIP of the index/middle finger and between the IP and MCP of the thumb and how necessary the additional sensors are.

Figures 4.32 (a)-(f) (page 96) demonstrate a comparison between these joints during pinch grasp motions (such as in Figure 4.30). Figures 4.32 (a), (c) and (e) show that some correlation exists between the movement of the joints, although this has not been true for all attempted grasps. This is evident from Figures 4.32 (b), (d) and (f) where the motion of one joint is plotted against the motion of its consecutive joint in the corresponding digit, in a similar way to Figure 4.6 (page 75) by Kamper et al. (2003). In the specific grasp examples of Figures 4.32, the relation of these joints in the index finger seems more reliable than the ones in the middle and the thumb. However, this has not been consistent in all experiments. It can be concluded that the index and middle fingers tend to have some correlation between the two joints in question while the thumb joints showed no evidence of maintaining any constant relationship.

Although some correlation has been demonstrated in some experiments, the repeatability and accuracy of this model would be unacceptable for high precision tasks required during surgical applications. This conclusion is supported by the fact that the correlation between these joints dissipates entirely during non-grasp motions, as demonstrated in Figures 4.33 (a)-(f) (page 97). Therefore, the sensors at the last joint of each digit are a necessary addition.

4.4 Summary

This Chapter presented a study on the kinematics of the human hand and detailed the research conducted in order to determine an efficient method of capturing the motion of a surgeon's hand digits according to the specified design criteria. Section 2.3.6 briefly reviewed a selection of such devices on offer and in research that comprise the state of the art. Amongst those, the master interfaces that capture

direct digit motion involve a variety of setbacks. Lack of detailed joint tracking and, thus, lack of the required information would not allow the model of the human hand presented in Section 4.1 to be used. Furthermore, the lack of adjustability to different users is not addressed in these devices, while vision based data gloves (e.g. Cyberglove) or trackers (e.g. Leapmotion) cannot support haptic feedback as standalone devices.

In order to help identify potential challenges in this endeavour, a readily available data glove was used. The experiments with the commercial 5DT Glove Ultra were not meant as a comparison, but rather to explore fibre optics technology as a sensing method and to highlight issues occurring in hand tracking, such as the opposition of the thumb. Following from this, three prototypes of a custom-made hand exoskeleton with ergonomic design for hand digit motion capture have been developed.

The final prototype's 13 DOFs allow for unrestricted motion, corresponding to the hand model of Section 4.1, and obtaining high resolution data of the joint angles. While these sensors have a resolution of 0.1° (for a range of 360°), depending on the calibration of the sensors to the required working range, the resolution of the sensors could be as low as 0.02° (for a range of about 80°). This level of joint sensing resolution can offer accurate information that will lead to precise tracking in comparison with other sensing methods that offer a more generalised depiction of the finger's curvature (as is the case for the 5DT Ultra Glove).

Prototype 3 of the exoskeleton has been the most successful with 19 sensors in total. It can capture the motion of all three digits and has excellent repeatability (error in the order of μm in digit abduction/adduction). The successful tracking of the digit motion and grasping is due to its high number of DOFs. However, the pronation/supination of the thumb's CMC joint was not successfully tracked. This did not inhibit tracking of the thumb's motion or attempted grasps. Nevertheless, it is possible that the lack of this measurement would limit motions of the thumb that can be tracked. Strategic repositioning of this sensor on the exoskeleton should be

carried out in future work to determine this. The design of the exoskeleton would also benefit from having a tighter fit on the user's hand to improve accuracy and repeatability of the joint measurements at the base of the hand digits.

Despite some degree of coupling between the joints, the trajectories that consecutive joints follow can differ significantly. Independent sensing of each joint is important for accurate depiction of the position and orientation of the fingertip in the Cartesian space. This is true even for the joints closest to the fingertips where the addition of sensors has proven necessary. Detection of these joint angles is often omitted in hand tracking devices (e.g. 5DT glove). Therefore, the tracking of the μ`Angelo` exoskeleton is more detailed compared to hand tracking systems that detect only the general curvature of a digit and can help represent the motion of the user better. In future work, comparison with simpler tracking systems could determine whether this is advantageous in surgical teleoperation.

The exoskeleton also includes potential for force feedback to the user, an important aspect in surgical procedures, while it is also lightweight to facilitate portability. The exoskeleton is adjustable to a range of digit lengths, however it does not include scaling for different digit diameters, a feature that, although beyond the scope of this thesis, should be included in future work. The exoskeleton was 3D printed in VeroWhitePlus (plastic material by Stratasys, UK) which made the manufacturing process fast and low-cost. However, using this material, the exoskeleton is not as robust as regular use would require. This can be improved in future work with the use of different materials such as Nanocure (Envisiontec, Germany), which prototype 1 and 2 of the exoskeleton were made of.

The simulation of the exoskeleton captured motion constitutes a basis for a surgical simulation environment, where the surgeon will be able to test the concept of anthropomorphic instruments in training. Further on, the surgeon can use the exoskeleton to directly control the instruments. The development of the μ`Angelo` instrument is presented in the following Chapter.

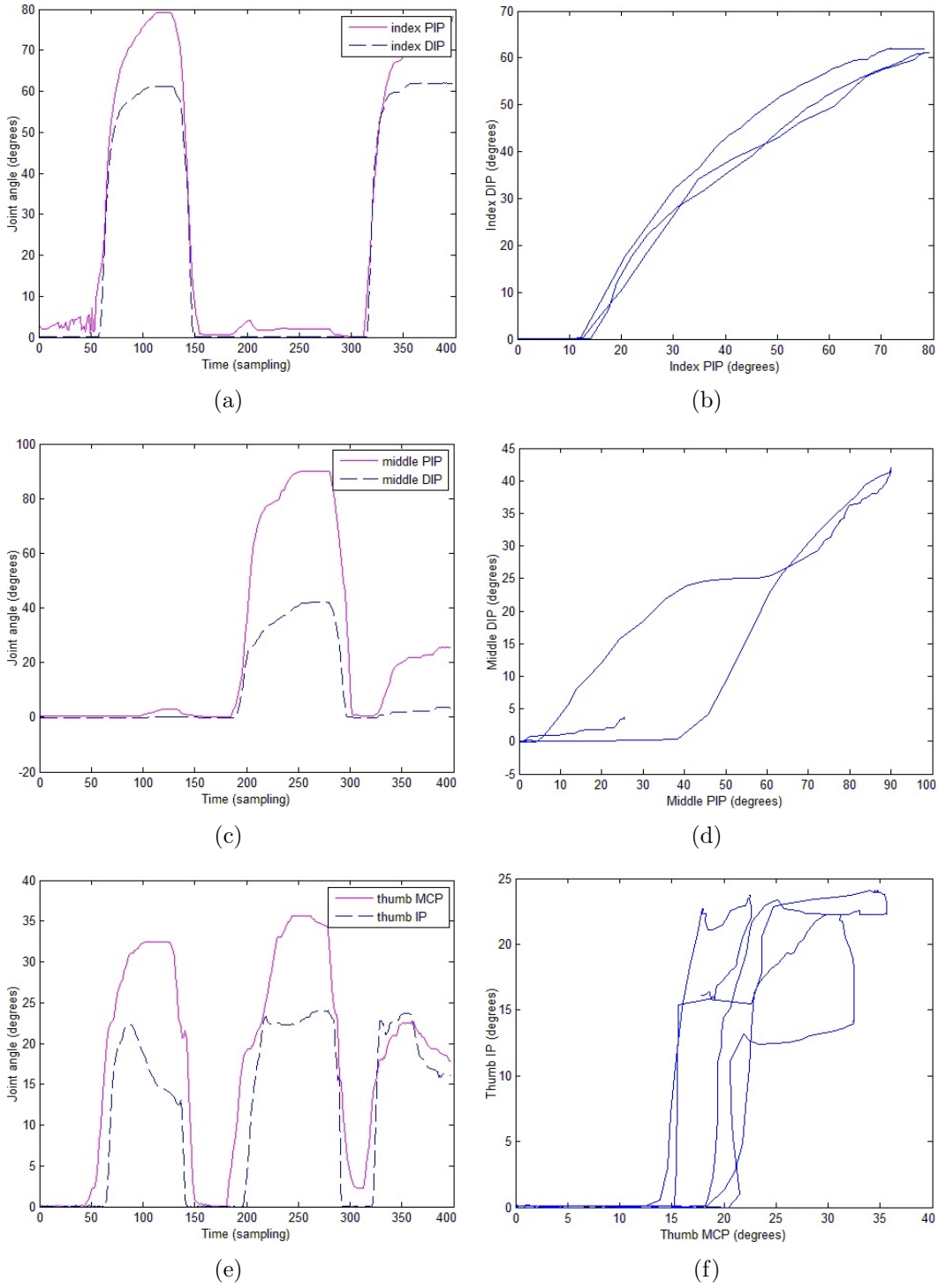

Figure 4.32: Comparison between the DIP and PIP joints of the index/middle finger and the IP and MCP of the thumb during execution of pinch grasps. (a),(c),(e): index-thumb during 50-150 and 300-400 sampling time and middle-thumb during 200-300. (b),(d),(f): graph of the relation between the corresponding joints of each digit during the pinch grasps

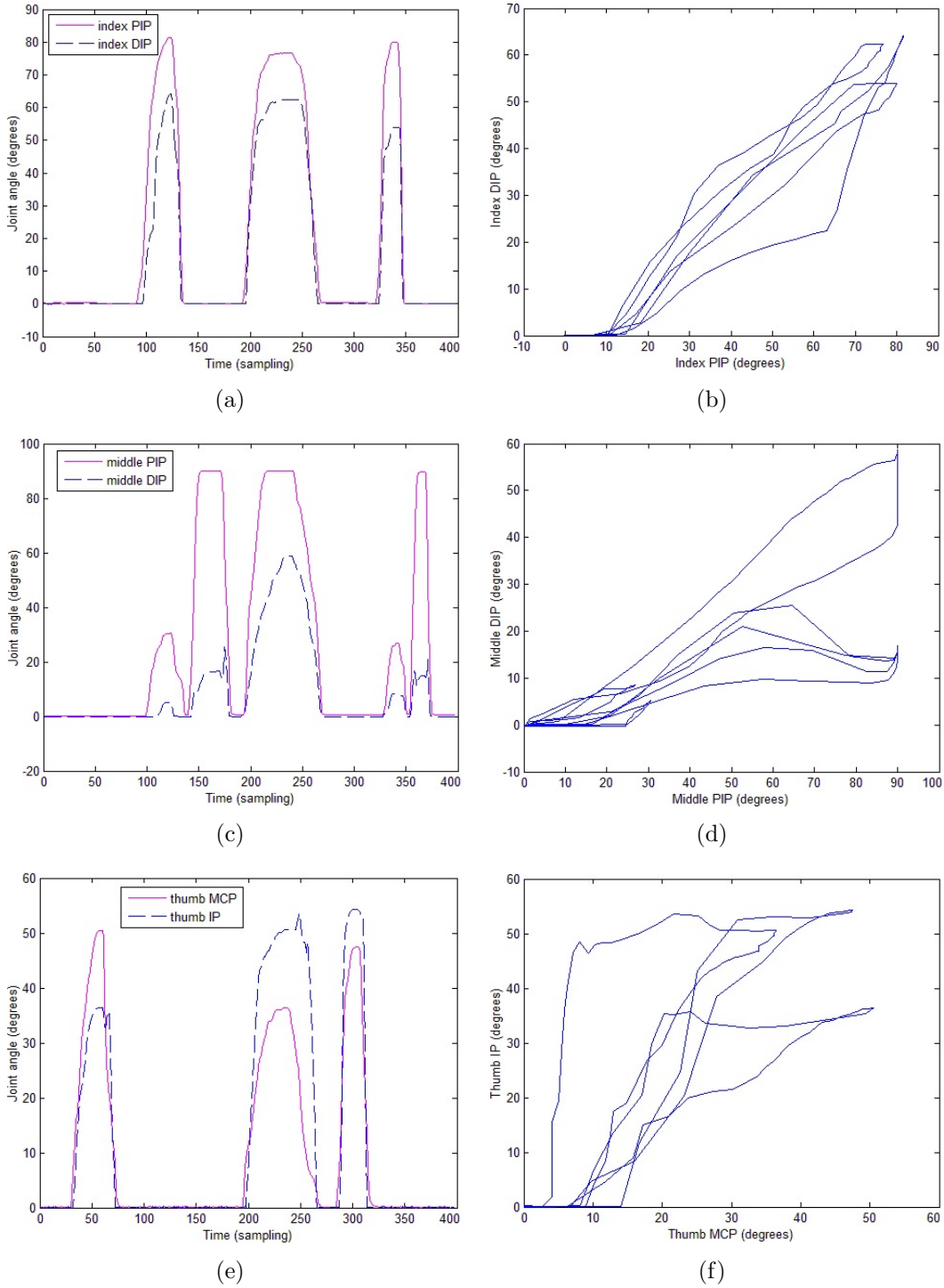

Figure 4.33: Comparison between the DIP and PIP joints of the index/middle finger and the IP and MCP of the thumb during execution of non-grasping digit motion. (a),(c),(e): moving only the thumb during 30-75 and 290-320 sampling time, only the index during 100-140 and 320-350, only the middle during 150-180 and 350-380 and all digits during 200-270. (b),(d),(f): graph of the relation between the corresponding joints of each digit

Chapter 5

Slave System

The concept of anthropomorphic instruments was introduced in Section 3.2, while an exoskeleton that controls the instrument has been developed and presented in Chapter 4. A first attempt to prototype an anthropomorphic instrument was made following the discussion and feedback from the focus group meetings and the results are described in this Chapter. The mapping between the exoskeleton and the instrument is discussed in Chapter 6.

The study of the human hand and the simulation of its joints (Section 4.1) have helped to develop instruments that could reproduce the motion of the hand digits. The surgical instruments are designed in CAD software and 3D printed. The prototypes are scaled up in comparison to the desired product size, in order to facilitate production using limited resources and budget. However, miniaturisation has been attempted to an extent in order to understand consequent challenges. Methods of actuation using SMA springs as well as a cable-driven mechanism have been considered.

The first prototype, actuated by SMA, facilitated an initial exploration of the concept and brought up a number of limitations and design challenges. Its development process is demonstrated and the potential of the materials used and actuation method are assessed. A second prototype, based on a cable-driven actuation mechanism, was developed in order to address the inadequacies of the first prototype. Two ways of routing the cable-driven mechanism have been investigated to optimise the cable control and their correspondence to the joint angle changes. The focus has been on the mechanism design and its kinematics and not the implementation of a complete system. For this reason, only open-loop control has been attempted.

The prototype analysis includes its workspace, capabilities for different grasping configurations and force measurements.

The research presented in Sections 5.1, 5.2, 5.3.1 and 5.3.5 is an edited version of the work published in:

Tzemanaki, A., Dogramadzi, S., Pipe, T., and Melhuish, C. (2012). Towards an anthropomorphic design of minimally invasive instrumentation for soft tissue robotic surgery. In Advances in Autonomous Robotics. Springer, pages 455-456 (with permission from Springer).

Tzemanaki, A., Walters, P., Pipe, A. G., Melhuish, C., and Dogramadzi, S. (2014). An anthropomorphic design for a minimally invasive surgical system based on a survey of surgical technologies, techniques and training. The International Journal of Medical Robotics and Computer Assisted Surgery, 10(3):368-378.

Tzemanaki, A., Burton, T. M., Gillatt, D., Melhuish, C., Persad, R., Pipe, A. G., and Dogramadzi, S. (2014). μAngelo: A novel minimally invasive surgical system based on an anthropomorphic design. In 2014 5th IEEE RAS EMBS International Conference on Biomedical Robotics and Biomechatronics, pages 369-374 (©2014 IEEE).

The research presented in Sections 5.3.2 and 5.3.3 is an edited version of the work that will be published in:

Tzemanaki, A., Fracczak, L., Gillatt, D., Koupparis, A., Melhuish, C., Persad, R., Pipe, A. G., Rowe, E. and Dogramadzi, S. (2016). Design of a multi-DOF cable-driven mechanism of a miniature serial manipulator for robot-assisted minimally invasive surgery. In 2016 6th IEEE RAS EMBS International Conference on Biomedical Robotics and Biomechatronics (accepted) (©2016 IEEE).

5.1 Kinematic Model of the Surgical Instrument

As the final goal is that the instruments have the potential to mimic the surgeon's hand, their kinematics should correspond to the kinematics of the human hand. Using the same model for the five and four-DOF digits as the one described in Section 4.1, the FK for the surgical instrument was solved. The main difference between the human hand and the instrument models is the relative position of the reference frames of each digit. In both models, the base frames of the index and middle fingers are expressed in the frame of the thumb base. Figure 5.1 shows the comparison of the relations between frames in the two models. The rotation matrix of the base of the index/middle finger base {I} with regard to the thumb base {T}, for both models, is:

$$R_{TI} = \begin{bmatrix} 0 & 1 & 0 \\ 0 & 0 & 1 \\ 1 & 0 & 0 \end{bmatrix} \tag{5.1}$$

For the model of the human hand, the translation vectors of the index base {I} and the middle base {M} with regard to {T} are respectively:

$$p_{TI} = \begin{bmatrix} 0 \\ D_Y \\ D_Z \end{bmatrix} \tag{5.2}$$

$$p_{TM} = \begin{bmatrix} \pm D_X \\ D_Y \\ D_Z \end{bmatrix} \tag{5.3}$$

where D_X, D_Y and D_Z are measured parameters of the user's hand, with $-D_X$ for the right and $+D_X$ for the left hand. In Figure 5.1, and for a specific user of the exoskeleton, $D_X = 30$ mm, $D_Y = 0$ mm and $D_Z = 75$ mm.

For the model of the anthropomorphic instrument, the thumb is placed between the index and middle finger. This is necessary as symmetry contributes to the reduction of the shaft diameter that accommodates the instrument digits (and thus, the size of the required surgical incision). The corresponding translation vectors are:

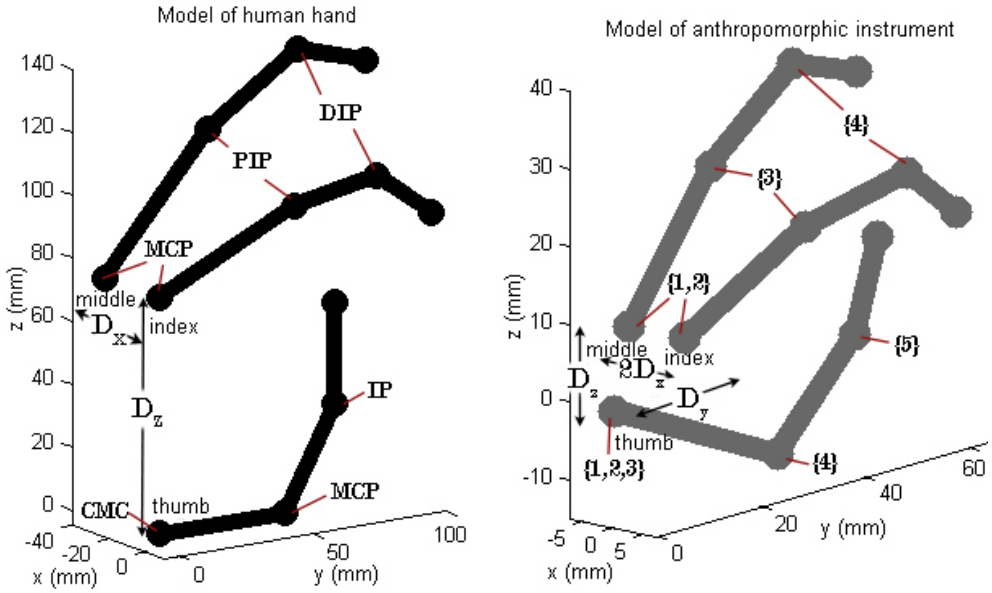

(a) (b)

Figure 5.1: Comparison between the kinematic model of (a) a human hand and (b) the μ`Angelo` instrument

$$p_{ti} = \begin{bmatrix} D_x \\ D_y \\ D_z \end{bmatrix} \qquad (5.4) \qquad p_{tm} = \begin{bmatrix} -D_x \\ D_y \\ D_z \end{bmatrix} \qquad (5.5)$$

where in Figure 5.1, $D_x = 4.5$ mm, $D_y = 8.3$ mm and $D_z = 8.5$ mm. Figure 5.2 shows both models in the same graph for comparison of their size.

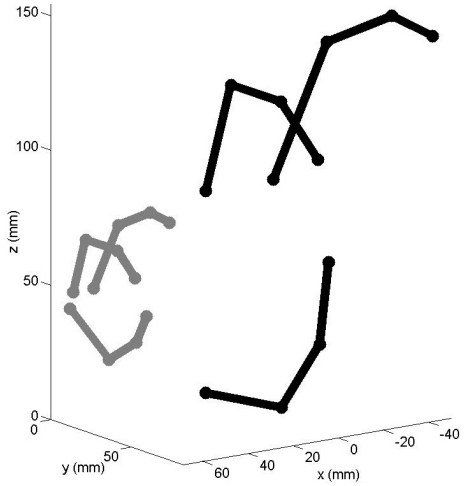

Figure 5.2: Size comparison of the instrument model (in grey) with the model of a human hand (in black)

Table 5.1: Range of the joints of the instruments

Digits	Type of joint	DOFs	Range (degrees)
Index and middle	DIP	1	[0, 90]
	PIP	1	[0, 90]
	MCP	2	[0, 90] [-27, 27]
Thumb	IP	1	[0, 90]
	MCP	1	[0, 90]
	CMC	3	[-180, 0] [-35, 35] [-20, 20]

In order to reduce the diameter of the shaft even further, the first joint of the instrument's thumb (corresponding to the flexion of the CMC) has a range of 180° (instead of 90° as in the human hand). This allows the digit to be folded into the shaft when the instrument enters the patient's abdomen. Figure 5.3 shows the two instruments along with the camera in the folded and extended position.

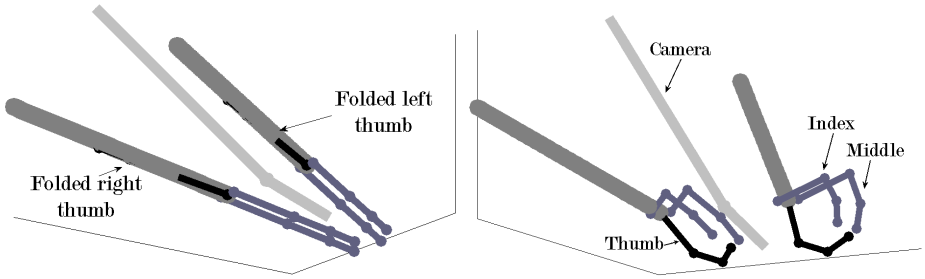

Figure 5.3: Simulation of instruments and camera in a folded and extended position

Table 5.1 summarises the chosen angle range of the different joints of the instrument. An experiment with ten participants (ratio of women to men being 1:1) showed that the opening between their index and middle fingers was never greater than 54° (the minimum being 17° with an average of 33.3° and a standard deviation of 12.3) and hence, the range for the MCP (abduction) joint was chosen to be [-27°, 27°]. Likewise, the ranges of the thumb CMC were chosen to be [-20°, 20°] for the pronation/supination and [-35°, 35°] for the abduction/adduction.

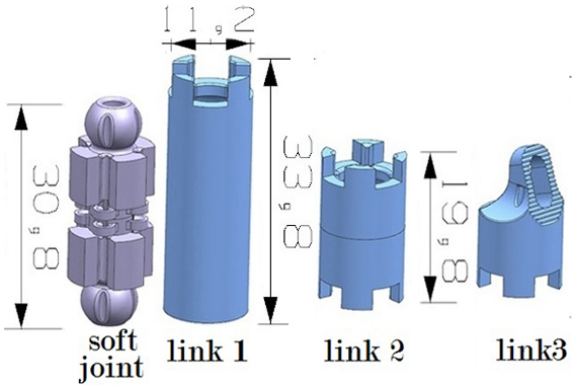

Figure 5.4: Links and joint of the digit in CAD software

5.2 SMA-Driven Prototype

The first (scaled-up) prototype was based on SMA helices which enable actuation by contracting when heated, similar to the methods used by Ho and Desai (2012). As with the exoskeleton, all parts were designed in CAD software (Figure 5.4), manufactured using 3D printing and assembled. However, not all parts are rigid: the robotic digit, with an overall length of 9.7 cm, comprises three rigid links which are connected via two soft links which assume the role of joints. The links were fabricated in a rigid, high temperature-resistant resin (NanoCure, Envisiontec, Germany) and the joints in a soft elastomer material (TangoPlus, Objet Geometries, Israel). The detailed drawings are given in Appendix III.

Each part can accommodate SMA helix actuators (Biometal Micro Helix, Toki, Japan), so that each joint is actuated by one or two antagonistic pairs of helices, which enable motion in one or two DOFs respectively.

The goal of this prototype was to explore the capabilities of this actuating method and to evaluate the use of compliant and rigid manufacturing materials, without developing a complex prototype with the full number of required DOFs employed by the kinematic model and the hand exoskeleton. At the same time, quick manufacturing and actuation of the prototype enabled better demonstration of the concept by visualisation of the instruments in order to understand their configuration and functionality.

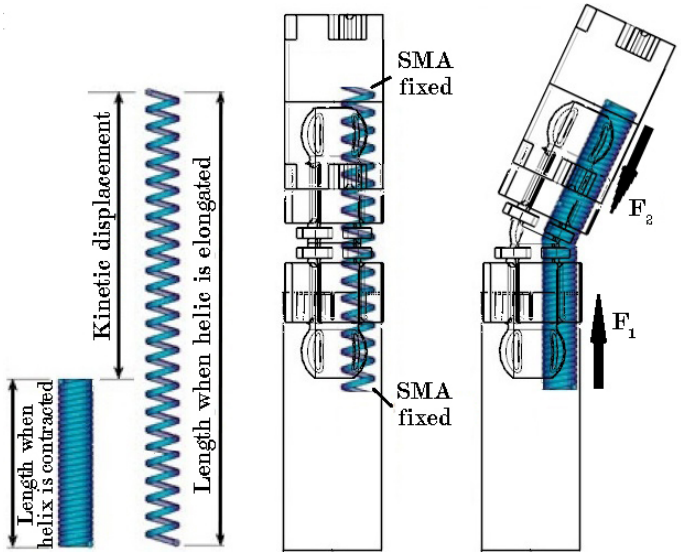

Figure 5.5: Operation of the SMA helix actuator

5.2.1 Material Properties and Operation

SMA actuators have been mentioned in the preceding literature review and briefly in Section 2.3.4. Most commonly, SMA wires are composed of nickel and titanium (thus frequently called NiTi). This alloy has two distinct temperature-dependent crystal structures called martensite (lower temperature) and austenite (higher temperature). When martensite NiTi is heated, at a specific temperature it starts to transform into austenite until the transformation is complete. In the reverse, when austenite NiTi is cooled, it begins to change into martensite until it is completely reverted. This process is characterised by a hysteresis as the temperature range for the martensite-to-austenite transformation is higher than that for the reverse transformation upon cooling (Mihálcz, 2001).

The SMA helix used in this work has a diameter of 0.62 mm and is composed of a 0.15 mm diameter wire. Each helix is elongated (200% of its original size) and is fixed into the structures. When current passes through the helix, it contracts due to the produced heat and two opposite forces F_1 and F_2 from either end result in actuating the joint. This operation principle is shown in Figure 5.5.

However, these actuators can only be used in the direction of contraction. Furthermore, due to the aforementioned hysteresis, the response time can be slow and

the resulting asymmetry complicates the position control. Pairs of helices, acting antagonistically, could improve response times and offer movement in two directions.

5.2.2 Range of Motion

The movement of the soft joint is depicted in Figure 5.6 and is similar to the one demonstrated by Walters and McGoran (2011). Compared to Figure 5.7, it is evident that the rigid structures limit the range of motion.

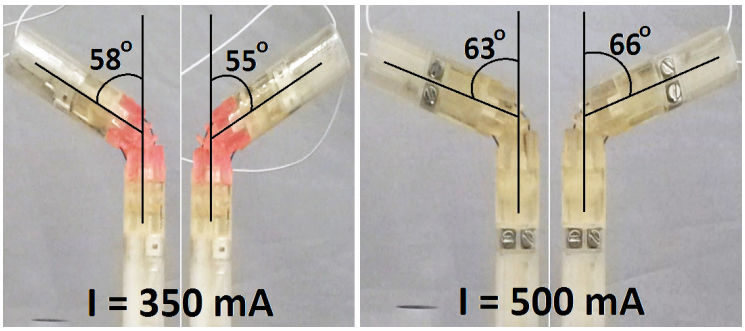

Figure 5.6: Angle measurement for current of 0.35/0.5 A

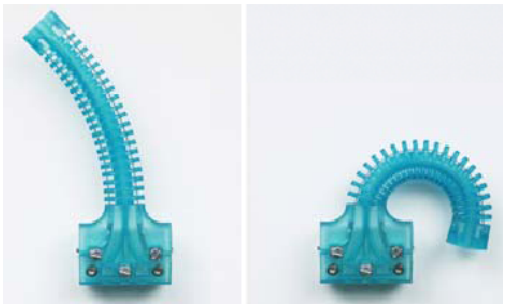

Figure 5.7: Tentacle-like structure actuated by antagonistic SMA (Walters and McGoran, 2011)

The helix, while integrated into the digit, was tested using a maximum of 500 mA, as greater current would considerably shorten the life of the SMA helix. The maximum range of the joint movement can be seen in Figure 5.6: [-58°, 55°] for current of 350 mA and [-63°, 66°] for 500 mA. The particular design is thus advantageous to the one presented by (Ho and Desai, 2012), as the range of motion demonstrated is greater than ±45°.

The asymmetry observed is due to small length differences between the helices

of each side of the digit as well as to the imprecision between the fixing points of each helix on the rigid structures. However, both of these factors can be controlled, while it is also possible to improve the range of the angle generated by changing the length of the helix. For this reason, screw terminals were fitted inside the rigid links to enable the active length of the SMA actuators to be adjusted and achieve the maximum angular displacement.

5.2.3 Degrees of Freedom

As already mentioned, the two pairs of antagonistic helices enable two independent DOFs, by enabling motion in two directions (pitch and yaw). Therefore the joint behaves as a universal joint, having the surface of a hemisphere as workspace.

The greatest advantage of the SMA actuators, apart from their small size, is the fact that they allow independent movement for each joint. As illustrated in Figure 5.8, the joints are not coupled and the second (top) joint moves without affecting the first one. This provides an advantage over cable-driven mechanisms where joint coupling complicates the control.

The combined motion of two digits is demonstrated in Figure 5.9, where the last link (end-effector) is also shown in more detail. The design is such that, when the two end-effectors are united (combinations of thumb-index and thumb-middle finger), their surfaces resemble those of laparoscopic forceps, in order to make the grasp more efficient. Since the control can allow the movement of the last link to be independent from the rest of the digit, it would be possible, when necessary, to use two digits as standard forceps by joining the bottom two links of each digit together and opening and closing the combination of the top links (as suggested in Section 3.3.4).

Three-digit grasping of a sphere (20 mm diameter, 5 g) made of compliant material was attempted (Figure 5.10) with three two-DOF digits, in a layout resembling a thumb, index and middle finger. This experiment was achieved by simply controlling the current passing through the SMA springs, rather than with a user-interface.

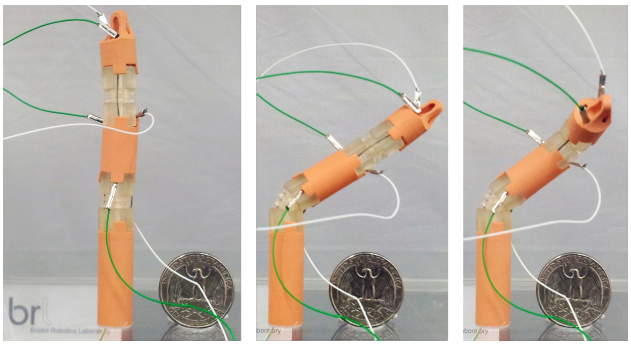

Figure 5.8: Actuation of each joint independently

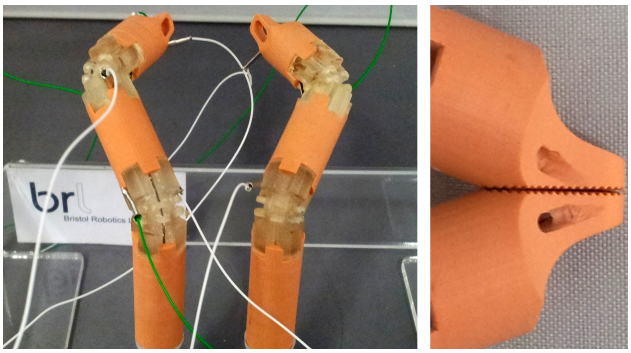

Figure 5.9: Two-digit grasping

Due to the arrangement of the SMA helices in the rigid structures, the type of grasp shown here is not similar to the way human digits grasp an object. Nevertheless, it was observed that the sphere was evenly grasped by all three digits and as a result there was little compression, while no complex control was needed for a secure grasp.

5.2.4 Force Measurement

Producing adequate force is a significant factor when choosing a method of actuation. As discussed in Section 2.3.4, force ranged between 2-9 N is required for pulling tissue

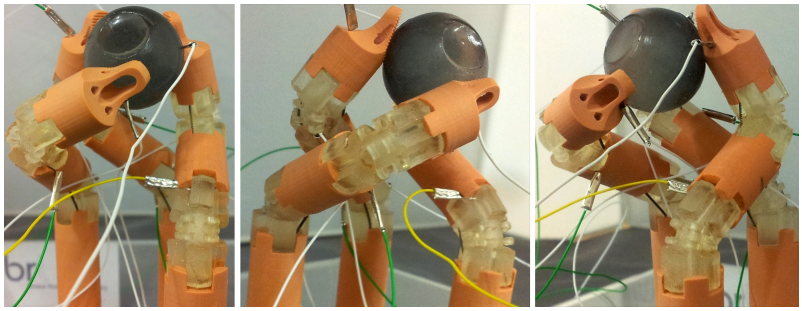

Figure 5.10: Three-digit grasping

(e.g. when suturing), while a force of a maximum of 48 N is needed for grasping a large needle (Madhani et al., 1998). One 20 mm SMA helix can produce 0.2-0.4 N and hence, an SMA only actuated prototype cannot be suitable for such tasks. However, a more complex network of SMAs in combination with other actuating methods could be considered, such as the hybrid actuator in the work by Raghavaiah et al. (2005).

In order to assess the SMA digits, the maximum applied force was measured when using *i*) a single SMA and *ii*) two SMA acting simultaneously. Figure 5.11 shows the set-up of the experiment when using a digit with two links and one joint. For this experiment, a pressure sensor (FS01, Honeywell, USA) with a sensing range of 0-6.7 N and $\pm$0.2 N accuracy was used. In order to distribute the applied force evenly on the sensing area and generate a more consistent output, a 3D printed hemisphere was attached on top of the sensor.

The maximum force observed when activating one SMA, using a current of 350 mA, was 0.18 N. This measurement is approximate and could underestimate the force applied due to the sensor's limitations, as the accuracy of the sensor is 0.2 N and the measuring force is at the low side of the sensing range. Nevertheless, the force is smaller than expected (0.4 N) and inadequate even when two SMA helices were used simultaneously (the maximum observed force was 0.25 N). The configuration of the SMA by Ho et al. (2011) produces a maximum of 1.4 N which the authors consider advantageous for applications in neurosurgery. However, this actuating method seems to be inadequate for the surgical grasping tasks of abdominal surgery, as the number of SMAs appropriate for achieving the required force is such that it would make it impossible to accommodate them in a miniature structure.

Although the miniature size and the relatively low cost of the SMA actuators make them advantageous compared with other methods, the produced force is too limited. Consequently, different actuation methods needed to be explored.

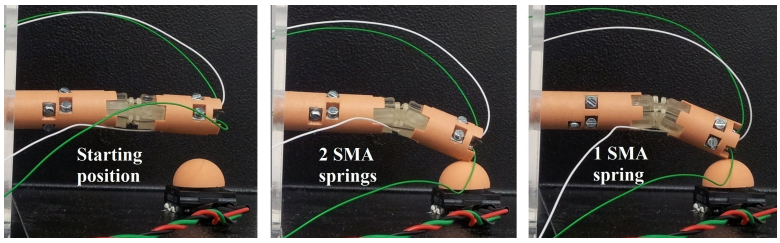

Figure 5.11: Testing the applied force using one and two SMA helices simultaneously

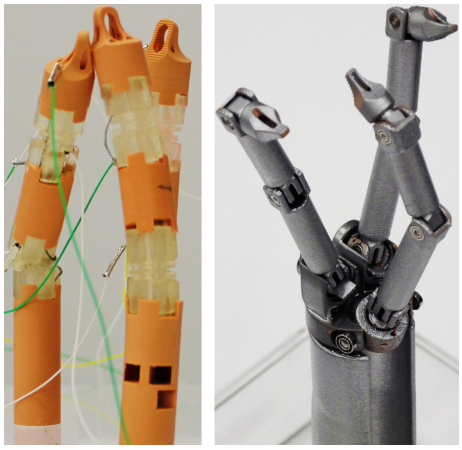

Figure 5.12: SMA and cable-driven versions of the three-digit instrument

5.3 Cable-Driven Prototype

As seen from Table 2.1 (page 48), one of the common methods of actuation is via cable/pulley mechanisms. Although such mechanisms can increase system complexity, produced forces seem closer to the desired range. Building on the knowledge gained from the first prototype, the second version of the anthropomorphic instrument carries a cable-driven mechanism, accommodated inside the digits and through the shaft supporting them. The configuration is kept similar to the first prototype: Figure 5.12 shows a comparison between the two prototypes.

5.3.1 The Instrument Design

The CAD drawings and the dimensions of the various components of the cable-driven prototype are shown in Figure 5.13 (index and middle fingers are identical) and can also be found in Appendix III. The digits were fabricated in VeroWhitePlus (Stratasys, UK), with the texture of the last links of the digits similar to the previous

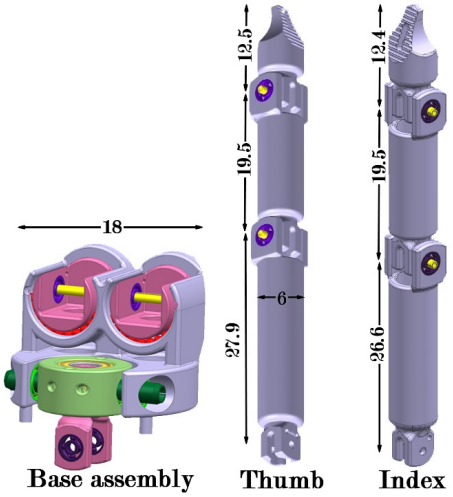

Figure 5.13: Computer-aided design of the structure (all dimensions in mm)

prototype for efficient grasping but with a smaller digit shaft diameter (6 mm).

The instrument has 13 DOFs, following the kinematic model presented in Table 5.1 (page 102) and matching the exoskeleton's motion sensing capabilities. The DIP and PIP joints of the index and middle fingers (Figure 4.1, page 69), as well as the IP and MCP of the thumb, are rotary joints with one DOF each. Figure 5.14 depicts the mechanism of a single DOF joint connecting the last and the middle link of a digit via two bearings and a shaft. Each DOF is controlled by two antagonistic cables attached to one of the links. The MCP joints of the index and middle fingers have two DOFs (flexion and abduction) and thus, each joint is controlled by two pairs of cables acting in two vertical directions. Similarly, the three DOFs of the thumb's CMC joint are controlled by three pairs of cables. The cable routing is analysed in Section 5.3.2. The cables are connected to the motors via springs, pulleys and gears (Section 5.3.3), which are located at the proximal side of the instrument.

As mentioned on page 102, the thumb is initially (before entering the abdomen) inside the shaft and beneath the index and middle fingers in order to make the instrument more compact and to minimise the required incision in the patient's body. Using such an arrangement, the overall diameter of the demonstrated instrument is 18 mm. This diameter is large in comparison with the Da Vinci instrument shaft (diameter of 8 mm). Nevertheless, this instrument includes a higher number of

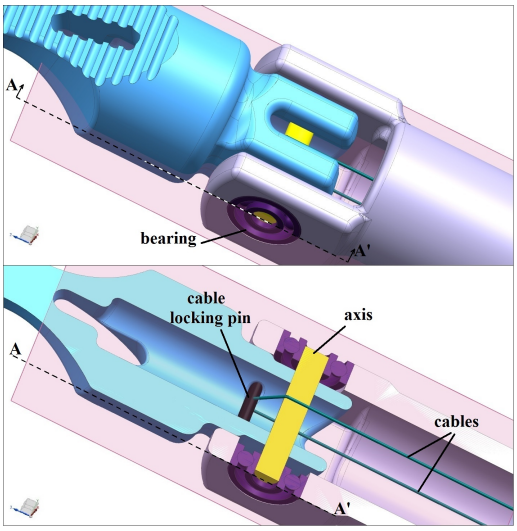

Figure 5.14: Mechanism of one-DOF joint: a) 3D aspect b) cross section

DOFs and increased potential dexterity. Compared to surgical instruments found in the related literature and which are summarised in Table 2.1 (page 48), the 18 mm diameter is a promising miniaturisation for an initial prototype. The three-digit gripper by Luo and Wang (2011) has a shaft diameter of 24 mm, while the '3f9d' hand by Oshima et al. (2010) has a smaller shaft diameter of 12.7 mm but needs assembling after insertion in the patient's abdomen.

After insertion in the abdomen, the thumb is unfolded from inside the shaft so that the surgeon can manipulate the digits. The unfolding is executed with a minimum workspace trajectory. The greatest distance of the compacted thumb from its base during this sequence is 42 mm (Figure 5.15). It is assumed that this distance is safe as, during this process, the abdominal cavity is inflated and hence, there is negligible risk of injuring surrounding tissues.

Different layouts and dimensions of the instrument are also shown in Figure 5.16 in more detail; a) insertion (initial position), b) unfolding, d) manipulation and e) grasping. The extended length of the instrument during insertion is 131 mm (the thumb is folded at this time - Figure 5.16a) and 66 mm when the thumb is unfolded (Figure 5.16c). Although the actual combined workspace of the three digits is more complex, it is possible to approximate it as the 3/4 of a 66 mm radius sphere (Figure 5.15).

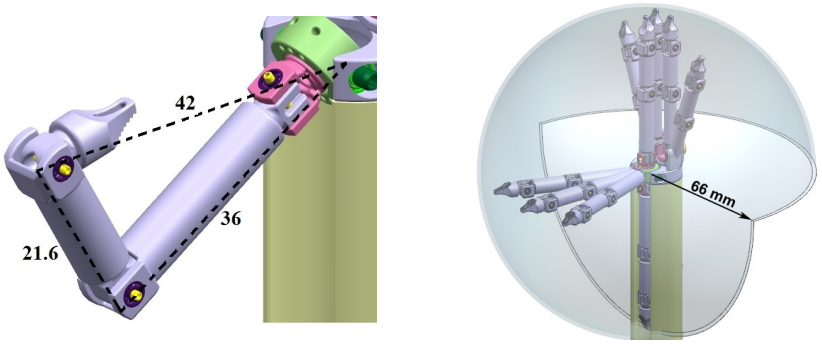

Figure 5.15: Workspace of the instrument during insertion and operation (dimensions in mm and measured to the edge of each body)

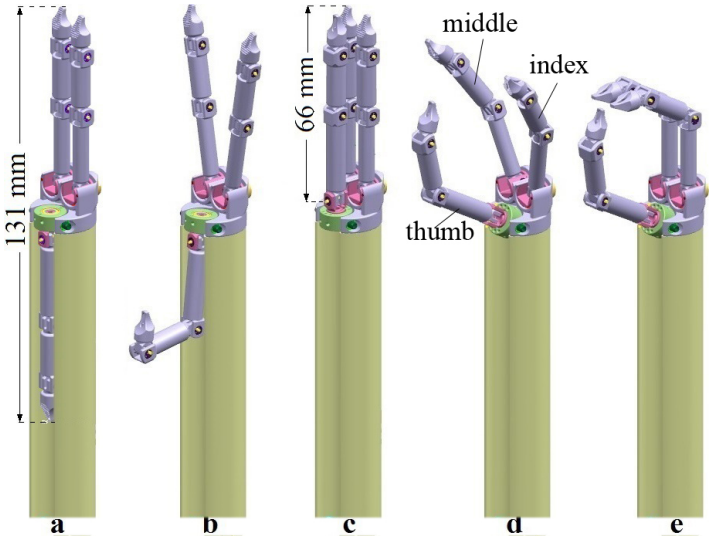

Figure 5.16: Different positions of the instrument

Each digit has a length of 66 mm (about half the length of an average human finger). This length is a compromise between having a miniaturized instrument and giving it the ability to grasp tissues or large organs without inflicting trauma. This is exceptionally important when the organ is sensitive, such as the liver, which could also be as heavy as 4 kg. Pinching it with a small gripper (e.g. forceps) could result in dangerous haemorrhage. Nevertheless, for when precision grasping is required, the digits are miniaturised to such an extent that the last link (7 mm length of grasping surface) of each digit has a similar size to the end-effector of standard surgical forceps (Da Vinci: needle drivers - 5 mm, Maryland forceps - 11 mm, prograsp forceps - 14 mm).

This miniaturisation agrees with suggestions from the focus groups regarding the

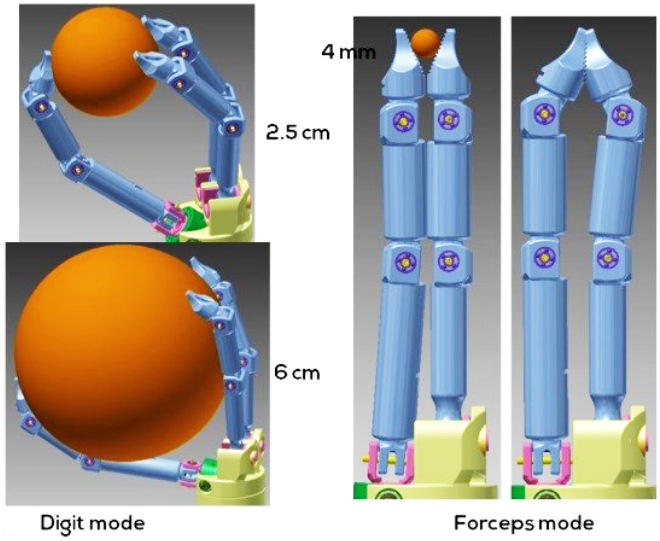

Figure 5.17: Dual grasping mode: the instrument can grasp and manipulate organs and tissues of large diameter as well as perform precision grasps

potential dual grasping mode of the instrument (Section 3.3.4). Figure 5.17 shows grasping modes of the μ`Angelo` end-effector. Spheres of 2.5 cm and 6 cm diameters simulate different size organs.

Illustration of surgical concept

The proposed instrument corresponds to the envisioned concept that was presented in Section 3.2. More specifically, Figures 5.18 (a)-(h) demonstrate the simulated surgical concept, showing insertion and unfolding of the anthropomorphic instruments. The illustrated mesh represents the patient's abdomen. After the instruments enter the inflated abdominal cavity, the thumbs are carefully unfolded, so that they occupy the minimum possible workspace. Then, the surgeon takes control and manipulates the digits (wearing the hand exoskeleton). At the end of the surgery, the digits return to the initial folded configuration and exit the abdominal cavity.

5.3.2 Cable routing

As the index and middle fingers of the instrument are identical and less complex than the thumb, having one DOF less, the description of the cable routing will centre

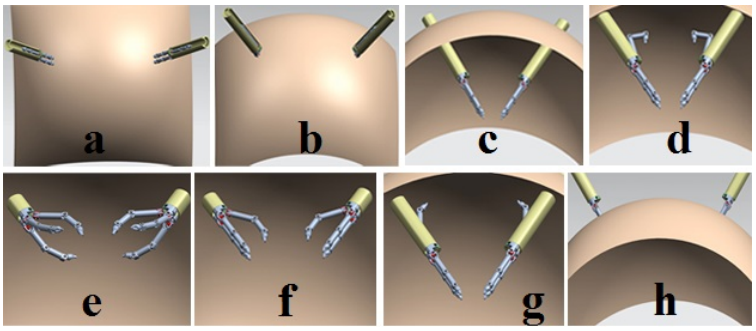

Figure 5.18: Concept of surgery using the anthropomorphic instruments: a)-c) entering the abdomen, d) unfolding of the thumb, e)-f) manipulation by the surgeon, g) folding back the thumb, h) exiting the abdominal cavity

on the thumb. The method of finding the driving equations of the index and middle finger can be derived from that of the thumb.

Unlike some of the aforementioned designs (Arata et al., 2005; Seibold et al., 2008), motors are located outside the instrument and connected to the joints via cables, as this can reduce the cost of the motors, their size being of little importance. As already mentioned, each of the thumb's five DOFs (Figure 5.19) is controlled by an antagonistic pair of cables, with two DOFs having axes that share a common origin ({1} and {3}). Ten cables in total offer potential for high precision when trying to imitate the surgeon's digits using the exoskeleton, as each joint can be actively controlled. Unlike robotic hands and grippers of a larger size, however, the μ`Angelo` digits have a 4 mm inner diameter and thus lack the space to accommodate pulleys (with the exception of the 1 mm joint shafts) or sheaths that will define specific cable paths inside this shaft. In order to achieve manipulation, a unique strategy of variable contact cable topology is hereby used.

Tension in the cables is assumed to be constant and cable elasticity and friction to be negligible. Each pair is attached to the link located above the corresponding joint. This means that for DOF {5} cable 'tJ_5' of the thumb is attached to link '3' (Figure 5.19). Likewise, cable 'tJ_4' is attached to link '2', 'tJ_3' is attached to link 'a', 'tJ_2' to link '1' and 'tJ_1' to link 'b'.

Cable 'tJ_5' has the most complex control because its length is not only affected by DOF {5}, but also by DOF {4}, {3} and {2} (DOF {1} does not contribute to

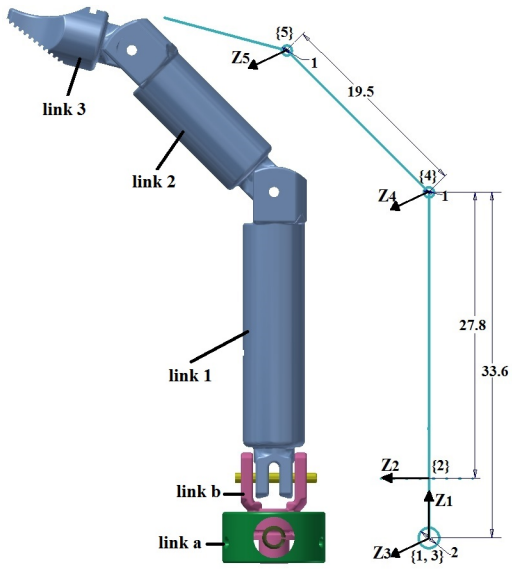

Figure 5.19: Degrees of freedom of the thumb, their axes and names of links ($l_0 = 33.6$ mm, $l_1 = 27.8$ mm, $l_2 = 19.5$ mm)

any change on the length of cables 'tJ_5'-'tJ_2', as its axis coincides with the axis of the digit as well as with the path of these cables). Therefore, the following analysis will focus on cable 'tJ_5', as the equations that drive the other cables can be derived in a similar manner. Section 5.3.2 presents two ways of routing the cable inside the digit as well as the method of deriving the equations of the cable's motion when affected only by DOF {3}, {4} and {5}. Section 5.3.2.4 discusses the effect that DOF {2} has on the same cable.

The following investigation distinguishes between cable routing and the paths that occur during motion. The way that each DOF affects each cable is dependent on the geometry of the digit links. In order to find the path that the cable follows, it is required to determine the key contact points that limit the space that the cable can move in. These points can be found from the design and are shown in Figure 5.20 (c). Generally, Q_x denotes a point Q that is referenced in frame $\{x\}$ and the points can be described as follows:

- P_5: position of the 'locking' pin in link '3', where the cable is attached
- G_5: narrowing of the shaft of link '2'

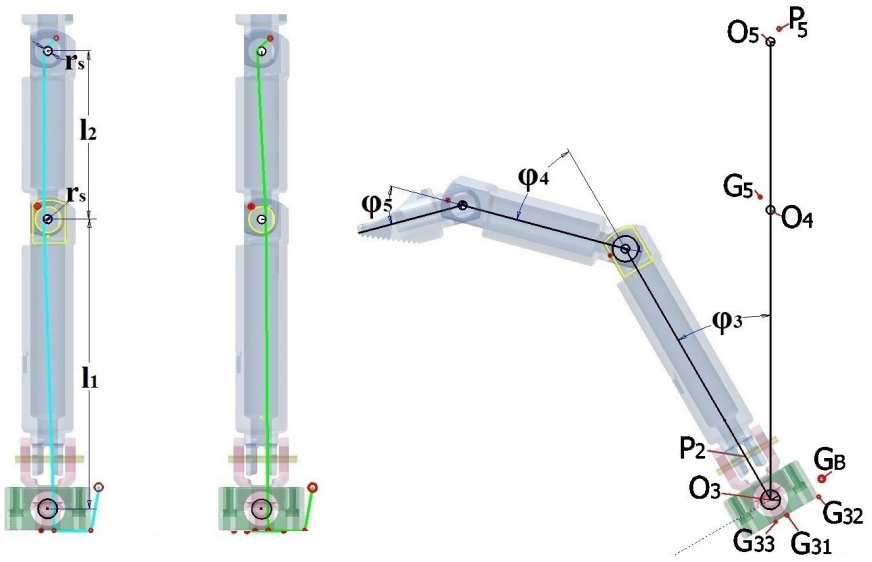

(a) (b) (c)

Figure 5.20: Two ways of cable routing: the cable is tangential to (a) the 'front' of the O_4 shaft or (b) the 'back'. (c) Key contact points of the cable inside the digit

- G_{31} and G_{33}: diametrical points of the through hole of link 'a' (inner diameter of a bearing placed inside this link)
- G_{32}: edge of link 'a'
- G_B: this point belongs to the reference frame of the instrument {B} which is coincident with frame {3} when $\phi_3 = 0$. Cable 'tJ_5' exits the thumb at this point and enters a sheath of constant length until it connects to the actuating motor.

The coordinates of each of these points are given in Table 5.2 with respect to their reference frame (e.g. P_5 is measured with regard to frame O_5. The distances between the reference frames (joint axes) are shown in Figure 5.19, while the shaft of each joint has a radius of $r_s = 0.5$ mm.

Figures 5.20 (a) and (b) demonstrate two different methods of routing the cable that drives DOF {5}. The manipulator shown is at $\phi_2 = \phi_3 = \phi_4 = \phi_5 = 0$. In Figure 5.20 (a), cable 'tJ_5' (cyan) starts at point P_5 and it is then tangential to an arc belonging to the 'front' (left in Figure 5.20) side of the O_5 shaft. It extends vertically until it touches the 'front' side of the O_4 shaft, continues to point G_{31},

Table 5.2: Design parameters

Point	Ref. frame	X(mm)	Y(mm)
P_5	{5}	1	1.5
G_5		1.2	16.3
G_{31}	{3}	0.75	2.5
G_{32}		5	2.5
G_{33}		0.75	2.5
P_2	{2}	1.25	1.5
G_B	{B}	5.95	2.5

through G_{32} and finally exits at G_B. In Figure 5.20 (b), the cable (green) is instead tangential to the 'back' (right in Figure 5.20) side of the O_4 shaft. Below, these two routes are denoted by L_a and L_b, to match the representation of Figures 5.20 (a) and (b).

5.3.2.1 L_a routing

Depending on ϕ_3-ϕ_5, the cable will pass through all or some of the key points of Figure 5.20c. The initial position as described in Figure 5.20 (a) in the previous Section can be symbolised as follows:

$$P_5 \rightarrow S(O_5) \rightarrow S(O_4) \rightarrow G_{31} \rightarrow G_{32} \rightarrow G_B$$

where S(O_i) denotes that the cable is tangential to the O_i shaft ('front' side). There are 22 possible paths for this configuration, denoted by A_i and summarised in Table 5.3. The specific path that the cable follows depends on $\phi_3 - \phi_5$. Using the limits shown in Table 5.4 (ω_{31}-ω_{36} for ϕ_3, ω_{41}-ω_{45} for ϕ_4 and ω_{51}-ω_{512} for ϕ_5), the combinations of $\phi_3 - \phi_5$ can be classified into fifty different categories (denoted AC in the Tables). These limits depend on the geometry of the digit and can also be functions of ϕ_3 and/or ϕ_4. The method of calculating ω_{32} and ω_{43} is shown in Appendix IV as an example. Table 5.5 (page 134) summarises the categories (AC) of different angle combinations. For example, Table 5.3 shows that path A_6 is followed when AC=131, which means that (from Table 5.5) $\phi_3 \in [0, \omega_{31}]$, $\phi_4 \in [\omega_{42}, 90]$ and $\phi_5 \in [0, \omega_{55}]$.

Table 5.3: Paths of cable 'tJ_5' when it passes 'in front of' the O_4 shaft

Symbol	Path	AC*
A_1	$P_5 \rightarrow S(O_5) \rightarrow S(O_4) \rightarrow G_{31} \rightarrow G_{32} \rightarrow G_B$	111
A_2	$P_5 \rightarrow S(O_4) \rightarrow G_{31} \rightarrow G_{32} \rightarrow G_B$	112
A_3	$P_5 \rightarrow G_{31} \rightarrow G_{32} \rightarrow G_B$	113, 122
A_4	$P_5 \rightarrow S(O_5) \rightarrow G_{31} \rightarrow G_{32} \rightarrow G_B$	121
A_5	$P_5 \rightarrow G_5 \rightarrow G_{31} \rightarrow G_{32} \rightarrow G_B$	123, 132
A_6	$P_5 \rightarrow S(O_5) \rightarrow G_5 \rightarrow G_{31} \rightarrow G_{32} \rightarrow G_B$	131
A_7	$P_5 \rightarrow S(O_5) \rightarrow S(O_4) \rightarrow G_{31} \rightarrow G_B$	211, 311
A_8	$P_5 \rightarrow S(O_4) \rightarrow G_{31} \rightarrow G_B$	212, 312
A_9	$P_5 \rightarrow G_{31} \rightarrow G_B$	213, 222, 313
A_{10}	$P_5 \rightarrow S(O_5) \rightarrow G_{31} \rightarrow G_B$	221
A_{11}	$P_5 \rightarrow G_5 \rightarrow G_{31} \rightarrow G_B$	223, 232
A_{12}	$P_5 \rightarrow S(O_5) \rightarrow G_5 \rightarrow G_{31} \rightarrow G_B$	231
A_{13}	$P_5 \rightarrow G_B$	314, 322, 413, 422, 512, 612
A_{14}	$P_5 \rightarrow G_5 \rightarrow G_B$	323, 332, 414, 423, 432, 513, 522
A_{15}	$P_5 \rightarrow S(O_5) \rightarrow G_B$	321, 421, 511, 611
A_{16}	$P_5 \rightarrow S(O_5) \rightarrow G_5 \rightarrow G_B$	331, 431, 521
A_{17}	$P_5 \rightarrow S(O_5) \rightarrow S(O_4) \rightarrow G_B$	411
A_{18}	$P_5 \rightarrow S(O_4) \rightarrow G_B$	412
A_{19}	$P_5 \rightarrow G_{33} \rightarrow G_B$	613, 712
A_{20}	$P_5 \rightarrow G_5 \rightarrow G_{33} \rightarrow G_B$	614, 622, 713, 722
A_{21}	$P_5 \rightarrow S(O_5) \rightarrow G_5 \rightarrow G_{33} \rightarrow G_B$	621, 721
A_{22}	$P_5 \rightarrow S(O_5) \rightarrow G_{33} \rightarrow G_B$	711

*AC: Angle Category (See Table 5.5)

At the initial position, the length of the cable is:

$$L_{A0} = P_5E_5 + \overset{\frown}{E_5F_A} + l_2 + \overset{\frown}{E_4I_A} + I_AG_{31} + G_{31}G_{32} + G_{32}G_B \tag{5.6}$$

where E_5 is a tangential point on the O_5 shaft (Figure 5.21a); F_A is the point where the cable intersects the horizontal from O_5; E_4 is a tangential point on the O_4 shaft; I_A is a second tangential point on the O_4 shaft as the cable extends to G_{31}. The above distances are calculated by:

$$R = \sqrt{x_p^2 + y_p^2} \tag{5.7}$$

$$P_5E_5 = \sqrt{R^2 - r_s^2} \tag{5.8}$$

$$\overset{\frown}{E_5F_A} = \frac{\pi r_s}{180}\left(180 - tan^{-1}\frac{y_p}{x_p} - cos^{-1}\frac{r_s}{R} - \phi_5\right) \tag{5.9}$$

Table 5.4: Limits for ϕ_3, ϕ_4 and ϕ_5

For L_a	**Description**	**Value or Range (deg)**
ω_{31}	$G_{31}G_{32}//G_{32}G_B$	45.58
ω_{32}	$G_5G_{31}//G_{31}G_B$	$f(\phi_4) \in [102.21, 104.39]$
ω_{33}	$I_AG_{31}//G_{31}G_B$	104.91
ω_{34}	$E_5I_A//I_AG_B$	117.44
ω_{35}	$G_5G_{33}//G_{33}G_B$	$f(\phi_4) \in [116.99, 119.06]$
ω_{36}	$E_5G_{33}//G_{33}G_B$	$f(\phi_4) \in [119.46, 119.62]$
ω_{41}	$E_5I_A//I_AG_{31}$	1.98
ω_{42}	$E_5G_5//G_5G_{31}$	5.77
ω_{43}	$E_5G_5//G_5G_B$	$f(\phi_3) \in [3.36, 6.07]$
ω_{44}	$E_5I_A//I_AG_B$	$f(\phi_3) \in [0.03, 1.98]$
ω_{45}	$E_5G_5//G_5G_{33}$	3.39
ω_{51}	$P_5F_A//F_AE_4$	49.79
ω_{52}	$P_5I_A//I_AG_{31}$	$f(\phi_4) \in [49.79, 76.35]$
ω_{53}	$P_5E_5//E_5G_{31}$	$f(\phi_4) \in [47.33, 49.79]$
ω_{54}	$P_5G_5//G_5G_{31}$	$f(\phi_4) \in [47.33, 90]$
ω_{55}	$P_5E_5//E_5G_5$	47.33
ω_{56}	$P_5G_{31}//G_{31}G_B$	$f(\phi_3, \phi_4) \in [49.79, 90]$
ω_{57}	$P_5E_5//E_5G_B$	$f(\phi_3, \phi_4) \in [47.33, 49.86]$
ω_{58}	$P_5G_5//G_5G_B$	$f(\phi_3, \phi_4) \in [84.62, 90]$
ω_{59}	$P_5I_A//I_AG_B$	$f(\phi_3, \phi_4) \in [49.79, 76.35]$
ω_{510}	$P_5G_{33}//G_{33}G_B$	$f(\phi_3, \phi_4) \in [47.33, 84.62]$
ω_{511}	$P_5G_5//G_5G_{33}$	$f(\phi_4) \in [47.33, 84.62]$
ω_{512}	$P_5E_5//E_5G_{33}$	$f(\phi_4) \in [47.33, 49.53]$
For L_b	**Description**	**Value (deg)**
α_{31}	$G_{31}G_{32}//G_{32}G_B$	45.93
α_{32}	$I_BG_{31}//G_{31}G_B$	106.03
α_{33}	$I_BG_{33}//G_{33}G_B$	120.73
α_{51}	$P_5E_5//E_5E_4$	52.73

$$\widehat{E_4I_A} = \frac{\pi r_s}{180}(\omega_{41} - \phi_4) \tag{5.10}$$

$$I_AG_{31} = \sqrt{O_4G_{31}^2 - r_s^2} \tag{5.11}$$

$$O_4G_{31} = \sqrt{x_{G_{31}}^2 + (l_0 + y_{G_{31}})^2} \tag{5.12}$$

$$G_{31}G_{32} = x_{G_{32}} - x_{G_{31}} \tag{5.13}$$

$$G_{32}G_B = \sqrt{O_3G_B^2 + O_3G_{32}^2 - 2 \cdot O_3G_B \cdot O_3G_{32} \cdot \cos\left(tan^{-1}\frac{y_{G_{32}}}{x_{G_{32}}} + tan^{-1}\frac{y_{G_B}}{x_{G_B}} - \phi_3\right)} \tag{5.14}$$

In a similar way, we can derive equations for each category of Table 5.3.

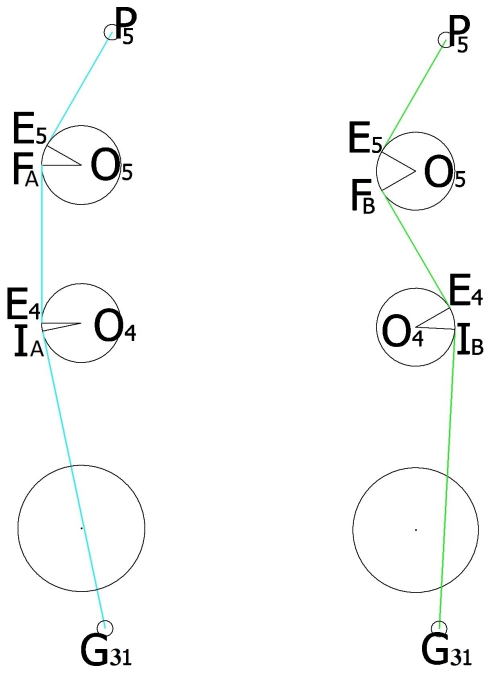

(a) (b)

Figure 5.21: Close up of a) L_a and b) L_b routing when $\phi_3 = \phi_4 = \phi_5 = 0$ (not actual dimensions)

5.3.2.2 L_b routing

The route is similar to the previous case, with the exception that the cable is tangential to the back of the O_4 shaft. This simplifies the computation greatly as there are only eight possible paths (also, eight combinations of $\phi_3 - \phi_5$ in Table 5.5), shown in Table 5.6 (page 135). The cable length at the initial position is:

$$L_{B0} = P_5E_5 + \overset{\frown}{E_5F_B} + F_BE_4 + \overset{\frown}{E_4I_B} + I_BG_{31} + G_{31}G_{32} + G_{32}G_B \tag{5.15}$$

where E_5 is a tangential point on the O_5 shaft (Figure 5.21b); F_B a second tangential point on the O_5 shaft as the cable extends to E_4 which is a tangential point on the O_4 shaft; I_B is a second tangential point on the O_4 shaft as the cable extends to G_{31}. The above distances are calculated:

$$\overset{\frown}{E_5F_B} = \frac{\pi r_s}{180}\left(270 - tan^{-1}\frac{y_p}{x_p} - cos^{-1}\frac{r_s}{R} - cos^{-1}\frac{2r_s}{l_2} - \phi_5\right) \tag{5.16}$$

$$F_BE_4 = 2\sqrt{\left(\frac{l_2}{2}\right)^2 - r_s^2} \tag{5.17}$$

$$\widehat{E_4 I_B} = \frac{\pi r_s}{180}\left(180 - cos^{-1}\frac{2r_s}{l_2} - cos^{-1}\frac{r_s}{O_4 G_{31}} - tan^{-1}\frac{x_{G_{31}}}{x_{G_{31}} + l_0} + \phi_4\right) \quad (5.18)$$

5.3.2.3 Comparison

Despite the computational simplicity of routing L_b, simulation shows that it is not ideal. This can be seen in Figures 5.22 (a) and (b), where the length difference (or cable pull) is shown for both routes for the entire range of one DOF while the other are at constant angles. These graphs essentially simulate the effect of each DOF on the cable as if it was independent from the others. DOF {4} (purple dotted line) almost cancels out the effect that DOF {5} (black dotted line) has on cable 'tJ_5'. Routing L_a seems to be the one that will give the most accurate results as otherwise, it would be possible to achieve more than one set of solutions with the same pull using L_b. For example, for $\phi_2 = 20°$ (for DOF {2} contribution, see Section 5.3.2.4) and $\phi_3 = 135°$, if $\phi_4 = \phi_5$, the cable pull is always 5.85 mm for any value of $\phi_4, \phi_5 \in [0, 90]$.

DOF {3} and {5} have an almost identical effect in both cases, especially when other DOFs are close to 0°. However, for greater angle values, L_a gives a greater (although constant) length difference. This is also beneficial as the resolution is higher and thus positioning can be more precise (a greater cable length range corresponds to the same angular range).

5.3.2.4 Abduction-adduction

DOF {2} of the instrument's thumb, as seen in Figure 5.19 (page 115), is the corresponding abduction/adduction motion of the human thumb and hence its axis is perpendicular to the axes of DOFs {3}, {4} and {5}. In order to include the effect that DOF {2} has on cable 'tJ_5', the superposition principle was applied: the total cable pull is the sum of the difference in length caused individually by DOF {2} and the combination of DOFs {3}, {4} and {5}.

The length difference caused by DOF {2} is calculated starting from shaft O_5, O_4 or point G_5 until point G_{31}, G_B or G_{33}, depending on ϕ_3-ϕ_5 and the path being

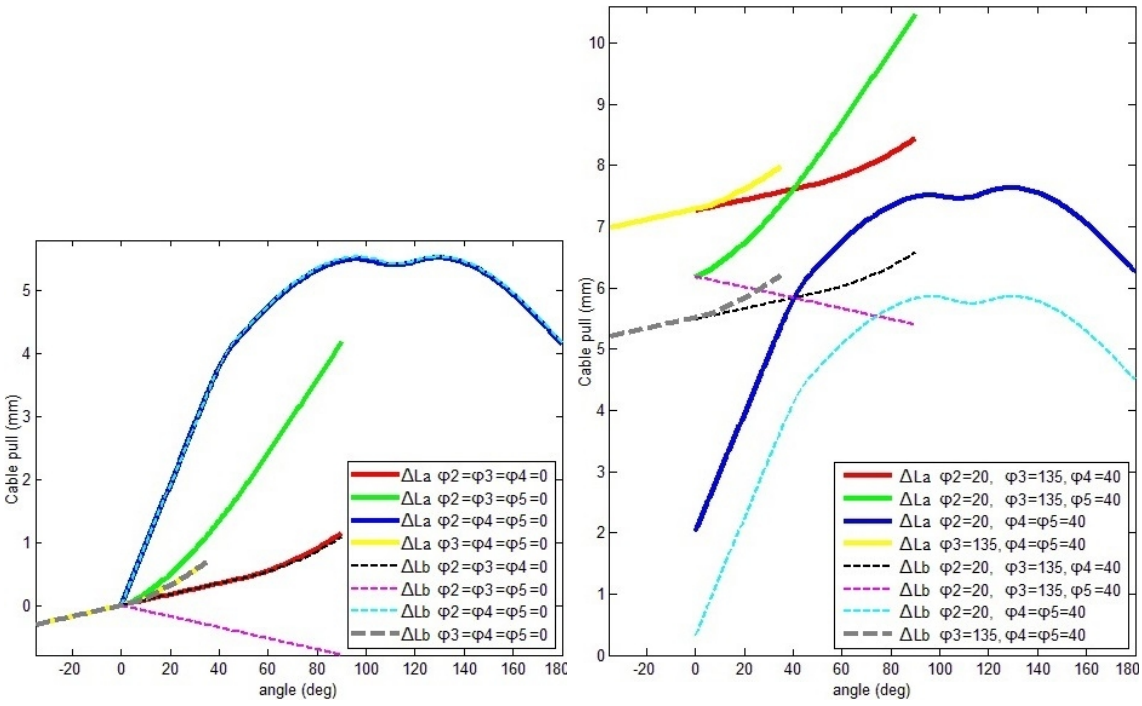

Figure 5.22: Difference in cable pull as a function of one DOF when the others are at (a) 0° and (b) a constant value
L_a - red: DOF {5}, green: DOF {4}, blue: DOF {3}, yellow: DOF {2}
L_b - black: DOF {5}, purple: DOF {4}, cyan: DOF {3}, grey: DOF {2}

followed. For example, for A_{13} and A_{15} the cable length is calculated from shaft O_5 until G_B and subtracted from that of the initial position (when all joints are 0°).

The routing and possible paths for each cable of all the DOFs of the thumb, index and middle fingers are given in Appendix IV.

5.3.3 Pulley and Gear Design

The calculation of the cable pull corresponding to each joint's angular change also contributes to calculations in order to design pulleys that will be attached to the shafts of the motors. Using L_a, we can find that the maximum pull for 'tJ_5' happens at $\phi_2 = 35°$, $\phi_3 = 129.49°$ and $\phi_4 = \phi_5 = 90°$ (path A_{20} in Table 5.3) and is 11.7 mm. The digit at this configuration is illustrated in Figure 5.23. Using this maximum, we can find the pulley radius for best resolution.

The motor that actuates the cable rotates from -90° to 90° (half a circle). For

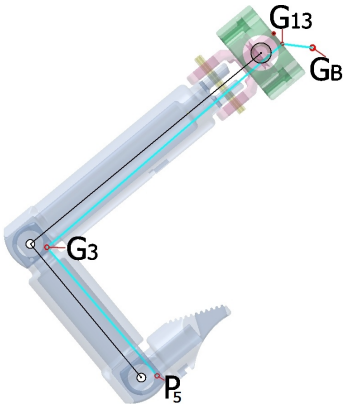

Figure 5.23: Position of the μ`Angelo` 'thumb' at the maximum length difference from the initial position

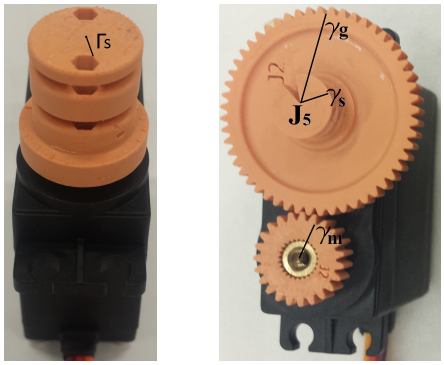

(a) (b)

Figure 5.24: Two designs for cable 'tJ_5' pulleys and gears: using equations (a) (5.19) and (b) (5.20)

maximum resolution, the maximum cable pull should be equal to the half circle circumference:

$$\pi\Gamma_S = \Delta L_{max} \tag{5.19}$$

where Γ_S is the radius of the pulley around which the cable wraps, shown in Figure 5.24 (a). From (5.19), Γ_S= 3.7 mm for cable 'tJ_5'.

For cables 'miJ_1'-'miJ_4' of the index or middle finger this radius would be too small for 3D printing resolution. Therefore, the gears shown in Figure 5.24 (b) have been designed. The radii of these gears can be found using the following equation:

$$\gamma_s = \frac{\Delta L_{max}\gamma_g}{\pi\gamma_m} \tag{5.20}$$

where γ_g is the radius of the gear supporting the pulley that the cable wraps around and γ_m refers to the gear attached to the motor's shaft. For example, for 'tJ_4' it can be calculated that $\Delta L_{max} = 7.4$ mm, and hence, a combination that satisfies (5.20) is $\gamma_s = 4$ mm, $\gamma_g = 8.4$ mm and $\gamma_m = 5$ mm. Table 5.7 (page 135) sums up the maximum cable pull for all cables of the three digits as well as the chosen radii for the corresponding pulleys and gears.

The analysis of Section 5.3.2 allows for control of the cable that bends a joint, taking into account all DOFs acting on it. However, since each joint is controlled by an antagonistic pair of cables, it is important to create a model for both the agonist and antagonist. In some joints of the instrument, the models of the two cables are not a perfect match. This is more evident in the effect that DOF {3} has on 'tJ_5' and 'tJ_4': both cables (agonist/antagonist) of each pair exit at G_B, which is located at one edge of link 'a' (see Figures 5.20 and 5.19 (c)) and hence the cable routings are asymmetric. In order to account for this difference in certain DOFs, the agonist and antagonist could be actuated by two motors instead of one, as in the work by Grebenstein et al. (2011). As this would considerably increase the cost, springs can instead be added between the antagonists and the motors.

5.3.4 Accuracy test

Figure 5.25 depicts a test rig of the instrument (painted in silver) including 13 motors. Each of the cables exits the shaft of the instrument at a specified point and enters a sheath of constant length. The sheaths are fixed both at the exit point of the shaft as well as at the test rig. Each cable exits the sheath and wraps around the pulley of the corresponding motor. The agonist-antagonist parts are wrapped clockwise and counter-clockwise respectively around two runners of the same pulley (the runners can be seen in Figure 5.24).

The sheaths are made of polytetrafluoroethylene (PTFE), which was used for its low friction coefficient. The sheath that was used in the test rig of Figure 5.25 has an inner diameter of 0.71 mm and an outer diameter of 1 mm. Its thin wall made

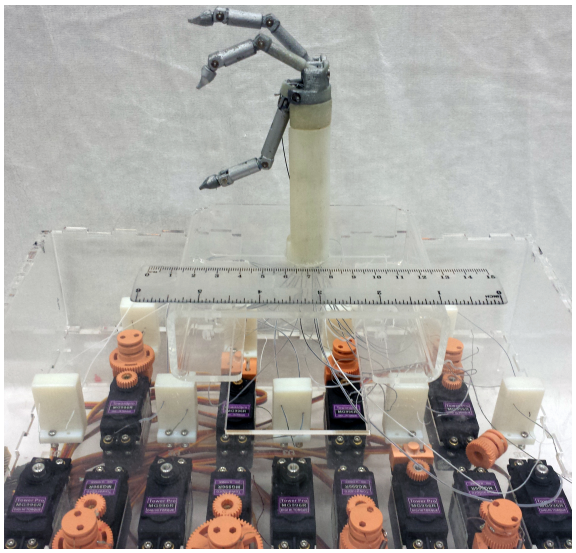

Figure 5.25: Instrument with all cables attached to the gears of the motors

it difficult to effectively pull the cable and move the joint, as even low tension on the cable (e.g. 1 N) would cause the sheath to buckle. For the mechanism to work correctly, the sheaths could not be bent which complicated the process of attaching the cables to the motors. To address this problem, PTFE sheaths of 0.5 mm inner and 1.6 mm outer diameter were used. This challenge delayed the manufacturing process and, consequently, only one digit (index) of the instrument was used for the accuracy tests. As the index and the middle finger of the instrument are identical, testing the theoretical model on the index finger was considered sufficient to identify possible issues.

The digit is shown in Figure 5.26. Eight sheaths deliver the eight cables to the pulleys attached to the gears of the four motors (1.02 Nm maximum torque). A spring with an experimentally measured constant of 530 N/m connects each of the antagonistic cables of DOFs {3} and {4} to the pulleys to account for the difference in maximum possible pull between the agonist and antagonist. The cable used in this experiment is high performance polyethylene fibre with 0.12 mm diameter and 89 N tensile strength.

In order to compare the behaviour of the 3D printed digit to the theoretical calculation, the process followed is similar to the one used for accuracy testing of

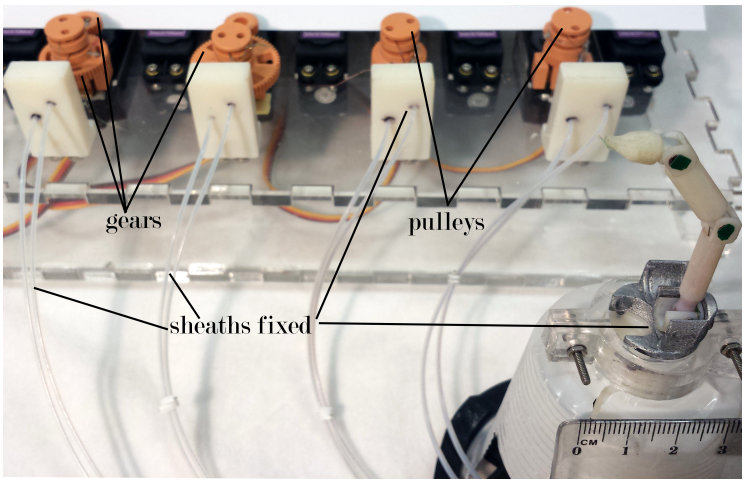

Figure 5.26: One digit of the instrument connected to the pulleys through constant length PTFE sheaths and gears

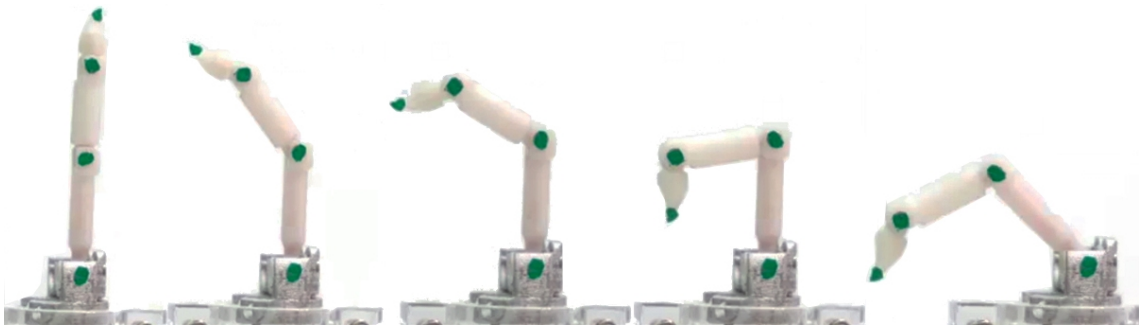

(a) (b) (c) (d) (e)

Figure 5.27: 3D printed digit when $[\phi_1\ \phi_2\ \phi_3\ \phi_4]$ is equal to (a) [0 0 0 0]°, (b) [0 0 45 45]°, (c) [0 0 60 60]°, (d) [0 0 90 90]° and (e) [0 45 45 45]°

the exoskeleton which is illustrated in Figure 4.25 (page 87). Figures 5.27 and 5.28 demonstrate the digit motion when actuating different combinations of its joints. Green markers are placed perpendicular to the axes of all DOFs and at the side and front of the end-effector for tracking them using video processing. The position of each green marker is tracked and links connecting the markers are plotted. Figures 5.29, 5.30 and 5.31 show a comparison of the expected result from simulation (black) and the produced result in hardware (purple). Blue dots indicate the expected end-effector's position and green dots indicate the position of the real end-effector tracked with image processing.

Figures 5.29 (a) and (b) illustrate the flexion of the digit while Figures 5.31 (a) and (b) show the abduction. To simplify the theoretical model, it was assumed that

(a) (b) (c) (d) (e) (f)

Figure 5.28: 3D printed digit when $[\phi_1\ \phi_2\ \phi_3\ \phi_4]$ is equal to (a) [27 0 0 0]°, (b) [0 0 0 0]°, (c) [-27 0 0 0]°, (d) [-27 0 45 45]°, (e) [-27 0 90 0]° and (f) [-27 0 90 90]°

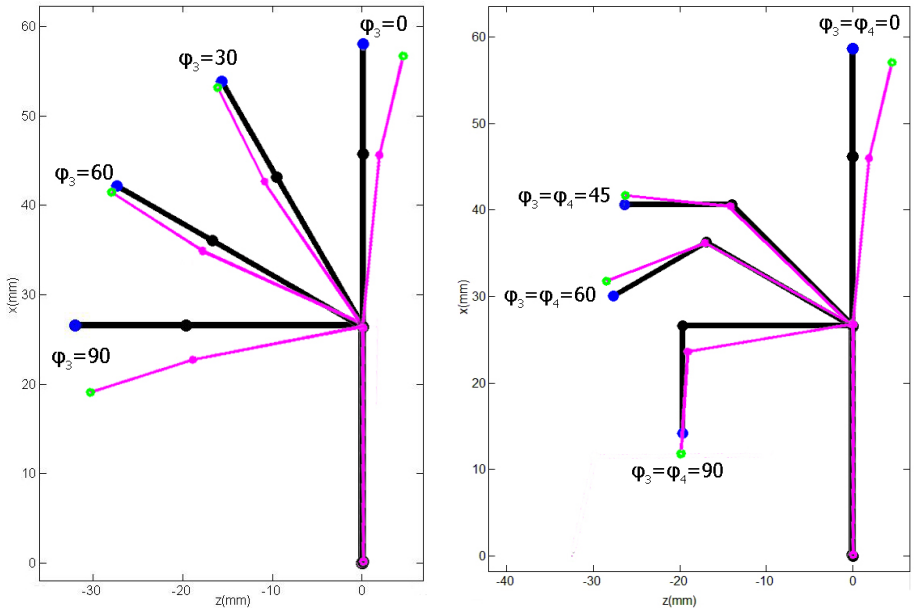

(a) (b)

Figure 5.29: Comparison of the experimental (purple) with the theoretical (black) result when actuating (a) DOF {3} and (b) DOFs {3} and {4}

friction and cable elasticity are negligible. As expected, this affects the joint angle, especially when actuating DOF {2} at the same time as DOFs {3} and {4}. The cable elasticity also introduces a degree of compliance in the joints which can lead to inaccuracy.

Figure 5.29 shows that even at the starting position ($[\phi_1\ \phi_2\ \phi_3\ \phi_4] = [0\ 0\ 0\ 0]°$), the simulated and the 3D printed digit differ slightly at DOFs {3} and {4} by -6° and -8° respectively. This is due to additional tension created by the springs attached

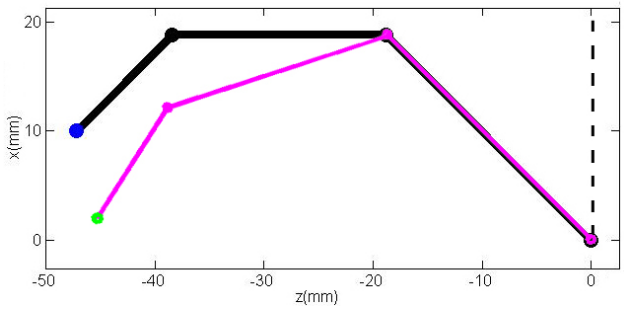

Figure 5.30: Comparison of the experimental (purple) with the theoretical (black) result when $[\phi_1\ \phi_2\ \phi_3\ \phi_4] = [0\ 45\ 45\ 45]^\circ$

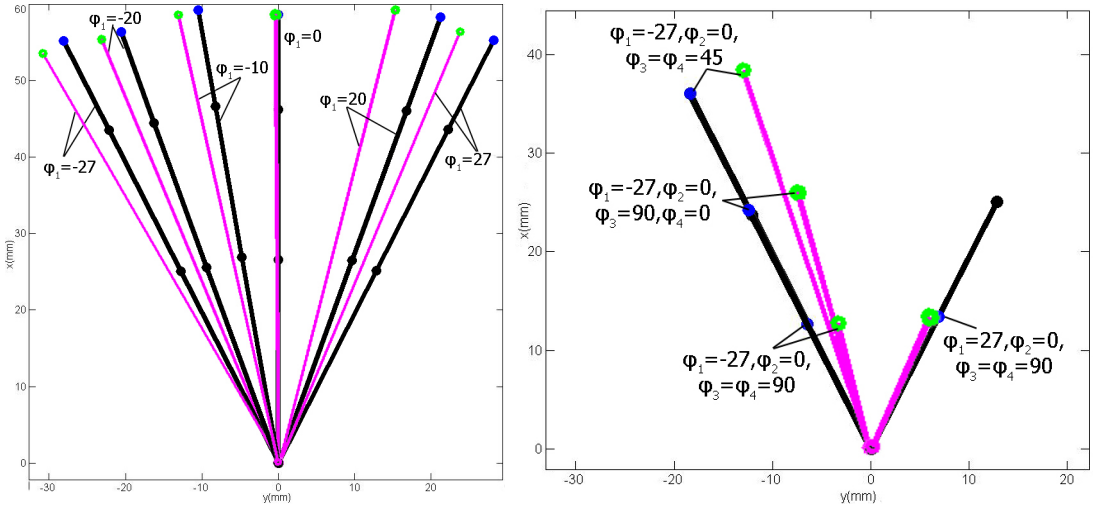

(a) (b)

Figure 5.31: Comparison of the experimental (purple) with the theoretical (black) result when actuating (a) DOF {1} and (b) DOFs {1}, {3} and {4}

to the antagonistic cables responsible for extending the two joints. The springs also contribute to the compliance in the digit. At the disadvantage of increasing the cost and complexity, using one motor per cable (two per DOF) could address this uncertainty. In addition, the resolution could be improved by using higher precision motors and gears with larger diameters and an increased number of teeth. Special cables, for example made of fluorocarbon or titanium alloy, with negligible elasticity could also improve the result.

As the process followed for the comparison includes video and image processing, the links' lengths can appear smaller or larger depending on the distance between the camera and the 3D printed digit. Therefore, the plot of the tracked digit was

enlarged so that the length of link '1' (Figure 5.19) matched that of the corresponding link of the simulated digit. It can be seen from Figures 5.30 and 5.31 (b) that the maximum observed error of the end-effectors' position is 8 mm, with a mean of 3.4 mm ($\sigma = 2.2$). The angular error of each joint depends on the values of the rest of the joints at a given time. For example, the average error over all trials for DOF {1} is 5.6° ($\sigma = 4.3$), whereas in trials that only DOF {1} is actuated the average error is 2.8° ($\sigma = 1.5$). The average error and standard deviation for each DOF is given in Table 5.8 (page 135).

5.3.5 Digit force

Figure 5.32 shows an one digit experiment based on the cable-spring-pulley mechanism, as in the previous experiment. DOFs {4} and {3} (DIP and PIP joint) of the instrument's index finger are actuated to assess force exerted by the end-effector. For this experiment, one cable per each joint was attached via a pulley to the shaft of a motor, while the other cable was connected to a linear spring applying tension to the cable and keeping the joint at 0°.

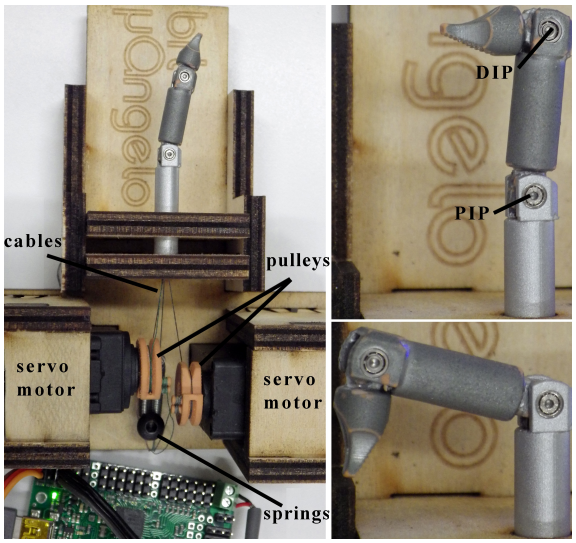

Figure 5.32: Testing one digit of the instrument using two servo-motors

In order to compare the two prototypes (SMA vs. cable and motor), the same method of force measurement as presented in Section 5.2.4 (page 107) was used.

The same pressure sensor (FS01, Honeywell, USA) was used while both DOFs {4} and {3} were active (Figure 5.33). The maximum measured force was 3 N (mean of 10 tests with σ=0.1). The elasticity of the cable and the introduced compliance means that the maximum force could be greater in a rigid mechanism where each cable is connected to an individual motor. However, the force capability of this prototype greatly exceeds the 0.18 N measured with the SMA-driven prototype. It is also within the range of required forces when pulling tissue as determined by (Madhani et al., 1998). This result can be further improved by using motors of a higher maximum torque.

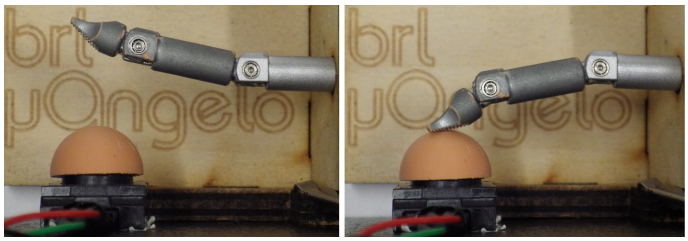

Figure 5.33: Testing the maximum applied force

5.4 Summary

This Chapter has presented the development of surgical instrument prototypes, in response to the second research question of Section 1.1 (page 3). The kinematic model of the instruments has been compared to the model of the human hand and the developed exoskeleton. As discussed on page 38, although evidence is sparse, studies suggest that three digits are adequate for precision grasping tasks (Zhang et al., 2006; Costello and Fragaszy, 1988). This finding is supported with regard to surgery by the participating medical collaborators of this project. In continuation, two instrument prototypes using different actuation methods were investigated.

The first prototype, based on SMA actuation, combines rigid and soft materials and the digit bends around the centre of the soft structures. Such flexible joints are of benefit, compared to a simple hinge, since it constitutes a simple way of creating multiple DOFs. Furthermore, using individual SMA segment helices for each

joint enables independent actuation for each DOF, further simplifying the actuation mechanism. Despite this, and although the range of motion achieved in each DOF, was satisfactory for grasping tasks, use of SMA includes force limitations. A network of such helices in combination with other actuating methods would potentially produce the required forces. However, this would prevent adequate miniaturisation.

In order to overcome the challenges of insufficient grasping force, the following prototype comprised a cable-driven mechanism. For increased dexterity, active actuation of each DOF has been attempted using an antagonistic pair of cables. Apart from the inevitable coupling between joints, the high number of cables required in combination with the narrow digit shafts impose a complex and computationally expensive way of actuation. For this reason, a unique strategy of variable contact cable topology is proposed which is based on the geometry and design of each digit of the instrument. This design strategy could allow further miniaturisation as it does not require pulleys.

The control of the instrument's motion and grasping has not been covered in this study but constitutes future work. The study of the instrument has focused on the mechanism design and its kinematics. The theoretical model of the cable-driven mechanism has been described with two ways of possible cable routing being investigated. The method of deriving the cable pull as a function of the joint angles accounts for all DOFs acting on each cable. Due to resulting asymmetry between the routing of the antagonistic cables of each joint, two motors are required to actuate each joint.

The theoretical model was experimentally tested on the index finger of the instrument, as its design is simpler to realise in hardware and it was considered sufficient to identify potential issues with the design or hardware implementation. In order to reduce the cost, each joint was actuated by only one motor. One of the cables for each of DOFs {3} and {4} was attached to a spring to absorb the difference in cable pull between agonist and antagonist. DOFs {1} and {2} had both cables attached directly to the corresponding pulley as the design of these joints is more symmetric.

The springs introduced a degree of compliance in the digit which, along with cable friction and elasticity, had an impact on the accuracy of the model. Although, the observed error of the end-effector's position had a maximum of 8 mm, better accuracy would be required for surgical tasks. The angular error of each DOF ranged from 0° to 14° depending on the values of the other DOFs, due to the coupling between the joints. The error generally increases when more DOFs are actuated at the same time, as the actuation becomes more complex with friction and elasticity having a greater impact. This error can be minimised by using *i*) two high precision motors for each asymmetric joint instead of the spring-motor system and *ii*) low elasticity and friction cables. It is also possible for the error to be further corrected, intuitively by the user, during teleoperation. As the slave imitates the master, the user of the master can, through visual feedback and interaction with the slave and its environment, update executed motions and grasps to achieve the desired result. This is a process which, at least to a small degree, will occur due to the differences between the lengths of the master's and slave's digit links.

Following the requirements arising from the survey and the focus group meetings, the design of the instrument adopts additional articulation, using an anthropomorphic approach which could facilitate movements occurring during conventional open surgery. At the same time, miniaturisation has been attempted during the design and manufacturing process, which made it possible to address subsequent challenges such as cable routing and actuation. The 18 mm diameter of the instrument shaft is the minimum that can be achieved when the instrument is manufactured by 3D printing, due to the resolution of the machine and the robustness of the material. 3D printing, becoming ever more affordable and accessible, has enabled fast prototyping and optimisation of the design. However, the prototype can have better resolution and smaller size when using other manufacturing methods such as metal sintering and micro-machining.

The cable's tensile strength is also reduced due to friction and buckling of the cable inside the digit. Future iterations of this assembly could utilise 'kink free'

titanium alloy wires with higher tensile strength. The prototype demonstrated a maximum force of 3N, which lies among the desired range of forces used in surgical tasks. This force can be further improved with use of higher torque motors, higher strength cables and manufacturing in different materials (such as surgical steel).

The identified differences between the kinematic models of the master and the slave impose the need for a mapping process between them during teleoperation, which is presented in the following Chapter.

Table 5.5: Categories depending on which range ϕ_3, ϕ_4 and ϕ_5 belong to

	Angle ranges														
$\boldsymbol{\phi_3}$	$[0, \omega_{31}]$								$[\omega_{34}, \omega_{35}]$						
$\boldsymbol{\phi_4}$	$[0, \omega_{41}]$				$[\omega_{41}, \omega_{42}]$			$[\omega_{42}, 90]$	$[0, \omega_{43}]$				$[\omega_{43}, 90]$		
$\boldsymbol{\phi_5}$	$[0, \omega_{51}]$		$[\omega_{51}, \omega_{52}]$	$[\omega_{52}, 90]$	$[0, \omega_{53}]$	$[\omega_{53}, \omega_{54}]$	$[\omega_{54}, 90]$	$[0, \omega_{55}]$	$[\omega_{55}, 90]$	$[0, \omega_{57}]$	$[\omega_{57}, \omega_{58}]$	$[\omega_{58}, 90]$	$[0, \omega_{55}]$	$[\omega_{55}, 90]$	
AC	111		112	113	121	122	123	131	132	511	512	513	521	522	
$\boldsymbol{\phi_3}$	$[\omega_{31}, \omega_{32}]$								$[\omega_{35}, \omega_{36}]$						
$\boldsymbol{\phi_4}$	$[0, \omega_{41}]$				$[\omega_{41}, \omega_{42}]$			$[\omega_{42}, 90]$	$[0, \omega_{45}]$				$[\omega_{45}, 90]$		
$\boldsymbol{\phi_5}$	$[0, \omega_{51}]$		$[\omega_{51}, \omega_{52}]$	$[\omega_{52}, 90]$	$[0, \omega_{53}]$	$[\omega_{53}, \omega_{54}]$	$[\omega_{54}, 90]$	$[0, \omega_{55}]$	$[\omega_{55}, 90]$	$[0, \omega_{57}]$	$[\omega_{57}, \omega_{510}]$	$[\omega_{510}, \omega_{511}]$	$[\omega_{511}, 90]$	$[0, \omega_{55}]$	$[\omega_{55}, 90]$
AC	211		212	213	221	222	223	231	232	611	612	613	614	621	622
$\boldsymbol{\phi_3}$	$[\omega_{32}, \omega_{33}]$								$[\omega_{36}, 180]$						
$\boldsymbol{\phi_4}$	$[0, \omega_{41}]$				$[\omega_{41}, \omega_{43}]$			$[\omega_{43}, 90]$	$[0, \omega_{45}]$				$[\omega_{45}, 90]$		
$\boldsymbol{\phi_5}$	$[0, \omega_{51}]$	$[\omega_{51}, \omega_{52}]$	$[\omega_{52}, \omega_{56}]$	$[\omega_{56}, 90]$	$[0, \omega_{57}]$	$[\omega_{57}, \omega_{58}]$	$[\omega_{58}, 90]$	$[0, \omega_{55}]$	$[\omega_{55}, 90]$	$[0, \omega_{512}]$	$[\omega_{512}, \omega_{511}]$	$[\omega_{511}, 90]$	$[0, \omega_{55}]$	$[\omega_{55}, 90]$	
AC	311	312	313	314	321	322	323	331	332	711	712	713	721	722	
$\boldsymbol{\phi_3}$	$[\omega_{33}, \omega_{34}]$								$[0, \alpha_{31}]$		$[\alpha_{31}, \alpha_{32}]$		$[\alpha_{32}, \alpha_{33}]$		$[\alpha_{33}, 180]$
$\boldsymbol{\phi_4}$	$[0, \omega_{44}]$				$[\omega_{44}, \omega_{43}]$			$[\omega_{43}, 90]$	$[0, 90]$						
$\boldsymbol{\phi_5}$	$[0, \omega_{51}]$	$[\omega_{51}, \omega_{59}]$	$[\omega_{59}, \omega_{58}]$	$[\omega_{58}, 90]$	$[0, \omega_{57}]$	$[\omega_{57}, \omega_{58}]$	$[\omega_{58}, 90]$	$[0, \omega_{55}]$	$[\omega_{55}, 90]$	$[0, \alpha_{51}]$	$[\alpha_{51}, 90]$	$[0, \alpha_{51}]$	$[\alpha_{51}, 90]$	$[0, \alpha_{51}]$	$[\alpha_{51}, 90]$
AC	411	412	413	414	421	422	423	431	432	811	812	821	822	831	832	841	842

See Table 5.4 for the values of each ω_i and α_i limit angle

AC: Angle Category

Table 5.6: Paths of cable 'tJ_5' when it passes 'behind' the O_4 shaft

Symbol	Path	AC*
B_1	$P_5 \rightarrow S(O_5) \rightarrow S(O_4) \rightarrow G_{31} \rightarrow G_{32} \rightarrow G_B$	811
B_2	$P_5 \rightarrow S(O_4) \rightarrow G_{31} \rightarrow G_{32} \rightarrow G_B$	812
B_3	$P_5 \rightarrow S(O_5) \rightarrow S(O_4) \rightarrow G_{31} \rightarrow G_B$	821
B_4	$P_5 \rightarrow S(O_4) \rightarrow G_{31} \rightarrow G_B$	822
B_5	$P_5 \rightarrow S(O_5) \rightarrow S(O_4) \rightarrow G_B$	831
B_6	$P_5 \rightarrow S(O_4) \rightarrow G_B$	832
B_7	$P_5 \rightarrow S(O_5) \rightarrow S(O_4) \rightarrow G_{33} \rightarrow G_B$	841
B_8	$P_5 \rightarrow S(O_4) \rightarrow G_{33} \rightarrow G_B$	842

*AC: Angle Category (See Table 5.5)

Table 5.7: Maximum cable pull and radii (in mm) of corresponding pulleys and gears for cables of the thumb (tJ_x), index and middle fingers (miJ_x)

Digit	Cable	Range (deg)	Max. cable pull	Γ_s	γ_s	γ_m	γ_g
Thumb	tJ_1	[-20, 20]	21.9	7	-	-	-
	tJ_2	[-35, 35]	13.8	4.4	-	-	-
	tJ_3	[0, 180]	14	4.5	-	-	-
	tJ_4	[0, 90]	7.4	-	4	5	8.4
	tJ_5	[0, 90]	11.7	3.7	-	-	-
Index and middle	miJ_1	[-27, 27]	3.1	-	2.3	5.2	12
	miJ_2	[0, 90]	1.24	-	1.2	5.2	15.7
	miJ_3	[0, 90]	3.9	-	2.2	5.4	9.5
	miJ_4	[0, 90]	8.1	-	3.7	5	7.2

Table 5.8: Average angular position error and standard deviation for the DOFs of the instrument's index finger

DOF	Average error	σ
1	5.6°	4.3
2	3.2°	2.6
3	4.6°	4.1
4	8.2°	2.5

Chapter 6

Kinematic mapping of the master-slave system

The preceding two Chapters presented the development of a sensory hand exoskeleton and an anthropomorphic surgical instrument. While control of the slave instrument is not the focus of the research of these two subsystems, this Chapter examines the correspondence of the two from a theoretical point of view. First, the relation of the instrument's design to the human hand and its degree of anthropomorphism is discussed. This description provides insight into the specific differences between the two subsystems and, in combination with the theoretical models presented in previous Chapters, a kinematic mapping between the two is devised. The analysis of the mapping process is presented and the correspondence of the user's hand motion to the instrument is demonstrated. Finally, the proposed mapping method is used to explore simpler configurations of the master and slave subsystems.

The research presented in Section 6.1 is an edited version of the work that will be published in:

Tzemanaki, A., Fracczak, L., Gillatt, D., Melhuish, C., Persad, R., Pipe, A. G., and Dogramadzi, S. (2016). Design of a multi-DOF cable-driven mechanism of a miniature serial manipulator for robot-assisted minimally invasive surgery. In 2016 6th IEEE RAS EMBS International Conference on Biomedical Robotics and Biomechatronics, pages 55-60 ().

6.1 Anthropomorphism in the μAngelo instrument

While the human hand digits (fingers and thumb) are an intricate mechanism, the μAngelo instrument provides a carefully chosen subset of human functional behaviour. Although it resembles a miniature hand, exact imitation would be unnecessary for R-A MIS applications. The following Sections compare the anthropomorphic instrument to the human hand, demonstrating their similarities as well as their differences.

6.1.1 Structure

As mentioned on page 38, the thumb, index and middle fingers are those primarily responsible for carrying out precision tasks in surgery. For this reason, and to keep the diameter of the instrument minimal, the μAngelo surgical instrument has only three digits. The index and the middle finger of the human hand have three phalanges, while the thumb has two. However, the first metacarpal bone of the thumb is ossified in the same manner as the phalanges, and this has led anatomists to regard the thumb as having three phalanges (Gray, 1919). Similarly, each μAngelo digit has three links.

Furthermore, the possibility of attaching different surgical tips for each digit has already been mentioned (page 64). The instrument would then be an extension to the surgeon's hand with added versatility, making it possible to perform tasks that they cannot do using just their hands. This offers the option of independently performing actions that normally require the help of an assistant.

6.1.2 Degrees of Freedom

The index and middle fingers comprise three joints each. Two (DIP and PIP) are responsible for flexion/extension of the phalanges while the MCP controls both flexion/extension and abduction/adduction. The thumb has three joints with the

addition of the CMC which offers pronation/supination, especially important for opposition (Brüser and Gilbert, 1999).

Similarly, each of the index and middle finger of the μAngelo have two 1-DOF joints (flexion/extension) and one 2-DOF (flexion/extension and abduction/adduction). The thumb has three 1-DOF joints and one 2-DOF joint: in Figure 5.19 (page 115), flexion/extension of the μAngelo thumb is indicated with frames {5}, {4} and {3}, abduction/adduction with {2} and pronation/supination with {1}. The joints of the μAngelo are simple rotary joints with range of motion similar to the corresponding joints of the hand, apart from DOF {3} of the thumb which has a range of 180°, so that it can fold into the shaft of the instrument.

6.1.3 Actuation

The digits of the human hand are remotely controlled; there are no muscles inside them. They are located in the palm and in the mid forearm, connected to the bones of the digits by tendons, which pull on and move the joints. The exact actuation system is complex, with each joint action controlled by one or more tendons. These agonist-antagonist tendons control the stiffness of the joints and the accuracy of the movement by co-contraction (Gribble et al., 2003). Likewise, μAngelo is controlled via a cable-driven mechanism which maintains the principal quality of the muscular actuation: each joint is controlled by a pair of antagonistic cables. The 13 rotary DOFs of the μAngelo are actuated by a minimum of 13 motors.

The digits also include smaller bones (sesamoids) which provide a smooth surface for tendons to slide over similarly to the μAngelo cables that slide over the joint shafts.

6.2 Mapping Algorithm

The similarities between the human hand and the surgical instrument can facilitate simple and direct teleoperation. Some methods of kinematic mapping have been

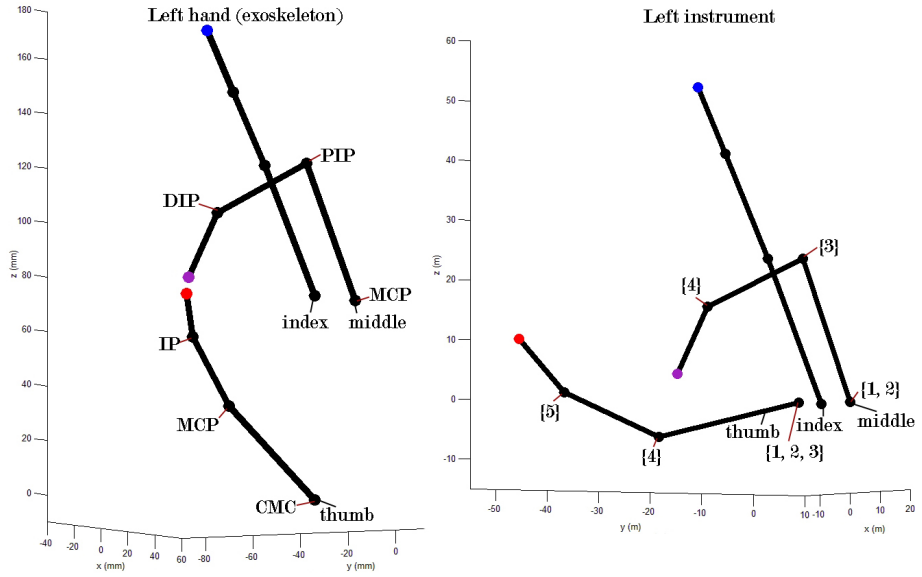

Figure 6.1: Comparison of the user's digit motion with the instruments' digit motion when using simple joint-to-joint mapping. The coloured dots indicate the end-tip of each digit: blue-index, purple-middle and red-thumb

reviewed in Section 2.3.7. From these, joint-to-joint mapping suits anthropomorphic manipulators (Peer et al., 2008), which makes it appropriate for the μ`Angelo` system. However, the differences indicated in the previous Section as well as the comparison of their kinematic models presented in Section 5.1, and specifically in Figure 5.1, (page 101), impose the use of a more complex mapping process between the two. The system, therefore, adopts a hybrid method where both joint-to-joint and point-to-point mapping strategies are used.

Figure 6.1 shows a snapshot of a user's digit motion while attempting a pinch grasp between the thumb and the middle finger (similar to the one in Figures 4.31 (c) and (d), page 92) and compares it to the configuration of the instrument's digits when using simple joint-to-joint mapping. Using this method alone, grasping attempts will fail. This is mainly due to the different position of the thumb's base with respect to the base of the index and middle fingers in the human hand and the instrument, but also due to the dissimilar lengths of the corresponding links, which can also differ between different users.

Nevertheless, the layout of the index and middle finger is similar in the two models and, thus, the mapping for these digits could be a joint-to-joint correspondence.

This can simplify the process greatly, with the thumb being the only digit that needs a complex mapping algorithm.

The proposed mapping process is summarised in Figure 6.2. It is based on the relative position between the fingertips of the user's hand, which can be considered as the vertices of a triangle. The geometry of such a system can be manipulated through triangle similarity to derive a relationship between the relative positions of the instrument's end-effectors. This method will be referred to as Similar Triangles Transform (STT). The data for all three digits are derived from the exoskeleton's sensors and the following steps are subsequently taken:

i) With the angles of the exoskeleton joints as input, the FK model of the surgical instrument is used to derive the positions of the tips of the index and middle finger (p_i and p_m). The aim is to find the position of the thumb's tip p_t.

ii) The FK model of the human hand is modified so that the layout of the digits is similar to the layout of the instrument's digits (vectors (6.1) and (6.2)). It is then used to derive the positions of the tips of the hand digits (p_I, p_M and p_T).

iii) Points p_I, p_M and p_T constitute the vertices of a triangle with sides A, B and C, which can be found as the magnitude of the vector connecting the vertices (equations (6.3)).

iv) A similar triangle with sides a, b and c can be formed for the tips of the instrument's digits. For this reason, the proportion of similarity is taken as the ratio of A to a (a is the magnitude of the vector connecting points p_i and p_m, equations (6.4) and (6.5)).

v) Sides b and c are calculated using the aforementioned ratio λ (equation (6.6)).

vi) The lengths of sides a, b and c are used to determine the location of the instrument's thumb p_t.

vii) As there are multiple solutions for p_t, an additional condition is required. Consequently, the p_t coordinate on the z axis (z_t) is calculated from the corresponding coordinate of the hand model using ratio λ (equations (6.7)).

viii) Conditions for z_t are derived and checked that they are satisfied (equations (6.19)).

ix) The orientation R_t is derived using the FK model of the instrument's thumb and the angles of the exoskeleton joints.

x) The combination of R_t and the calculated p_t is the input into the IK model of the instrument's thumb to derive the required values of its joints.

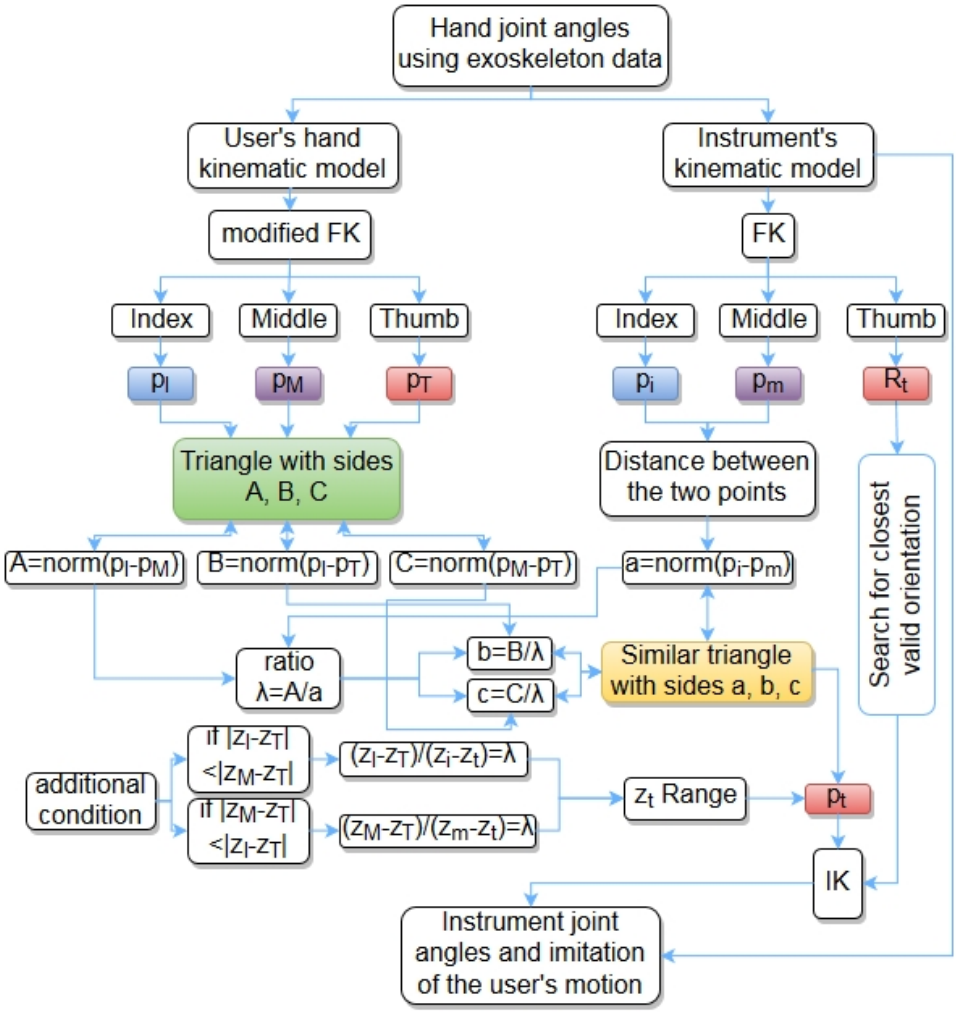

Figure 6.2: Similar Triangle Transform (STT) method for mapping the user's digit joint angles to the instrument's joint angles in order to mimic the user's hand digit motion

For the modification of the FK of the human hand, the translation vectors of the frames of the index and middle fingers with regard to the frame of the thumb are replaced. In Section 5.1 the translation vectors were given as:

$$p_{TI} = \begin{bmatrix} 0 \\ D_Y \\ D_Z \end{bmatrix} \qquad (5.2) \qquad p_{TM} = \begin{bmatrix} \pm D_X \\ D_Y \\ D_Z \end{bmatrix} \qquad (5.3)$$

For the mapping process, these vectors are replaced with:

$$p'_{TI} = \begin{bmatrix} -\frac{D_X}{2} \\ D_Y \\ D_Z \end{bmatrix} \qquad (6.1) \qquad p'_{TM} = \begin{bmatrix} \frac{D_X}{2} \\ D_Y \\ D_Z \end{bmatrix} \qquad (6.2)$$

Without this modification, the position of the thumb's tip is located at the far side of the index finger (left hand). Conversely, vectors (6.1) and (6.2) place the tip of the thumb in an area between the index and middle finger, which is beneficial due to the layout of the instrument's digits. Although the distance between the tip of the thumb and the other two fingertips changes, this modification is paramount at a later stage of the algorithm, when using the z coordinate of the thumb's tip's position to calculate the desired p_t as will be shown from the conditions (6.7).

Figure 6.3 shows the two similar triangles formed with the tips of the digits as vertices, coloured with green (modified human hand) and yellow (instrument). The sides of the green triangle can be calculated as follows:

$$\begin{cases} A = \sqrt{(x_I - x_M)^2 + (y_I - y_M)^2 + (z_I - z_M)^2} \\ B = \sqrt{(x_I - x_T)^2 + (y_I - y_T)^2 + (z_I - z_T)^2} \\ C = \sqrt{(x_M - x_T)^2 + (y_M - y_T)^2 + (z_M - z_T)^2} \end{cases} \qquad (6.3)$$

where (x_j, y_j, z_j) are the coordinates of p_j, for $j = I, M, T$. Similarly, side a of the

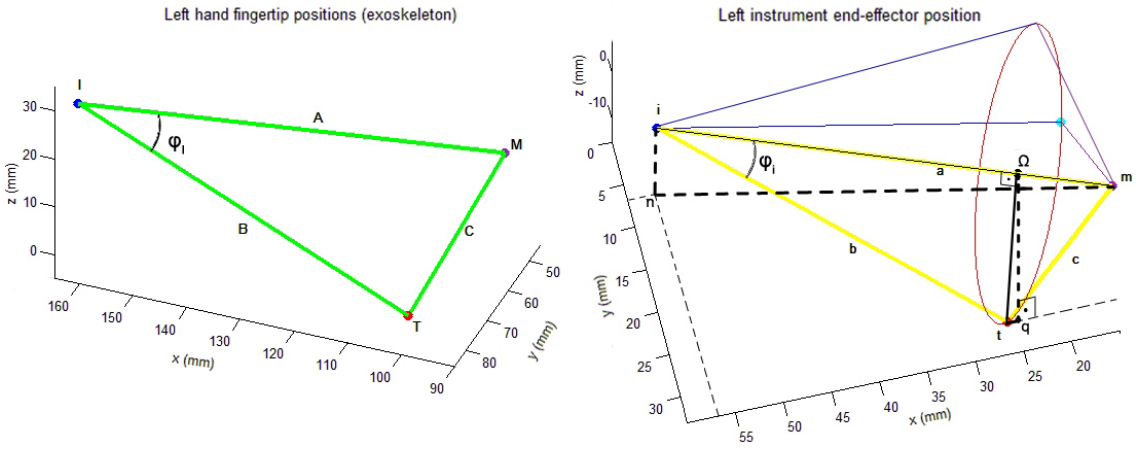

(a) (b)

Figure 6.3: Triangles formed with the tips of the digits as vertices: (a) I, M and T for the user's index, middle and thumb (green triangle) and (b) i, m and t for the instrument (yellow triangle). In (b), two solutions for z_t satisfy the polynomial (6.20) and are represented with red and cyan coloured dots

yellow triangle is calculated by:

$$a = \sqrt{(x_i - x_m)^2 + (y_i - y_m)^2 + (z_i - z_m)^2} \tag{6.4}$$

where (x_j, y_j, z_j) are the coordinates of p_j, for $j = i, m$. The similarity proportion is chosen as:

$$\lambda = \frac{A}{a} \tag{6.5}$$

and, therefore, sides b and c of the yellow triangle can be derived:

$$\begin{cases} b = \frac{B}{\lambda} \\ c = \frac{C}{\lambda} \end{cases} \tag{6.6}$$

In order to limit the possible solutions for p_t the following assumption is made:

$$\begin{cases} if \quad |z_T - z_I| \leq |z_T - z_M| \text{: } \frac{z_T - z_I}{z_t - z_i} = \lambda \Rightarrow z_t = z_i + \frac{z_T - z_I}{\lambda} \\ if \quad |z_T - z_M| < |z_T - z_I| \text{: } \frac{z_T - z_M}{z_t - z_m} = \lambda \Rightarrow z_t = z_m + \frac{z_T - z_M}{\lambda} \end{cases} \tag{6.7}$$

However, this solution for z_t may not always be possible as the following set of

equations must be satisfied at the same time:

$$\begin{cases} (x_i - x_t)^2 + (y_i - y_t)^2 = b^2 - d^2 \\ (x_m - x_t)^2 + (y_m - y_t)^2 = c^2 - e^2 \end{cases} \tag{6.8}$$

where $d = z_i - z_t$ and $e = z_m - z_t$. It can be observed from Figure 6.3 that two cones are formed with vertices p_i and p_m and a common base of radius Ωt, where $\Omega(x_\omega, y_\omega, z_\omega)$ is the centre of the circular base. For equations (6.8) to be satisfied, z_t must belong to the area that is covered by the base of the cones. The heights $i\Omega$ and $m\Omega$ are aligned with side a of the yellow triangle and constitute the axis of the two cones. By finding Ωq (projection of Ωt on z axis), the allowed range of z_t can be calculated. Angle ϕ_i has the same measure as angle ϕ_I due to the similarity of the triangles. From cosine law:

$$\phi_i = cos^{-1} \frac{A^2 + B^2 - C^2}{2AB} \tag{6.9}$$

It follows that

$$\Omega t = |b \sin(\phi_i)| \tag{6.10}$$

$$i\Omega = |b \cos(\phi_i)| \tag{6.11}$$

The axis (side a) of the two cones can be described as a line in 3D space using the following parametric equations:

$$\begin{cases} x = (x_m - x_i)t + x_i \\ y = (y_m - y_i)t + y_i \\ z = (z_m - z_i)t + z_i \end{cases} \tag{6.12}$$

where t is a parameter expressing a point on the line. If $t = 0$ when $(x, y, z) \equiv (x_i, y_i, z_i)$ and $t = 1$ when $(x, y, z) \equiv (x_m, y_m, z_m)$, then $(x, y, z) \equiv (x_\omega, y_\omega, z_\omega)$ for

$t = t_\omega$ which can be calculated as:

$$t_\omega = \frac{i\Omega}{a} \tag{6.13}$$

From equation (6.12), z_ω can be calculated:

$$z_\omega = (z_m - z_i)t_\omega + z_i \tag{6.14}$$

It can also be seen from triangles nim and $q\Omega m$, in Figure 6.3, that $n\hat{i}m = q\hat{\Omega}m$. Using cosine law:

$$q\hat{\Omega}m = cos^{-1}(\frac{a^2 + in^2 - nm^2}{2a \cdot in}) \tag{6.15}$$

where $in = |z_i|$ and $nm = \sqrt{(x_m - x_i)^2 + (y_m - y_i)^2 + z_m^2}$. When point t is at the lowest possible point, the projection Ωq is aligned with plane (i, m, t) and, thus, equation (6.15) is used to find angle $q\hat{\Omega}t$:

$$q\hat{\Omega}t = 90 - q\hat{\Omega}m \tag{6.16}$$

Finally, it can be calculated that

$$\Omega q = \Omega t \cos(q\hat{\Omega}t) \tag{6.17}$$

The vertical distance Ωq can be used to derive the limits for z_t:

$$z_t \in [z_\omega - \Omega q, z_\omega + \Omega q] \tag{6.18}$$

Subsequently, it is examined whether the calculated value of z_t (equation 6.7) satisfies the range (6.18). Depending on the result, its value may change to the

upper or lower limit:

$$\begin{cases} if\, z_t < z_\omega - \Omega q \Rightarrow z_t = z_\omega - \Omega q \\ if\, z_t > z_\omega + \Omega q \Rightarrow z_t = z_\omega + \Omega q \end{cases} \tag{6.19}$$

With z_t known, equations (6.8) can be combined to give the following polynomial:

$$(k_2^2 + 1)y_t^2 + 2(x_i k_2 - k_1 k_2 - y_i)y_t + k_1^2 - 2k_1 x_i + x_i^2 + y_i^2 - b^2 + d^2 = 0 \tag{6.20}$$

where $k_1 = \frac{x_i^2 - x_m^2 + y_i^2 - y_m^2 - b^2 + c^2 + d^2 - e^2}{2(x_i - x_m)}$ and $k_2 = \frac{y_i - y_m}{x_i - x_m}$. The roots of the polynomial (represented with red and cyan coloured dots in Figure 6.3) are the solution for y_t, while x_t can be calculated by:

$$x_t = k_1 - k_2 y_t \tag{6.21}$$

Figures 6.4 (a)-(c) show the layout of the instrument's digits as the result of the STT mapping method and Figure 6.5 demonstrates the similarity between the two triangles. In comparison with Figure 6.1, the digits of the instrument go beyond simply indicating the intention of the user: they are representative of the user's digits by imitating their layout but are also set for successful grasping. The angle vectors of the exoskeleton joints of Figure 6.4 and the joints of the surgical instrument post-mapping are respectively:

$$\begin{cases} \theta_I = [3.55\ 25.13\ 1.95\ 0.02]^{\circ\, T} \\ \theta_M = [8.77\ 25.45\ 89.98\ 41.97]^{\circ\, T} \\ \theta_T = [0\ 0.06\ 75.66\ 34.59\ 23.96]^{\circ\, T} \end{cases} \tag{6.22}$$

$$\begin{cases} \theta_i = [3.55\ 25.13\ 1.95\ 0.02]^{\circ\, T} \\ \theta_m = [8.77\ 25.45\ 89.98\ 41.97]^{\circ\, T} \\ \theta_t = [0\ 23.77\ 44.22\ 106.54\ 75.49]^{\circ\, T} \end{cases} \tag{6.23}$$

The same process can be used, if the correspondence between master and slave for the index and middle finger changes. For example, Figure 6.6 (a) shows the layout of the slave when the PIP and flexion of MCP joints of the index and middle fingers are 2/3 of the value of the equivalent exoskeleton joints. In comparison with

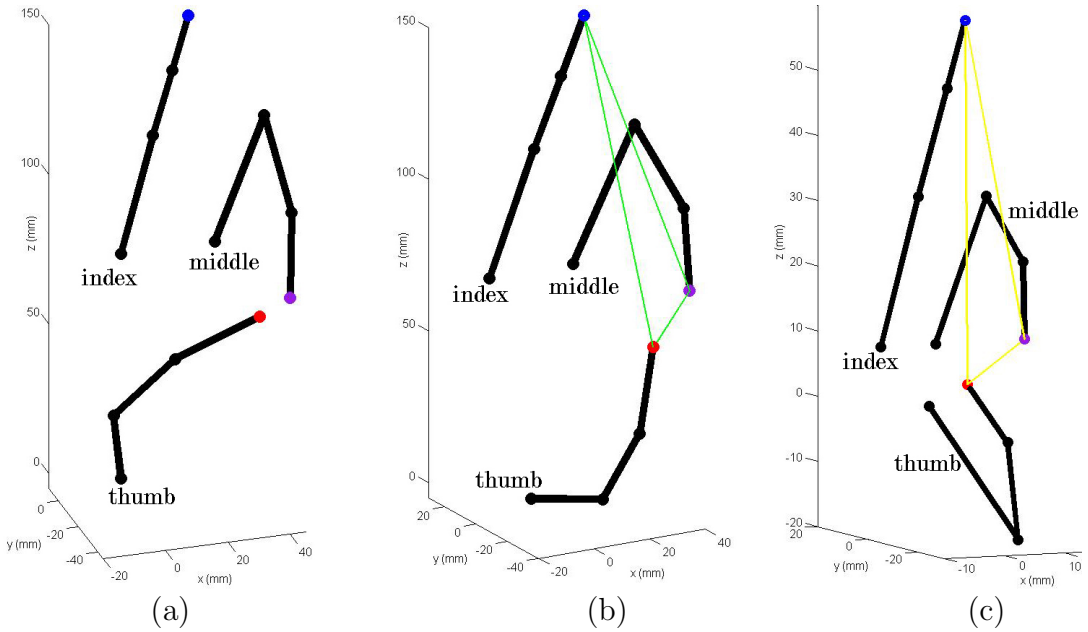

Figure 6.4: Comparison of (a) the user's digits' pose with (b) the modified hand model and (c) the instruments' digits' pose after the mapping process

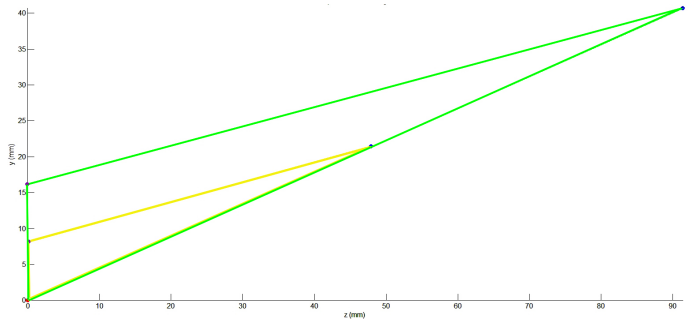

Figure 6.5: Demonstration of similarity of the triangles that are formed between the digit tips of the master (green) and the slave (yellow)

Figures 6.6 (b) and (c) where the layout of instrument and the human hand are shown respectively, the index and middle finger imitation of Figure 6.6 (a) is not as accurate. Nevertheless, the joint angles of the thumb are not at the extremes of their range and thus, impossible positions due to hardware limitations can be more easily avoided. The PIP joint of the instrument's thumb is at 106° in Figure 6.6 (b) and 43° in 6.6 (a), while this joint in the 3D printed prototype has a range of

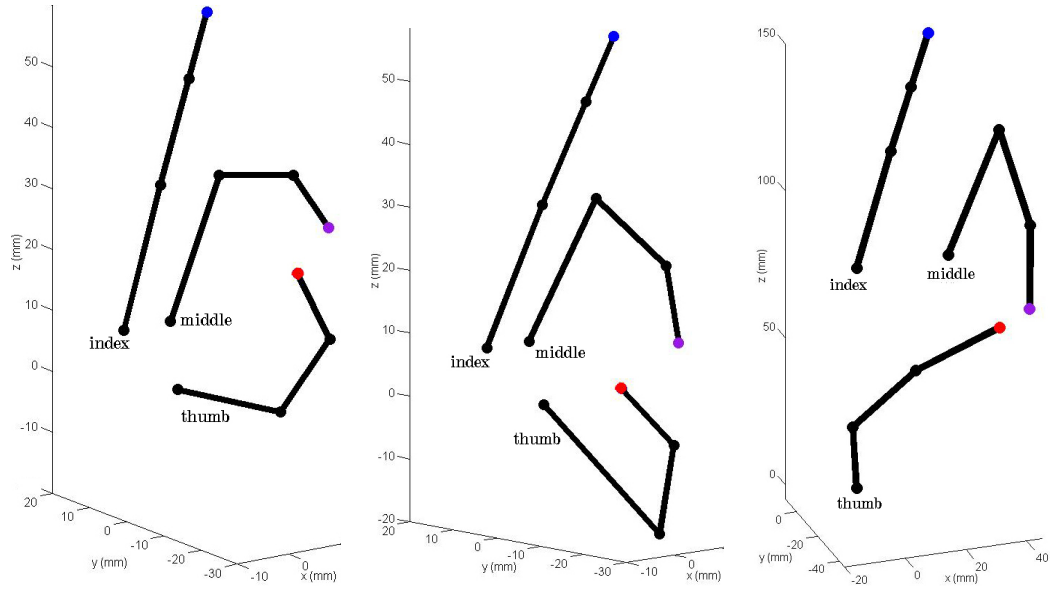

(a) (b) (c)

Figure 6.6: Comparison of the digit layout for (a) the instrument when the PIP and flexion of MCP of the index and middle fingers are equal to 2/3 of the value of the equivalent joint of the user's hand (b) the instruments when the index and middle fingers have a direct joint-to-joint mapping and (c) the user's hand

$[0, 90°]$. The angle vectors for the instrument's joints in Figure 6.6 (a) are:

$$\begin{cases} \theta'_i = [3.55\ 16.76\ 1.3\ 0.02]^{\circ\,T} \\ \theta'_m = [8.77\ 16.97\ 59.99\ 41.97]^{\circ\,T} \\ \theta'_t = [0\ 2.03\ 95.71\ 43.59\ 86.96]^{\circ\,T} \end{cases} \tag{6.24}$$

The mapping process uses the orientation R_T of the user's thumb, calculated by the corresponding FK model, as the orientation R_t which is used as input to the instrument's IK model. It has to be noted that the combination of this orientation and the desired end-effector position is not always feasible. Besides, as mentioned on page 88, the pronation/supination sensor of the CMC joint of the exoskeleton's thumb records no angle change due to its position. This sensor would provide useful information regarding the orientation of the user's thumb which would contribute to determining the correct orientation of the instrument's thumb, especially in relation to the orientation of the index and middle fingers when attempting grasping. To

address this challenge, the algorithm initially uses R_T as input to the IK model of the instrument and when this is not a valid orientation for the desired position, it investigates the closest feasible orientation that suits the grasp.

The STT method can be used to represent most poses of the user's digits. Figures 6.7 and 6.8 illustrate the digit layout of the user's hand in comparison to the mapped instrument. However, when the hand is in full open position and the digits are extended, the thumb's extension is not reproduced, as can be seen from Figure 6.9. This happens because the process gives priority to the relative distance between fingertips which, through the IK model, leads to different joint angles.

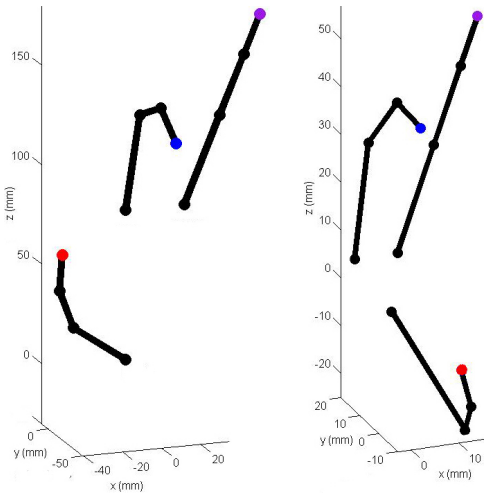

Figure 6.7: Correspondence between the instrument (right) and the user's hand (left) before an attempted index-thumb grasp using the mapping process

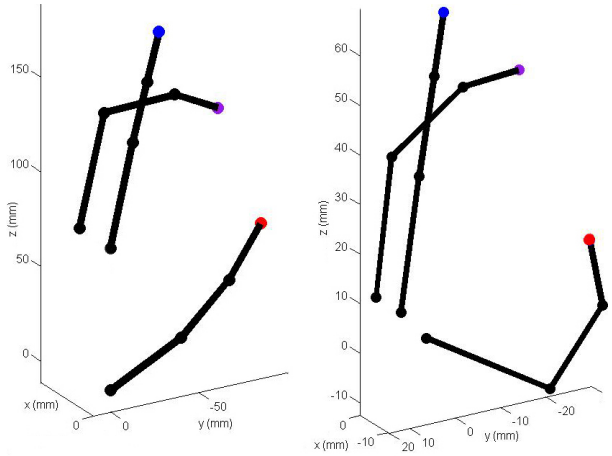

Figure 6.8: Correspondence between the instrument (right) and the user's hand (left) before an attempted middle-thumb grasp using the mapping process

Using the STT, the mapping error during an attempt for grasping can be considered as the difference:

$$e_j = \frac{norm(p_T - p_J)}{\lambda} - norm(p_t - p_j) \tag{6.25}$$

where j can be either i or m if the finger that is collaborating with the thumb for the grasp is the index or the middle respectively (the algorithm uses data of the finger with its tip closer to the tip of the thumb), p_T and p_J are the position of tip of the user's thumb and J finger, λ is the similarity ratio as calculated from equation (6.5),

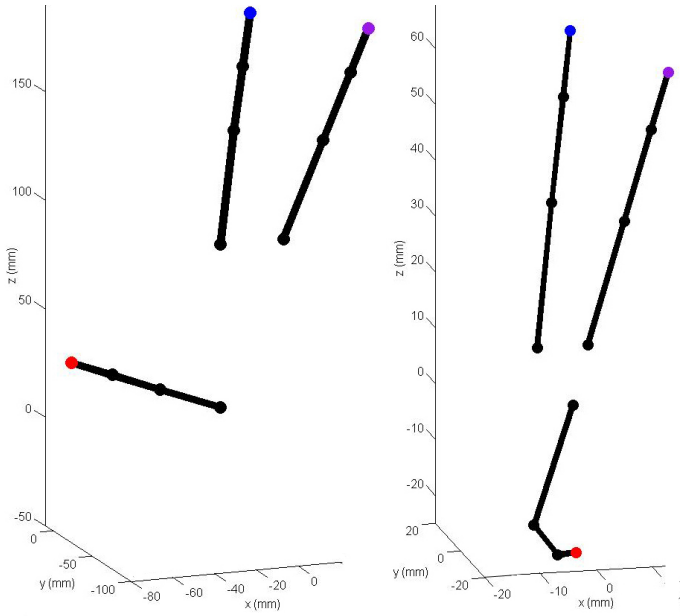

Figure 6.9: Correspondence between the instrument (right) and the user's hand (left) when the hand is open and the digits fully stretched using the mapping process

p_t and p_j are the position of the end-effectors of the instrument's thumb and j digit, and *norm* indicates the length of the corresponding vectors. For the specific joint angles of the user's digits (angle vectors (6.22)), the error is 3.04 mm for the case of Figure 6.6 (b) and 2.37 mm for Figure 6.6 (a) (angles of PIP and flexion of MCP are equal to 2/3 of the exoskeleton value).

Iterative STT Mapping

This result can be improved using a modification in the mapping process, where an iterative step is added: the STT is first applied to the 'modified human hand model' of step ii (page 140) and then, again, to the instrument model. Therefore, instead of simply modifying the FK model of the human hand to position the thumb between the index and middle fingers using vectors (6.1) and (6.2), the position of the thumb's end effector is calculated through the IK model of the hand using the STT method.

Figures 6.10 and 6.11 show the result of the modified mapping process when the angles of PIP and flexion of MCP are equal to the full or 2/3 of the exoskeleton value respectively. The error (6.25) is 0.028 mm and 0.034 mm respectively, while

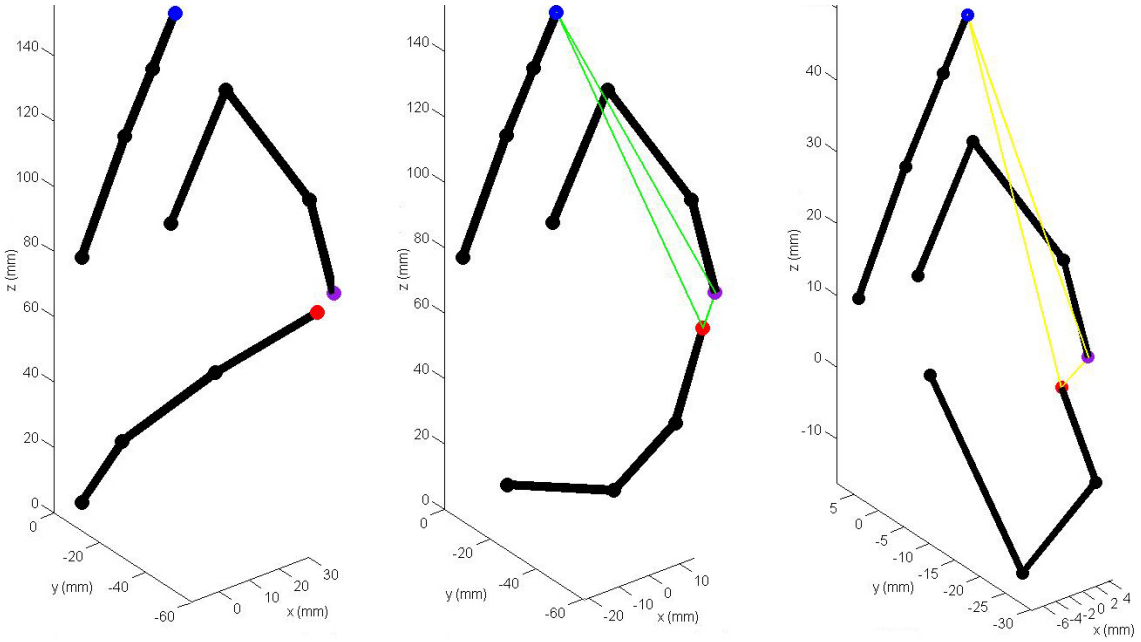

(a) (b) (c)

Figure 6.10: Result using the modified mapping process: (a) the user's digits, (b) modified hand model, (c) the instruments' digits

the resulting angle vectors of the instrument's thumb are:

$$\theta_t'' = [0\ 11.23\ 53.79\ 94.23\ 78.23]^{\circ\,T} \tag{6.26}$$

$$\theta_{t2/3}'' = [0\ 3.73\ 99.65\ 44.09\ 82.52]^{\circ\,T} \tag{6.27}$$

This modification, however, makes mapping problematic when the digits of the user are extended to an opened hand. This is due to the position of the thumb's tip, which, when the thumb is extended, is located away from the possible instrument's workspace. The algorithm, therefore, cannot find a feasible orientation for the thumb for such positions. A combination of joint-to-joint mapping (when the hand is opened) with the iterative STT during grasping attempts could lead to more accurate depiction of the user's motion.

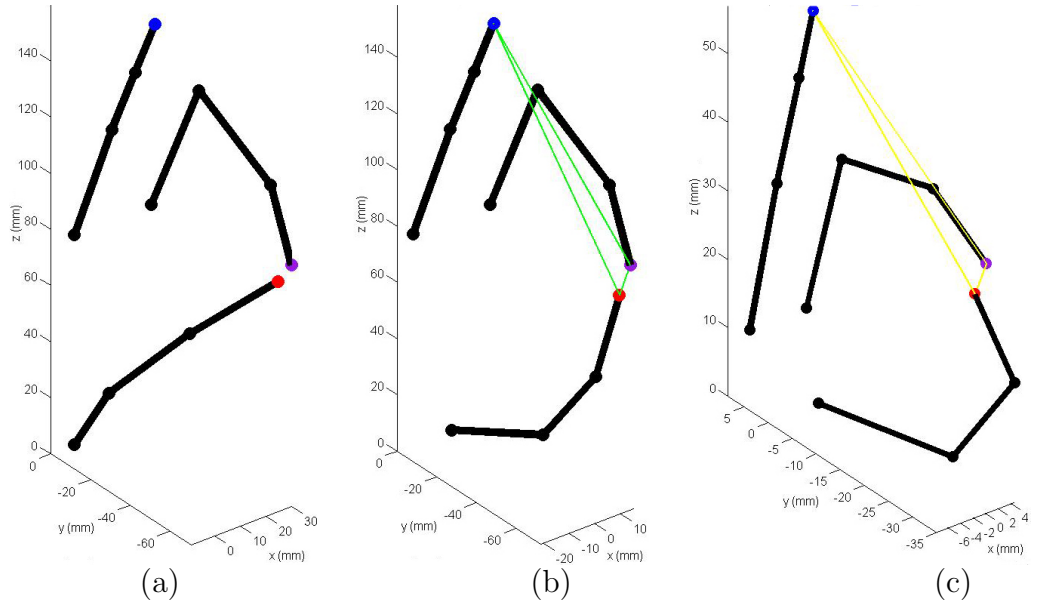

Figure 6.11: Result using the modified mapping process when the angles of PIP and MCP are 2/3 of the exoskeleton values: (a) the user's digits, (b) modified hand model, (c) the instruments' digits

6.3 Effect of Design Simplification on Accuracy

Section 4.3.3.3 examined the relationship between the PIP and DIP joints of the index and middle fingers and between MCP and IP joints of the thumb. The data from the exoskeleton suggested that there is little or no correlation between the motions of these joints. Despite some degree of coupling, the position of the PIP and MCP joints cannot generally be used to determine the position of DIP and IP respectively. This further indicates that hand tracking devices with simpler designs that do not account for all digit joints could be problematic in fine motions that require precision such as pinch grasping.

To examine this matter further and evaluate the effects, this has been tested on the μ`Angelo` system. The following two sections consider a simplified system design with fewer DOFs, where the exoskeleton has one less sensor and the instrument one less joint on each digit or where only the instrument has decreased number of DOFs. Such design alterations would reduce the complexity of actuation and decrease the cost of the system. In both cases, the exoskeleton has been mapped to the instrument using the iterative STT mapping method.

6.3.1 Reduced Number of Exoskeleton and Instrument DOFs

This experiment aims to evaluate the result of the mapping if *i*) the exoskeleton did not include sensors for the DIP joints of the index and middle fingers and the IP of the thumb and *ii*) the instrument digits did not have these joints, thus one less joint on each digit (10 DOFs instead of 13). To accomplish this, the same FK models were used except for the last joint which was kept at 0° while the IK models were modified accordingly.

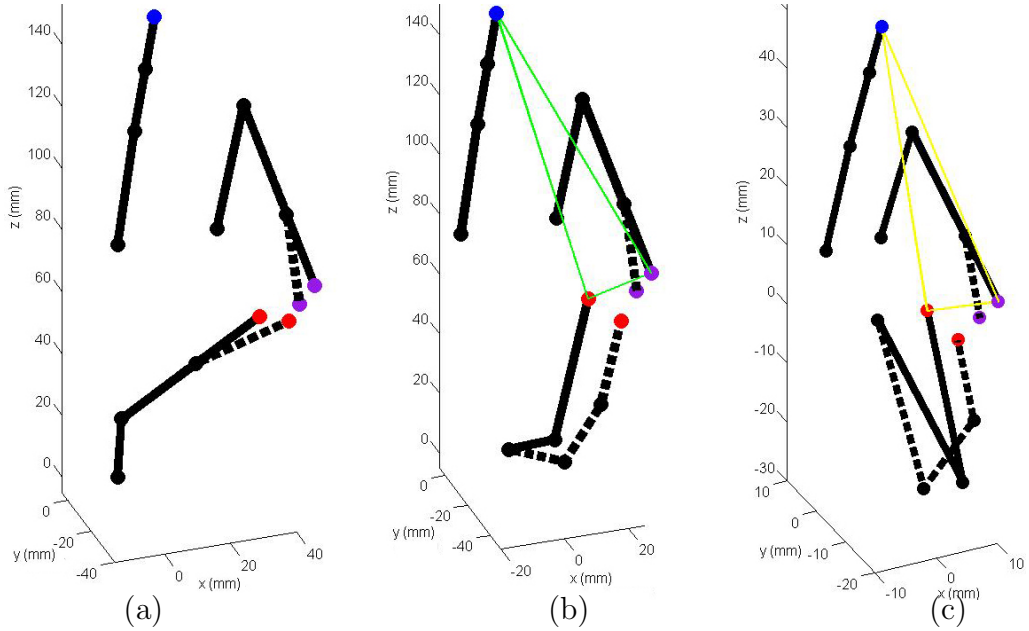

Figure 6.12: Result of mapping using exoskeleton sensors for 10 (solid line) or 13 DOFs (dotted line): (a) user's hand (b) modified hand for the mapping process and (c) instrument

Figure 6.12 (a) illustrates the actual layout of the user's digits with all DOFs (according to the model of Section 4.1) with dotted lines, while the solid lines represent the model that does not include the additional sensors. The dotted lines represent the same layout as in Figure 6.4. Figure 6.12 (b) shows the 'intermediate' step of modifying the hand model. Here, the thumb is not mapped joint-to-joint to the exoskeleton thumb, but instead derived using the iterative STT which employs the IK model of the thumb. Likewise, Figure 6.12 (c) compares how the instrument digits would be mapped using 10 (solid line) or 13 (dotted line) DOFs.

For the configuration of Figure 6.12, which can be described with vectors (6.22) except for the last angle which is kept at 0°, the error given by equation (6.25) is 6.87 mm. In comparison with the error of 0.028 mm that occurs when all 13 DOFs are used, it is obvious that, using the specific mapping method, the lack of these sensors and joints affects the accuracy of the hand tracking and mapping to the instrument greatly.

6.3.2 Reduced Number of Instrument DOFs

It would be interesting to examine the results of the proposed mapping process if all exoskeleton sensors were used, tracking 13 DOFs in total, while the instrument only had 10 DOFs, omitting the last joint of each digit.

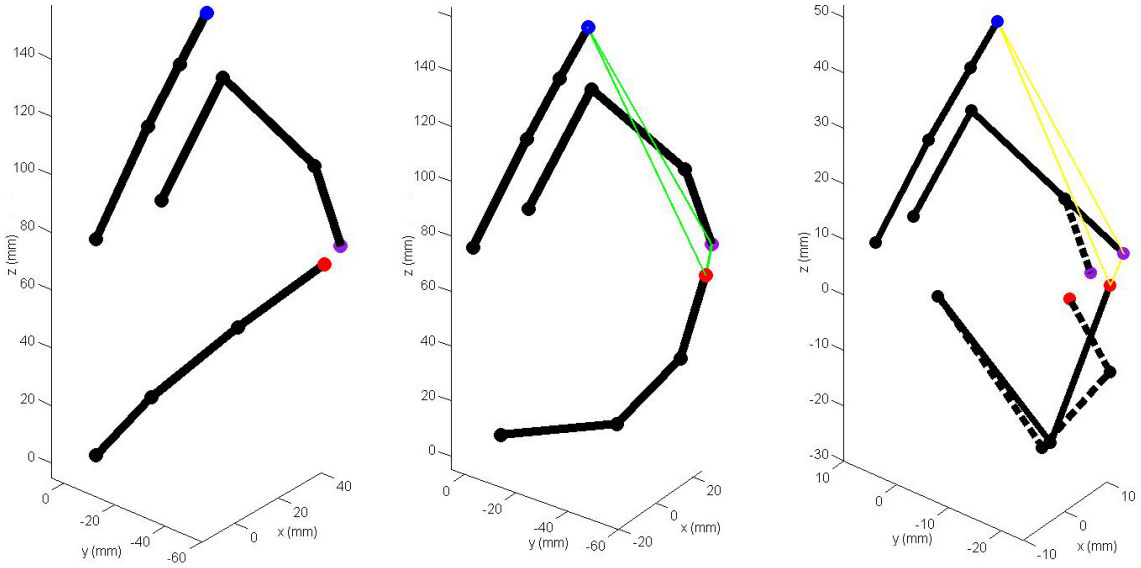

Figure 6.13: Result of mapping using all exoskeleton sensors for a 10 (solid line) or 13 DOFs (dotted line) instrument: (a) user's hand (b) modified hand for the mapping process and (c) instrument

Similar to the previous Section, Figure 6.13 compares the result of using all exoskeleton sensors and a 13-DOF instrument (dotted line) with the result of using all exoskeleton sensors and a 10-DOF instrument (solid line). In this case, the error (6.25) is 0.42 mm, which is about 6% of the error occurring when the exoskeleton does not include the additional sensors. Although this error is 15 times greater than

the error when using all DOFs of the instrument, it could still be within acceptable limits for surgical tasks, depending on the desired accuracy. Figure 6.14 shows the error during a grasping attempt sequence between the thumb and the middle finger for the three configurations between exoskeleton and instrument that were discussed.

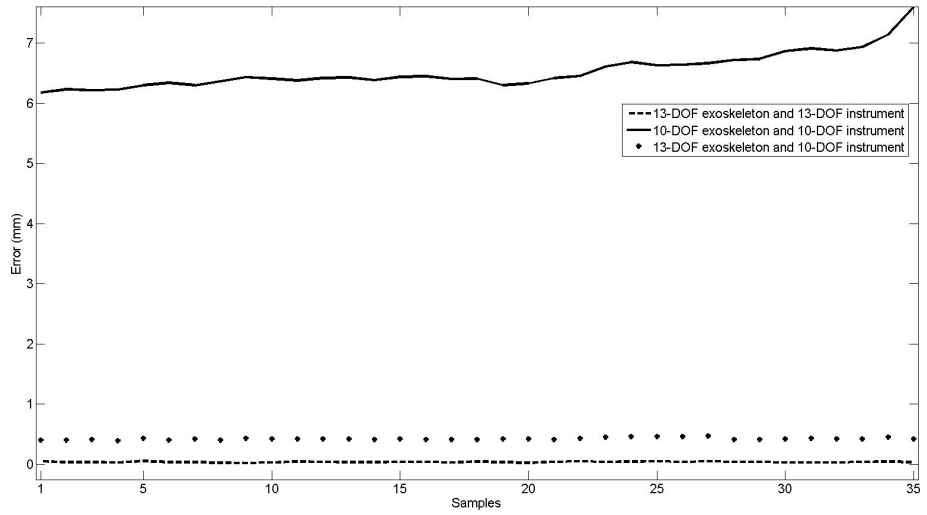

Figure 6.14: Error in the distance between digits during a thumb-middle finger grasp attempt

6.4 Summary

This Chapter examined the relationship between the master and slave subsystems of the µAngelo system as well as the similarities and differences of the slave and the human hand. Based on this comparison, the anthropomorphic nature of the system was determined. The design follows the utilities of the human hand, such as supination, adduction and rotation. The range of each joint is similar to the corresponding joint in the human hand, apart from the flexion of the thumb which has a range of 180°. This allows the thumb to fold inside the shaft of the instrument as well as to increase the operating workspace of the instrument.

The resulting anthropomorphism makes it possible for a simple joint-to-joint mapping to be applied between the exoskeleton and the instrument. Using this mapping method, the motion of the user's digits has been replicated in simulation.

However, joint-to-joint mapping fails when performing a pinch grasp. The combination of a joint-to-joint and point-to-point method has been proposed, where the position of the instrument's thumb is calculated in relation to the position of the index and middle fingers (STT). While the position and layout of the slave's thumb is derived through the model's IK, the layout of the index and middle fingers is acquired via a joint-to-joint relation to the master. The lengths of the user's digit links are not only greater than the corresponding links of the slave, but also do not have a specific correlation to them, as the exoskeleton is adjustable to different hand sizes. Therefore, the exact position of each of the slave's end-effectors is not as important as the relative distance between the three end-effectors.

The experiments using the proposed mapping method included tracking of different grasps involving the thumb and one of the index or middle fingers. Note that even when only two digits are used, the mapping algorithm takes into account the relative position of all three digit tips to form the similar triangles. Following this method, three-digit grasps can be further explored in future work. The experiments demonstrated an error in the order of 10^{-2}mm during grasping attempts. For open hand and extended digit motions, joint-to-joint mapping has better results for imitation of the thumb and therefore, a combination of the two approaches can be used. This hybrid solution, however, could lead to unpredictable 'jumps' between different end-effector positions, orientations and eventually unsafe poses. Determining an algorithm that smooths transition between approaches includes future work.

The necessity of multiple DOFs has been investigated by considering the exoskeleton and the instrument to lack one joint per digit. This is common among exoskeletons, e.g. the one by Luo and Wang (2011), and data gloves, e.g. 5DT Glove Ultra, found in the literature. Using the specific mapping method, the experiments show an increase in the error, unsuitable for surgical applications, when both the instrument and the exoskeleton lack three DOFs. No information about the last joint of each digit places the end-effector of all digits of the instrument at configurations unfit for grasping. This case should be investigated by exploring different mapping

methods in future work. Nevertheless, when information from the exoskeleton is complete for all joints, the proposed mapping process balances the largest part of the error even when the instrument digits lack three DOFs.

The desired number of DOFs for the instrument can be decided based on the requirements for specific types of surgery. For example, vascular surgery would require submillimetre accuracy, whereas millimetre accuracy could be sufficient for abdominal surgical tasks. However, more factors need to be considered such as reduction of the instrument's workspace without the additional joint and last link of the digit. Furthermore, as mentioned on page 113, the last link and joint offers the possibility for different operation modes that include using the index and middle finger of the instrument as common forceps when fine grasping is required.

Chapter 7

Conclusion and Future Work

7.1 Thesis Conclusions and Contributions

This thesis has presented the investigation for the development of novel instrumentation for MIS of soft tissue. The research focused on both the design and construction of a teleoperation system with application in abdominal surgical operations. Through a user-centred design and the anthropomorphic nature of its instruments, the system aims to bridge the gap between R-A MIS and open surgery by enabling three-digit movements commonly performed during the latter.

The background research that was presented helped to shape the methods of investigation as well as to determine the concept design of the system. In answer to the first research question "What are the issues and setbacks in R-A MIS when compared to other MIS techniques and open surgery?", Chapters 2 and 3 examined existing systems and techniques used in the literature as well as presented studies carried out for acquiring surgeons' views on the matter.

One of the thesis contributions has been the quantitative and qualitative research presented in Chapter 3, which further identified challenges and limitations of R-A MIS and other surgical techniques currently used. According to the survey, surgeons encounter challenges when transitioning from open surgery to MIS or R-A MIS (although to a lesser degree for the latter) due to the large gap between the nature of the techniques. Increased dexterity, manoeuvrability, larger instrument workspace and more natural manipulation could lead to adoption of R-A MIS in more complex surgical procedures. The survey and the focus group meetings suggested that surgeons are not satisfied with the current approaches in surgery and the dexterity

and ergonomics of available systems. This agreed with the existing literature on the subject, such as the findings of the Center for Devices and Radiological Health et al. (2013) where experienced surgeons considered the Da Vinci to have a complex user-interface. Additionally, the results of the survey, conducted as part of this thesis, further challenge the use of SPA as a valuable surgical technique.

In answer to the research question "Can R-A MIS instruments be designed to utilise dexterous manipulations and ergonomics associated with open soft tissue (abdominal) surgery?", the µAngelo slave instruments have been proposed. Multi-port R-A MIS surgery combined with benefits of HALS has been the foundation of this research, taking into account their limitations and attempting to integrate elements of open surgery techniques. Discussions with surgeons about the concept of the system have been valuable in determining positive and negative elements in it. The system has the potential to contribute to different type of grasps, as pinch-grasping is not its only capability because of its opposable thumb.

The thesis also posed the research question: "How can an appropriate user interface be designed to match the dexterity of the instrument and enable remote manipulation". In answer to this, Chapter 4 detailed the development and the components of the master off the µAngelo system, while Chapter 6 discussed the mapping between the master and the slave to enable teleoperation.

Consequently, a contribution of the thesis is the concept of anthropomorphism in teleoperation and especially in surgery. The µAngelo exoskeleton can track the user's hand digits in detail with a design that has provision for haptic feedback. It comprises a lightweight, portable and wearable surgical interface with a user-centred, adjustable design. The three prototypes were developed in an effort to improve on the performance of the data glove that was initially used for motion tracking. Each prototype helped identify challenges and problems in capturing the complex motion of the human hand. Prototype 3 has 19 sensors in total, with high resolution and accuracy and can offer detailed data of the angular position of the user's digit joints. The experiments showed that motion tracking has a few millimetres accuracy which,

however, due to the sensors' high performance, can be reduced with a more stable and tighter fit of the exoskeleton on the user's hand. This can be also extrapolated from experiments including only the abduction/adduction of the digits. During this motion, the exoskeleton stays in place and the results showed high repeatability.

A third contribution of the thesis regards the developed surgical instruments, which resemble human hands, having a miniature thumb, index and middle finger. The concept of anthropomorphism in surgical instruments is novel and, while a few multi-fingered designs exist in the literature, these are mainly aimed for use as simple retractors or for executing basic movements. Successful manipulation of soft objects is a critical issue for surgery and, consequently, the `µAngelo` instruments were designed for high dexterity with multiple DOFs. The instrument comprises three digits instead of five, as in the human hand, so that the incision is kept to a minimum. Besides, the thumb, index and middle finger can be adequate for most precision movements carried out in surgical tasks. Based on this concept, the two prototypes aspired to adhere to requirements for miniaturisation and force capabilities. The SMA instrument prototype demonstrated a wide range of motion in its joints and, therefore, could exhibit good manoeuvrability in confined spaces and around obstacles. As the miniature SMA helix actuators that were trialled in this prototype could not produce satisfactory pushing/grasping force, the second prototype was actuated by a cable-driven mechanism with the motors located away from the instrument's body. Miniaturisation of such a mechanism constitutes a challenge due to the lack of space for pulleys and specified routes for the cables inside the digits. Through a detailed inspection of the geometry of each digit and by identifying possible pathways for the cables, an input-output function was derived for each cable. This theoretical model for the cable actuation accounts for all DOFs. With the angle values of every DOF as input, the function outputs the length of each cable that needs to be pulled so that the joints move and the digit adopts the specified configuration. The cable pull is then converted to angular rotation of each motor. During the experiments, each cable was controlled by one motor,

whereas springs connected some cables to the corresponding motors to account for differences in maximum cable pull between the antagonistic cables. However, the compliance originating from the springs, in combination with effects from friction in the cables, contributed to positional inaccuracy. Two motors per DOF could eliminate the compliance and reduce the error.

A final contribution is the proposed STT algorithm that is presented in Chapter 6, a novel method to map the movements of the master to the slave that can be applied to any three-fingered robotic hand. It is a hybrid method of joint-to-joint and point-to-point mapping, with stress on the relative distance between the user's fingertips, which is preserved, although scaled down, in the slave's end-effectors. While more generalised methods can be found in the literature (Gioioso et al., 2013), STT comprises a simple method that guarantees that the layout of the slave's index and middle fingers is imitating the corresponding fingers of the master, while the thumb is positioned for successful grasping.

The importance of tracking the distal joints of the hands' digits was examined by comparing their trajectories to the ones of their proximal joints. Often, hand tracking devices disregard sensing for these joints and, instead, assume coupling between them and their proximal ones. Nevertheless, using data from the exoskeleton, little or no correlation was determined, suggesting that the position of the distal joint cannot be extrapolated from the proximal. Testing this in simulation using the STT algorithm, the error increased greatly when no information about the distal joints was available. On the contrary, the experiments showed that with the STT method, it is possible for the slave to have a simpler design and fewer DOFs and still correspond to the operation of the master, as long as information about all joints of the master is available. In such a case, however, the capability of the instrument to operate in 'dual mode' would have to be reviewed. This regards the mentioned concepts of digit-mode vs. forceps-mode (Figure 5.17, page 113); as the goal is also to be able to grasp tissues or organs of a large diameter, the 'middle' link of each digit (becoming the last link when the distal joint is removed) cannot

be small. However, this would inhibit precision grasping during 'forceps mode'.

In summary, the advantages of the proposed design over the existing ones include higher number of DOFs, anthropomorphic design of instruments, possibility for interchangeable tips and dual grasping mode for the instrument, adjustable sensory exoskeleton and potential for integration of haptic feedback. By adopting a design similar to the human hand, the system could make robots more accessible not only in the surgical domain, but, beyond, in areas that benefit from teleoperation, mechatronics and user-centred design, as well as in areas where safety issues prevent use of autonomous robots, such as assistive technologies and nuclear industry (Nagatani et al., 2013).

7.2 Limitations and Future work

One of the major challenges in this research has been the process of prototyping the two subsystems. The material of the 3D printed prototypes of both the exoskeleton and the instrument is not as robust as required when parts are built to a small scale to make the design lightweight or miniature. Other methods of manufacturing can be expensive and also escape the scope of this thesis. However, modifications to the design of the prototypes can improve the robustness of the prototypes. The exoskeleton could include both rigid and flexible parts in order to improve usability and have a snug fit. A comparison of the exoskeleton to other hand digit tracking methods (e.g. data gloves) would evaluate it further.

Furthermore, having pinpointed issues of the instrument actuation using the index finger, actuation should be extended to the thumb and the middle finger, using two motors to actuate each DOF. This would also increase the force generated in both directions of movement (when bending the digits as well as when extending them). This way, it will be possible not only to grasp tissues, but also to push them and use the digits to create traction, as is frequently needed in MIS. Furthermore, it has been mentioned that three digits can be adequate for precision grasps and

motions as indicated in the literature. It would also be interesting, through tests of the proposed system, to assess the concept of three-digit grasping versus two-digit grasping, especially in the context of surgical tasks.

A topic for future work, and integral for the implementation of the system as a whole, is the development of the control module for the slave instrument. Despite being a teleoperated system, control strategies will be required for grasping as well as to ensure the correct positioning of each instrument digit and, thus, representative mapping. This is a challenging topic as due to miniaturisation, the instrument lacks the space for additional sensors to track position. This is also the case for sensors that provide information about the applied force. However, such information is required for implementation of haptic feedback. It can be attempted to derive information about the force generated at the tips using the torque of the motors while sensing the motor current.

The improvements and additions to the master-slave system mentioned in the previous paragraphs will help to conduct more experiments and user studies in order to validate the µAngelo surgical system concept further and compare it with existing MIS techniques. This would address another limitation of the thesis, i.e. the lack of usability testing of the system. Considering the duration and scope of the thesis, the focus group feedback presented in Chapter 3 was believed to be adequate for an initial exploration of this aspect of the research. In future work, however, participants, both experienced and non-experienced in surgery, will be asked to complete a series of tasks similar to the FLS (Ragle, 2012), such as pick and place an object with precision, cut a circle and tie knots, in a comparison study using the *i*) µAngelo surgical system, *ii*) laparoscopic instruments and/or *iii*) the Da Vinci instruments. A continuation of this exploration would be a second survey among the participants of the aforementioned user study, in order to receive additional feedback and identify points for improvement. Subsequently, studies where the cognitive load and the fatigue of the users are assessed should be carried out to further evaluate the µAngelo system in terms of ergonomics.

The existing µAngelo system can be extended in order to create a more realistic surgical set-up: the exoskeleton's wrist will be attached to a haptic device such as the Virtuose 6D desktop (Haption, France) in order to provide information about the wrist and arm movements of the user and position the instrument in 3D space (Figure 7.1). Similarly, the instruments will be attached to the end of a (commercially available) robotic arm in order to emulate the robotic arms of the Da Vinci robot.

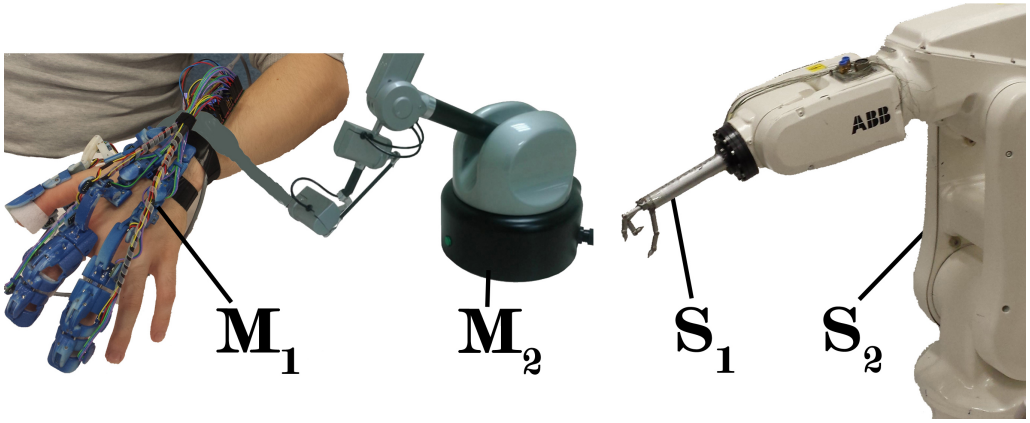

Figure 7.1: Envisioned system setup for future work:
M_1 - sensory exoskeleton, M_2 - Haptic device,
S_1 - slave anthropomorphic instrument, S_2 - 6 DOF slave arm

Although the concept promises to reduce the cognitive gap between surgical instrument operation and everyday hand gestures, surgeons need more options and flexibility during procedures. Therefore, additions to the system such as dual operation mode (digit-mode vs. forceps-mode) and potential for interchangeable tools should be realised and tested in hardware.

Finally, the mapping of the two subsystems that was presented in Chapter 6 included an algorithm that maps the master to the slave with minimal error during grasping attempts. Mapping has also been discussed for the case that the digits are extended. However, the combination of these two methods, which will ensure a smooth transition between them, constitutes future work. Furthermore, future work should also include a comparison of the proposed mapping algorithm to other mapping methods.

Publication Abstracts

The progress made so far has led to the publication of articles, the abstracts of which are as follows:

Towards an Anthropomorphic Design of Minimally Invasive Instrumentation for Soft Tissue Robotic Surgery

Minimally invasive procedures, such as laparoscopy, have significantly decreased blood loss, postoperative morbidity and length of hospital stay. R-A MIS has offered refined accuracy and more ergonomic instruments for surgeons, further minimising trauma to the patient. On the other hand, training surgeons in minimally invasive surgical procedures is becoming increasingly long and arduous. In this paper, we outline the rationale of a novel design of instruments for robotic surgery with increased dexterity that will provide more natural manipulation of soft tissues. The proposed system will not only reduce the training time for surgeons but also improve the ergonomics of the procedure. (Tzemanaki et al., 2012)

Hand exoskeleton for remote control of minimally invasive surgical anthropomorphic instrumentation

MIS has evolved from traditional laparoscopy to robotically assisted surgery. Advances in the design, articulation and flexibility of the instruments have added to the popularity of robotically assisted MIS. Nevertheless, the way that these instruments are controlled affects not only their efficacy, but also the ergonomics and the learning process for the surgeon. This paper reports on the development of a lightweight and adjustable hand exoskeleton that can sense movements of the surgeon's finger's joints and translate it to movements in the joints of a hand-like instrument. (Tzemanaki et al., 2013)

An Anthropomorphic Design for a Minimally Invasive Surgical System based on a Survey of Surgical Technologies, Techniques and Training

Background Over the past century, abdominal surgery has seen a rapid transition from open procedures to less invasive methods such as R-A MIS. This paper aims to investigate and discuss the needs of MIS in terms of instrumentation and to inform the design of a novel instrument.

Methods A survey was conducted among surgeons regarding their opinions on surgical training, surgical systems, how satisfied they are with them and how easy they are to use. A concept for MIS robotic instrumentation was then developed and a series of focus groups with surgeons were run to discuss it. The initial prototype of the robotic instruments, herein demonstrated, comprises modular rigid links with soft joints actuated by shape memory alloy helix actuators; these instruments are controlled using a sensory hand exoskeleton.

Results The results of the survey, as well as the ones of the focus groups, are presented here. A first prototype of the system was built and initial laboratory tests have been conducted in order to evaluate this approach.

Conclusions The analysed data from both the survey and the focus groups justify the chosen concept of an anthropomorphic MIS robotic system which imitates the natural motion of the hands. (Tzemanaki et al., 2014b)

μAngelo: A Novel Minimally Invasive Surgical System Based on an Anthropomorphic Design

Abdominal surgery has seen a rapid transition from open procedures to R-A MIS. The learning process for new surgeons is long compared to open surgery, and the desired dexterity cannot always be achieved using the current surgical instruments.

Furthermore, the way that these instruments are controlled plays an important role in their effectiveness and the ergonomics of the procedure. This paper presents the μAngelo surgical system for abdominal R-A MIS, based on an anthropomorphic design comprising two three-digit surgical instruments and a sensory hand exoskeleton. The operation of these subsystems and the efficacy of their corresponding performance are demonstrated. (Tzemanaki et al., 2014a)

Design of a multi-DOF cable-driven mechanism of a miniature serial manipulator for robot-assisted minimally invasive surgery

While multi-fingered robotic hands have been developed for decades, none has been used for surgical operations. μAngelo is an anthropomorphic master-slave system for teleoperated robot-assisted surgery. As part of this system, this paper focuses on its slave instrument, a miniature three-digit hand. The design of the mechanism of such a manipulator poses a challenge due to the required miniaturization and the many active degrees of freedom. As the instrument has a human-centred design, its relation to the human hand is discussed. Two ways of routing its cable-driven mechanism are investigated and the method of deriving the input-output functions that drive the mechanism is presented. (Tzemanaki et al., 2016)

Bibliography

Abbott, D. J., Becke, C., Rothstein, R. I., and Peine, W. J. (2007). Design of an endoluminal NOTES robotic system. In *International Conference on Intelligent Robots and Systems*. IEEE, San Diego, CA, pages 410–416.

Al-Naami, M., Anjum, M. N., Aldohayan, A., Al-Khayal, K., and Alkharji, H. (2013). Robotic general surgery experience: a gradual progress from simple to more complex procedures. *The International Journal of Medical Robotics and Computer Assisted Surgery*. URL `http://dx.doi.org/10.1002/rcs.1521`. Accessed 3/11/13.

Allemann, P., Leroy, J., Asakuma, M., Al Abeidi, F., Dallemagne, B., and Marescaux, J. (2010). Robotics may overcome technical limitations of single-trocar surgery: an experimental prospective study of Nissen fundoplication. *Archives of surgery (Chicago, Ill. : 1960)*, 145(3):267–71.

Arata, J., Mitsuishi, M., Warisawa, S., Tanaka, K., Yoshizawa, T., and Hashizume, M. (2005). Development of a dexterous minimally-invasive surgical system with augmented force feedback capability. In *IEEE/RSJ International Conference on Intelligent Robots and Systems*. pages 3207–3212.

Arulampalam, T., Paterson-Brown, S., Morris, A., and Parker, M. (2009). Natural orifice transluminal endoscopic surgery consensus statement. *Annals of The Royal College of Surgeons of England*, 91(1):456–459.

Baik, S. H. (2008). Robotic colorectal surgery. *Yonsei Medical Journal*, 49(6):891–896.

Bajo, A., Goldman, R. E., Wang, L., Fowler, D., and Simaan, N. (2012). Integration and preliminary evaluation of an insertable robotic effectors platform for single port access surgery. In *International Conference on Robotics and Automation*. IEEE, Saint Paul, MN, pages 3381–3387.

Berguer, R. and Hreljac, a. (2004). The relationship between hand size and difficulty using surgical instruments: a survey of 726 laparoscopic surgeons. *Surgical endoscopy*, 18(3):508–12.

Boston Business Journal (2005). EndoVia Medical purchased by California company. URL `http://www.bizjournals.com/boston/blog/mass-high-tech/2005/04/endovia-medical-purchased-by-california.html`. Accessed 26/10/13.

Boynton, P. M. (2004). Administering, analysing, and reporting your questionnaire. *BMJ (Clinical research ed.)*, 328(7452):1372–5.

Boynton, P. M. and Greenhalgh, T. (2004). Selecting, designing, and developing your questionnaire. *BMJ (Clinical research ed.)*, 328(7451):1312–5.

Brüser, P. and Gilbert, A. (1999). *Finger bone and joint injuries*. CRC Press.

Buchholz, B. and Armstrong, T. J. (1992). A kinematic model of the human hand to evaluate its prehensile capabilities. *Journal of biomechanics*, 25(2):149–62.

Buchholz, B., Armstrong, T. J., and Goldstein, S. A. (1992). Anthropometric data for describing the kinematics of the human hand. *Ergonomics*, 35(3):261–273. PMID: 1572336.

Burton, T. M. W., Vaidyanathan, R., Burgess, S., Turton, A. J., and Melhuish, C. (2011). Development of a parametric kinematic model of the human hand and a novel robotic exoskeleton. In *2011 IEEE International Conference on Rehabilitation Robotics*. pages 1–7.

Cancer Research UK (2012). Cancer incidence statistics for the UK. Technical Report May, Cancer Research UK [online]. URL `http://publications.cancerresearchuk.org/downloads/Product/CS\_CS\_INCIDENCE.pdf`. Accessed 21/10/13.

Cardenas-Goicoechea, J., Adams, S., Bhat, S. B., and Randall, T. C. (2010). Surgical outcomes of robotic-assisted surgical staging for endometrial cancer are equivalent to traditional laparoscopic staging at a minimally invasive surgical center. *Gynecologic oncology*, 117(2):224–8.

Center for Devices and Radiological Health, Office of Surveillance and Biometrics, and Medical Product Safety Network (2013). MedSun Survey Report: da Vinci Surgical System. Technical report, Food and Drug Administration. URL `http://www.fda.gov/downloads/MedicalDevices/ProductsandMedicalProcedures/SurgeryandLifeSupport/ComputerAssistedRoboticSurgicalSystems/UCM374095.pdf`. Accessed 13/03/16.

Cerveri, P., Momi, E., Lopomo, N., Baud-Bovy, G., Barros, R. M. L., and Ferrigno, G. (2007). Finger kinematic modeling and real-time hand motion estimation. *Annals of Biomedical Engineering*, 35(11):1989–2002.

Chandler, J. G., Corson, S. L., and Way, L. W. (2001). Three spectra of laparoscopic entry access injuries. *Journal of the American College of Surgeons*, 192(4):478–90; discussion 490–1.

Chiu, C., Nguyen, N., and Bloom, S. (2011). Single-incision laparoscopic appendectomy using conventional instruments: an initial experience using a novel technique. *Surgical Endoscopy*, 25(4):1153–1159.

Choi, J. (2008). *Developing a 3-dimensional kinematic model of the hand for ergonomic analyses of hand posture, hand space envelope, and tendon excursion.* Ph.D. thesis, The University of Michigan.

Cobos, S., Ferre, M., Urán, M., Ortego, J., and Pena, C. (2008). Efficient human hand kinematics for manipulation tasks. In *IEEE/RSJ International Conference on Intelligent Robots and Systems*. IEEE, pages 2246–2251.

Costello, M. B. and Fragaszy, D. M. (1988). Prehension in Cebus and Saimiri: I. Grip type and hand preference. *American Journal of Primatology*, 15(3):235–245.

CyberGlove Systems LLC (2016). CyberGrasp. URL `http://www.cyberglovesystems.com/cybergrasp`. Accessed 11/03/16.

Dagnino, G., Georgilas, I., Tarassoli, P., Atkins, R., and Dogramadzi, S. (2015). Intra-operative 3d imaging system for robot-assisted fracture manipulation. In *Engineering in Medicine and Biology Society (EMBC), 2015 37th Annual International Conference of the IEEE*. IEEE, pages 9–12.

Dakin, G. F. and Gagner, M. (2003). Comparison of laparoscopic skills performance between standard instruments and two surgical robotic systems. *Surgical endoscopy*, 17(4):574–9.

Dankelman, J., Painter, F., Schanker, B., Samaha, D., and Hansen, J. (2010). Increasing complexity of medical technology and consequences for training and outcome of care. Technical report, World Health Organization. URL `whqlibdoc.who.int/hq/2010/WHO_HSS_EHT_DIM_10.4_eng.pdf`. Accessed 19/10/13.

Dapri, G., Casali, L., Dumont, H., Van Der Goot, L., Herrandou, L., Pastijn, E., Sosnowski, M., Himpens, J., and Cadière, G.-B. (2011). Single-access transumbilical laparoscopic appendectomy and cholecystectomy using new curved reusable instruments: a pilot feasibility study. *Surgical Endoscopy*, 25(4):1325–1332.

Dikaiakos, G., Tzemanaki, A., Pipe, A., and Dogramadzi, S. (2014). Mechatronic implementation in minimally invasive surgical instruments. In *5th IEEE RAS EMBS International Conference on Biomedical Robotics and Biomechatronics*. pages 357–362.

Dipietro, L., Sabatini, A. M., and Dario, P. (2008). A survey of glove-based systems and their applications. *IEEE Transactions on Systems Man and Cybernetics Part C Applications and Reviews*, 38(4):461–482.

Doné, K., DiMartino, A., Judkins, T., Hallbeck, S., and Oleynikov, D. (2004). Evaluation of laparoscopic tools for usability and comfort. *Proceedings of the Human Factors and Ergonomics Society Annual Meeting*, 48(12):1359–1362.

Dragulescu, D., Perdereau, V., Drouin, M., Ungureanu, L., and Menyhardt, K. (2007). 3d active workspace of human hand anatomical model. *Biomed. Eng. Online*, 6:15.

Duchene, D. A., Moinzadeh, A., Gill, I. S., Clayman, R. V., and Winfield, H. N. (2006). Survey of residency training in laparoscopic and robotic surgery. *The Journal of Urology*, 176(5):2158–2166; discussion 2167.

ECRI Institute (2014). Top 10 Health Technology Hazards for 2015. Technical report, ECRI Institute. URL `www.ecri.org/2015hazards`.

Fifth Dimension Technologies (2005). 5DT Data Glove 14 Ultra. URL `http://www.5dt.com/products/pdataglove14.html`. Accessed 1/05/16.

Flora, E. D., Hons, B., Wilson, T. G., Martin, I. J., Rourke, N. A. O., Maddern, G. J., and O'Rourke, N. A. (2008). A review of natural orifice translumenal endoscopic surgery (NOTES) for intra-abdominal surgery: experimental models, techniques, and applicability to the clinical setting. *Annals of surgery*, 247(4):583–602.

Freschi, C., Ferrari, V., Melfi, F., Ferrari, M., Mosca, F., and Cuschieri, A. (2012). Technical review of the Da Vinci surgical telemanipulator. *The international journal of medical robotics and computer assisted surgery*.

Furriel, F. T., Laguna, M. P., Figueiredo, A. J., Nunes, P. T., and Rassweiler, J. J. (2013). Training of european urology residents in laparoscopy: results of a pan-european survey. *BJU International*, 112(8):1223–1228. URL `http://dx.doi.org/10.1111/bju.12410`.

Geomagic (2013). Geomagic Touch (formerly Geomagic Phantom Omni). URL `http://geomagic.com/en/products/phantom-omni/overview`. Accessed 26/10/13.

Gioioso, G., Salvietti, G., Malvezzi, M., and Prattichizzo, D. (2013). Mapping synergies from human to robotic hands with dissimilar kinematics: An approach in the object domain. *IEEE Transactions on Robotics*, 29(4):825–837.

Gobern, J. M., Novak, C. M., and Lockrow, E. G. (2011). Survey of robotic surgery training in obstetrics and gynecology residency. *J Minim Invasive Gynecol*, 18(6):755–760.

Golash, V. and Willson, P. D. (2005). Early laparoscopy as a routine procedure in the management of acute abdominal pain: a review of 1,320 patients. *Surgical endoscopy*, 19(7):882–5.

Gorce, P. and Rezzoug, N. (2004). A method to learn hand grasping posture from noisy sensing information. *Robotica*, 22:309–318. URL `http://journals.cambridge.org/article_S0263574704000025`.

Gray, H. (1919). *Anatomy of the Human Body*. Lea & Febiger, 1918.

Grebenstein, M., Albu-Schffer, A., Bahls, T., Chalon, M., Eiberger, O., Friedl, W., Gruber, R., Haddadin, S., Hagn, U., Haslinger, R., Hppner, H., Jrg, S., Nickl, M., Nothhelfer, A., Petit, F., Reill, J., Seitz, N., Wimbck, T., Wolf, S., Wsthoff, T., and Hirzinger, G. (2011). The dlr hand arm system. In *IEEE International Conference on Robotics and Automation*. pages 3175–3182.

Greenberg, H. (2013). Marketing Is Key to Surgical Robots Success. URL `http://www.cnbc.com/id/100652922`. Accessed 11/03/16.

Gribble, P. L., Mullin, L. I., Cothros, N., and Mattar, A. (2003). Role of cocontraction in arm movement accuracy. *Journal of Neurophysiology*, 89(5):2396–2405.

Gunther, S., Rosen, J., Hannaford, B., and Sinanan, M. (2007). The Red DRAGON: A Multi-Modality System for Simulation and Training in Minimally Invasive Surgery. *Studies in health technology and informatics*, 125:149–154. URL `http://ebooks.iospress.nl/publication/10734`.

Gwilliam, J., Mahvash, M., Vagvolgyi, B., Vacharat, A., Yuh, D. D., and Okamura, A. (2009). Effects of haptic and graphical force feedback on teleoperated palpation. In *IEEE International Conference on Robotics and Automation*. pages 677–682.

Hagn, U., Konietschke, R., Tobergte, A., Nickl, M., Jörg, S., Kübler, B., Passig, G., Gröger, M., Fröhlich, F., Seibold, U., Le-Tien, L., Albu-Schäffer, A., Nothhelfer, A., Hacker, F., Grebenstein, M., and Hirzinger, G. (2010). DLR MiroSurge: a versatile system for research in endoscopic telesurgery. *International journal of computer assisted radiology and surgery*, 5(2):183–93.

Hanl, E. J., Miller, B. E., Kumar, R., Hasser, C. J., Coste-Maniere, E., Talamini, M. A., Aurora, A. A., Schenkman, N. S., and Marohn, M. R. (2006). Mentoring console improves collaboration and teaching in surgical robotics. *Journal of Laparoendoscopic & Advanced Surgical Techniques*, 16(5):445–451. `arXiv:1011.1669v3`.

Hannaford, B., Rosen, J., Friedman, D. W., King, H., Roan, P., Cheng, L., Glozman, D., Ma, J., Kosari, S. N., and White, L. (2013). Raven-II: an open platform for surgical robotics research. *IEEE transactions on bio-medical engineering*, 60(4):954–9.

Hashizume, M., Sugimachi, K., and Group, S. (1997). Needle and trocar injury during laparoscopic surgery in Japan. *Surgical endoscopy*, 11(12):1198–1201.

Heijnsdijk, E. A. M., Dankelman, J., and Gouma, D. J. (2002). Effectiveness of grasping and duration of clamping using laparoscopic graspers. *Surgical endoscopy*, 16(9):1329–31.

Herron, D. M. and Marohn, M. (2007). A consensus document on robotic surgery : prepared by the SAGES-MIRA robotic surgery consensus group. Technical report, Society of American Gastrointestinal and Endoscopic Surgeons, Los Angeles, CA.

Hesselink, V. J., Luijendijk, R. W., de Wilt, J. H., Heide, R., and Jeekel, J. (1993). An evaluation of risk factors in incisional hernia recurrence. *Surgery, gynecology & obstetrics*, 176(3):228–234.

Hillel, A. T., Kapoor, A., Simaan, N., Taylor, R. H., and Flint, P. (2008). Applications of robotics for laryngeal surgery. *Otolaryngologic clinics of North America*, 41(4):781–91, vii.

Ho, M. and Desai, J. P. (2012). Towards the development of an SMA-actuated MRI-compatible tendon-driven neurosurgical robot. In *IEEE International Conference on Robotics and Automation*. Saint Paul, MN, pages 683–688.

Ho, M., Koltz, M., Simard, J. M., Gullapalli, R., Desai, J. P., and Member, S. (2011). Towards a MR Image-guided SMA-actuated neurosurgical robot. In *International Conference on Robotics and Automation*. IEEE, Shangai, China, pages 1153–1158.

Hoffman, A. (2010). Intuitive surgical, inc.: How long can their monopoly last? *Bentley University and RSM Case Development Case Center*.

Iberall, T. (1987). The nature of human prehension: Three dextrous hands in one. In *Robotics and Automation. Proceedings. 1987 IEEE International Conference on*, volume 4. pages 396–401.

Ikuta, K., Hasegawa, T., and Daifu, S. (2003). Hyper redundant miniature manipulator "Hyper Finger" for remote minimally invasive surgery in deep area. In *IEEE International Conference on Robotics and Automation*, volume 1. pages 1098–1102.

Intuitive Surgical (2011). Media - press release. URL `http://investor.intuitivesurgical.com/phoenix.zhtml?c=122359&p=irol-newsArticle&ID=1638907`. Accessed 18/10/13.

Intuitive Surgical (2016). Intuitive Surgical - Company Profile. URL http://www.intuitivesurgical.com/company/profile.html. Accessed 11/03/16.

Intuitive Surgical, Inc. (2016a). Da Vinci Surgery - Robotic-Assisted Minimally Invasive Surgery. URL www.davincisurgery.com/davinci-surgery. Accessed 11/03/16.

Intuitive Surgical, Inc. (2016b). Intuitive surgical - endowrist instruments. URL www.intuitivesurgical.com/products/instruments. Accessed 11/03/16.

Intuitive Surgical, Inc. (2016c). Intuitive Surgical - Image Gallery - da Vinci Si System. URL www.intuitivesurgical.com/company/media/images/davinci_si_images.html. Accessed 11/04/16.

Ito, M., Asano, Y., Horiguchi, A., Shimizu, T., Yamamoto, T., Uyama, I., and Miyakawa, S. (2010). Cholecystectomy using single-incision laparoscopic surgery with a new sils port. *Journal of Hepato-Biliary-Pancreatic Sciences*, 17(5):688–691.

Jackson, T. D., Wannares, J. J., Lancaster, R. T., Rattner, D. W., and Hutter, M. M. (2011). Does speed matter? the impact of operative time on outcome in laparoscopic surgery. *Surgical Endoscopy*, 25(7):2288–2295.

Jones, J. (2011). Robotic surgery. URL http://spinoff.nasa.gov/spinoff2000/hm1.htm. Accessed 18/10/13.

Jonsdottir, G. M., Jorgensen, S., Cohen, S. L., Wright, K. N., Shah, N. T., Chavan, N., and Einarsson, J. I. (2011). Increasing minimally invasive hysterectomy: effect on cost and complications. *Obstetrics and gynecology*, 117(5):1142–9.

Kadar, N., Reich, H., Liu, C. Y., Manko, G. F., and Gimpelson, R. (1993). Incisional hernias after major laparoscopic gynecologic procedures. *American Journal of Obstetrics and Gynecology*, 168(5):1493–1495.

Kamper, D. G., Cruz, E. G., and Siegel, M. P. (2003). Stereotypical fingertip trajectories during grasp. *Journal of Neurophysiology*, 90(6):3702–3710.

Kano, N., Takeshi, A., Kusanagi, H., Watarai, Y., Mike, M., Yamada, S., Mishima, O., Uwafuji, S., Kitagawa, M., Watanabe, H., Kitahama, S., Matsuda, S., Endo, S., and Gremillion, D. (2010). Current surgical training: simultaneous training in open and laparoscopic surgery. *Surgical endoscopy*, 24(12):2927–9.

Khiangte, E., Newme, I., Phukan, P., and Medhi, S. (2010). Improvised transumbilical glove port: A cost effective method for single port laparoscopic surgery. *Indian Journal of Surgery*, 73(2):142–145.

Kim, D., Hilliges, O., Izadi, S., Butler, A. D., Chen, J., Oikonomidis, I., and Olivier, P. (2012). Digits: freehand 3D interactions anywhere using a wrist-worn gloveless sensor. In *Proceedings of the 25th annual ACM symposium on User interface software and technology*, UIST '12. ACM, New York, NY, USA, pages 167–176.

Kitagawa, M., Dokko, D., Okamura, A. M., and Yuh, D. D. (2005). Effect of sensory substitution on suture-manipulation forces for robotic surgical systems. *The Journal of Thoracic and Cardiovascular Surgery*, 129(1):151–158.

Ko, S. Y. and Rodriguez y Baena, F. (2013). Toward a Miniaturized Needle Steering System With Path Planning for Obstacle Avoidance. *IEEE Transactions on Biomedical Engineering*, 60(4):910–917.

Koechlin, F., Lorenzoni, L., and Schreyer, P. (2010). Comparing price levels of hospital services across countries. In *OECD Health Working Papers*, 53. OECD Publishing, Paris, France, pages 1–60.

Krippendorff, K. (2004). *Content Analysis: An Introduction to its Methodology*. SAGE Publications, Inc, California, 2nd edition.

Kroh, M., El-Hayek, K., Rosenblatt, S., Chand, B., Escobar, P., Kaouk, J., and Chalikonda, S. (2011). First human surgery with a novel single-port robotic system: cholecystectomy using the da Vinci Single-Site platform. *Surgical endoscopy*, 25(11):3566–73.

Krukowski, Z., Leroy, J., and Marescaux, J. (2010). Single port cholecystectomy: impact of instrumentation in getting the critical view of safety. URL `http://www.websurg.com/doi-vd01en2929.htm`. Accessed 30/10/13.

Leap Motion Inc (2016). Leap Motion — Mac & PC Motion Controller for Games, Design, Virtual Reality & More. URL `www.leapmotion.com/`. Accessed 01/05/16.

Liarokapis, M. V., Bechlioulis, C. P., Kyriakopoulos, K. J., and Artemiadis, P. K. (2013). Directions, methods and metrics for mapping human to robot motion with functional anthropomorphism: a review. Technical report, School of Mechanical Engineering, National Technical University of Athens, Tech. Rep. URL `http://www.minasliarokapis.com/TR2013_Liarokapis_MappingSkillTransfer.pdf`.

Lin, J. J. and Liu, F. L. (2015). Hand-assisted laparoscopic colorectal surgery. In *Minimally Invasive Coloproctology*. Springer, pages 27–34.

Liu, A., Tendick, F., Cleary, K., and Kaufmann, C. (2003). A survey of surgical simulation: Applications, technology, and education. *Presence Teleoperators and Virtual Environments*, 12(6):599–614.

Lum, M. J. H., Friedman, D. C. W., Sankaranarayanan, G., King, H., Fodero, K., Leuschke, R., Hannaford, B., Rosen, J., and Sinanan, M. N. (2009). The RAVEN: design and validation of a telesurgery system. *The International Journal of Robotics Research*, 28(9):1183–1197.

Luo, H. and Wang, S. (2011). Multi-manipulation with a Metamorphic Instrumental Hand for Robot-assisted Minimally Invasive Surgery. In *IEEE/ICME International Conference on Complex Medical Engineering*. Harbin, China, pages 363–368.

Lysaght, M. J. (2005). Robot-assisted surgery: Da Vinci. URL `http://biomed.brown.edu/Courses/BI108/BI108\_2005\_Groups/04/davinci.html`. Accessed 18/10/13.

Macgregor, J. M., Kim, R. S., Gallagher, J. T., Soliman, M. K., Ferrara, A., Baldwin, K., Pigalarga, R., and Glanville, C. (2012). Fundamentals of Robotic Surgery. URL `http://thesagesmeeting.org/fundamentals-of-robotic-surgery/`. Accessed 19/10/13.

Mack, M. J. (2001). Minimally invasive and robotic surgery. *Jama*, 285(5):568–572.

Madhani, A., Niemeyer, G., and Salisbury, J. (1998). The Black Falcon: a teleoperated surgical instrument for minimally invasive surgery. In *1998 IEEE/RSJ International Conference on Intelligent Robots and Systems*, volume 2. pages 936–944.

Malik, K. (2013). Human Development Report 2013 - The Rise of the South: Human Progress in a diverse world. Technical report, United Nations Development Programme. URL `http://hdr.undp.org/en/reports/global/hdr2013/`. Accessed 18/10/13.

Marcus, H. J., Hughes-Hallet, A., Candy, T. P., Nandi, D., Yang, G.-Z., and Darzi, A. (2013). Electronic response to Paul, S. et al., Robotic surgery: revisiting "no innovation without evaluation". *BMJ*, 346:f1573. URL `http://www.bmj.com/content/346/bmj.f1573?tab=responses`. Accessed 03/11/13.

Marescaux, J. (2002). Code name: "Lindbergh operation ". *Annales de chirurgie*, 127(1):2–4.

Matern, U., Waller, P., Giebmeyer, C., Rckauer, K., and Farthmann, E. (2001). Ergonomics: requirements for adjusting the height of laparoscopic operating tables. *JSLS : Journal of the Society of Laparoendoscopic Surgeons / Society of Laparoendoscopic Surgeons*, 5(1):712.

Mayring, P. (2000). Qualitative content analysis [28 paragraphs]. *Forum: Qualitative Social Research*, 1(2).

Meijden, O. and Schijven, M. (2009). The value of haptic feedback in conventional and robot-assisted minimal invasive surgery and virtual reality training: a current review. *Surgical Endoscopy*, 23(6):1180–1190.

Meijer, D. W., Bannenberg, J. J. G., and Jakimowicz, J. J. (2000). Hand-assisted laparoscopic surgery. *Surgical Endoscopy Ultrasound and Interventional Techniques*, 14:891–895.

Microsoft (2016). Kinect for Xbox One. URL `www.xbox.com/en-GB/xbox-one/accessories/kinect-for-xbox-one{\#}fbid=jmWuaYYIVL6`. Accessed 01/05/16.

Mihálcz, I. (2001). Fundamental characteristics and design method for nickel-titanium shape memory alloy. *Periodica Polytechnica. Engineering. Mechanical Engineering*, 45(1):75.

Montellano Lopez, A., Richardson, R., Dehghani, A., Roshan, R., Jayne, D., and Neville, A. (2012). Preliminary adhesion control of a miniature intra-abdominal robot for laparoscopic surgery. In *The 5th Hamlyn Symposium on Medical Robotics*. London, pages 75–76.

Morimoto, T. K., Greer, J. D., Hsieh, M. H., and Okamura, A. M. (2016). Surgeon design interface for patient-specific concentric tube robots. *2016 6th IEEE International Conference on Biomedical Robotics and Biomechatronics (BioRob)*:41–48.

Mutter, D. and Marescaux, J. (2004). Standard laparoscopic cholecystectomy - WeBSurg, the e-surgical reference of laparoscopic surgery. URL `http://www.websurg.com/Standard\_laparoscopic\_cholecystectomy-vd01en1608e.htm`. Accessed 19/10/13.

Nagatani, K., Kiribayashi, S., Okada, Y., Otake, K., Yoshida, K., Tadokoro, S., Nishimura, T., Yoshida, T., Koyanagi, E., Fukushima, M., and Kawatsuma, S. (2013). Emergency response to the nuclear accident at the fukushima daiichi nuclear power plants using mobile rescue robots. *Journal of Field Robotics*, 30(1):44–63.

Nam, E. J., Kim, S. W. S., Lee, M., Yim, G. W., Paek, J. H., Lee, S. H., Kim, J. H. W., and Kim, Y. T. (2011). Robotic single-port transumbilical total hysterectomy: a pilot study. *Journal of gynecologic oncology*, 22(2):120–126.

Napier, J. R. (1956). The Prehensile Movements of the Human Hand. *Journal of Bone & Joint Surgery, British Volume*, 38-B(4):902–913.

Natali, C. D., Member, S., Ranzani, T., Simi, M., Menciassi, A., and Valdastri, P. (2012). Trans-abdominal active magnetic linkage for robotic surgery. In *International Conference on Intelligent Robots and Systems*. IEEE, Saint Paul, MN, pages 695–700.

Nawrat, Z. and Kostka, P. (2014). Robin Heart Surgery Robotic System. Challenges in Mechanical Construction, Control System and Stuff Training Before First Clinical Application. *Archive of Mechanical Engineering*, 61(1):163–178.

Niewola, A., Podsedkowski, L., Wróblewski, P., Zawiasa, P., and Zawierucha, M. (2013). Selected aspects of robin heart robot control. *Archive of Mechanical Engineering*, 60(4):575–593.

Novara, G., Catto, J. W., Wilson, T., Annerstedt, M., Chan, K., Murphy, D. G., Motttrie, A., Peabody, J. O., Skinner, E. C., Wiklund, P. N., et al. (2015). Systematic review and cumulative analysis of perioperative outcomes and complications after robot-assisted radical cystectomy. *European urology*, 67(3):376–401.

Ohshima, R., Takayama, T., Omata, T., Ohya, T., Kojima, K., Takase, K., and Tanaka, N. (2008). Assemblable three fingered five-DOF hand for laparoscopic surgery. In *IEEE International Conference on Robotics and Automation*. pages 3896–3901.

Oshima, R., Takayama, T., Omata, T., Kojima, K., Takase, K., and Tanaka, N. (2010). Assemblable three-fingered nine-degrees-of-freedom hand for laparoscopic surgery. *IEEE/ASME Transactions on Mechatronics*, 15(6):862–870.

Ota, T., Degani, A., Schwartzman, D., Zubiate, B., McGarvey, J., Choset, H., and Zenati, M. a. (2008). A novel highly articulated robotic surgical system for epicardial ablation. In *International Conference of Engineering in Medicine and Biology Society*. Division of Cardiac Surgery, The Bioengineering Department, University of Pittsburgh, Pittsburgh, Pennsylvania, USA, IEEE, pages 250–253.

Park, A. E. and Lee, T. H. (2011). *Minimally Invasive Surgical Oncology: State-of- the-Art Cancer Management*, chapter Evolution of Minimally Invasive Surgery and Its Impact on Surgical Residency Training. Springer Berlin Heidelberg, Berlin, Heidelberg, pages 11–22.

Park, J. S., Choi, G.-S., Lim, K. H., Jang, Y. S., and Jun, S. H. (2011). S052: a comparison of robot-assisted, laparoscopic, and open surgery in the treatment of rectal cancer. *Surgical endoscopy*, 25(1):240–8.

Patel, R. and Stifelman, M. D. (2004). Hand-assisted laparoscopic devices: The second generation. *Journal of Endourology*, 18(7):649–653.

Paul, S., McCulloch, P., and Sedrakyan, A. (2013). Robotic surgery: revisiting "no innovation without evaluation". *BMJ*, 346:f1573.

Peer, A., Einenkel, S., and Buss, M. (2008). Multi-fingered telemanipulation-mapping of a human hand to a three finger gripper. In *Robot and Human Interactive Communication, 2008. RO-MAN 2008. The 17th IEEE International Symposium on*. IEEE, pages 465–470.

Pheasant, S. and Haslegrave, C. (2006). *Bodyspace: Anthropometry, Ergonomics, and the Design of Work*. Taylor & Francis.

Piccigallo, M., Scarfogliero, U., Quaglia, C., Petroni, G., Valdastri, P., Menciassi, A., and Dario, P. (2010). Design of a novel bimanual robotic system for single-port laparoscopy. *IEEE/ASME Transactions on Mechatronics*, 15(6):871–878.

Qian, K., Niu, J., and Yang, H. (2013). Developing a gesture based remote human-robot interaction system using kinect. *International Journal of Smart Home*, 7(4).

Raghavaiah, V., Kode, C., Cavusoglu, M. C., and Azar, M. T. (2005). Design and characterization of a novel hybrid actuator using shape memory alloy and d.c. motor for minimally invasive surgery applications. In *International Conference on Mechatronics & Automation*. IEEE, Niagara Falls, Canada, pages 416–420.

Ragle, C. (2012). Fundamental Laparoscopic Skills. In *Advances in Equine Laparoscopy*, chapter 2. Wiley-Blackwell, pages 13–20. URL `http://www.acvs.org/Symposium/Proceedings2011/data/papers/147.pdf`. Accessed 18/10/13.

Rané, A. and Dasgupta, P. (2003). Prospective experience with a second-generation hand-assisted laparoscopic device and comparison with first-generation devices. *Journal of endourology Endourological Society*, 17(10):895–897.

Rané, A. and Wolf, J. S. (2005). The role of hand-assisted laparoscopy in urology : a critical appraisal. *BJU International*, 96(1):13–16.

Rao, P. P., Rao, P. P., Bhagwat, S., et al. (2011). Single-incision laparoscopic surgery-current status and controversies. *Journal of minimal access surgery*, 7(1):6.

Reyes, D. a. G., Tang, B., and Cuschieri, a. (2006). Minimal access surgery (MAS)-related surgeon morbidity syndromes. *Surgical endoscopy*, 20(1):1–13.

Roke, C., Melhuish, C., Pipe, T., Drury, D., and Chorley, C. (2012). Lump localisation through a deformation-based tactile feedback system using a biologically inspired finger sensor. *Robotics and Autonomous Systems*, 60(11):1442–1448.

Rottman, S. J., Podolsky, E. R., Kim, E., Kern, J., and Curcillo, P. G. (2010). Single port access (SPA) splenectomy. *JSLS : Journal of the Society of Laparoendoscopic Surgeons / Society of Laparoendoscopic Surgeons*, 14(1):48–52.

Rozet, F., Jaffe, J., Braud, G., Harmon, J., Cathelineau, X., Barret, E., and Vallancien, G. (2007). A direct comparison of robotic assisted versus pure laparoscopic radical prostatectomy: a single institution experience. *The Journal of urology*, 178(2):478–82.

Sampat, A., Parakati, I., Kunnavakkam, R., Glick, D. B., Lee, N. K., Tenney, M., Eggener, S., and Roth, S. (2015). Corneal Abrasion in Hysterectomy and Prostatectomy: Role of Laparoscopic and Robotic Assistance. *Anesthesiology*, 122(5):994–1001.

Sánchez, L. A., Petroni, G., Piccigallo, M., Scarfogliero, U., Niccolini, M., Liu, C., Stefanini, C., Zemiti, N., Menciassi, A., Poignet, P., and Dario, P. (2011). Real-time control and evaluation of a teleoperated miniature arm for single port laparoscopy. In *Annual International Conference of the IEEE Engineering in Medicine and Biology Society*. Boston, Massachusetts, pages 7049–53.

Sang, H., Wang, S., Li, J., He, C., Zhang, L., and Wang, X. (2011). Control design and implementation of a novel masterslave surgery robot system, microhand a. *The International Journal of Medical Robotics and Computer Assisted Surgery*, 7(3):334–347.

Santello, M., Flanders, M., and Soechting, J. F. (1998). Postural hand synergies for tool use. *The Journal of Neuroscience*, 18(23):10105–10115.

Santos-Carreras, L., Hagen, M., Gassert, R., and Bleuler, H. (2012). Survey on surgical instrument handle design: Ergonomics and acceptance. *Surgical Innovation*, 19(1):50–59.

Scott-Conner, C. E. H. (2012). Hand-assisted laparoscopic surgery. In Soper, N. J. and Scott-Conner, C. E., eds., *The SAGES Manual*, volume 1 Basic Laparoscopy and Endoscopy, chapter 8. Springer Verlag, New York, NY, pages 99–104.

Seibold, U., Kuebler, B., and Hirzinger, G. (2008). Prototypic force feedback instrument for minimally invasive robotic surgery. In Bozovic, V., ed., *Medical Robotics*, volume 44. InTech, pages 377–400.

Shang, J., Noonan, D. P., Payne, C., Clark, J., Sodergren, M. H., Darzi, A., and Yang, G. Z. (2011). An articulated universal joint based flexible access robot for minimally invasive surgery. In *IEEE International Conference on Robotics and Automation*. pages 1147–1152.

Simaan, N. (2005). Snake-like units using flexible backbones and actuation redundancy for enhanced miniaturization. In *International Conference on Robotics and Automation*. IEEE, Barcelona, Spain, pages 3023–3028.

Simaan, N., Taylor, R., and Flint, P. (2004). High dexterity snake-like robotic slaves for minimally invasive telesurgery of the upper airway. In Barillot, C., Haynor, D., and Hellier, P., eds., *Medical Image Computing and Computer-Assisted Intervention MICCAI 2004*, volume 3217 of *Lecture Notes in Computer Science*. Springer Berlin Heidelberg, pages 17–24.

Simorov, A., Otte, R. S., Kopietz, C. M., and Oleynikov, D. (2012). Review of surgical robotics user interface: what is the best way to control robotic surgery? *Surgical Endoscopy*, 26(8):2117–2125.

Smith, A. B., Raynor, M., Amling, C. L., Busby, J. E., Castle, E., Davis, R., Nielsen, M., Thomas, R., Wallen, E. M., Woods, M., et al. (2012). Multi-institutional analysis of robotic radical cystectomy for bladder cancer: perioperative outcomes and complications in 227 patients. *Journal of Laparoendoscopic & Advanced Surgical Techniques*, 22(1):17–21.

Society of American Gastrointestinal and Endoscopic Surgeons (2009). Integrating advanced laparoscopy into surgical residency training: A sages position paper - curriculum guidelines in advanced laparoscopic surgery. Technical report, Society of American Gastrointestinal and Endoscopic Surgeons, Los Angeles, CA. URL `http://www.sages.org/publications/guidelines/integrating-advanced-laparoscopy-into-surgical-residency-training-a-sages-position-paper`. Accessed 18/10/13.

Solly, J., Bunce, C., and Cowley, S. (2006). Focus on cholecystectomy. *The Journal of One-Day Surgery*, 17(1):15–18.

Soot, S. J., Eshraghi, N., Farahmand, M., Sheppard, B. C., and Deveney, C. W. (1999). Transition from open to laparoscopic fundoplication: The learning curve. *Archives of Surgery*, 134(3):278–282.

Spiers, A., Baillie, S., Pipe, T., and Persad, R. (2012). Experimentally driven design of a palpating gripper with minimally invasive surgery considerations. In *Haptics Symposium (HAPTICS)*, volume 1. IEEE, Vancouver, BC, pages 261–266.

St Peter, S. D. and Holcomb, G. W. I. (2008). *Atlas of Pediatric Laparoscopy and Thoracoscopy*, chapter History of Minimally Invasive Surgery. Elsevier Health Sciences, pages 1–5.

Stein, R. J., White, W. M., Goel, R. K., Irwin, B. H., Haber, G. P., and Kaouk, J. H. (2010). Robotic laparoendoscopic single-site surgery using GelPort as the access platform. *European urology*, 57(1):132–6.

Stifelman, M. and Nieder, A. M. (2002). Prospective comparison of hand-assisted laparoscopic devices. *Urology*, 59(5):668 – 672.

Sung, G. T., Gill, I. S., Urology, A., and Article, C. M. E. (2001). Robotic laparoscopic surgery: a comparison of the da Vinci and Zeus systems. *Urology*, 58(6):893–898.

Tan, L. C., Samanta, S., and Hosking, S. W. (2002). Safe transition from open to laparoscopic fundoplication by an established consultant–the importance of repeated audit. *Annals of the Royal College of Surgeons of England*, 84(2):84–8.

Tavakoli, M., Aziminejad, A., Patel, R., and Moallem, M. (2006). Methods and mechanisms for contact feedback in a robot-assisted minimally invasive environment. *Surgical Endoscopy And Other Interventional Techniques*, 20(10):1570–1579.

Taylor, R. H. (2006). A perspective on medical robotics. *Proceedings of the IEEE*, 94(9):1652–1664.

Thielmann, S., Seibold, U., Haslinger, R., Passig, G., Bahls, T., Stefan, J., Nickl, M., Nothhelfer, A., Hagn, U., and Hirzinger, G. (2010). MICA - A new generation of versatile instruments in robotic surgery task specific. In *International Conference on Intelligent Robots and Systems*. Tapei, Taiwan, pages 871–878.

Thirsk, R., Williams, D., and Anvari, M. (2007). NEEMO 7 undersea mission. *Acta Astronautica*, 60(47):512 – 517.

Tholey, G. and Desai, J. P. (2007). A modular, automated laparoscopic grasper with three-dimensional force measurement capability. In *Proceedings 2007 IEEE International Conference on Robotics and Automation*. IEEE, pages 250–255.

Trehan, A. and Dunn, T. J. (2013). The robotic surgery monopoly is a poor deal. *BMJ*, 347.

Tyson, M. D. and Humphreys, M. R. (2014). Urological applications of natural orifice transluminal endoscopic surgery (NOTES). *Nat Rev Urol*, 11(6):324–332.

Tzemanaki, A., Burton, T. M., Gillatt, D., Melhuish, C., Persad, R., Pipe, A. G., and Dogramadzi, S. (2014a). Microangelo: A novel minimally invasive surgical system based on an anthropomorphic design. In *2014 5th IEEE RAS EMBS International Conference on Biomedical Robotics and Biomechatronics*. pages 369–374.

Tzemanaki, A., Dogramadzi, S., Pipe, T., and Melhuish, C. (2012). Towards an anthropomorphic design of minimally invasive instrumentation for soft tissue robotic surgery. In *Advances in Autonomous Robotics*. Springer, pages 455–456.

Tzemanaki, A., Fracczak, L., Gillatt, D., Melhuish, C., Persad, R., Pipe, A. G., and Dogramadzi, S. (2016). Design of a multi-dof cable-driven mechanism of a miniature serial manipulator for robot-assisted minimally invasive surgery. In *2016 6th IEEE RAS EMBS International Conference on Biomedical Robotics and Biomechatronics*. pages 55–60.

Tzemanaki, A., Gao, X., Pipe, A. G., Melhuish, C., and Dogramadzi, S. (2013). Hand exoskeleton for remote control of minimally invasive surgical anthropomorphic instrumentation. In Yang, G.-Z. and Darzi, A., eds., *The 6th Hamlyn Symposium on Medical Robotics*. Imperial College London, pages 81–82. URL `http://ubimon.doc.ic.ac.uk/Hamlyn2013/public/Proceedings\_2013\_2.pdf`. Accessed 21/10/13.

Tzemanaki, A., Walters, P., Pipe, A. G., Melhuish, C., and Dogramadzi, S. (2014b). An anthropomorphic design for a minimally invasive surgical system based on a survey of surgical technologies, techniques and training. *The International Journal of Medical Robotics and Computer Assisted Surgery*, 10(3):368–378.

Uygun, I., Okur, M. H., Aydogdu, B., Arslan, M. S., Cimen, H., and Otcu, S. (2013). Transumbilical scarless surgery with thoracic trocar: easy and low-cost. *Journal of the Korean Surgical Society*, 84(6):360–366.

Vitiello, V., Lee, S. L., Cundy, T. P., and Yang, G. Z. (2013). Emerging robotic platforms for minimally invasive surgery. *IEEE Reviews in Biomedical Engineering*, 6:111–126.

Walonick, D. S. (2010). A selection from survival statistics. *StatPac, Inc.* URL `https://www.statpac.com/surveys/surveys.pdf`. Accessed 27/10/14.

Walters, P. and McGoran, D. (2011). Digital fabrication of smart structures and mechanisms - creative applications in art and design. In *IS&T Digital Fbrication 2011*. Minneapolis, MN, pages 185–188.

Watanabe, T., Kawamura, K., Harada, K., Susilo, E., Menciassi, A., Dario, P., Fujie, M. G., and Member, S. (2010). A reconfigurable master device for a modular surgical robot and evaluation of its feasibility. In *International Conference on Biomedical Robotics and Biomechatronics*. Tokyo, Japan, pages 114–119.

Wege, A. and Hommel, G. (2005). Development and control of a hand exoskeleton for rehabilitation of hand injuries. In *2005 IEEE/RSJ International Conference on Intelligent Robots and Systems*. pages 3046–3051.

Weghe, M. V., Rogers, M., Weissert, M., and Matsuoka, Y. (2004). The ACT Hand : Design of the Skeletal Structure. In *IEEE International Conference on Robotics and Automation*. pages 3375–3379.

Weichert, F., Bachmann, D., Rudak, B., and Fisseler, D. (2013). Analysis of the accuracy and robustness of the leap motion controller. *Sensors (Basel, Switzerland)*, 13(5):6380–93.

Wolfe, S. W., Hotchkiss, R. N., Pederson, W. C., and Kozin, S. H. (2010). Goals of Treatment; Biomechanics of the Injured Hand. In *Greens Operative Hand Surgery*. Elsevier, sixth edition, pages 1609–1612.

Wright, J. D., Kostolias, A., Ananth, C. V., Burke, W. M., Tergas, A. I., Prendergast, E., Ramsey, S. D., Neugut, A. I., and Hershman, D. L. (2014). Comparative effectiveness of robotically assisted compared with laparoscopic adnexal surgery for benign gynecologic disease. *Obstetrics and gynecology*, 124(5):886896.

Xu, K., Goldman, R. E., Ding, J., Allen, P. K., Fowler, D. L., and Simaan, N. (2009). System design of an insertable robotic effector platform for single port access (SPA) surgery. In *International Conference on Intelligent Robots and Systems*. IEEE/RSJ, St. Louis, pages 5546–5552.

Xu, K. and Zheng, X. (2012). Configuration comparison for surgical robotic systems using a single access port and continuum mechanisms. In *International Conference on Intelligent Robots and Systems*. IEEE, Saint Paul, MN, pages 3367–3374.

Yang, X., Park, J., Jung, K., and You, H. (2007). Development and evaluation of a 25-degree of freedom hand kinematic model. *Science and Technology*:1–4.

Yeung, B. P. M. and Gourlay, T. (2012). A technical review of flexible endoscopic multitasking platforms. *International journal of surgery*, 10(7):345–354.

Yoon, H.-S., Choi, Y., and Yi, B.-J. (2010). A 4-DOF bendable endoscope mechanism for single port access surgery. In *IEEE ICRA 2010 Workshop on Snakes, Worms and Catheters : Continuum and Serpentine Robots for Minimally Invasive Surgery*. Anchorage, Alaska, pages 54–56.

Yoon, H.-S. and Yi, B.-J. (2015). Design of a master device for controlling multi-moduled continuum robots. *Proceedings of the Institution of Mechanical Engineers, Part C: Journal of Mechanical Engineering Science*. URL `http://pic.sagepub.com/content/early/2015/12/31/0954406215625359.abstract`. `http://pic.sagepub.com/content/early/2015/12/31/0954406215625359.full.pdf+html`.

Zecca, M., Endo, N., Itoh, K., Imanishi, K., Saito, M., Nanba, N., Takanobu, H., and Takanishi, A. (2007). On the development of the bioinstrumentation system wb-1r for the evaluation of human-robot interaction - head and hands motion capture systems-. In *2007 IEEE/ASME international conference on Advanced intelligent mechatronics*. pages 1–6.

Zhang, C., Robb, B., Waters, J., Selzer, D., Wiebke, E., and Virgilio, G. (2012). Incidence of incisional hernias increase with single port laparoscopic technique. URL `http://www.sages.org/wp-content/uploads/posters/2012/39416.jpg?0d5076`. Accessed 18/10/13.

Zhang, L., Zhou, N., and Wang, S. (2013). Direct manipulation of tool-like masters for controlling a masterslave surgical robotic system. *The International Journal of Medical Robotics and Computer Assisted Surgery*. URL `http://dx.doi.org/10.1002/rcs.1545`.

Zhang, R., Kunz, A., Lochmatter, P., and Kovacs, G. (2006). Dielectric elastomer spring roll actuators for a portable force feedback device. In *14th Symposium on Haptic Interfaces for Virtual Environment and Teleoperator Systems*. pages 347–353.

Appendix I

Questionnaire title:

Optimal minimally invasive instrumentation design and laparoscopic and robotic surgery training survey

Thank you for participating in this survey. Your feedback (regardless whether you are a junior or a senior surgeon) is invaluable and constitutes a fundamental part of our research.

The particular research project focuses on determining and designing new instrumentation for minimally invasive robotic surgery, in order to expand the already proven benefits of this type of surgery, but also on improving the ergonomics of the procedure for the surgeon. The project is being funded by the Bristol Urological Institute via North Bristol NHS Trust.

This survey should take about 15 minutes of your time. This questionnaire is the first part of two, the second being the use of your expertise and professional opinion to evaluate and test the final design.
We would appreciate if you could return the questionnaire **within 15 days.**

Your answers will be treated with confidentiality and anonymity. Your personal and contact information will be kept private and will not be shared or revealed to anyone.

We are based at the Bristol Robotics Laboratory in Bristol, UK, which is collaboration between two Bristol universities: the University of the West of England and the University of Bristol. Please feel free to contact us for information and further questions:

www.brl.ac.uk

Antonia.tzemanaki@brl.ac.uk

Sanja.dogramadzi@uwe.ac.uk

With kind regards,

Antonia Tzemanaki

Bristol Robotics Laboratory
T Building
Frenchay Campus
BS16 1QY
Bristol, UK
+44 (0)117 328 3394

Optimal minimally invasive instrumentation design and laparoscopic and robotic surgery training survey

Instructions:

Please read each question first before answering. The questionnaire consists of open as well as closed questions. You can use as much white space for your answers as you need, and also feel free to add explanations where you consider that it is needed. All the questions are marked in italics, please answer all them (writing N/A = not applicable where appropriate).

1 *Please indicate which of the following robotic surgical systems you have already heard of. (Please select all that apply to you)*

- ☐ DaVinci Surgical System
- ☐ Zeus Surgical System
- ☐ CyberKnife
- ☐ ARAKNES project
- ☐ MiroSurge System
- ☐ Others (please specify):

2 *Please indicate which of the following robotic surgical systems you have already used. (Please select all that apply to you and/or add others that are not mentioned)*

- ☐ DaVinci Surgical System
- ☐ Zeus Surgical System
- ☐ CyberKnife
- ☐ Others (please specify):

3 *How satisfied are you with the following systems?*

	Very satisfied	Satisfied	Dissatisfied	Very dissatisfied	I have not used it
DaVinci Surgical System	☐	☐	☐	☐	☐
Cyberknife	☐	☐	☐	☐	☐

4 *What in your opinion are the main <u>benefits</u> of the DaVinci Surgical System (N/A if you have not used it)? Please write in capitals.*

5 *What in your opinion are the main <u>shortcomings</u> of the DaVinci Surgical System (N/A if you have not used it)? Please write in capitals.*

6 *How would you rate the <u>cost</u> of the DaVinci Surgical System in relation to its performance?*

☐ Too expensive to buy ☐ Expensive, but worth buying ☐ Fair cost/performance balance ☐ I have not used it

7 *How experienced would you consider yourself in the following types of surgery?*

	I have never performed one	Junior surgeon	Intermediate	Senior surgeon
Open surgery	☐	☐	☐	☐
Laparoscopy	☐	☐	☐	☐
Robotic surgery	☐	☐	☐	☐

8 *How long was the duration of your training for <u>open</u> surgery (estimation of duration in hours, or please write "none" if you did not have any)? Please write in capitals.*

9 *How long was the duration of your (traditional) <u>laparoscopic</u> surgery training (estimation of duration in hours, or please write "none" if you did not have any)? Please write in capitals.*

10 *How long was the duration of your <u>robotic</u> surgery training (estimation of duration in hours, or please write "none" if you did not have any)? Please write in capitals.*

11 *How would you rate the complexity of the following types of surgery training?*

	Very complex	Complex	Not so complex	Simple	N/A
Traditional laparoscopic surgery training	☐	☐	☐	☐	☐
Robotic surgery training	☐	☐	☐	☐	☐

12 *How would you rate the following transitions?*

	Very difficult	Difficult	Manageable	Easy	N/A
Open surgery to Laparoscopy	☐	☐	☐	☐	☐
Laparoscopic to Robotic surgery	☐	☐	☐	☐	☐
Open to Robotic surgery	☐	☐	☐	☐	☐

13 *Which type of minimally invasive surgery do you prefer to practice?*

☐ Multi-port access ☐ Single port access ☐ Single port, but I do not have the option in my place of work

14 *What in your opinion are the <u>benefits</u> of single port (or single incision) surgery? Please write in capitals.*

15 *What in your opinion are the <u>drawbacks</u> of single port (or single incision) surgery? Please write in capitals.*

16 *What do you consider as the maximum size of a surgical incision in minimally invasive surgery, without high risk of hernia? (please answer in mm)*

17	*There are cases where the incisions during a minimally invasive surgery are minimal, however in the end the surgeon has to lengthen one of them in order to remove a large piece of tissue e.g. the prostate. How important is <u>miniaturisation</u> to you and would you prefer other ways of avoiding big incisions (e.g. <u>morcellation</u> or breaking the specimen into smaller pieces prior to removal)? Please write in capitals.*

18	*Which do you think is the most demanding task during minimally invasive surgery (e.g. suturing) and why? Please write in capitals.*

19	*Are there certain movements that you would like to perform but are unable to, due to the limitation of the existing instrumentation? (during robotic surgery or laparoscopy) Please write in capitals.*

20	*How willing are you to try new instrumentation that <u>does not change the main concept</u> of the method you are using during minimally invasive surgery? Please rate in the scale of 1-4 :* *1=I do not want to try new tools, 4=I am very happy to try new tools*

☐ 1 ☐ 2 ☐ 3 ☐ 4

21 *How willing are you to adapt to new methods of manipulating instruments that <u>may change your routine</u> during minimally invasive surgery? Please rate in the scale of 1-4 :*
1=I do not want to adapt to a new concept, 4=I am very happy to try

☐ 1 ☐ 2 ☐ 3 ☐ 4

22 *How happy are you with your position and posture during the following types of surgery?*

	Very unhappy	Unhappy	Happy	Very happy	N/A
Traditional laparoscopic surgery	☐	☐	☐	☐	☐
Robotic surgery	☐	☐	☐	☐	☐

23 *What would in your opinion be the optimum <u>posture</u> and surgeon-machine interface during a minimally invasive surgery? E.g. sitting down/ standing up, away/on top of the patient, head in a monitor or watching a wider screen, wearing gloves that control the instruments/ manipulating tools that control the instruments. Please write in capitals.*

Please fill your details below; they will be kept confidential and will only be used to derive statistical data.

Name:

☐ Male ☐ Female

Company:

Speciality:

Age:

☐ 30-34 ☐ 35-39 ☐ 40-44 ☐ 45-49 ☐ 50-54 ☐ 55-59 ☐ 60-64 ☐ 64-70

How many years have you been performing open surgery:

☐ Less than 1 ☐ 1-2 ☐ 3-4 ☐ 5-6 ☐ More than 7

How many years have you been performing minimally invasive surgery (traditional or robotic):

☐ Less than 1 ☐ 1-2 ☐ 3-4 ☐ 5-6 ☐ More than 7

Email address:

Would like to be contacted for the 2nd part of the survey?
(evaluation of a new design of instrumentation for robotic minimally invasive surgery of soft tissue)

☐ Yes ☐ No

Would like to be notified about the results of this survey?

☐ Yes ☐ No

Focus Group Sessions – Total time: 65 min

1. Refreshments, settling down and camera setting. (5 minutes)
   The participants introduce themselves and the moderator explains the procedure. (5 minutes)
2. The moderator reads Part I and gives the participants time to read it again. After reading, A is discussed for 10 minutes. Comparisons with B may occur (in such a case, this will last 20 minutes). If B is not being covered, the moderator takes at least another 10 minutes for B. Key questions:
   What is good about the surgical approach in this scenario?
   What is bad?
3. The moderator reads Part II and gives the participants time to read it again. Key questions:
   What is good about this scenario? (10 min)
   What is bad? (10 min)
   How could this scenario be different? (extend it, change it) / what are your expectations for a new device? (10 min)

Part I

Archie is a 45 year old man and suffers from a condition that requires him to have abdominal surgery.

A. *His surgeon, Mr Turner, told him that there are different ways of performing this intervention: open surgery or minimal invasive surgery (MIS) using robotic technology. Mr Turner has had thorough training in open surgery and according to him this approach would be the best option. He explains to Archie that performing the operation in this way would be the current "gold standard" with excellent long term results, compared to the MIS approach, where such results are still missing. He points out that the main advantage of the open approach would be that the surgeon could use the best tool - the human hand.*

B. *Not knowing the exact benefits of MIS, Archie got a second opinion. The second surgeon, Ms Blue, recommended using the newest robotic surgical technology, the Da Vinci Surgical System. After her training in open surgery, she underwent extensive training in robotic surgery and has been performing the procedure for years. Despite not having long term results yet, Ms Blue believes in this approach. Questioned, she admits that the current instruments, although highly articulated and intuitively controlled, are not yet ideal. However, she claims that apart from the excellent visual system that the robot offers, there are several advantages to it, such as better precision, tremor reduction and enhanced ergonomics.*

Part II

Ms Blue knows that many patents held by Intuitive Surgical (the company of Da Vinci) are due to expire relatively soon and that there are competitors developing new surgical systems.
One of the systems she is aware of focuses on instrument design. The instruments (fig. i) that the robot carries are hand-like and each comprises three fingers that are foldable in order to enter the abdomen through a small incision. Two fingers are used as grasping forceps (or Maryland forceps), while the third is used for extra support and also carries a retractable blade or other knot-tying assisting gripper.
The surgeon remotely controls the instruments via a 3-finger exoskeleton (fig. ii) that he/she wears on his/her hands. This way, the surgeon uses natural hand movements to grasp organs/tissues.

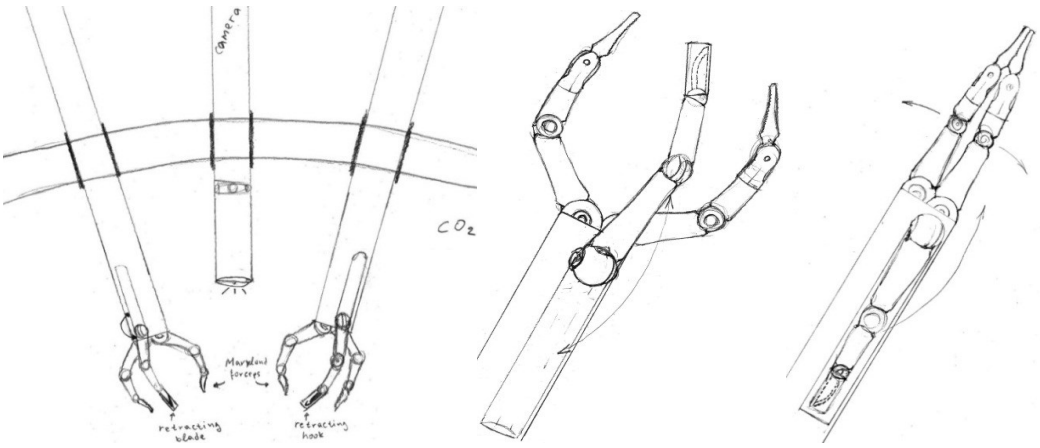

Fig. i - Hand-like instruments

Fig. ii - Example of an exoskeleton

Appendix II

Forward Kinematics of a 5 DOF digit

The next two tables illustrate the Denavit-Hartenberg parameters:

Proximal (Craig) Approach				
joint	$\mathbf{a_{i-1}}$	$\mathbf{\alpha_{i-1}}$	$\mathbf{d_i}$	$\mathbf{\theta_i}$
1	0	0	0	θ_1
2	0	-90	0	θ_2
3	0	-90	0	θ_3
4	ℓ_1	0	0	θ_4
5	ℓ_2	0	0	θ_5
t	ℓ_3	0	0	0

Terminology:

ℓ_i Length of the finger's i link

θ_i The angle of the finger's i joint

Auxiliary variables:

$$h_{10} = \ell_1 c_3 + \ell_2 c_{34} + \ell_3 c_{345}, \quad h_{12} = \ell_2 c_{34} + \ell_3 c_{345}, \quad h_{14} = \ell_3 c_{345}$$
$$h_{11} = \ell_1 s_3 + \ell_2 s_{34} + \ell_3 s_{345}, \quad h_{13} = \ell_2 s_{34} + \ell_3 s_{345}, \quad h_{15} = \ell_3 s_{345}$$

- *The axes of the 3rd, 4th and 5th joints of the system are parallel and make the finger move as if it was planar. Therefore, the variables h_{10} και h_{11} describe the fingertip's distance from the vertical axes of the plane that the 1st and 2nd joints define.*

The homogenous transformations g_{ij} that relate the consecutive links i, j are:

$$g_{01} = \begin{bmatrix} c_1 & -s_1 & 0 & 0 \\ s_1 & c_1 & 0 & 0 \\ 0 & 0 & 1 & 0 \\ 0 & 0 & 0 & 1 \end{bmatrix}, \quad g_{12} = \begin{bmatrix} c_2 & -s_2 & 0 & 0 \\ 0 & 0 & 1 & 0 \\ -s_2 & -c_2 & 0 & 0 \\ 0 & 0 & 0 & 1 \end{bmatrix}, \quad g_{23} = \begin{bmatrix} c_3 & -s_3 & 0 & 0 \\ 0 & 0 & 1 & 0 \\ -s_3 & -c_3 & 0 & 0 \\ 0 & 0 & 0 & 1 \end{bmatrix},$$

$$g_{34} = \begin{bmatrix} c_4 & -s_4 & 0 & \ell_1 \\ s_4 & c_4 & 0 & 0 \\ 0 & 0 & 1 & 0 \\ 0 & 0 & 0 & 1 \end{bmatrix}, \quad g_{45} = \begin{bmatrix} c_5 & -s_5 & 0 & \ell_2 \\ s_5 & c_5 & 0 & 0 \\ 0 & 0 & 1 & 0 \\ 0 & 0 & 0 & 1 \end{bmatrix}, \quad g_{5t} = \begin{bmatrix} 1 & 0 & 0 & \ell_3 \\ 0 & 1 & 0 & 0 \\ 0 & 0 & 1 & 0 \\ 0 & 0 & 0 & 1 \end{bmatrix},$$

$$g_{02}=\begin{bmatrix} c_1c_2 & -c_1s_2 & -s_1 & 0\\ s_1c_2 & -s_1s_2 & c_1 & 0\\ -s_2 & -c_2 & 1 & 0\\ 0 & 0 & 0 & 1\end{bmatrix},\qquad g_{03}=\begin{bmatrix} c_1c_2c_3+s_1s_3 & -c_1c_2s_3+s_1c_3 & -c_1s_2 & 0\\ s_1c_2c_3-c_1s_3 & -s_1c_2s_3-c_1c_3 & -s_1s_2 & 0\\ -s_2c_3 & s_2s_3 & -c_2 & 0\\ 0 & 0 & 0 & 1\end{bmatrix},$$

$$g_{04}=\begin{bmatrix} c_1c_2c_{43}+s_1s_{34} & -c_1c_2s_{34}+s_1c_{34} & -c_1s_2 & \ell_1\left(c_1c_2c_3+s_1s_3\right)\\ s_1c_2c_{34}-c_1s_{34} & -s_1c_2s_{34}-c_1c_{34} & -s_1s_2 & \ell_1\left(s_1c_2c_3-c_1s_3\right)\\ -s_2c_{34} & s_2s_{34} & -c_2 & -\ell_1s_2c_3\\ 0 & 0 & 0 & 1\end{bmatrix},$$

$$g_{05}=\begin{bmatrix} c_1c_2c_{435}+s_1s_{345} & -c_1c_2s_{345}+s_1c_{345} & -c_1s_2 & c_1c_2\left(\ell_1c_3+\ell_2c_{34}\right)+s_1\left(\ell_1s_3+\ell_2s_{34}\right)\\ s_1c_2c_{345}-c_1s_{345} & -s_1c_2s_{345}-c_1c_{345} & -s_1s_2 & s_1c_2\left(\ell_1c_3+\ell_2c_{34}\right)-c_1\left(\ell_1s_3+\ell_2s_{34}\right)\\ -s_2c_{345} & s_2s_{345} & -c_2 & -s_2\left(\ell_1c_3+\ell_2c_{34}\right)\\ 0 & 0 & 0 & 1\end{bmatrix}$$

The homogenous transformation that connects the fingertip to the inertial frame and consists of the fingertip position vector $\mathbf{p_{0t}}$ and its rotation matrix R_{0t} is the following:

$$g_{0t}=\begin{bmatrix} R_{0t} & \mathbf{p_{0t}}\\ 0_{1\times3} & 1\end{bmatrix}=\begin{bmatrix} c_1c_2c_{345}+s_1s_{345} & -c_1c_2s_{345}+s_1c_{345} & -c_1s_2 & c_1c_2h_{10}+s_1h_{11}\\ s_1c_2c_{345}-c_1s_{345} & -s_1c_2s_{345}-c_1c_{345} & -s_1s_2 & s_1c_2h_{10}-c_1h_{11}\\ -s_2c_{345} & s_2s_{345} & -c_2 & -s_2h_{10}\\ 0 & 0 & 0 & 1\end{bmatrix}$$

The <u>Jacobian matrix of the fingertip</u> J_t maps the joint velocity vector to the fingertip velocity expressed in the fingertip's frame $\{t\}$. The columns J_{it} of the Jacobian can be calculated using the corresponding homogenous transformation

$$g_{it}=\begin{bmatrix} n_x & o_x & a_x & p_x\\ n_y & o_y & a_y & p_y\\ n_z & o_z & a_z & p_z\\ 0 & 0 & 0 & 1\end{bmatrix}$$

using the formulas:

$$V_{tx}=-n_xp_y+n_yp_x \qquad V_{ty}=-o_xp_y+o_yp_x \qquad V_{tz}=-a_xp_y+a_yp_x$$

$$\omega_{tx}=n_z \qquad \omega_{ty}=o_z \qquad \omega_{tz}=a_z$$

$$J_{it}=\begin{bmatrix} V_{it}\\ \omega_{it}\end{bmatrix}$$

Also:

$$g_{4t}=\begin{bmatrix} c_5 & -s_5 & 0 & c_5\ell_3+\ell_2 \\ s_5 & c_5 & 0 & s_5\ell_3 \\ 0 & 0 & 1 & 0 \\ 0 & 0 & 0 & 1 \end{bmatrix}, \qquad g_{3t}=\begin{bmatrix} c_{45} & -s_{45} & 0 & \ell_1+c_4\ell_2+c_{45}\ell_3 \\ s_{45} & c_{45} & 0 & s_4\ell_2+s_{45}\ell_3 \\ 0 & 0 & 1 & 0 \\ 0 & 0 & 0 & 1 \end{bmatrix},$$

$$g_{2t}=\begin{bmatrix} c_{345} & -s_{345} & 0 & h_{10} \\ 0 & 0 & 1 & 0 \\ -s_{345} & -c_{345} & 0 & -h_{11} \\ 0 & 0 & 0 & 1 \end{bmatrix}, \qquad g_{1t}=\begin{bmatrix} c_2c_{345} & -c_2s_{345} & -s_2 & c_2h_{10} \\ -s_{345} & -c_{345} & 1 & -h_{11} \\ -s_2c_{345} & -s_2s_{345} & 0 & -s_2h_{10} \\ 0 & 0 & 0 & 1 \end{bmatrix}$$

Substituting, we derive:

$$J_t=\begin{bmatrix} J_{1t} & J_{2t} & J_{3t} & J_{4t} & J_{5t} \end{bmatrix}=\begin{bmatrix} c_2\left(\ell_1s_{45}+\ell_2s_5\right) & 0 & \ell_1s_{45}+\ell_2s_5 & \ell_2s_5 & 0 \\ -c_2\left(\ell_1c_{45}+\ell_2c_5+\ell_3\right) & 0 & \ell_1c_{45}+\ell_2c_5+\ell_3 & \ell_2c_5+\ell_3 & \ell_3 \\ -s_2h_{11} & h_{10} & 0 & 0 & 0 \\ -s_2c_{345} & -s_{345} & 0 & 0 & 0 \\ -s_2s_{345} & -c_{345} & 0 & 0 & 0 \\ -c_2 & 0 & 1 & 1 & 1 \end{bmatrix}$$

The <u>system's Jacobian</u> J can be calculated from fingertip's Jacobian as follows:

$$J=\begin{bmatrix} R_{0t} & 0_{3\times3} \\ 0_{3\times3} & R_{0t} \end{bmatrix}J_t$$

$$J=\begin{bmatrix} J_v \\ J_\omega \end{bmatrix}=\begin{bmatrix} -s_1c_2h_{10}+c_1h_{11} & -c_1s_2h_{10} & s_1h_{10}-c_1c_2h_{11} & s_1h_{12}-c_1c_2h_{13} & s_1h_{14}-c_1c_2h_{15} \\ c_1c_2h_{10}+s_1h_{11} & -s_1s_2h_{10} & -c_1h_{10}-s_1c_2h_{11} & -c_1h_{12}-s_1c_2h_{13} & -c_1h_{14}-s_1c_2h_{15} \\ 0 & -c_2h_{10} & s_2h_{11} & s_2h_{13} & s_2h_{15} \\ 0 & -s_1 & -c_1s_2 & -c_1s_2 & -c_1s_2 \\ 0 & c_1 & -s_1s_2 & -s_1s_2 & -s_1s_2 \\ 1 & 0 & -c_2 & -c_2 & -c_2 \end{bmatrix}$$

Forward Kinematics of a 4 DOF digit

The analysis that follows is identical to the one for the 5 DOF digit, and hence, it will be less detailed.

Proximal (Craig) Approach				
joint	a_{i-1}	α_{i-1}	d_i	θ_i
1	0	0	0	θ_1
2	0	-90	0	θ_2
3	ℓ_1	0	0	θ_3
4	ℓ_2	0	0	θ_4
t	ℓ_3	0	0	0

Auxiliary variables:

$h_{20} = \ell_1 c_2 + \ell_2 c_{23} + \ell_3 c_{234}$, $h_{22} = \ell_2 c_{23} + \ell_3 c_{234}$, $h_{24} = \ell_3 c_{234}$

$h_{21} = \ell_1 s_2 + \ell_2 s_{23} + \ell_3 s_{234}$, $h_{23} = \ell_2 s_{23} + \ell_3 s_{234}$, $h_{25} = \ell_3 s_{234}$

Homogenous transformations:

$$g_{01} = \begin{bmatrix} c_1 & -s_1 & 0 & 0 \\ s_1 & c_1 & 0 & 0 \\ 0 & 0 & 1 & 0 \\ 0 & 0 & 0 & 1 \end{bmatrix}, \quad g_{12} = \begin{bmatrix} c_2 & -s_2 & 0 & 0 \\ 0 & 0 & 1 & 0 \\ -s_2 & -c_2 & 0 & 0 \\ 0 & 0 & 0 & 1 \end{bmatrix}, \quad g_{23} = \begin{bmatrix} c_3 & -s_3 & 0 & \ell_1 \\ s_3 & c_3 & 0 & 0 \\ 0 & 0 & 1 & 0 \\ 0 & 0 & 0 & 1 \end{bmatrix},$$

$$g_{34} = \begin{bmatrix} c_4 & -s_4 & 0 & \ell_2 \\ s_4 & c_4 & 0 & 0 \\ 0 & 0 & 1 & 0 \\ 0 & 0 & 0 & 1 \end{bmatrix}, \quad g_{4t} = \begin{bmatrix} 1 & 0 & 0 & \ell_3 \\ 0 & 1 & 0 & 0 \\ 0 & 0 & 1 & 0 \\ 0 & 0 & 0 & 1 \end{bmatrix}, g_{02} = \begin{bmatrix} c_1 c_2 & -c_1 s_2 & -s_1 & 0 \\ s_1 c_2 & -s_1 s_2 & c_1 & 0 \\ -s_2 & -c_2 & 0 & 0 \\ 0 & 0 & 0 & 1 \end{bmatrix},$$

$$g_{03} = \begin{bmatrix} c_1 c_{23} & -c_1 s_{23} & -s_1 & c_1 (h_{20} - h_{22}) \\ s_1 c_{23} & -s_1 s_{23} & c_1 & s_1 (h_{20} - h_{22}) \\ -s_{23} & -c_{23} & 0 & -(h_{21} - h_{23}) \\ 0 & 0 & 0 & 1 \end{bmatrix}, \quad g_{04} = \begin{bmatrix} c_1 c_{234} & -c_1 s_{234} & -s_1 & c_1 (h_{20} - h_{24}) \\ s_1 c_{234} & -s_1 s_{234} & c_1 & s_1 (h_{20} - h_{24}) \\ -s_{234} & -c_{234} & 0 & -(h_{21} - h_{25}) \\ 0 & 0 & 0 & 1 \end{bmatrix}$$

$$g_{0t} = \begin{bmatrix} c_1 c_{234} & -c_1 s_{234} & -s_1 & c_1 h_{20} \\ s_1 c_{234} & -s_1 s_{234} & c_1 & s_1 h_{20} \\ -s_{234} & -c_{234} & 0 & -h_{21} \\ 0 & 0 & 0 & 1 \end{bmatrix}$$

Fingertip's Jacobian J_t :

$$g_{4t}=\begin{bmatrix}1&0&0&\ell_3\\0&1&0&0\\0&0&1&0\\0&0&0&1\end{bmatrix},\qquad g_{3t}=\begin{bmatrix}c_4&-s_4&0&\ell_2+\ell_3c_4\\s_4&c_4&0&\ell_3s_4\\0&0&1&0\\0&0&0&1\end{bmatrix},$$

$$g_{2t}=\begin{bmatrix}c_{34}&-s_{34}&0&\ell_1+\ell_2c_3+\ell_3c_{34}\\s_{34}&c_{34}&0&\ell_2s_3+\ell_3s_{34}\\0&0&1&0\\0&0&0&1\end{bmatrix},\qquad g_{1t}=\begin{bmatrix}c_{234}&-s_{234}&0&h_{20}\\0&0&1&0\\-s_{234}&-c_{234}&0&-h_{21}\\0&0&0&1\end{bmatrix}$$

$$J_t=\begin{bmatrix}0&\ell_1s_{34}+\ell_2s_4&\ell_2s_4&0\\0&\ell_1c_{34}+\ell_2c_4+\ell_3&\ell_2c_4+\ell_3&\ell_3\\h_{20}&0&0&0\\-s_{234}&0&0&0\\-c_{234}&0&0&0\\0&1&1&1\end{bmatrix}$$

Finger's Jacobian:

$$J=\begin{bmatrix}J_v\\J_\omega\end{bmatrix}=\begin{bmatrix}-s_1h_{20}&-c_1h_{21}&-c_1h_{23}&-c_1h_{25}\\c_1h_{20}&-s_1h_{21}&-s_1h_{23}&-s_1h_{25}\\h_{20}&-h_{20}&-h_{22}&-h_{24}\\-s_{234}&0&0&0\\-c_{234}&0&0&0\\0&1&1&1\end{bmatrix}$$

Appendix III

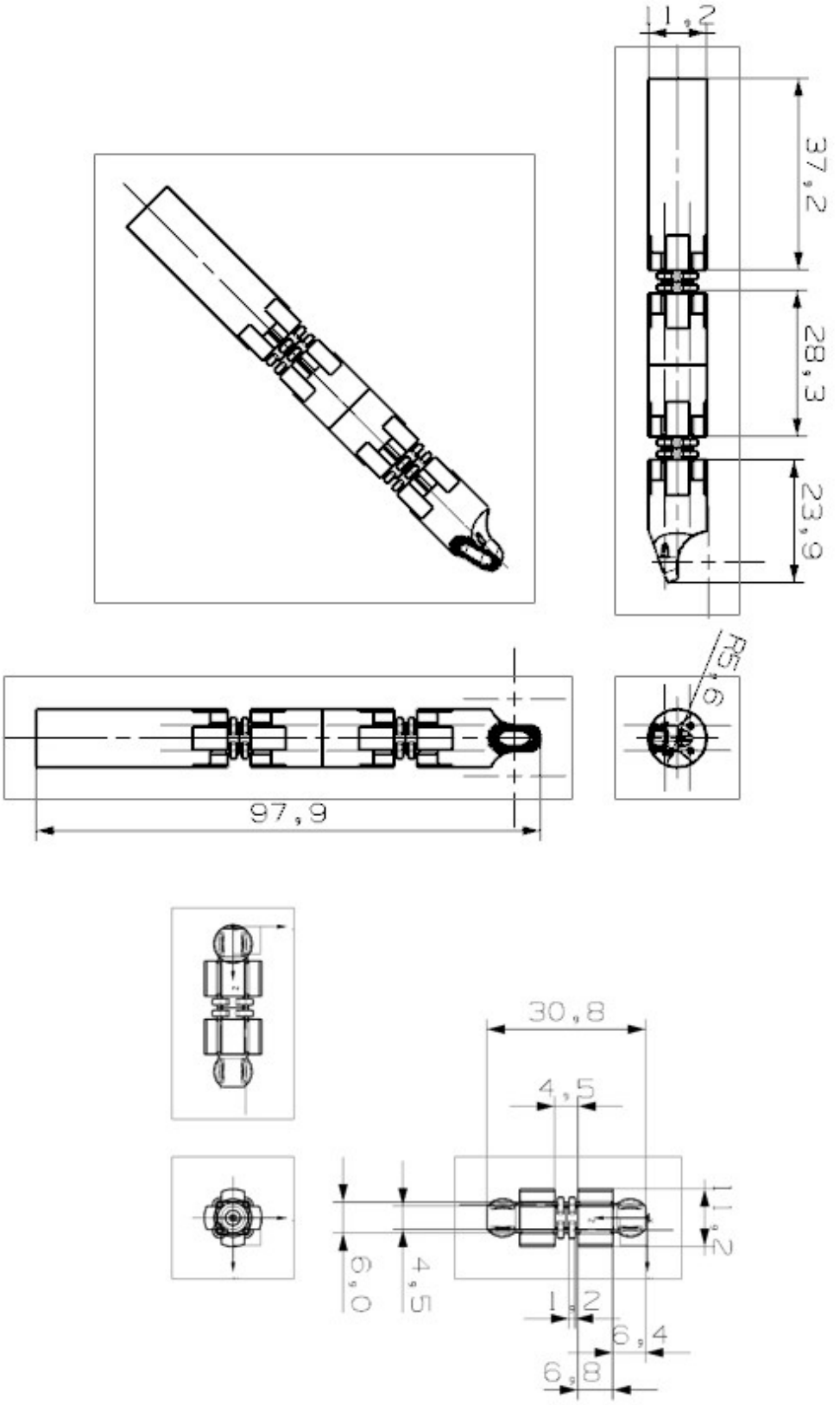

Figure 7.2: CAD drawings of SMA-driven instrument prototype (assembly and soft joint)

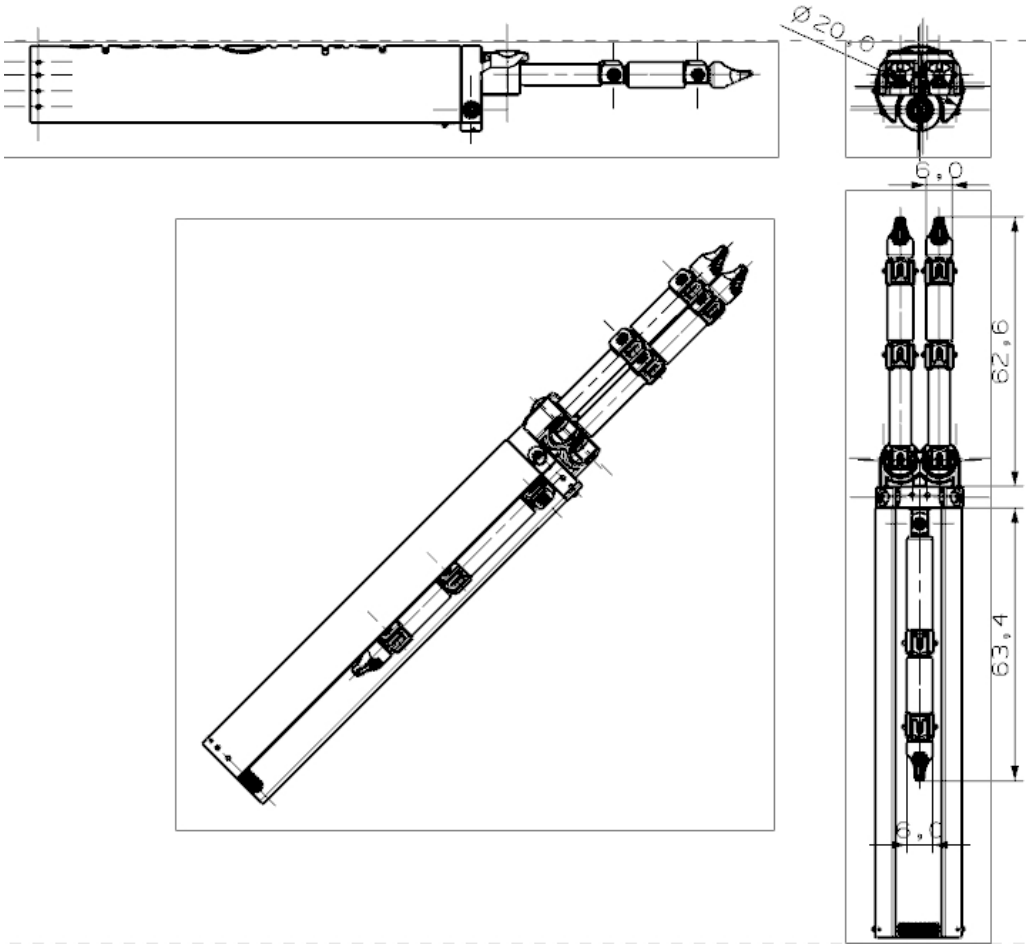

Figure 7.3: CAD drawings of cable-driven instrument prototype (assembly)

Appendix IV

Limit Angles of Cable 'tJ_5'

Calculation of ω_{32}

In the following equations, x_i and y_i denote the x and y coordinate of point i with regard to its reference frame as presented in Table 5.2.

When $\phi_3 = \omega_{32}$, the points G_5, G_{31} and G_B are aligned as shown in Fig. 7.4a, hence, it can be written as $G_5G_{31}//G_{31}G_B$. G'_{31} is the pivot point when $\phi_3 = 0$ and G_{31} when $\phi_3 = \omega_{32}$, i.e. the angle between G'_{31} and G_{31} is ω_{32}. Using cosine law, we get:

$$\psi_0 = cos^{-1}\left(\frac{O_3G_5^2 + G_5G_{31}^2 - O_3G_{31}^2}{2 \cdot O_3G_5 \cdot O_3G_{31}}\right) \tag{Iα}$$

where:

$$O_3G_5 = \sqrt{\left(O_4G_5 \sin\left(\phi_4 + tan^{-1}\frac{x_{G_5}}{l_2 - y_{G_5}}\right)\right)^2 + \left(O_4G_5 \cos\left(\phi_4 + tan^{-1}\frac{x_{G_5}}{l_2 - y_{G_5}} + l_0\right)\right)^2}$$

$$O_4G_5 = \sqrt{x_{G_5}^2 + (l_2 - y_{G_5})^2}$$
$$O_3G_{31} = \sqrt{x_{G_{31}}^2 + y_{G_{31}}^2}$$
$$G_5G_{31} = \sqrt{(x_{G_{31}} + O_4G_{5x})^2 + (l_0 + y_{G_{31}} + O_4G_{5y})^2}$$
$$O_4G_{5x} = O_4G_5 \sin\left(\phi_4 + tan^{-1}\tfrac{x_{G_5}}{l_2 - y_{G_5}}\right)$$
$$O_4G_{5y} = O_4G_5 \cos\left(\phi_4 + tan^{-1}\tfrac{x_{G_5}}{l_2 - y_{G_5}}\right)$$

Again, using cosine law, length G_5G_B can be derived as the root of the polynomial:

$$G_5G_B^2 + 2O_3G_5 \cdot \cos\psi_0 \cdot G_5G_B + O_3G_5^2 - O_3G_B^2 = 0 \tag{Iβ}$$

Furthermore,

$$\psi_1 = cos^{-1}\frac{O_3G_B^2 + O_3G_{31}^2 - G_{31}G_B^2}{2 \cdot O_3G_B \cdot O_3G_{31}} \tag{Iγ}$$

where $G_{31}G_B = G_5G_B - G_5G_{31}$ and $O_3G_B = \sqrt{x_{G_B}^2 + y_{G_B}^2}$. Finally:

$$\omega_{32} = 180 - \gamma_0 - \gamma_1 - \psi_1 \tag{I}$$

where $\gamma_0 = tan^{-1}\frac{x_{G_{31}}}{y_{G_{31}}}$ and $\gamma_1 = tan^{-1}\frac{x_{G_B}}{y_{G_B}}$.

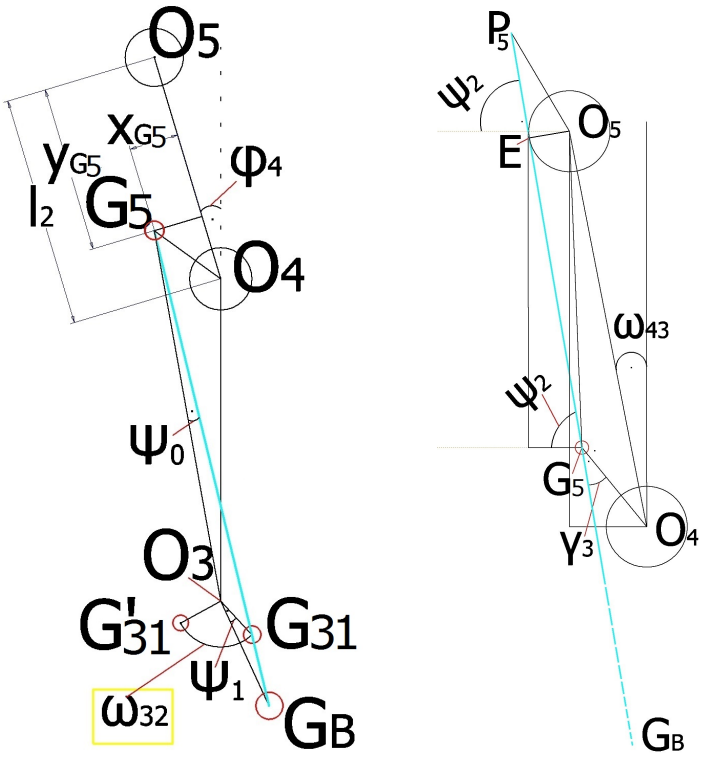

(a) (b)

Figure 7.4: Geometry for calculation of ω_{32} and ω_{43} (not actual dimensions)

Calculation of ω_{43}

When $\phi_4 = \omega_{43}$, the cable is tangential to the O_5 shaft and passes straight through G_5 and G_B (Fig. 7.4b), i.e. $E_5G_5 // G_5G_B$. In this case:

$$\gamma_3 = 180 - sin^{-1}\frac{r_s}{O_5G_5} - tan^{-1}\frac{y_{G_5}}{x_{G_5}} - tan^{-1}\frac{l_2 - y_{G_5}}{x_{G_5}} \tag{IIα}$$

where $O_5G_5 = \sqrt{x_{G_5}^2 + y_{G_5}^2}$. For angle ψ_2, there are two cases; i) when G_B is on the right side and ii) left side of O_4:

$$\psi_2 = \begin{cases} tan^{-1}\frac{O_4G_{B_x}}{O_4G_{B_y}} - sin^{-1}\left(O_4G_5 \sin\frac{\gamma_3}{O_4G_B}\right) & \phi_3 \leq 180 - \gamma_1 \\ 180 + tan^{-1}\frac{O_4G_{B_x}}{O_4G_{B_y}} - sin^{-1}\left(O_4G_5 \sin\frac{\gamma_3}{O_4G_B}\right) & \phi_3 > 180 - \gamma_1 \end{cases} \tag{IIβ}$$

where

$$O_4G_{B_x} = O_3G_B \sin(180 - \gamma_1 - \phi_3)$$

$$O_4G_{B_y} = O_3G_B \cos(180 - \gamma_1 - \phi_3) + l_0$$

Finally:

$$\omega_{43} = cos^{-1}\frac{r_s}{O_5G_5} + tan^{-1}\frac{x_{G_5}}{y_{G_5}} - \psi_2 \tag{II}$$

Routings of the Thumb and Index Finger Cables

Similar to the method presented in Section 5.3.2, the paths and angle categories regarding the cables of the other DOFs of the thumb and the index/middle fingers can be derived. For the thumb, Tables 7.1, 7.2 and 7.3 regard cable 'tJ_4', Table 7.4 regards 'tJ_3', Tables 7.5, 7.6 regard 'tJ_2' and Table 7.7 regards 'tJ_1'. For the index or middle finger, Tables 7.8, 7.9 and 7.10 regard cable 'miJ_4', Tables 7.11, 7.12 and 7.13 regard 'miJ_3', Table 7.14 regards 'miJ_2' and equation (7.1) regards 'miJ_1'.

Routing of cable 'tJ_4' of the thumb

For reference of symbols, see Figure 5.20c, on page 116.

Table 7.1: Paths of cable 'tJ_4' of the thumb

Path	Cat.
$P_4 \rightarrow S(O_4) \rightarrow G_{31} \rightarrow G_{32} \rightarrow G_B$	11
$P_4 \rightarrow G_{31} \rightarrow G_{32} \rightarrow G_B$	12
$P_4 \rightarrow S(O_4) \rightarrow G_{31} \rightarrow G_B$	21, 31
$P_4 \rightarrow G_{31} \rightarrow G_B$	22, 32
$P_4 \rightarrow G_B$	33
$P_4 \rightarrow S(O_4) \rightarrow G_B$	41, 51
$P_4 \rightarrow G_B$	42, 52
$P_4 \rightarrow G_{33} \rightarrow G_B$	53
$P_4 \rightarrow S(O_4) \rightarrow G_{33} \rightarrow G_B$	61
$P_4 \rightarrow G_{33} \rightarrow G_B$	62

*Cat: angle category (See Table 7.3)

Table 7.2: Limits for ϕ_3, ϕ_4 regarding 'tJ_4' of the thumb

Symbol	Description	Value or Range (deg)
ω_{31}	$G_{31}G_{32}//G_{32}G_B$	45.58
ω_{37}	$P_4G_{31}//G_{31}G_B$	104.01
ω_{33}	$I_AG_{31}//G_{31}G_B$	104.91
ω_{38}	$E_5I_A//I_AG_B$	118.76
ω_{39}	$G_5G_{33}//G_{33}G_B$	119.71
ω_{46}	$E_5I_A//I_AG_{31}$	51.78
ω_{47}	$E_5G_5//G_5G_{31}$	$f(\phi_3) \in [51.78, 90]$
ω_{48}	$E_5G_5//G_5G_B$	$f(\phi_3) \in [49.39, 51.78]$
ω_{49}	$E_5I_A//I_AG_B$	$f(\phi_3) \in [49.39, 90]$
ω_{410}	$E_5G_5//G_5G_{33}$	49.39

Table 7.3: Categories that ϕ_3, ϕ_4 and ϕ_5 are classified to regarding 'tJ_4' cable

	Angle ranges						
$\boldsymbol{\phi_3}$	$[0, \omega_{31}]$		$[\omega_{31}, \omega_{37}]$		$[\omega_{37}, \omega_{33}]$		
$\boldsymbol{\phi_4}$	$[0, \omega_{46}]$	$[\omega_{46}, 90]$	$[0, \omega_{46}]$	$[\omega_{46}, 90]$	$[0, \omega_{46}]$	$[\omega_{46}, \omega_{47}]$	$[\omega_{47}, 90]$
Cat.	11	12	21	22	31	32	33
$\boldsymbol{\phi_3}$	$[\omega_{33}, \omega_{38}]$		$[\omega_{38}, \omega_{39}]$		$[\omega_{39}, 180]$		
$\boldsymbol{\phi_4}$	$[0, \omega_{48}]$	$[\omega_{48}, 90]$	$[0, \omega_{48}]$	$[\omega_{48}, \omega_{49}]$	$[\omega_{49}, 90]$	$[0, \omega_{410}]$	$[\omega_{410}, 90]$
Cat.	41	42	51	52	53	61	62

See Table 7.2 for the values of each ω_i limit angle

Routing of cable 'tJ_3' of the thumb

Figures 7.5 (a) and (b) show the top and bottom sides of link 'a' (Figure 5.19) with the points where cable 'tJ_3' passes from. The cable is starts from 'S', which is the centre of the through hole at its bottom side and travels through to 'A', the corresponding point at its top side. The cable crosses the top surface until the opposite edge, symbolised with 'C' until it vertically continues and exits at 'D', a hole at the shaft of the instrument where it enters a sheath of constant length until it connects to the motor. 'O_3' is the centre of rotation, origin of DOF {3}. Figure 7.6 shows the cable routing when ϕ_3=0.

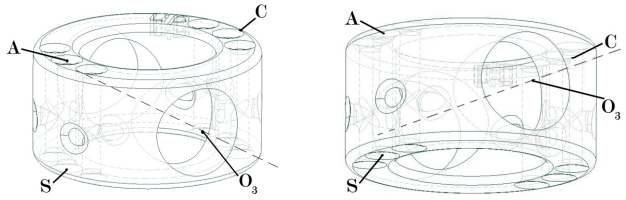

(a) (b)

Figure 7.5: a) Top and b) bottom sides of link 'a' which controls DOF {3}

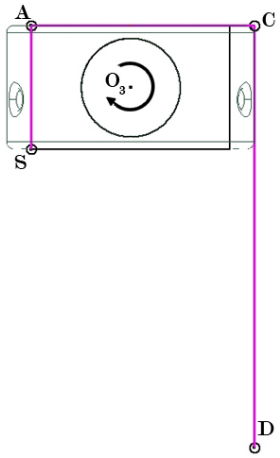

Figure 7.6: Profile of link 'a' and routing of 'tJ_3' when ϕ_3=0 (not actual dimensions)

Table 7.4: Paths of cable 'tJ_3' of the thumb

Path	**Cat.**	Angle Range
$S \rightarrow A \rightarrow C \rightarrow D$	1	$[0, \omega_{310}*]$
$S \rightarrow A \rightarrow D$	2	$[\omega_{310}, 180]$

*when $\phi_3 = \omega_{310}$(=87.88°): AC//CD

Routing of cable 'tJ_2' of the thumb

Figures 7.7 (a) and (b) show three parts of the thumb assembly with the contact points of cable 'tJ_2'. The cable is starts from 'P_2', which is the centre of a locking pin on link '1', while it travels inside link 'b' via 'G_{21} and 'G_{22}'. 'G_{21}' is the edge of a narrowing of link 'b' and 'G_{22}' is the edge on the exit of the same link. 'G_{23}' is the edge of link 'a' that the cable passes from before it exits at 'G_B' inside the shaft of the instrument (same exit point with 'tJ_4' and 'tJ_5'). 'O_2' is the centre of rotation of DOF {2}. Figure 7.8 shows the cable routing when ϕ_2=0.

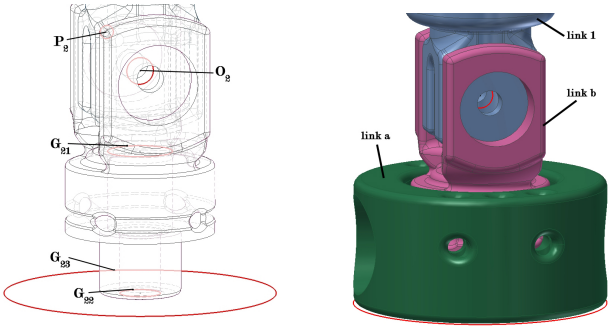

(a) (b)

Figure 7.7: a) Cable contact points of 'tJ_2' and b) assembly for control of DOF {2}

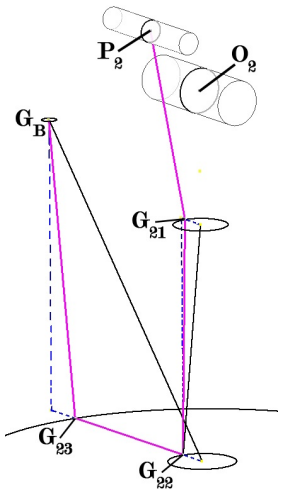

Figure 7.8: Routing of 'tJ_2' when ϕ_2=0

Table 7.5: Paths of cable 'tJ_2' of the thumb

Path	**Cat.**	Angle Range
$P_2 \rightarrow G_{21} \rightarrow G_{22} \rightarrow G_B$	3	$[0, \omega_{311}]$
$P_2 \rightarrow G_{21} \rightarrow G_{22} \rightarrow G_B$	4	$[\omega_{311}, \omega_{312}]$
$P_2 \rightarrow G_{21} \rightarrow G_B$	5	$[\omega_{312}, \omega_{313}]$
$P_2 \rightarrow G_{21} \rightarrow G_{24} \rightarrow G_B$	6	$[\omega_{313}, 180]$

See Table 7.6 for each ωi limit angle

Table 7.6: Limits for ϕ_3, ϕ_4 regarding 'tJ_2' of the thumb

Symbol	**Description**	**Value or Range (deg)**
ω_{311}	$G_{22}G_{23}//G_{23}G_B$	53.43
ω_{312}	$G_{21}G_{22}//G_{22}G_B$	116.57
ω_{313}	$G_{21}G_{24}//G_{24}G_B$	136.8

Routing of cable 'tJ_1' of the thumb

Figures 7.9 (a) and (b) show link 'a' and 'b': their relative movement is responsible for DOF {1}. Cable 'tJ_1' starts at point 'H' of link 'b' and goes through it to reach point 'K'. Then, it wraps around the part's external circumference counter-clockwise until it reaches the opening 'L′'. At this point the cable enters link 'a' via point 'L'. Inside link 'a' and through a vertical path, it reaches point 'M', before it crosses to the opposite edge 'N' of the same part. Finally, it exits at point 'N′', which is located at the shaft of the instrument, and into a constant length sheath.

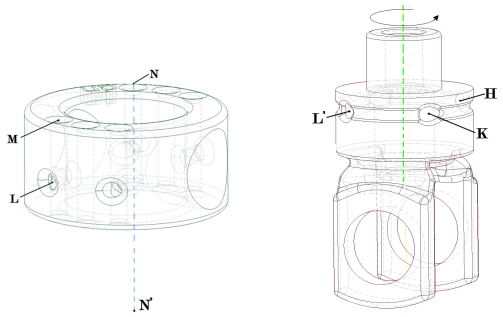

(a) (b)

Figure 7.9: Contact points of 'tJ_1' on a) link 'a' and b) link 'b' for control of DOF {1}

Table 7.7: Paths of cable 'tJ_1' of the thumb

Path	**Cat.**	Angle Range
$H \rightarrow K \rightarrow L' \rightarrow L \rightarrow M \rightarrow N \rightarrow N'$	7	$[0, \omega_{314}*]$
$H \rightarrow K \rightarrow L' \rightarrow L \rightarrow M \rightarrow N'$	8	$[\omega_{314}, 180]$

*when $\phi_3 = \omega_{314}(=89°)$: $MN//NB_1$

Routing of cable 'miJ_4' of the index/middle finger

Similar to cable 'tJ_5' of the thumb, 'miJ_4' starts at 'P_4' and exits at 'G_{B4}' (shaft) via various points shown in Figure 7.10. Table 7.8 summarises the possible paths.

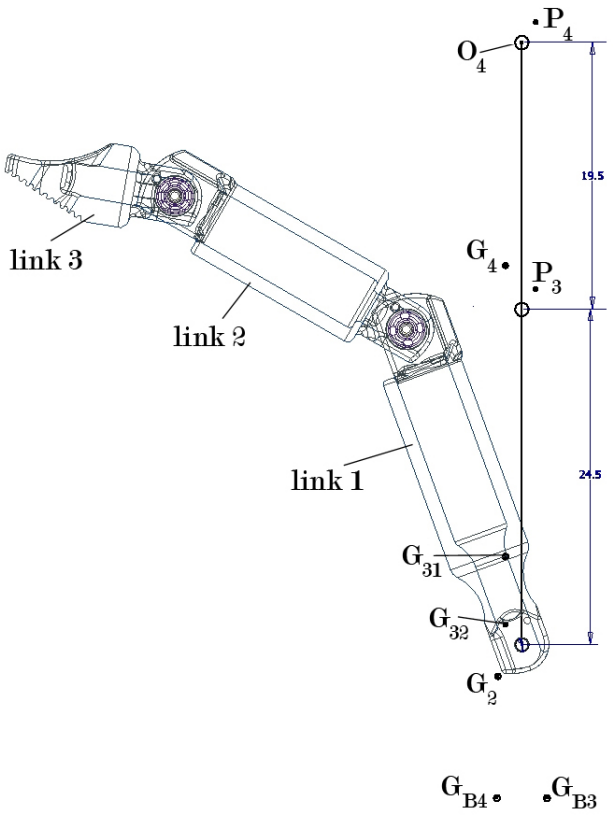

Figure 7.10: Links of the index/middle finger and contact points of 'miJ_4' and 'miJ_3'

Table 7.8: Paths of cable 'miJ_4' of the index/middle finger

Path	Cat.
$P_4 \rightarrow S(O_4) \rightarrow G_{32} \rightarrow G_{B4}$	111
$P_4 \rightarrow G_{32} \rightarrow G_{B4}$	112
$P_4 \rightarrow G_{31} \rightarrow G_{32} \rightarrow G_{B4}$	113, 122
$P_4 \rightarrow G_4 \rightarrow G_{31} \rightarrow G_{32} \rightarrow G_{B4}$	114, 123, 132
$P_4 \rightarrow S(O_4) \rightarrow G_{31} \rightarrow G_{32} \rightarrow G_{B4}$	121
$P_4 \rightarrow S(O_4) \rightarrow G_4 \rightarrow G_{31} \rightarrow G_{32} \rightarrow G_{B4}$	131
$P_4 \rightarrow S(O_4) \rightarrow G_{32} \rightarrow G_2 \rightarrow G_{B4}$	211
$P_4 \rightarrow G_{32} \rightarrow G_2 \rightarrow G_{B4}$	212
$P_4 \rightarrow G_{31} \rightarrow G_{32} \rightarrow G_2 \rightarrow G_{B4}$	213, 222
$P_4 \rightarrow G_4 \rightarrow G_{31} \rightarrow G_{32} \rightarrow G_2 \rightarrow G_{B4}$	214, 223, 232
$P_4 \rightarrow S(O_4) \rightarrow G_{31} \rightarrow G_{32} \rightarrow G_2 \rightarrow G_{B4}$	221
$P_4 \rightarrow S(O_4) \rightarrow G_4 \rightarrow G_{31} \rightarrow G_{32} \rightarrow G_2 \rightarrow G_{B4}$	231

*Cat: angle category (See Table 7.10)

Table 7.9: Limits for ϕ_3, ϕ_4 regarding 'miJ_4' of the index/middle finger

Symbol	Description	Value or Range (deg)
β_{21}	$G_{32}G_2//G_2G_{B4}$	25.18
β_{31}	$IG_{31}//G_{31}G_{32}$	2.06
β_{32}	$IG_4//G_4G_{31}$	2.89
β_{41}	$P_4I//IG_{32}$	$f(\phi_3) \in [47.74, 48.85]$
β_{42}	$G_4G_{31}//G_{31}G_{32}$	$f(\phi_3) \in [47.74, 75.42]$
β_{43}	$P_4G_4//G_4G_{31}$	$f(\phi_3) \in [47.33, 75.42]$
β_{44}	$P_4I//IG_{31}$	$f(\phi_3) \in [47.33, 47.74]$
β_{45}	$P_4I//IG_4$	47.33

Table 7.10: Categories that ϕ_3, ϕ_4 and ϕ_5 are classified to regarding 'miJ_4' cable

	Angle ranges								
$\boldsymbol{\phi_2}$	$[0, \beta_{21}]$								
$\boldsymbol{\phi_3}$	$[0, \beta_{31}]$				$[\beta_{31}, \beta_{32}]$			$[\beta_{32}, 90]$	
$\boldsymbol{\phi_4}$	$[0, \beta_{41}]$	$[\beta_{41}, \beta_{42}]$	$[\beta_{42}, \beta_{43}]$	$[\beta_{43}, 90]$	$[0, \beta_{44}]$	$[\beta_{44}, \beta_{43}]$	$[\beta_{43}, 90]$	$[0, \beta_{45}]$	$[\beta_{45}, 90]$
Cat.	111	112	113	114	121	122	123	131	132
$\boldsymbol{\phi_2}$	$[\beta_{21}, 90]$								
$\boldsymbol{\phi_3}$	$[0, \beta_{31}]$				$[\beta_{31}, \beta_{32}]$			$[\beta_{32}, 90]$	
$\boldsymbol{\phi_4}$	$[0, \beta_{41}]$	$[\beta_{41}, \beta_{42}]$	$[\beta_{42}, \beta_{43}]$	$[\beta_{43}, 90]$	$[0, \beta_{44}]$	$[\beta_{44}, \beta_{43}]$	$[\beta_{43}, 90]$	$[0, \beta_{45}]$	$[\beta_{45}, 90]$
Cat.	211	212	213	214	221	222	223	231	232

See Table 7.9 for the values of each β_i limit angle

Routing of cable 'miJ_3' of the index/middle finger

Cable 'miJ_3' has similar contact points with 'miJ_4' (Figure 7.10). The main difference is that it starts from locking pin 'P_3', attached to link '2'. Potential paths are summarised in Table 7.11.

Table 7.11: Paths of cable 'miJ_3' of the thumb

Path	Cat.
$P_3 \rightarrow S(O_3) \rightarrow G_{32} \rightarrow G_{B3}$	11
$P_3 \rightarrow G_{32} \rightarrow G_{B3}$	12
$P_3 \rightarrow G_{31} \rightarrow G_{32} \rightarrow G_{B3}$	13
$P_3 \rightarrow S(O_3) \rightarrow G_{32} \rightarrow G_2 \rightarrow G_{B3}$	21
$P_3 \rightarrow G_{32} \rightarrow G_2 \rightarrow G_{B3}$	22
$P_3 \rightarrow G_{31} \rightarrow G_{32} \rightarrow G_2 \rightarrow G_{B3}$	23

*Cat: angle category (See Table 7.12)

Table 7.12: Categories that ϕ_3, ϕ_4 and ϕ_5 are classified to regarding 'miJ_3' cable

	Angle ranges					
$\boldsymbol{\phi_2}$	$[0, \beta_{21}]$			$[\beta_{21}, 90]$		
$\boldsymbol{\phi_3}$	$[0, \beta_{33}]$	$[\beta_{33}, \beta_{34}]$	$[\beta_{34}, 90]$	$[0, \beta_{33}]$	$[\beta_{33}, \beta_{34}]$	$[\beta_{34}, 90]$
Cat.	11	12	13	21	22	23

See Table 7.13 for the values of each β_i limit angle

Table 7.13: Limits for ϕ_3, ϕ_4 regarding 'miJ_3' of the thumb

Symbol	Description	Value or Range (deg)
β_{21}	$G_{32}G_2//G_2G_{B3}$	25.18
β_{33}	$P_3J//JG_{32}$	48.05
β_{34}	$P_3G_{31}//G_{31}G_{32}$	75.42

Routing of cable 'miJ_2' of the index/middle finger

Figure 7.11 shows the contact points of cable 'miJ_2', as well as the path when ϕ_2=0. There only two possible paths, described in Table 7.14.

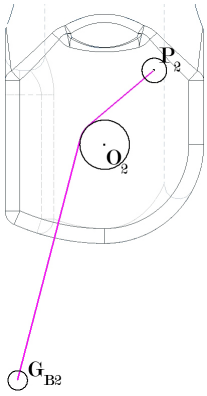

Figure 7.11: Contact points of 'miJ_2' and cable path when ϕ_2=0

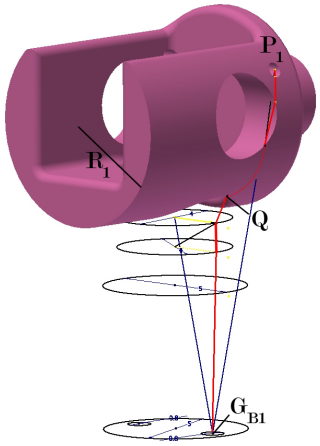

Figure 7.12: Contact points of cable 'miJ_1'

Table 7.14: Paths of cable 'miJ_2' of the thumb

Path	Cat.	Angle Range
$P_2 \rightarrow S(O_2) \rightarrow G_{B2}$	1	$[0, \beta_{22}*]$
$P_2 \rightarrow G_{B2}$	2	$[\beta_{22}, 90]$

*when $\phi_2 = \beta_{22}(= 87.88°)$: $P_2K//KG_{B2}$

Routing of cable 'miJ_1' of the index/middle finger

Figure 7.12 shows the part that connects link '1' of the index (or middle finger) to the base assembly of the instrument (Figure 5.13). Cable 'miJ_1' starts at 'P_1', wraps around the surface of the cylindrical part until point 'Q' and exits at 'G_{B1}' into its sheath. Change of angle ϕ_1 of DOF {1} causes change of the length of the $\overset{\frown}{P_2E}$ arc. The difference in cable length can be approximated by the following formula:

$$\Delta L = \frac{\phi_1 R_1 \pi}{180} \tag{7.1}$$

where R_1 is the radius of the cylindrical part.